Modification of poly(vinyl alcohol) hydrogels for small diameter vascular graft application

by

Yuan Yao

A thesis
presented to the University of Waterloo
in fulfillment of the
thesis requirement for the degree of
Doctor of Philosophy
in
Chemical Engineering

Waterloo, Ontario, Canada, 2021

©Yuan Yao 2021

Examining Committee Membership

The following served on the Examining Committee for this thesis. The decision of the Examining Committee is by majority vote.

External Examiner	Prof. Christopher Moraes Department of Chemical Engineering, McGill University
Supervisor	Prof. Evelyn Yim Department of Chemical Engineering, University of Waterloo
Internal Member	Prof. Boxin Zhao Department of Chemical Engineering, University of Waterloo
Internal Member	Prof. Michael Tam Department of Chemical Engineering, University of Waterloo
Internal-external Member	Prof. Alfred Yu Department of Electrical & Computer Engineering, University of Waterloo

Author's Declaration

This thesis consists of materials all of which I authored or co-authored: see Statement of Contributions included in the thesis. This is a true copy of the thesis, including any required final revisions, as accepted by my examiners.

I understand that my thesis may be made electronically available to the public.

Statement of Contributions

Chapter 2 of this thesis contains parts of two unpublished manuscripts.

Section 2.5 is a part of a published paper that was co-authored by myself and my supervisor (Dr. Evelyn Yim). I did the literature research, writing and editing; Dr. Evelyn Yim did the review and editing.

Yuan Yao, Evelyn Yim. "Fucoidan for cardiovascular application and the factors mediating its activities". *Carbohydrate polymers*. 270 (2021) 118347. DOI: 10.1016/j.carbpol.2021.118347 © 2021 Elsevier Ltd.

Section 2.6.1 is a part of a published paper that was co-authored by my colleague (Ms. Linan Cui), myself, and my supervisor (Dr. Evelyn Yim). For the section that was included in this thesis, I did the literature research, writing and editing; Ms. Linan Cui did the editing; Dr. Evelyn Yim did the review and editing.

Linan Cui[†], Yuan Yao[†], Evelyn Yim. "The effects of surface topography modification on hydrogel properties". *APL Bioengineering*. 5 (2021) 031509. DOI: 10.1063/5.0046076 ([†]authors contribute equally). Reproduced with the permission of AIP Publishing.

Chapter 3 of this thesis consists of the following paper that was co-authored by myself, my supervisor (Dr. Evelyn Yim), my colleague (Dr. Aung Moe Zaw), and two collaborators (Dr. Deirdre E.J. Anderson and Dr. Monica T. Hinds). I designed and conducted the experiments and did the writing and revision of the manuscript; Dr. Aung Moe Zaw helped with the animal surgery and the review and editing of the manuscript; Dr. Deirdre E.J. Anderson and Dr. Monica T. Hinds did the *ex-vivo* shunt study and helped with the review and editing of the manuscript; Dr. Evelyn Yim supervised the study and did the review and editing of the manuscript.

Yuan Yao, Aung Moe Zaw, Deirdre E.J. Anderson, Monica T. Hinds, Evelyn K.F. Yim. "Fucoidan functionalization on poly(vinyl alcohol) hydrogels for improved endothelialization and hemocompatibility". *Biomaterials* 249 (2020) 120011. DOI: 10.1016/j.biomaterials.2020.120011. © 2020 Elsevier Ltd.

Chapter 4 of this thesis is a manuscript under-preparation that will be co-authored by myself, my supervisor, and two collaborators (Dr. Deirdre E.J. Anderson and Dr. Monica T. Hinds). I designed and conducted the experiments and did the writing; Dr. Deirdre E.J. Anderson and Dr. Monica T. Hinds did the *ex-vivo* shunt study; Dr. Evelyn Yim supervised the study.

Chapter 5 of this thesis is a manuscript under-preparation that will be co-authored by myself, my supervisor, and my colleague (Dr. Aung Moe Zaw and Ms. YeJin Jeong). I designed and conducted the experiments and did the writing; Dr. Aung Moe Zaw and Ms. YeJin Jeong helped with the animal study; Dr. Evelyn Yim supervised the study.

Abstract

Vascular disease remains the leading cause of death globally. Bypass grafting is one of the common surgical interventions to restore the blood flow. Autologous grafts, especially internal thoracic arteries and saphenous veins are the gold standard bypass grafts, but the source can be limited. Synthetic grafts have been extensively developed as alternatives to autografts. Despite the progresses in the past decades, complications, such as thrombosis and intimal hyperplasia formation, persist in synthetic small diameter vascular grafts (<6 mm), leading to their fast occlusion. Polyvinyl alcohol (PVA) is a biocompatible material that has been extensively studied for various biomedical applications. PVA hydrogels prepared by a food grade crosslinker, sodium trimetaphosphate (STMP), were shown to have the potential to for use as small diameter vascular grafts due to its low thrombogenicity and tunable mechanical properties. However, PVA does not support endothelialization due to the lack of cell attaching sites and its hydrophilic nature. Endothelialization on synthetic surface is believed to be crucial to prevent thrombus and intimal hyperplasia formation, and thus affecting the long-term patency. Various approaches including biochemical and biophysical modifications can be employed to improve endothelial cell responses. In this thesis, it is hypothesized that the combination of biochemical and biophysical cues can enhance endothelialization on PVA and therefore improving the patency of PVA vascular grafts. The thesis was set out to investigate the effects of a bioactive sulfated polysaccharide and topographies on endothelial cell responses and develop modification methods to improve endothelialization on PVA hydrogels for small diameter vascular graft application.

Fucoidan is a sulfated polysaccharide, isolated mainly from brown seaweeds. It has been known to have multiple bioactivities, including anticoagulant and antithrombotic, anticancer, and anti-inflammatory activities. In the first part of the thesis, we assessed the effect of fucoidan molecule on hemocompatibility and endothelial cell adhesion. Fucoidan was mixed into PVA solution and co-crosslinked by STMP. The endothelialization and hemocompatibility of fucoidan modified hydrogels were evaluated *in vitro*, *ex vivo* and *in vivo*. The results demonstrated that fucoidan improved endothelial cell adhesion on PVA both *in vitro* and *in vivo* without affecting the mechanical properties of PVA. Additionally, *in vitro* and *ex vivo* hemocompatibility tests showed that modified PVA-fucoidan hydrogels maintained good hemocompatibility with minimal platelet adhesion and activation and low thrombin generation. The results suggest that fucoidan is a promising molecule that can be used to improve endothelialization without sacrificing hemocompatibility.

Cells are surrounded by a complex microenvironment with geometrically defined structures *in vivo*. The extracellular environment provided three-dimensional (3D) physical cues in micron and sub-micron scale, that plays an essential role in diverse cell processes. Many studies have demonstrated that micro- and nano-topographies can be used to mimic the natural extracellular environment and thus regulate cell processes and behaviors. PVA hydrogels can be topographically patterned using casting methods. However, topography alone on PVA is not sufficient to support endothelial cell adhesion. In the second part of the thesis, we developed a fucoidan conjugation method that is compatible with topographical patterning. The conjugation was achieved through carbonyldiimidazole (CDI) reaction, and fucoidan was aminated using ethylenediamine (EDA) to facilitate the conjugation. This fucoidan conjugation method improved endothelialization on PVA significantly without affecting the mechanical properties of PVA. It also yielded a surface that has a significantly lower thrombogenicity compared to PVA modified by other fucoidan modification methods. Additionally, this conjugation method can be applied to other material, such as expanded polytetrafluoroethylene (ePTFE), which is the typical material for synthetic vascular grafts. The results in this section showed that the fucoidan can be chemically conjugated on synthetic surfaces to improve endothelial cell responses. More importantly, the study suggested that the methods to present fucoidan on the surfaces can significantly alter the surface chemistry and the bioactivities for endothelial cell responses and hemocompatibility.

In the last part of the thesis, PVA hydrogels was modified with fucoidan and topographies of various dimensions. The synergistic effect of fucoidan and topographies on endothelial cell adhesion and functions as well as hemocompatibility were evaluated. The results showed that the topographies on PVA-fucoidan hydrogels could affect endothelial cell adhesion, monolayer formation, and function, while not affecting the hemocompatibility significantly. Among 6 isotropic and anisotropic topographical patterns evaluated, the 2 μm grating appeared to be the most promising topography and was used for *in vivo* studies. The *in vivo* results showed a significantly improvement on the blood flow in the fucoidan-conjugated PVA grafts and fucoidan-conjugated PVA grafts with 2 μm grating. Furthermore, the luminal endothelialization on PVA small vascular grafts was achieved by fucoidan and 2 μm grating modification. Finally, we investigated the potential mechanism underlying the improvement on endothelialization by the modification with fucoidan and topography. The results indicated that fucoidan may function similarly as extracellular matrix (ECM) proteins. Fucoidan provides binding ligands for integrins, β_1, α_2, α_5, α_6, and $\alpha_v\beta_5$, that are actively involved in endothelial cell adhesion to ECM proteins. Vascular endothelial cells formed similar number and size of focal adhesions on fucoidan compared to those on gelatin, although size of focal adhesions was smaller

compared to those on laminin. Topographies further affected focal adhesion size and alignment, and 2 μm grating promoted cell migration.

Overall, this thesis has demonstrated the hypothesis of presenting a sulfated polysaccharide and topography as luminal modification to improve performance of PVA small diameter vascular graft. The findings of the research work suggest that both fucoidan and topographical cues can benefit the endothelial cell adhesion and regeneration of endothelial monolayer both *in vitro* and *in vivo*, and thus are promising modification strategies for blood contact materials and vascular devices.

Acknowledgements

Foremost, I would like to express my deepest gratitude to my supervisor Prof. Evelyn Yim for her constant support and encouragement throughout my four-year PhD program. I appreciate that she is always there to provide her guidance and suggestions for the project. Her insight and knowledge in this field have steered me through this research.

I would also like to acknowledge our collaborators Dr. Deirdre Anderson and Dr. Monica Hinds from Oregon Health & Science University. They not only helped with our *ex vivo* shunt experiments, but also provided insightful feedback and suggestions to carry the research forward. I would also like to thank Prof Boxin Zhao for sharing the equipment in his lab. I would like to thank Prof. Alfred Yu, Dr. Adrian Chee, Dr. Billy Yiu, and Mr Richard Shangguan for their help with the ultrasound imaging.

Many thanks to all my lab-mates at Regenerative Nanomedicine Lab for sharing their experiences, the scientific discussion, their timely help and their suggestions for my projects. I would also like to thank all the co-op students that I have mentored for their help with my experiments.

I would like to give my special thanks to everyone in our animal research team. The animal study would have been impossible to accomplish without their support and help, especially during the pandemic time. Many thanks to Ms. Jean Flanagan and Ms. Angela Wagler from the Central Animal Facility, for supporting our animal surgeries and taking care of our animals. I'm grateful to our surgeon Dr. Filip Konecny, who has always been professional, open to discussions and supportive for our projects. Many thanks to my colleague Dr. Aung Moe Zaw and Ms. YeJin Jeong. I'm truly grateful to their support and the huge efforts they have spent in the animal surgeries and in the post-surgery animal care. I would also like to thank Ms. Sabrina Mattiassi, my former colleague Ms. Grace Pohan, and everyone else who have helped with the surgery and the animal care.

I would like to thank my parents, who have always given me the freedom to choose the path that I like. I appreciate their unwavering support and trust in me. I thank my boyfriend for being there whenever I need help and thank him for cheering me up during the difficult times.

Lastly, I would like to thank National Institutes of Health and NSERC-CREATE program at University of Waterloo for funding of my research.

Table of Contents

Examining Committee Membership ii
Author's Declaration iii
Statement of Contributions iv
Abstract vi
Acknowledgements ix
List of Figures xiv
List of Tables xxiii
List of Publications xxiv
Chapter 1 Introduction 1
1.1 Background 1
1.2 Hypotheses and objectives 2
1.3 Research contributions 4
1.4 Organization of the thesis 5
Chapter 2 Literature Review 6
2.1 Vascular system and vascular disease 6
2.1.1 Vascular system 6
2.1.2 Pathogenesis of vascular disease 8
2.2 Vascular graft as surgical intervention for cardiovascular diseases 10
2.2.1 Autologous graft 10
2.2.2 Synthetic vascular graft 11
2.2.3 Failure of small diameter vascular graft 11
2.3 Efforts to improve performance of small diameter vascular grafts 13
2.3.1 Surface modification 13
2.3.2 Tissue engineered small diameter vascular graft 17
2.4 Polyvinyl alcohol (PVA) hydrogels 20
2.4.1 Crosslinking of PVA 20
2.4.2 STMP-PVA small diameter vascular graft 20
2.4.3 Endothelialization of PVA 22
2.5 Fucoidan as a bioactive molecule 23
2.5.1 Anticoagulant and antithrombotic activities 24
2.5.2 Anti-inflammatory activities 27

2.5.3 Directing vascular cell behaviors 29
2.6 Topographical cues for improved cell responses 31
2.6.1 Topographical cues on hydrogels 31
2.6.2 Topographical cues for improved endothelial cell responses 35
2.7 Summary 36
Chapter 3 Effect of Fucoidan on Endothelial Cell Adhesion and Hemocompatibility of PVA 38
3.1 Introduction 38
3.2 Materials and methods 40
3.2.1 Preparation of PVA hydrogels 40
3.2.2 Sterilization of PVA hydrogels 40
3.2.3 Scanning electron microscope (SEM) measurement 40
3.2.4 Static water contact angle (WCA) measurement 40
3.2.5 Fucoidan concentration determination 41
3.2.6 Crosslinking density measurement 41
3.2.7 Water content measurement 42
3.2.8 Mechanical property test 42
3.2.9 Endothelial cell adhesion and function assay 42
3.2.10 *In vitro* hemocompatibility test 43
3.2.11 *Ex vivo* shunt assay 43
3.2.12 Implantation of fucoidan modified small diameter vascular grafts 44
3.2.13 Statistics 45
3.3 Results 46
3.3.1 Characterization of fucoidan modified PVA hydrogels 46
3.3.2 Biomechanical properties of fucoidan modified PVA hydrogels 48
3.3.3 Endothelial cell adhesion on fucoidan modified PVA hydrogels 49
3.3.4 *In vitro* hemocompatibility of fucoidan modified PVA hydrogels 51
3.3.5 Gamma sterilization of fucoidan modified PVA hydrogels 52
3.3.6 *Ex-vivo* shunt study of fucoidan-modified PVA grafts 55
3.3.7 *In-vivo* study of fucoidan modified PVA small diameter vascular graft 56
3.4 Discussion 61
3.5 Conclusions 68

Chapter 4 Development and Optimization of Fucoidan Conjugation for Enhanced Endothelial Attachment and Hemocompatibility **70**
4.1 Introduction 70
4.2 Materials and methods 71
4.2.1 Preparation of PVA hydrogels 71
4.2.2 Amination of fucoidan 72
4.2.3 Modification of PVA hydrogels with fucoidan 72
4.2.4 Toluidine blue staining 73
4.2.5 X-ray photoelectron spectroscopy (XPS) measurement 73
4.2.6 Water contact angle measurement 73
4.2.7 Mechanical property test 73
4.2.8 Sterilization treatment 73
4.2.9 Endothelial cell adhesion assays 74
4.2.10 *In vitro* hemocompatibility test 74
4.2.11 Ex-vivo hemocompatibility test 74
4.2.12 Fucoidan modification on ePTFE 74
4.2.13 Implantation of ePTFE vascular graft 75
4.2.14 Statistics 75
4.3 Results 75
4.3.1 Comparison of fucoidan conjugation with other fucoidan modification methods 75
4.3.2 Characterization of aminated fucoidan-conjugated PVA hydrogel with various preparation methods 85
4.3.3 Optimization of fucoidan conjugation based on surface and biological characterization 88
4.3.4 Fucoidan conjugation on ePTFE 92
4.4 Discussion 96
4.5 Conclusion 99
Chapter 5 Combination of Fucoidan and Topographical Modification for Small Diameter Vascular Graft Application **101**
5.1 Introduction 101
5.2 Materials and methods 103
5.2.1 Fabrication of patterned PVA hydrogels 103
5.2.2 Fucoidan conjugation on unpatterned and patterned PVA hydrogels 103

5.2.3 Scanning electron microscope (SEM) measurement 103
5.2.4 Water contact angle measurement 103
5.2.5 Sterilization of PVA vascular grafts 103
5.2.6 Endothelial cell adhesion and function assays 103
5.2.7 Monocyte adhesion assay 104
5.2.8 Gelatin and laminin conjugation on PVA 104
5.2.9 Focal adhesion and integrin staining 104
5.2.10 Wound healing assay 105
5.2.11 *In vitro* hemocompatibility test 105
5.2.12 Implantation of PVA small diameter vascular graft 105
5.2.13 Statistics 106
5.3 Results 106
5.3.1 Surface characterization of unpatterned and patterned PVA-CDI-aF 106
5.3.2 *In vitro* hemocompatibility of unpatterned and patterned PVA-CDI-aF 107
5.3.3 Endothelial cell adhesion and function 109
5.3.4 *In vivo* performance of PVA small diameter vascular graft with fucoidan and topography modification 111
5.3.5 Endothelialization was improved through integrin and focal adhesion formation 116
5.4 Discussion 122
5.5 Conclusion 126
Chapter 6 Conclusions and Recommendations 127
6.1 Conclusions 127
6.2 Recommendations 128
6.2.1 Effect of modification on smooth muscle cells and inflammatory responses 128
6.2.2 The role of mechanical properties 129
6.2.3 Purification of fucoidan 129
List of Copyright Permissions 131
Bibliography 137

List of Figures

Figure 2-1 The structure of blood vessels 7
Figure 2-2 Pathogenesis of atherosclerosis [35]. Copyright © 2017, Nature Publishing Group. 8
Figure 2-3. Fucoidan structure with mono-(1-3)-α-$_L$-fucopyranose backbone and repeated (1-3)- and (1-4)-α-$_L$-fucopyranose backbone 23
Figure 2-4. Coagulation pathways and the role of fucoidan. Fucoidan exhibits anticoagulant activity by inhibiting FXa formation in the intrinsic pathway [194, 195, 198]. Fucoidan improves the activity of heparin cofactor II and antithrombin III in inactivating thrombin by binding to antithrombin III and heparin cofactor II [199-201]. Fucoidan inhibits fibrinogen-thrombin reaction by binding to the thrombin attacking site in fibrinogen [202, 203]. Fucoidan also promotes fibrinolytic effect by simulating t-PA catalyzed plasminogen activation [204, 205]. 25
Figure 2-5. Three complement activation pathways and the role of fucoidan in complement activation. Fucoidan inhibits complement activation through the classical pathway by preventing active C1 formation, inhibiting C4 activity by forming a complex with C4, and preventing the binding of C4b and C2a [216, 220]. Fucoidan also inhibits complement activation through the alternative pathway by preventing the binding of factor B to C3b [216]. 28
Figure 3-1. Absorbance of Toluidine blue staining at 631 nm with different concentration of free fucoidan solution. 41
Figure 3-2. (A) Schematic diagram of polyvinyl alcohol-fucoidan (PVA-F) preparation procedure. (B) Scanning electron microscopy (SEM) images showed the structures on PVA (left) and PVA-F (right) surfaces. (C) Static water contact angle of PVA and PVA-F surfaces. (n=6, p=0.0554). (D) Fucoidan density on PVA-F samples was determined by toluidine blue staining. (E) Stability of fucoidan modification was determined by toluidine blue staining at day 0, 15, 30 and 60. n=3, no significant decrease was observed. (F) EDX spectrum of PVA-F samples showed sulfur element, confirming the presence of fucoidan. The table shows the atomic percentage of carbo, oxygen, sodium and sulfur and SD (n=3). 47
Figure 3-3. Mechanical properties of PVA and PVA-F samples. (A) Crosslinking density of PVA-F samples is significantly higher than PVA samples (n=5). (B) Water content of PVA and PVA-F hydrogels (n=3). (C) Compliance of PVA and PVA-F samples (n=3). (D) Burst pressure of PVA and PVA-F samples (n=5). (E) Longitudinal tensile Young's modulus of PVA and PVA-F samples (n=3). (F) Circumferential tensile Young's modulus of PVA and PVA-F samples (n=3). * denotes statistical significance using t-test with $p < 0.05$, n=3 48

Figure 3-4. Endothelial cell adhesion on PVA and PVA-F samples. (A) Representative fluorescence images of human umbilical vein endothelial cells (HUVECs) on PVA and PVA-F samples after 48 hr culture. Scale bar = 50 μm. (B) Average cell density on PVA and PVA-F samples. **** denotes statistical significance using one-way ANOVA with $p < 0.0001$, n=5. (C) CD31, VE-cadherin and eNOS expression of HUVEC monolayer on PVA-F samples (data normalized to glass). HUVECs on glass cover slip were included in analysis as a positive control. HUVECs on PVA samples were not taken into analysis. * denotes statistical significance using t-test with $p < 0.05$, n=5. (D) Representative fluorescence images of collagen type IV (COL IV) and laminin (LM) deposited by HUVECs on PVA and PVA-F samples after 24 hr culture samples (data normalized to glass). HUVECs on glass cover slip were included in analysis as a positive control. Scale bar = 50 μm. (E) Collagen type IV and laminin expression of HUVECs on PVA-F samples (data normalized to glass). HUVECs on PVA samples were not taken into analysis due to low cell number. No statistical significance was observed, n=3. 50
Figure 3-5. Representative images of human umbilical vein endothelial cells (HUVECs) on glass coverslips, PVA and PVA-F samples at a high magnification. (Scale bar =50 μm)..... 51
Figure 3-6. *In vitro* hemocompatibility tests of PVA and PVA-F samples. (A) Platelet adhesion and morphology on collagen coated glass cover (positive control), ePTFE (clinical control, platelets are as indicated with arrows), PVA and PVA-F. (B) Quantification of platelet adhesion determined by lactate dehydrogenase (LDH) assay. (C) Real-time thrombin generation assay. Lag-time (D) represents the time taken to start forming thrombin. Peak (E) represents the maximum thrombin generation rate. (F) represents endogenous thrombin potential (ETP). n=5, *, **and *** indicate a significant difference using one-way ANOVA with $p < 0.05$, $p < 0.01$, and $p < 0.001$, respectively. 52
Figure 3-7. Compliance (A), burst pressure (B), and water contact angle (C) of PVA and PVA-F samples with and without gamma sterilization. No significant difference was observed among all groups of samples. 53
Figure 3-8. Representative images of HUVECs on non-gamma treated PVA-F and gamma sterilized (PVA-Fg) samples. Glass coverslips were included as positive control. (Scale bar =50 μm). 54
Figure 3-9. Gamma sterilization effect on PVA-F samples. (A) Average cell density on PVA-F samples non-treated (PVA-F) and gamma sterilized (PVA-Fg). CD31 (B) and eNOS (C) expression of HUVECs on before and after gamma sterilized PVA-F sample (data normalized to glass). n=5, * and ** denotes statistical significance using one-way ANOVA with $p < 0.05$ and $p < 0.01$, respectively. Lagtime (D), Peak (E) and ETP (F) of real-time thrombin generation on non-treated and gamma sterilized samples (n=3). 54

Figure 3-10. *Ex-vivo* shunt study. Platelet accumulation (A), fibrin accumulation (B) and average luminal patent area (C) data are displayed as mean ± SD for all samples. Collagen and ePTFE controls are shown for comparison but were not included in the statistical comparison due to low sample size. No significant differences were observed between the various PVA samples for the platelet (p=0.0523), fibrin (p=0.201 for the 1-way ANOVA), or patent area (p=0.109 for the 1-way ANOVA) data. 56
Figure 3-11. Implantation of PVA-based small vascular graft (2 mm in diameter and 2 cm in length) in rabbit right common carotid artery model with end-to-side anastomosis. 57
Figure 3-12. Implantation of ePTFE, PVAg, and PVA-Fg grafts. (A) Dimensions of implanted grafts. (B) Patency rate of ePTFE (n=4), PVAg (N=5), and PVA-Fg (n=5). (C) Representative images of ePTFE graft, PVAg graft, and PVA-Fg graft after implantation. Scale bar=1cm. (D) Ultrasound images of PVAg, PVA-Fg and ePTFE grafts and corresponded arteries and peak systolic flow velocity inside the grafts and arteries after 14 days and 30 days implantation. (N.D. indicates not determined). (E) Peak systolic velocity (PSV) inside the grafts and arteries at day 14 and day 30. Non-detectable PSV was regarded as 0. 57
Figure 3-13. *In-vivo* endothelialization of PVA-Fg grafts. (A) Schematic diagram of sectioning positions of the grafts. (B) H&E staining of middle section of explanted vascular grafts. PVA-Fg showed a layer of cells on the luminal surfaces. Scale bar = 50 μm. (C) Immunofluorescence staining of the middle section of explanted vascular grafts. Arrows indicate luminal surfaces. Scale bar = 100 μm. CD31 positive signals in PVA-Fg samples indicated the presence of endothelial cells. (D) Immunofluorescence staining of the middle section of explanted vascular grafts. Arrows indicate luminal surfaces. Scale bar = 100 μm. The eNOS positive signals indicated that the endothelial cells inside PVA-Fg samples expressed eNOS proteins. 58
Figure 3-14. CD31 and DAPI staining showed endothelial cells at the proximal anastomoses (P) and distal anastomoses (D) and in the middle of the PVA-Fg graft (M). Arrows indicate luminal side of graft. (C) eNOS and DAPI staining showed the endothelial cells expressed eNOS. Arrows indicate luminal side of graft. Scale bar = 50μm. 59
Figure 3-15. Proximal and distal anastomotic stenosis of ePTFE, PVAg, and PVA-Fg grafts. (A) Representative H&E staining images of patent ePTFE, occluded ePTFE, PVAg, and PVA-Fg grafts. IH indicates intimal hyperplasia. (B) Stenosis percentage of ePTFE, PVAg, and PVA-Fg grafts at proximal anastomoses. (C) Stenosis percentage of ePTFE, PVAg, and PVA-Fg grafts at distal anastomoses. (Graft sections with missing pieces were not taken into calculation.) PVA-Fg grafts showed lower percentage of stenosis at both proximal and distal anastomosis than unmodified PVAg

grafts. (D) α-SMA staining of patent ePTFE, occluded ePTFE, PVAg and PVA-Fg grafts confirmed the presence of smooth muscle cells in the intimal hyperplasia. Scale bar=200 μm. (E) Ki67 staining of patent ePTFE, occluded ePTFE, PVAg and PVA-Fg grafts showed the presence of proliferating cells, but in a low density. Scale bar=50 μm. 60
Figure 3-16. Proposed crosslinking process of PVA and PVA-F hydrogels by sodium trimetaphosphate (STMP). 64
Figure 4-1. SEM images of unpatterned PVA-MF and PVA-MF with 2 μm gratings and 1.8 μ concave lenses. 76
Figure 4-2. Schematic diagram of preparation procedure of PVA-SF, PVA-CDI-F and PVA-CDI-aF. 76
Figure 4-3. Chemical structure of fucoidan (A) and ^{1}H NMR spectra of fucoidan, CDI-activated fucoidan and EDA aminated fucoidan (B and C). 77
Figure 4-4. X-ray photoelectron spectroscopy (XPS) survey scan of PVA, PVA-CDI, PVA-CDI-F, and PVA-CDI-aF. The table shows the atomic %age of carbon, nitrogen and oxygen and sulfur. SD (n = 3). N.D. = not detectable. 78
Figure 4-5. SEM images of unpatterned and 5 μm gratings PVA, PVA-MF, PVA-SF, PVA-CDI-F and PVA-CDI-aF. 79
Figure 4-6. Effect of fucoidan modification methods on the surface properties. (A) Water contact angle. N=4, * and ** indicate a significant difference using one-way ANOVA with $p < 0.05$ and $p < 0.01$, respectively. (B) Toluidine blue staining. N=3, * , **, *** and **** indicate a significant difference using one-way ANOVA with $p<0.05$, $p < 0.01$, $p < 0.005$ and $p < 0.0005$, respectively. 80
Figure 4-7. Compliance (A) and burst pressure (B) of PVA, PVA-SF, PVA-CDI-F and PVA-CDI-aF grafts. N=3, no significant difference was observed. 81
Figure 4-8. Endothelialization on fucoidan modified PVA with different modification methods. (A) Representative live/dead staining of cells on PVA and fucoidan modified PVA samples. Scale bar = 200 μm. (B) Endothelial cell monolayer formation on PVA and fucoidan modified PVA. Representative immunofluorescent images of endothelial cells on PVA and fucoidan modified PVA. Scale bar = 50 μm. Blue denotes nuclei, green denotes VE-cadherin and red denotes CD31. Cell viability (C), cell density (D) and VE-cadherin and CD31 expression (E) of endothelial cells on PVA and fucoidan modified PVA. N=6, *, **, *** and **** indicate a significant difference using one-way ANOVA with $p < 0.05$, $p < 0.01$, $p < 0.005$ and $p < 0.0005$, respectively. 82

Figure 4-9. *In vitro* hemocompatibility of fucoidan modified PVA. (A) Representative SEM images of platelets on PVA and fucoidan modified PVA. (B) Quantification of platelet adhesion determined by lactate dehydrogenase (LDH) assay. (C) (D) and (E) Realtime thrombin generation. Lag-time (C) represents the time taken to start forming thrombin. Peak (D) represents the maximum thrombin generation rate. ETP (E) represents endogenous thrombin potential. n=5, *, ** and **** indicate a significant difference using one-way ANOVA with $p < 0.05$, $p < 0.01$ and $p < 0.0005$, respectively. 83
Figure 4-10. *Ex vivo* hemocompatibility of plain PVA and fucoidan modified PVA vascular graft. Platelet accumulation (A), fibrin accumulation (B) and average luminal patent area (C) data are displayed as mean ± SD for all samples. Collagen–coated ePTFE, (n=2), ePTFE (n=2), PVA (n=2) and fucoidan modified PVA (n=6) grafts were tested. Statistical analysis was performed using a one-way ANOVA with Tukey's HSD *post hoc* testing ($p < 0.001$). * indicates statistical significance. (D) Three-dimensional surface volume renderings of microCT cross-sectional ROI selections showing thrombi in the lumen of tested samples. 85
Figure 4-11. Comparison of amination methods. (A) Amine quantification of fucoidan aminated by EDA and borane reduction reaction. N=3, ** indicates a significant difference using unpaired t test with $p < 0.01$. (B)(C)(D) Hemocompatibility of PVA modified by aminated fucoidan using different amination methods. N=2, * indicates a significant difference using unpaired t test with $p < 0.05$..... 86
Figure 4-12. Comparison of fucoidan from *Fucus vesiculosus* and *Undaria pinnatifida.* (A) Endothelialization on PVA-CDI-aF_{fv} and PVA-CDI-aF_{up}. Scale bar = 200 μm. Blue denotes nuclei, and red denotes F-actin. N=3, *, *** and **** indicate a significant difference using one-way ANOVA with $p < 0.05$, $p < 0.005$ and $p < 0.0005$, respectively. (B) Thrombin generation on PVA-CDI-aF_{fv} and PVA-CDI-aF_{up}. N=2, no statistical significance was observed. 87
Figure 4-13. Effect of terminal sterilization methods on endothelial cell adhesion and thrombin generation of PVA-CDI-aF. (A) Representative immunofluorescence staining images of HUVECs on PVA-CDI-aF sterilized by different methods. Scale bar = 200 μm. Blue denotes nuclei, and red denotes F-actin. (B) Cell density on PVA and PVA-CDI-aF samples with different sterilization methods. N=3, **** indicate a significant difference using two-way ANOVA with $p < 0.0005$. (C)(D)(E) Thrombin generation on PVA and PVA-CDI-aF samples with different sterilization methods. N=3, ** indicate a significant difference using two-way ANOVA with $p < 0.01$ 88
Figure 4-14. Preparation of aminated fucoidan with different EDA ratio. (A) Preparation of aminated fucoidan (aF) using different concentration of ethylenediamine (EDA). (B) Quantification of amine

groups on aminated fucoidan. N=3, *, **, *** and **** indicate a significant difference using one-way ANOVA with $p < 0.05$, $p < 0.01$, $p < 0.005$ and $p < 0.0005$, respectively. 89
Figure 4-15. Effect of EDA ratio on the surface properties of PVA-CDI-aF samples. (A) Water contact angle of PVA-CDI-aF. N=4, * and ** indicate a significant difference using one-way ANOVA with $p < 0.05$ and $p < 0.01$, respectively. (B) Toluidine blue staining of PVA-CDI-aF. N=3, * indicates a significant difference using one-way ANOVA with $p < 0.05$. 89
Figure 4-16. Effect of EDA ratio on endothelial cell adhesion on PVA with aminated fucoidan (PVA-CDI-aF)**.** (A) Representative live/dead staining images of HUVECs on PVA-CDI-aF. Scale bar = 200 μm. (B) Representative immunofluorescent images of HCAECs on PVA-CDI-aF. Scale bar = 100 μm. Blue denotes nuclei, green denotes VE-cadherin and red denotes F-actin. Cell viability (C) and density (D) of endothelial cells on PVA with aminated fucoidan. N=3, *, **, *** and **** indicate a significant difference using one-way ANOVA with $p < 0.05$, $p < 0.01$, $p < 0.005$ and $p < 0.0005$, respectively. 90
Figure 4-17. Effect of EDA ratio on hemocompatibility of PVA with aminated fucoidan (PVA-CDI-aF). (A) Representative SEM images of platelets on PVA-CDI-aF samples. Scale bar = 10 μm. (B) Quantification of platelet adhesion determined by lactate dehydrogenase (LDH) assay. (C) (D) and (E) Realtime thrombin generation. N=4, * and ** indicate a significant difference using one-way ANOVA with $p < 0.05$ and $p < 0.01$, respectively. 91
Figure 4-18. Characterization and cell adhesion on fucoidan conjugated ePTFE. (A) Toluidine blue staining of ePTFE and fucoidan modified ePTFE. (B) Representative live/dead staining images of HUVECs on ePTFE and fucoidan modified ePTFE. Scale bar = 200 μm. (C) Cell density of endothelial cells on ePTFE and fucoidan modified ePTFE. N=3, **, *** and **** indicate a significant difference using one-way ANOVA with $p < 0.01$, $p < 0.005$ and $p < 0.0005$, respectively. 93
Figure 4-19. *In vitro* hemocompatibility of fucoidan modified ePTFE. (A) Representative SEM images of platelets on collagen coated glass, ePTFE and ePTFE-plas-NaOH-aF. Scale bar = 10 μm. (B) Quantification of platelet adhesion determined by lactate dehydrogenase (LDH) assay. (C) (D) and (E) Realtime thrombin generation. Lag-time (C) represents the time taken to start forming thrombin. Peak (D) represents the maximum thrombin generation rate. ETP (E) represents endogenous thrombin potential. n=3, * indicates a significant difference using one-way ANOVA with $p < 0.05$..... 94
Figure 4-20. *In vivo* study of fucoidan modified ePTFE graft. (A) Blood flow inside the fucoidan modified ePTFE graft at week 1, week 2, and week 4 detected by ultrasound imaging. (B) Cell attachment in the luminal surfaces of fucoidan modified ePTFE grafts. Scale bar = 50 μm. (C)

Representative immunofluorescent images of cells in the lumen of fucoidan modified ePTFE graft. Scale bar = 200 μm. 95
Figure 5-1. Surface characterization of unpatterned and patterned PVA-CDI-aF. (A) SEM images of unpatterned and patterned PVA-CDI-aF. (B) Water contact angel of plain PVA (unmodified and unpatterned), unpatterned and patterned PVA-CDI-aF. n=3, * and ** indicate a significant difference using one-way ANOVA with $p < 0.05$ and $p < 0.01$, respectively. 107
Figure 5-2. *In vitro* hemocompatibility of unpatterned and patterned PVA-CDI-aF. (A) Representative SEM images of platelets on unpatterned and patterned PVA-CDI-aF. (B) Quantification of platelet adhesion determined by lactate dehydrogenase (LDH) assay. (C-E) Realtime thrombin generation. Lag-time (C) represents the time taken to start forming thrombin. Peak (D) represents the maximum thrombin generation rate. ETP (F) represents endogenous thrombin potential. N=4, * and *** indicate a significant difference using one-way ANOVA with $p < 0.05$ and $p < 0.005$, respectively, n.s. indicates no significance was seen between plain PVA and PVA-CDI-aF samples. 108
Figure 5-3. Endothelialization on unpatterned and patterned PVA-CDI-aF. (A) Representative immunofluorescent images of endothelial cells plain PVA, unpatterned, and patterned PVA-CDI-aF. Scale bar = 50 μm. Blue denotes nuclei, green denotes VE-cadherin and orange denotes F-actin. Cell density (B), average cell area (C), VE-cadherin expression (D) and cell circularity (E) of endothelial cells on unpatterned and patterned PVA-CDI-aF. N=6, **, *** and **** indicate a significant difference using one-way ANOVA with $p < 0.01$, $p < 0.005$, and $p < 0.0005$, respectively. 110
Figure 5-4. Monocyte adhesion on endothelial cells on unpatterned and patterned PVA-CDI-aF. (A) Representative immunofluorescent images of monocytes and endothelial cells on unpatterned and patterned PVA-CDI-aF. Scale bar = 100 μm. Blue denotes nuclei, green denotes monocytes and orange denotes CD31. (B) Monocyte density on unpatterned and patterned PVA-CDI-aF. N=6, * and ** indicate a significant difference using one-way ANOVA with $p < 0.05$ and $p < 0.01$, respectively. (C) CD31 expression of endothelial cells on unpatterned and patterned PVA-CDI-aF. N=6, no statistical significance was observed. 111
Figure 5-5. Ultrasound imaging of blood flow inside unmodified and modified PVA grafts. (A) Representative ultrasound images of blood flow inside the grafts before surgery, 2 weeks after surgery and 4 weeks after surgery. Flow velocity inside the grafts at midpoint (2 weeks) (B) and at endpoint (after 4-week). UP indicates unpatterned grafts, and 2μG indicates grafts with 2 μm gratings. No statistical significance was observed. 112

Figure 5-6. *In vivo* endothelialization of PVA small diameter grafts after 4 weeks of implantation. (A) Representative immunofluorescent images of endothelial cells in the lumen of PVA grafts. Scale = 100 μm. Blue denotes nuclei, green denotes VE-cadherin, and orange denotes CD31. (B) Schematic diagram of the sample location. (C) Percentage of grafts that have higher than 50% endothelial cell coverage at each position. (D) Endothelial coverage percentage of patent grafts. N=3 for plain PVA and UP PVA-CDI-aF, n=4 for 2μG PVA-CDI-aF. *, *** and **** indicate a significant difference using two-way ANOVA with $p < 0.05$, $p < 0.005$, and $p < 0.0005$, respectively. 113
Figure 5-7. Stenosis at the anastomoses of the explanted grafts. (A) Representative hematoxylin and eosin (H&E) images of proximal and distal anastomoses and stenosis percentage. Scale = 500 μm. (B) Stenosis percentage at proximal and distal anastomoses. N=4 for plain PVA and UP PVA-CDI-aF, n=5 for 2μG PVA-CDI-aF, no significance was observed. 114
Figure 5-8. Composition of intimal hyperplasia (IH) in proximal and distal anastomoses of grafts. (A) Representative Masson's trichrome staining images of the stenosis in proximal and distal anastomoses of plain PVA, unpatterned PVA-CDI-aF and PVA-CDI-aF grafts with 2 μm gratings. Scale = 500 μm. Blue denotes collagen and red denotes muscle fibers. (B) Percentage of the area collagen and muscle fiber to the area of total IH in the stenosis. P and D indicated the percentage at the proximal and distal anastomosis, respectively. N=4 for plain PVA and UP PVA-CDI-aF, n=5 for 2μG PVA-CDI-aF. No significance was observed. 115
Figure 5-9. Integrin formation by HUVECs on fucoidan. (A) Representative images of integrin subunits β_1, α_2, α_5, α_6, and integrin $\alpha_v\beta_5$ formed by endothelial cells on PVA-CDI-aF. Scale bar = 30 μm. Inset shows magnified view (scale bar = 5 μm). (B) Staining of integrin $\alpha_M\beta_2$ did not show positive signals. Scale bar = 30 μm. 117
Figure 5-10. Comparison of focal adhesion formation by HUVECs on fucoidan, laminin and gelatin. (A) Representative images of focal adhesions formed by endothelial cells on unmodified PVA, fucoidan conjugated PVA (PVA-CDI-aF), laminin-conjugated PVA (PVA-CDI-LMN) and gelatin conjugated PVA (PVA-CDI-GEL). Blue denotes nuclei, green denotes F-actin and orange denotes vinculin. Scale bar = 30 μm. Inset shows magnified view (scale bar = 5 μm). Number of focal adhesions per cell (B), average focal adhesion size (C) and total area of focal adhesions per cell (D) on unpatterned and patterned PVA-CDI-aF. N=6, *, ** and *** indicate a significant difference using one-way ANOVA with $p < 0.05$, $p < 0.01$ and $p < 0.005$, respectively. 119
Figure 5-11. Focal adhesion formation by HUVECs on unpatterned and patterned PVA-CDI-aF. (A) Representative immunofluorescence images of focal adhesion formed by HUVECs on unpatterned and

patterned PVA-CDI-aF. Scale bar = 20 μm. Blue denotes nuclei, green denotes F-actin and orange denotes vinculin. Inset shows magnified view (scale bar = 5 μm). Number of focal adhesions per cell (B), average focal adhesion size (C) and total area of focal adhesions per cell (D) on unpatterned and patterned PVA-CDI-aF. N=6, *, **, *** and **** indicate a significant difference using one-way ANOVA with $p < 0.05$, $p < 0.01$, $p < 0.005$ and $p < 0.0005$, respectively. 120

Figure 5-12. Endothelial cell migration with a wound healing assay. Representative images of HUVECs on unpatterned PVA-CDI-aF and PVA-CDI-aF with 2 μm gratings at 0h, 24h, 48h, and 72h after the scratches were made. Scale bar = 200 μm. Arrow indicates the direction of the 2 μm gratings. N=4, * and ** indicate a significant difference using one-way ANOVA with $p < 0.05$ and $p < 0.01$, respectively. 121

List of Tables

Table 3-1. Parameters and mechanical properties of implanted ePTFE, PVAg, PVA-Fg grafts and rabbit common carotid arteries (Rb CCA). Human saphenous vein (SV) and internal thoracic artery (ITA) were included as clinical comparisons. 45

Table 5-1. Integrins form by ECs on extracellular matrix proteins. 117

List of Publications

Journal papers:

Yuan Yao, Aung Moe Zaw, Deirdre E.J. Anderson, Monica T. Hinds, Evelyn K.F. Yim. "Fucoidan functionalization on poly(vinyl alcohol) hydrogels for improved endothelialization and hemocompatibility". *Biomaterials,* 2020, 249, 120011. DOI: 10.1016/j.biomaterials.2020.120011.

Yuan Yao, Evelyn K.F. Yim. "Fucoidan for cardiovascular application and the factors mediating its activities". *Carbohydrate Polymers*, 270 (2021) 118347. DOI: 10.1016/j.carbpol.2021.118347

Marek Kukumberg[†], **Yuan Yao**[†], Seok Hong Goh, Dawn J. H. Neo, Jia Yi Yao, and Evelyn K. F. Yim. "Evaluation of the topographical influence on the cellular behavior of human umbilical vein endothelial cells". *Advanced Biosystems*, 2018, 2, 1700217. DOI: 10.1002/adbi.201700217. ([†]authors contribute equally)

Linan Cui[†], **Yuan Yao**[†], Evelyn Yim. "The effects of surface topography modification on hydrogel properties". *APL Bioengineering*, 5 (2021) 031509. DOI: 10.1063/5.0046076 ([†]authors contribute equally).

YeJin Jeong, **Yuan Yao**, Tizazu H. Mekonnen and Evelyn K. F. Yim. "Changing compliance of poly(vinyl alcohol) tubular scaffold for vascular graft applications through modifying interlayer adhesion and crosslinking density". *Frontiers in materials*, 2020, 7, 595295. DOI: 10.3389/fmats.2020.595295

Muhammad Rizwan, **Yuan Yao**, Maud B. Gorbet, John W. Tse, Deirdre E. J. Anderson, Monica T. Hinds, and Evelyn K. F. Yim. "One-Pot Covalent Grafting of Gelatin on Poly(Vinyl Alcohol) Hydrogel to Enhance Endothelialization and Hemocompatibility for Synthetic Vascular Graft Applications". *ACS Applied. Bio Materials*. 2020, 3, 693−703. DOI: 10.1021/acsabm.9b01026

YeJin Jeong, **Yuan Yao**, and Evelyn K. F. Yim. "Current understanding of intimal hyperplasia and effect of compliance in synthetic small diameter vascular grafts". *Biomaterials Science*, 2020, 8, 4383–4395. DOI: 10.1039/d0bm00226g

Grace Pohan, Sabrina Mattiassi, **Yuan Yao**, Aung Moe Zaw, Deirdre E.J. Anderson, Marie F.A. Cutiongco, Monica T. Hinds, and Evelyn K.F. Yim. "Effect of Ethylene Oxide Sterilization on Polyvinyl Alcohol Hydrogel Compared with Gamma Radiation". *Tissue Engineering: Part A*, 26 (19-20), 1077-1090. DOI: 10.1089/ten.tea.2020.0002

Novella M. Bates, Heather E. Heidenreich, Meghan E. Fallon, **Yuan Yao**, Evelyn K. F. Yim, Monica T. Hinds and Deirdre E. J. Anderson. "Bioconjugation of a collagen-mimicking peptide onto poly(vinyl alcohol) encourages endothelialization while minimizing thrombosis". *Frontiers in Bioengineering and Biotechnology*, 8:621768. DOI: 10.3389/fbioe.2020.621768

Grace Pohan, Pascale Chevallier, Deirdre E. J. Anderson, John W. Tse, **Yuan Yao**, Matthew W. Hagen, Diego Mantovani, Monica T. Hinds and Evelyn K. F. Yim. "Luminal plasma treatment for small diameter polyvinyl alcohol tubular scaffolds". *Frontiers in Bioengineering and Biotechnology*, 7:117. doi: 10.3389/fbioe.2019.00117

Book chapters:

Yuan Yao, YeJin Jeong, Aung Moe Zaw, Marek Kukumberg, Evelyn K.F. Yim. "Rabbit Surgery Protocol for End-to-End and End-to-Side Vascular Graft Anastomosis". *Methods Molecular Biology*, Vol. 2375, Feng Zhao and KamW. Leong (Eds): Vascular Tissue Engineering, 978-1-0716-1707-6, 485275_1_En, (Chapter 15) (Accepted)

Aung Moe Zaw, Richard Shangguan, **Yuan Yao**, YeJin Jeong, Billy Y. S. Yiu, Adrian J. Y. Chee, Alfred C. H. Yu, Evelyn K. F. Yim. "Imaging in a small animal vascular blood flow with conventional ultrasound". *Methods Molecular Biology*, Vol. 2375, Feng Zhao and KamW. Leong (Eds): Vascular Tissue Engineering, 978-1-0716-1707-6, 485275_1_En, (Chapter 16) (Accepted)

Chapter 1
Introduction

1.1 Background

Cardiovascular disease remains the leading cause of death around the globe, accounting for more than 17.9 millions of death each year [1]. Atherosclerosis is recognized as one of the main pathogenesis of cardiovascular diseases. The progression of atherosclerosis narrows the lumen of a vessel, slows down the blood flow rate and eventually causes vessel blockage. Although the development of medications and percutaneous intervention reduces the requirement of surgical interventions in treating cardiovascular diseases, bypass surgeries are still required for severely affected patients to effectively restore blood perfusion. Autologous arteries or veins, such as internal thoracic arteries and saphenous veins from the patients, are common graft choices for replacing the damaged blood vessels or bypassing blocked vessels. However, the autologous grafts are not always available, which has inspired the exploration on prosthetic vascular grafts.

Synthetic bypass vascular grafts have been investigated to serve as alternatives to autologous grafts since last century. Commercially available synthetic grafts, such as expanded polytetrafluoroethylene (ePTFE) and polyethylene terephthalate (PET, better known as Dacron®) exhibit satisfactory long-term patency in large diameter (>6mm) [2]. However, when being applied to replace small diameter vessels, they occlude quickly due to acute thrombosis and intimal hyperplasia formation. Tissue engineered vascular grafts have also attracted broad research interests. Degradable prosthetic grafts, made of synthetic materials or natural materials, and decellularized vascular scaffolds from bovine have been commercialized and applied to clinical studies. However, in small diameter vessels, these grafts did not exhibit superior performance than conventional synthetic vascular grafts [3].

The low success rate of prosthetic and decellularized small diameter vascular grafts has been associated with multiple factors, such as inherent thrombogenicity [4] and inadequate endothelialization [5]. To this end, many researchers have investigated surface modification strategies to improve the surface hemocompatibility and endothelialization. Immobilization of extracellular matrix (ECM) proteins [6], peptides [7], and growth factors [8] on synthetic surfaces has proven efficiency in promoting endothelial cell adhesion and proliferation. However, increasing endothelialization while maintaining a low thrombogenicity remains challenging. Mismatch in mechanical properties has been suggested to be another critical contributor to graft failure [9]. The

mismatched mechanical properties between a graft and its adjacent native artery induces blood flow turbulence and disturbed fluid shear stress, which contribute to the formation of intimal hyperplasia [10]. Polyvinyl alcohol (PVA) is a biocompatible and FDA approved material. PVA hydrogels prepared by sodium trimetaphosphate have tunable mechanical properties that could match the mechanical properties of native vessels. By using a dip casting method, small diameter tubular grafts with sufficient mechanical strength can be easily fabricated [11]. However, the lack of endothelial cell adhesion limits the application of PVA vascular grafts. Driven by the drawbacks of the current synthetic vascular grafts and unmet need of a versatile modification strategy, this thesis aims to develop a surface modification method that is capable of enhancing both endothelialization and hemocompatibility to improve the performance of PVA small diameter vascular graft.

1.2 Hypotheses and objectives

Fucoidan is a sulfated polysaccharide with diverse biological functions. It plays an important role in hemostatic system, by interacting with coagulation factor Xa, inhibiting thrombin generation, and regulating platelet adhesion and activation [12]. The activity of fucoidan in mediating vascular cell behaviors has been demonstrated. Fucoidan exhibits endothelial protective function [13] and antiproliferative effect on smooth muscle cells [14] (see detailed review in chapte 2). These bioactivites suggest that fucoidan could be promising molecules for cardiovascular application.

Topographical cues have demonstrated a regulatory effect on endothelial adhesion and proliferation [15]. Grating and lens topographies have showed a promotion on endothelial cell attachment [16]. In native blood vessels, endothelial cells are exposed to fluid shear stress. Cells adapt to the shear stress and form an elongated and aligned morphology. This morphology has been reported to be beneficial for the anticoagulant and anti-atherogenic activities of endothelial cells. Surface topographies, more specifically anisotropic topographies, are capable of inducing aligned morphology of EC *in vitro* [17]. Our previous study showed that PVA hydrogels can be easily patterned using casting method or nanoimprinting methods. The patterns on PVA hydrogels have good fidelity and are stable in both dry and hydrated conditions.

These findings have led us to the hypothesis that luminal modification with fucoidan and topographical patterning could improve the patency and endothelialization of PVA vascular grafts. This can be divided into three sub-hypotheses:

1. Fucoidan could improve endothelial cell adhesion without sacrificing hemocompatibility of PVA hydrogels.
2. The method of presenting fucoidan on PVA could affect the surface properties and bioactivity of modified PVA hydrogels. Conjugation method that would preserve the fucoidan bioactivities could improve the endothelialization and hemocompatibility, without affecting the surface morphology, patterning and the graft mechanical properties.
3. Combination of fucoidan and topographical modification on PVA could promote the endothelialization of PVA small diameter vascular graft. Fucoidan could enhance vascular endothelial cells via integrin binding.

Based on the hypotheses, I have divided the project into three main aims:

1. Evaluate the effect of fucoidan molecule on endothelialization and hemocompatibility.

This aim will assess the change on endothelial cell adhesion and hemocompatibility of PVA caused by presenting fucoidan in PVA. Fucoidan was mixed into PVA solution and co-crosslinked to form a hydrogel. The endothelial cell adhesion on fucoidan modified hydrogel was tested. *In vitro* and *ex vivo* hemocompatibility test were done to assess the effect of fucoidan on the hemocompatibility. *In vivo* endothelialization was examined in a rabbit right common carotid artery model.

2. Develop and optimize of fucoidan conjugation method with surface characterization and biological assays.

This aim will address the need to develop a fucoidan conjugation method that is compatible with topographical patterning while presenting favorable biological functions. Native and aminated fucoidan were conjugated on PVA hydrogels. The effects of the modification method, amination reagents, sterilization, and the species of seaweeds that fucoidan was isolated were assessed with surface characterization and biological assays, including endothelial cell responses and hemocompatibility tests. The effect of the modification on mechanical properties of PVA hydrogels were examined. The possibility of conjugating fucoidan on other materials was examined with a conventional vascular graft material, such as ePTFE.

3. Examine the synergistic effect of fucoidan conjugation and topographical patterning on the performance of PVA hydrogels.

This aim evaluates the synergistic effects of PVA hydrogels modified by both fucoidan conjugation and topographical patterning. PVA hydrogels with micro-sized isotropic and anisotropic patterns were prepared, and subsequently modified with fucoidan through chemical conjugation. The cell adhesion, function, and hemocompatibility of fucoidan modified PVA with different topographies were examined. Topography that had best *in vitro* performance was selected for *in vivo* study. Small diameter vascular grafts of unmodified PVA, fucoidan conjugated PVA and fucoidan conjugated PVA with topographical patterns were implanted in rabbit right common carotid arteries to evaluate the *in vivo* performance. Furthermore, the mechanism of the modulation activity of fucoidan and topography on endothelial cells was studied by integrin and focal adhesion expression, and preliminary cell migration was accessed via a wound healing assay.

1.3 Research contributions

This PhD thesis is motivated by the need of both durable off-the-shelf available small diameter vascular grafts and an appropriate modification strategy to improve surface hemocompatibility and endothelialization. The research work done in this thesis will expand the knowledge by four major contributions. First, this work has demonstrated that fucoidan is a promising modification molecule for vascular graft. The presentation of fucoidan molecule on synthetic materials could improve endothelialization significantly without compromising the hemocompatibility. This could advance the application of fucoidan in cardiovascular field and contribute to the development of surface modification strategies for blood contact materials and vascular devices. Secondly, the fact that the bioactivities of fucoidan are dependent on molecular weight and structural features has been well accepted; however, the effects of immobilization method have not been explored. The findings from this work revealed that the different modification methods with fucoidan could cause drastic changes on the surface properties and the biological activities, which sheds light on the importance of selecting proper modification methods in the further application of fucoidan. Thirdly, this work demonstrated that the interaction of endothelial cells and fucoidan are through the formation of focal adhesion with integrins β_1, α_2, $\alpha_{5,}$ α_6, and $\alpha_v\beta_5$, and the topographies could further regulate the focal adhesion formation by endothelial cells on fucoidan. The topography also presented contact guidance to enhance cell migration. Lastly, this study presented a promising modification strategy with fucoidan and topography to improve endothelialization of PVA small diameter vascular grafts. This could benefit the application of PVA in vascular engineering, and the modification method could be applied to other synthetic materials for treating cardiovascular diseases.

1.4 Organization of the thesis

This thesis is composed of 6 chapters.

Chapter 1 presents an overview on the research background of the thesis project and introduces the thesis hypotheses, objectives and significance of the study.

Chapter 2 reviews the relevant literature including vascular biology, pathogenesis of cardiovascular diseases, development progresses of vascular grafts, PVA hydrogels, bioactivities of fucoidan and topographical cues on hydrogels for cell responses.

Chapter 3 describes the effects of fucoidan modification, by mixing fucoidan into PVA, on vascular endothelial cell adhesion and hemocompatibility of PVA.

Chapter 4 outlines the development and optimization of fucoidan conjugation methods based on surface characterization and biological assays.

Chapter 5 presents the synergistic effects of fucoidan conjugation and topographical patterning on endothelialization and performance of PVA small diameter vascular grafts.

Chapter 6 concludes the major findings of the thesis and provides recommendations for future directions to contribute the field of vascular engineering.

Chapter 2
Literature Review

Synthetic vascular grafts are commonly used in bypass surgeries to treat cardiovascular diseases. Currently available synthetic vascular grafts have high success rate when the diameter is larger than 6 mm, however, small diameter (< 6 mm) synthetic vascular grafts are subjected to fast occlusion. In this chapter, I will introduce the structure of vascular walls, pathogenesis of vascular disease and currently available vascular grafts. Further, progresses to improve the performance of synthetic small diameter vascular graft will be discussed. Polyvinyl alcohol (PVA) hydrogels will be introduced and their potential and limitations for use as small diameter vascular grafts will be focused. An introduction on fucoidan and topographical cues will be presented along with their potential uses in vascular graft application.

2.1 Vascular system and vascular disease

2.1.1 Vascular system

Vascular system transports oxygen and nutrients to organs and tissue and remove waste through different types of blood vessels, including arteries, veins and capillaries. Native blood vessels are comprised of three layers: tunica intima, tunica media and tunica externa (adventitia) (**Fig 2-1**). The tunica intima is the innermost layer formed by endothelium, a single layer of endothelial cells (ECs) , and an endothelial-specialized basement membrane, which contains laminin, collagen type IV, glycosaminoglycans and proteoglycans, such as heparan sulfate proteoglycans [18-20]. Vascular smooth muscle cells (SMCs), elastin tissue, and collagen formed the medial layer of native blood vessel walls. Externa, the outermost layer of native blood vessel, consists of collagen-rich extracellular matrix, loosely packed fibroblasts and a few quiescent resident inflammatory cells.

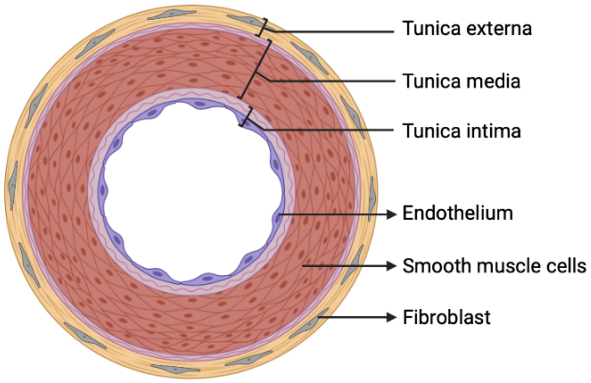


Figure 2-1 The structure of blood vessels

The endothelium in tunica intima is indispensable for normal vascular development and homeostasis. It serves as a non-thrombogenic barrier between blood and tissues and participates actively in maintaining homeostasis [21]. In mature and healthy blood vessels, ECs are in quiescent state. They secret various molecules, such as nitric oxide (NO) and prostacyclin (PGI_2) to prevent platelet aggregation [22]. Anticoagulant heparin-like glycosaminoglycans and thrombomodulin are present on the surfaces of ECs, which reduce blood coagulation by inactivating thrombin [23]. ECs also synthesize tissue factor pathway inhibitor and participate in fibrinolysis [24]. ECs are involved in inflammatory and immunological processes. Quiescent ECs do not interact with leukocytes. Upon activation by inflammatory stimuli, ECs change to pro-inflammatory phenotype and expressed adhesion molecules which mediate tethering of leukocytes to the surface of ECs [25].

In addition to the roles in coagulation system and inflammation, ECs also control the tone of SMCs by releasing vasoactive factors, such as NO and PGI_2, or vasoconstrictive factors such as thromboxane and endothelin-1 [26, 27]. SMCs are the major cells of tunic media. SMCs can sense the tensile stress of the blood vessel walls directly and react to shear stress indirectly through the interaction with ECs [28]. In normal blood vessel, SMCs are contractile, differentiated and quiescent, regulating blood vessel tone and blood flow through dynamic cell contraction and relaxation. Upon vessel injury or vascular interventional process, SMCs will change phenotype to a proliferating state and eventually migrate to intima, causing atherosclerosis, restenosis of vascular intervention and failure of vascular grafts.

The fibroblasts are abundant in the tunica externa. They are commonly regarded as supporting cells for the vessel structures. Research found out that fibroblasts could migrate from adventitia to intima

and form myofibroblasts [29-32]. Many studies have also evidenced the presence of progenitor cells and pericytes in the tunica externa [33]. Those cells have the ability to differentiate into ECs and SMCs [34].

2.1.2 Pathogenesis of vascular disease

Cardiovascular disease is the leading cause of mortality across the globe. Atherosclerosis is known to be the primary cause of various cardiovascular diseases, such as myocardial infarction and stroke. Atherosclerosis describes the buildup of plaque, containing cholesterol, calcium and waste products, inside the lining of the artery walls. The atherosclerotic plaque is exposed to pulsatile force from the blood stream and is vulnerable to rupture, resulting in thrombosis and vessel occlusion. Atherosclerosis progression involves endothelial dysfunction, smooth muscle cell proliferation, extracellular matrix accumulation and complex inflammation responses, as shown in **Fig 2-2**.

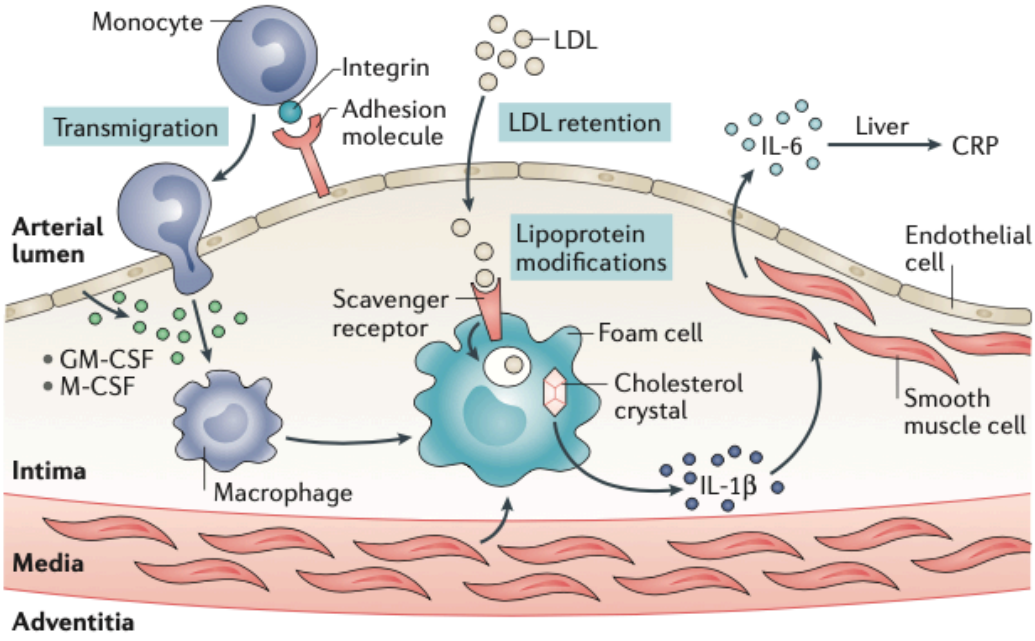


Figure 2-2 Pathogenesis of atherosclerosis [35]. Copyright © 2017, Nature Publishing Group.

Current evidence suggested that endothelial dysfunction is the initial step in atherogenesis and contributes to the progression of atherosclerotic plaque [36]. Dysfunctional ECs accelerate reactive oxygen species (ROS) formation and reduces the production of NO. NO plays an important role in modulating SMC proliferation through cGMP-dependent activation of the cAMP kinase [37, 38],

regulating platelets aggregation through cyclic GMP[39, 40], and inhibiting leukocyte chemotaxis. The endothelial dysfunction results in increased vascular permeability to lipoproteins and further leads to the accumulation of low-density lipoproteins (LDLs) in the intima [41]. Furthermore, various inflammatory cytokines induce the endothelial cells to express vascular adhesion molecules, such as vascular cell adhesion molecule (VCAM) and intracellular adhesion molecule (ICAM), consequently promoting the adhesion of monocytes to the endothelium and migration of monocytes to the subendothelial space. Monocytes in the intima acquire the characteristics of proinflammatory macrophages, augment the expression of scavenger receptor, internalize oxidized lipoproteins, and eventually transform into foam cells [42].

Phenotype switching, proliferation and migration of SMCs has been revealed as the main pathological processes in atherosclerosis. During the atherosclerosis development, SMCs migrate from media to intima and change from contractile phenotype to synthetic phenotype. The synthetic SMCs have high proliferation rate and synthesize 25 to 46 times more collagen than contractile SMCs [43], leading to arterial wall fibrosis and thickening. Those activated SMCs have also been reported to express scavenger receptors and uptake of oxidized LDLs, switching to macro-phage like cells and enhancing the formation of foam cells [44]. Additionally, similar to ECs, SMCs in the intimal lesions also expressed VCAM and ICAM and are capable to retain monocytes and macrophages within the lesion [45].

Compelling evidence has demonstrated that the adventitia is also actively involved in atherosclerosis. Adventitial fibroblasts proliferate, differentiate into myofibroblasts, and migrate to the intima after intimal injury and during the atherosclerotic lesion formation. Activation of adventitial fibroblasts was evidenced to contribute to early development of atherosclerosis [46]. The accelerated proliferation of adventitial fibroblasts was observed in the early stage of atherosclerosis, followed by an increase on collagen and elastin production in adventitia [47]. The deposition of adventitial extracellular matrix (ECM) affects the stiffness of arteries, and in turn further contribute to the proliferation of fibroblasts. Furthermore, the activation of adventitial fibroblasts induces their differentiation into myofibroblasts. Myofibroblasts are capable of migrating from the adventitia to intima within a few days, and become another source of intimal SMCs [32]. The contribution of adventitial progenitor cells to atherosclerosis has also been reported [34, 48]. These cells exhibit the capability of differentiating into SMCs, ECs, and myofibroblasts and macrophages [49]. In the atherosclerotic vessels, adventitial inflammation occurs and results in the production of cytokines, such as stromal cell-derived factor-1, tumor necrosis

factor-α, and transforming growth factor-β, which may lead to the differentiation of adventitial progenitor cells [50].

2.2 Vascular graft as surgical intervention for cardiovascular diseases

Treatments of cardiovascular disease range from dietary to pharmaceutical and surgical interventions. Early stage of atherosclerosis can be mitigated by taking therapeutic agents such as anticoagulant/ antiplatelets to reduce the blood clotting or angiotensin-converting enzyme (ACE) inhibitor and Beta-blocker to decrease blood pressure [51]. As the atherosclerotic lesion deteriorates, vascular surgeries may be required. Endovascular procedures, including angioplasty, stent insertion and atherectomy, could be carried out to widen the stenosed vessels or remove the plaque. For damaged or occluded vessels, vascular grafts are required to replace or bypass the blocked vessels to restore blood flow. Choices of clinically available bypass grafts could be divided into two main categories: autologous graft and synthetic graft.

2.2.1 Autologous graft

Autologous vessels, such as internal thoracic artery and saphenous vein from calf or thigh, have been used as bypass grafts. Internal thoracic artery and saphenous vein have been reported to have a ten-year patency rate of 90%-95% and 40%-60% [52, 53], respectively, and thus internal thoracic artery has become the preferred vessel of choice for coronary artery bypass grafts. The high long-term patency of internal thoracic artery graft is related to its low tendency of arteriosclerosis formation.

Although saphenous veins have lower patency rate, they are still extensively used as bypass grafts due to the ease of harvest. The failure of saphenous vein grafts are associated with the formation of intimal hyperplasia and accelerated atherosclerosis [54]. When being implanted as arterial bypass, vein grafts are exposed to arterial pressure, turbulent blood flow and shear stress, which could damage the endothelium, leading to platelet activation, macrophage migration and SMC proliferation. To improve the patency, many researchers have focused on improving the mechanical properties of vein grafts. Metal wire mesh has been used as external reinforcement around the saphenous vein grafts. With the reinforcement, a twofold decrease in the percentage of stenosis was observed [55]. The reduction on stenosis was proposed to be related to the controlling of dilatation of vein grafts by the wire mesh. Despite the promising results observed with reinforced vein grafts, the wire mesh is not biodegradable and may induce risk of complications. Additionally, about one-third of patients do not have suitable veins for grafting due to pre-existing vascular diseases or vein striping. Significant morbidity and

surgical costs associated with the harvesting of autologous vessels also combine to limit their application for small-diameter vascular grafts.

2.2.2 Synthetic vascular graft

Synthetic materials have attracted broad attention in vascular graft design. Since mid-twentieth century, development of a dependable and durable synthetic non-autogenous vascular conduit has experienced tremendous growth in the application of bypass and native vessel replacement [56, 57]. Existing synthetic materials for vascular graft are expanded polytetrafluoroethylene (ePTFE), polyethylene terephthalate (PET, better known as Dacron®) and polyurethane. These synthetic grafts showed sufficient long-term *in vivo* performance for large scale arterial reconstruction and larger diameter vessels (>6 mm), where the rate of blood flow is high. However, they have been proven to display inferior performance in small-diameter application (<6mm) [58-60]. The patency rate of ePTFE and Dacron® small diameter bypass were reported to be 79% and 75%, respectively, at 6 months [61]; and 50% and 45%, respectively, at 5 years [62]. In small diameter settings, these grafts are susceptible to inflammation, thrombosis and substantial development of intimal hyperplasia due to inherent thrombogenicity, lack of functional endothelium and compliance mismatch [63, 64].

2.2.3 Failure of small diameter vascular graft

Despite the endeavors in the past decades, developing a durable off-the-shelf small diameter vascular graft (<6mm) remains challenging. Small diameter synthetic vascular grafts have a high chance of re-stenosis due to acute thrombus formation and intimal hyperplasia at the anastomotic junctions [58]. Thrombogenicity is inherent due to the lack of endothelial layer of synthetic materials, and the development of intimal hyperplasia is attributed to a combination of the compliance mismatch between the synthetic grafts and native vessels, the lack of endothelial coverage and the continuous interactions of SMCs with non-typical cellular microenvironment [65]. Additionally, surgical trauma and the bio-incompatibility of the synthetic materials also contribute to the failure of synthetic small diameter vascular graft.

2.2.3.1 Lack of endothelial cells

In a native arterial wall, endothelium is in close contact with blood and intimately involves in preventing thrombosis [66]. However, synthetic materials lack of endothelial cell lining and /or do not binding sites for endothelial cells, and thus are exposed directly to blood flow. Upon implantation of the vascular graft, plasma protein immediately adsorbs to the wall, presenting sites for integrin receptors.

Platelet adhesion as well as platelet activation by the synthetic vessel walls cause thrombosis occurrence and early occlusion of the grafts. Thus, patients with prosthetic vascular grafts require long-term antithrombin mediations. Additionally, graft kinking, especially in bypass grafts, results in gross turbulence, providing a highly thrombogenic environment.

2.2.3.2 Surgical trauma

During vascular surgeries, the blood vessels suffered from injuries including the damage of cell wall in suturing and the removal of adventitia. The removal or denudation of endothelial cells causes downregulation of nitric oxide synthase. The inadequate availability of NO increases smooth muscle cell proliferation [67, 68], platelets aggregation [22, 69] and inflammation responses, and eventually trigger the formation of IH. Adventitia was usually removed during the surgery to facilitate suturing, which may trigger inflammation response [70] and initiate the intimal hyperplasia [71-73].

2.2.3.3 Material biocompatibility

Synthetic materials are prone to trigger vascular inflammatory responses. Previous study showed equal contribution of inflammatory response and arterial injury to intimal hyperplasia formation [74]. Macrophages were observed in ePTFE graft stenosis [75], and studies showed suppressed IH by depleting macrophages, indicating the macrophages may regulate IH formation [76]. Also, the inflammatory mediator stimulate the metalloproteinases (MMPs) production, which facilitate the migration and proliferation of SMCs [77, 78]. T-lymphocytes was also be observed in the intimal, and T-lymphocytes secrets tumor necrosis factor-α (TNF-α), which is proven to induce migration of SMCs [79]. In addition to inflammation, due to the lack of endothelial lining on the luminal surface of synthetic materials, platelets aggregation and thrombosis formation will be triggered, which will narrow down the lumen. Activated platelets and thrombin have also been well-studied as a mitogen of SMCs and stimulates SMCs proliferation [80-82].

2.2.3.4 Mismatch of mechanical properties

The mismatch of mechanical properties between grafts and native blood vessels is the most important factor that leads to intimal hyperplasia in vascular grafts. Compliant arterial wall acts as an elastic reservoir, absorbing energy during systole and release in diastole. Introduction of a rigid segment, such as stiff synthetic graft, even with relatively benign flow surfaces, interferes with the function. Due to the configuration and mechanical mismatch of native vessel and graft, there is a turbulence or flow separation around anastomosis area. The flow separation causes endothelial injury at the heel and the

toe, releasing growth factor and causing smooth muscle cells and myofibroblast proliferation [83, 84]. The disturb flow in downstream will trap platelets and cause platelets aggregation, and will also promote fibrin thrombus formation [85].

Wall shear stress, derived from blood flow, regulates the function and composition of blood vessels by affects phenotype and integrity of endothelial cells [86, 87]. Under physiological shear stress, the phenotype of ECs changes from random orientation to aligned along with flow direction. With increased steady shear force, ECs produced more NO, lowering the proliferation of SMCs and thus control the formation of intimal hyperplasia [88]. However, in vascular grafts, ECs are exposed to oscillatory shear stress and fail to produce NO. Distal anastomosis appears to have a sharp temporal shear stress change, with directional change of shear force, which may lead to endothelial deformation [89]. Wall shear stress also regulates SMC proliferation, protein synthesis, and mitogenic activity [90]. In contrast to ECs, SMCs have increased proliferation, DNA synthesis and cell survival in response to oscillatory shear stress [91].

Vascular vessel stress also plays an important role in IH formation in vascular grafts. The high wall stress in vascular grafts may serve as a initiator of inflammatory response, such as increased DGF and MMP expression, followed by SMC proliferation [92-94]. Platelet-derived growth factors (PDGF) are important for smooth muscle cells to proliferate. Studies on PDGF response to stress showed that upon increased wall stress, PDGF secretion is promoted, leading to accelerated SMC proliferation [95].

The combination of all the complications lead to the clinical failures of synthetic small diameter vascular grafts. There is an urgent need for an effective and long-lasting graft to overcome limitations and fulfill the need from the market of vascular engineering.

2.3 Efforts to improve performance of small diameter vascular grafts

2.3.1 Surface modification

The luminal surface of vascular graft is in direct contact with blood stream, and the implantation of a vascular graft may trigger protein adsorption, thrombogenesis and inflammatory responses. Thus, developing a surface that is hemocompatible and supports fast endothelialization is a crucial step to prevent acute thrombosis and improve long term patency.

2.3.1.1 Anticoagulant and antiplatelet

Thrombosis following implantation of synthetic small diameter vascular grafts is a major cause of graft occlusion. Heparin is one of the commonly used anticoagulant and has been frequently applied to modify the synthetic surfaces to reduce thrombogenicity [96]. Heparin-bonded ePTFE vascular grafts have been commercially available and applied to clinical studies. In clinical trials, the 1-year an d 2-year patency rate of heparin-bonded ePTFE in femoropopliteal bypasses was 92% and 83%, respectively, which was comparable to that of saphenous vein grafts [97]. Results also showed that heparin immobilization on ePTFE diminished fibrin formation and thrombin-mediated platelet activation [98]. Additionally, a significant reduction in neointimal cell proliferation and neointimal area were observed in heparin coated ePTFE grafts [99]. The immobilization of heparin to aminated poly(1,8-octanediol-co-citrate) modified ePTFE also improved the interaction between the surface of ePTFE and blood and vascular cells. The immobilized heparin enhanced the adhesion, viability, proliferation and NO production of primary EC and blood outgrowth EC were enhanced by heparin and reduced the proliferation of SMC [100]. Inspired by the promising results on heparin modified ePTFE grafts, heparin has also been used to other vascular graft materials. Heparin immobilization on poly(L-lactic acid) [101], poly(ε-caprolactone) [102, 103], and decellularized scaffolds [104] has shown promoted the proliferation and adhesion of endothelial cells and inhibited the adhesion and spreading of smooth muscle cells. Continuous release of heparin from synthetic grafts was also shown to reduce platelet adhesion, prolong coagulation time, suppress thrombus formation as well as maintain graft patency [105].

Although heparin modification on vascular graft materials has shown promising results, serious shortcomings of heparin exist. The administration of heparin causes hemorrhage, and heparin-induced thrombocytopenia can be fatal. Moreover, the stability of heparin modification may not be stable *in vivo*. Degradation or desulfation of heparin by heparinase could result in loss of bioactivity. To overcome the problems, development of heparin mimetic polymers has attracted broad interest. Low molecular weight heparin (LMWH) prepared by degrading heparin with heparinase showed longer half-life, and reduced side effect compared to heparin, and was proven to have anticoagulant, antiangiogenic and antifibrotic activities [106]. Fucoidan is a bioactive molecule that has structure and anticoagulant activities similar to heparin, and it does not cause hemorrhagic effects, making it a promising alternative to heparin [107]. Bioactivities of fucoidan and its potential for cardiovascular application will be introduced in section 2.5.

2.3.1.2 Extracellular matrix proteins and peptides

ECM proteins in the vascular tissue support endothelial cell growth and function. The ECM proteins can be recognized by cell receptors and present ligands for cells to bind to through integrins. Thus, modification of small diameter vascular material with extracellular proteins has been extensively investigated to encourage endothelial cell adhesion.

Collagen is the most abundant component in the basement membrane of ECs. Immobilization of collagen on a PU-based vascular graft promoted EC adhesion and proliferation [108]. Vascular scaffolds prepared by knitting of collagen blended poly(lactic acid) (PLA) yarn also exhibited promoted recruitment and proliferation of endothelial cells [109]. Laminin modification on ePTFE grafts exhibited accelerated neovascularization and endothelialization. The explanted graft showed coverage of endothelial cells in the luminal surface. The presence of laminin also promoted the neovascularization of the interstices of the grafts [110]. Coating fibronectin on ePTFE grafts at a concentration of 20 μg/ml significantly endothelial attachment [111]. Small diameter polyester grafts were coated with fibronectin and stem cell homing factor. The modification significantly improved endothelial coverage from 27% to 48%, decreased the thickness of intimal hyperplasia from 1.03 mm to 0.69 mm, and reduced thrombotic coverage from 2.21 mm^2 to 1.35 mm^2 [112].

Arginine-glycine-aspartate, or RGD, is widely studied adhesive peptide, and has been proven to be effective in promoting cell attachment [113]. Covalent conjugation of RGD on poly(ε-caprolactone) biodegradable grafts increased endothelial cell viability *in vitro* and enhanced the formation of endothelial cell monolayer *in vivo* after 1 month of implantation [114]. RGD-coating also facilitated the formation of a confluent monolayer of ECs on ePTFE grafts. However, the RGD-coated grafts did not exhibit different patency rate compared to unmodified grafts. Additionally, the modified grafts had higher neointima to lumen area ratio compared to unmodified grafts [115]. REDV (Arg-Glu-Asp-Val) sequence and YIGSR (Tyr–Ile–Gly-Ser-Arg) sequence bind to ECs while inhibit the adhesion of SMCs and platelets [116, 117]. The effects of RGD, REDV and YIGSR modification on silk fibroin scaffolds have been compared [118]. Only combination of YIGSR and RGD significantly enhances the proliferation of endothelial cells. YIGSR improved EC migration more substantially than REDV and RGD.

Although the ECM proteins and peptides are efficient in improving endothelialization, the direct contact of ECM component with blood could induce significant acute thrombosis and platelet activation [119].

2.3.1.3 Other bioactive molecules

In addition to ECM components and anticoagulants, other bioactive molecules, such as growth factors and antibodies, can also be applied to improve endothelialization. Vascular endothelial growth factor (VEGF) and basic fibroblast growth factors (bFGF) regulate the angiogenesis, vascular growth and maturation. They have been identified as promoters for endothelialization. Incorporation of VEGF and RGD peptide were shown to be equally efficient in promoting endothelial cell attachment and deposition of ECM proteins. Both modifications increased primary patency rate three-fold [120]. Modifying decellularized grafts with VEGF has been proven to enhance endothelial function and revascularization. ECs culture on VEGF modified poly(ε-caprolactone) grafts exhibited increased NO production, PGI_2 release, uptake of LDL [121]. The modified grafts also had markedly improved endothelialization, vascularization and smooth muscle regeneration compared to unmodified grafts after being implanted in rat abdominal aorta for 1 month. bFGF is another growth factor that is frequently used to improve vascularization of degradable vascular graft. Incorporation of bFGF in poly(ε-caprolactone) grafts have shown to promote the migration of SMCs and fibroblasts into the grafts [122]. The same group later developed a two-layer vascular graft with VEGF in the inner layer and bFGF and stromal cell–derived factor-1α in the outer layer. The graft exhibited faster endothelialization compared to grafts with VEGF alone and the bFGF induced a rapid formation of SMC layer [123].

Antibodies can target and recruit ECs from the vasculature and capturing the circulating EC and endothelial progenitor cells (EPCs) by engaging the antigens and receptors on the cell membrane. Coating the lumen of vascular grafts with EC- or EPC-specific antibodies is efficient in improving endothelialization. EC-specific antibodies, including platelet endothelial cell adhesion molecule (CD31) and vascular endothelial cadherin (VE-cadherin), vascular endothelial growth factor receptor 2 (VEGFR2), and von Willebrand factor (vWF), were compared. The antibodies were conjugated to poly(ε-caprolactone) (PCL)/collagen scaffolds to compare their efficacy in capturing ECs. Scaffolds modified with VEGFR2 alone showed significantly improved EC capture than unmodified surface, and scaffolds conjugated with both VEGFR2 and CD31 and VEGFR2 and VE-cadherin captured more ECs [124]. Several studies showed that CD34 antibody coating enhances the recruitment and adhesion of ECs and circulating EPCs [125, 126]. However, CD34 antibody presented a risk of increased platelet adhesion, protein adsorption and intimal hyperplasia [127, 128], thus alternative antibodies have been investigated. CD133 is EPC-specific antibody. ePTFE grafts coated with CD133 antibody showed accelerated endothelialization and higher patency after 7-day implantation in pig models [129].

2.3.2 Tissue engineered small diameter vascular graft

Tissue engineered vascular graft can grow and remodel *in vivo* and eventually be integrated into blood vessel configuration, and thus represents an attractive solution for vascular surgeries. The fundamental requirement of tissue engineered vascular grafts is the ability to degrade and support rapid cell adhesion and growth. Additionally, they should possess sufficient mechanical strength to withstand the pressure produced by blood flow and bio- and hemo-compatible luminal surfaces to prevent immunogenic responses and acute thrombosis before endothelial cell remodeling. A number of approaches have been employed to produce tissue engineered vascular grafts. They can be categorized into biodegradable polymers, decellularized ECM scaffolds and self-assembly cell sheets.

2.3.2.1 Biodegradable polymers

Both synthetic and natural biodegradable polymers have been used as degradable scaffolds for tissue engineered grafts. Biodegradable synthetic polymers, such as polyglycolide (PGA), poly(lactic acid) (PLA) and poly-ε-caprolactone (PCL), have good biocompatibility but requires modifications with bioactive molecules to improve cell responses to serve as long lasting small diameter vascular grafts. Compared to synthetic degradable materials, natural biodegradable polymers, such as collagen, elastin and silk fibroin, offers better biocompatibility and lower inflammatory and antigenic responses. Silk fibroin is natural protein produced by silkworm and appears to be one of the most promising polymers for tissue engineered graft. It has high biocompatibility, controllable biodegradability, and more importantly, it possesses mechanical properties that are superior to other natural materials. Electrospun silk fibroin grafts were reported to have higher compliance than ePTFE, Dacron and bovine heterografts, and have burst pressure four times higher than the upper physiological pressure [130]. Small diameter vascular grafts made of silk fibroin exhibited significantly higher 1-year patency rate (85.1%) compared to ePTFE grafts (30%) when being implanted in a rat abdominal aorta model. EC and SMC remodeling were observed after 1 month and organized into endothelial and medial layers [131]. Similar results were observed with silk fibroin grafts with 0.9 mm inner diameter. The grafts remained patency up to 6 months in mice [132]. To improve the hemocompatibility of silk fibroin grafts, sulfonation has been investigated to increase the EC attachment and prevent platelet adhesion. Sulfated silk fibroin prepared by reacting with chlorosulphonic acid had significantly enhanced EC and SMC attachment and anticoagulant activity compared to non-sulfated controls [133]. However, no large animal study has been reported on silk fibroin grafts, and the silk fibroin suffers from batch to batch variation and thus may result in inconsistent quality of product [134].

In an effort to improve biocompatibility and cell adhesion of synthetic materials while providing reinforcement of natural polymer scaffolds, hybrid polymer scaffolds have been widely investigated. A bilayered scaffold with an inner layer of human elastin and an outer layer of PCL possessed compliance and burst pressure comparable to those of human internal thoracic arteries. The elastin component supported cell attached and reduced platelet attachment, and the graft exhibited 100% patency rate with minimal thrombosis in a rabbit carotid artery model [135]. Promising results have also been observed in PCL grafts combined with gelatin, collagen and silk [136]. Additionally, different materials present different degradation profile, and thus hybrid scaffolds also offer an opportunity to manipulate the *in vivo* degradation rate of the grafts. Therefore, the use of hybrid degradable scaffolds has the potential to exploit the best of both synthetic and natural polymer scaffold systems to produce tissue engineered vascular grafts.

2.3.2.2 Decellularized ECM graft

Decellularized ECM vascular grafts are promising strategy as they have no immunological rejection, preserve native vessel architecture and allow for autologous recellularization. Common decellularized grafts can be derived from allogenic or xenogenic sources. Decellularized vascular graft, derived from bovine veins and arteries, have been used for hemodialysis and peripheral arterial bypass in clinical trials. However, the decellularized xenogenic grafts did not show superior clinical performance compared to established synthetic grafts due to thrombosis, infection and aneurysm. Alternative options for decellularized grafts, such as human umbilical artery and veins and small intestinal submucosa, have been continuously explored.

Decellularized scaffolds are mainly composed of collagen, elastin, fibronectin, laminin, glycosaminoglycans and growth factors, providing a favorable environment for host cell attachment, proliferation and migration [137]. However, the ECM components can also lead to platelet activation and thrombosis, and thus surface modification is usually required. Heparinization of decellularized ECM has shown to be effective to generate an antithrombotic surface both *in vitro* and *in vivo* [138]. Additionally, decellularized ECM grafts have a risk of incomplete endothelialization. Immobilization of growth factors is beneficial for graft patency and *in vivo* remodeling. Effects of heparin and VEGF functionalization on small intestinal submucosa small diameter vascular grafts have been investigated. The modified grafts demonstrated high patency rate and significant host cell infiltration when being implanted into the carotid artery of an ovine model. Endothelial cell monolayer was present in the lumen and the vascular wall exhibited infiltration of SMCs after 1 month. After 3 months, the ECs

showed alignment along the direction of flow and SMCs exhibited circumferential alignment. Additionally, the grafts also demonstrated mechanical properties and contractility comparable to native arteries [139].

The decellularized scaffolds offer several advantages for use in tissue engineered small diameter vascular grafts. They have inherent mechanical strength and as the scaffolds remodel, they release chemoattractants that stimulate host cell invasion and facilitate vascular graft integration and remodeling. However, decellularized ECM scaffolds face the challenge of decellularization technique. Insufficient decellularization has been associated with adverse immunes and failure, while aggressive decellularization may lead to the loss of mechanical properties.

2.3.2.3 Self-assembly grafts

Tissue engineered vascular graft can also be fabricated from a cell sheet approach, where layers of cell sheets will be cultured and matured *in vitro*, shaped into tubular constructs, and subsequently cultured in dynamic condition to unify the layers into vascular structure. The first cell sheet-based tissue engineered vascular graft used human umbilical vein SMCs and human skin fibroblasts [140]. The cell sheets were cultured for 4 weeks and another 8-week of culture were allowed to fuse the layers together. The generated grafts demonstrated burst pressure above 2000 mmHg, higher than commonly used human saphenous vein grafts. In clinical trials, cell sheet-based grafts have been used as arteriovenous grafts. The most promising cell sheet-based grafts are composed of autologous ECs and fibroblasts. The grafts displayed patency rate of 60% at 6 months [141]. The development of 3D bioprinting has also enabled the fabrication of cell-based vascular graft by using cell suspension as bioink. The major challenge in bioprinting is to optimize the printing technique that will allow for high cell viability [142].

Self-assembly graft solved a number of drawbacks associated with acellular tissue engineered graft. However, the fabrication of self-assembly grafts requires extended *in vitro* cell culture. Cells need several weeks to grow and mature. Additional months will be necessary to yield sufficient integrity and mechanical strength. The long-term *in vitro* cell culture may impair the functions of the cells. Additionally, the adult vascular cells may have limited replicative and regenerative capabilities, which may limit *in vitro* cell culture times. Alternative cell types, such as progenitor cells, stem cells and induced pluripotent stem cells could be considered as sources for self-assembly grafts due to their ability to differentiation into ECs and SMCs [3].

2.4 Polyvinyl alcohol (PVA) hydrogels

Polyvinyl alcohol (PVA) is a hydrophilic polymer and has been FDA approved for clinical uses in human. PVA is resistant to most organic solvent and has been described to have high oxygen and aroma barrier properties [143]. It has been used as a component for tablet coating to protect active ingredients. PVA-based hydrogels have been recognized as promising materials for various biomedical applications, such as drug delivery [144, 145], tissue engineering [146] and wound dressing [147], due to its low toxicity and biocompatibility.

2.4.1 Crosslinking of PVA

Fabrication of PVA hydrogels can be achieved by several crosslinking methods, including physical, chemical and radiation crosslinking. Physical crosslinking of PVA can be performed by cyclic freezing and thawing of aqueous PVA solution. The freeze-thaw crosslinking of PVA involves phase separation and crystalline formation [148]. Hydrogen bonds form in the aqueous solution of PVA. During the freezing of PVA solution, ice forms, which induces the growth of polymer crystals. The growth of polymer crystals acts as physical crosslinking points. Subsequently, water-insoluble hydrogels are formed in the later thermal cycles. PVA hydrogels crosslinked using freeze-thawing have been shown to have tailored mechanical properties by varying the number of freeze-thawing cycles [149, 150], and have shown promise for use as soft tissue substitutes [151] and artificial cartilage.

The abundant hydroxyl groups in the backbones of PVA polymer chains also provide reactive sites for chemical crosslinking of PVA [152]. One of the most commonly used crosslinking agents for PVA is glutaraldehyde (GA). It reacts with hydroxyl groups to form an ester bond to crosslink PVA [153]. However, the addition of GA may decrease the biocompatibility of PVA due to cytotoxicity of GA [154].

PVA hydrogels can also be crosslinked by radiation. With the addition of photo-initiator, PVA can also be crosslinked by UV irradiation [155]. Gamma irradiation of polyvinyl polymer generates free radicals and promotes the formation C-C bonds for crosslinking [156]. Gamma irradiation on PVA has been reported to successfully produce PVA hydrogels with different physical properties by changing the radiation dose [157].

2.4.2 STMP-PVA small diameter vascular graft

Sodium trimetaphosphate (STMP) is a food-grade crosslinker with low toxicity and low adverse effects on humans. STMP is able to crosslink polysaccharides in alkaline conditions, and it has been widely

used to prepare food-grade starch phosphates [158, 159]. Several studies also reported STMP crosslinking on hyaluronan [160], xanthan [161] and pullulan [162, 163]. Mechanism of STMP crosslinking with polysaccharide (ROH) has been proposed by many studies and proven by ^{31}P-nuclear magnetic resonance [164]. The reaction involves: (1) alcoholate formation; (2) STMP ring open; (3) monophosphate crosslink; (4) pyrophosphate crosslink; and (5) alkaline degradation [165]. The physiochemical behaviors of the generated polysaccharide-STMP hydrogels were reported to vary with different synthesis conditions, including polymer and STMP concentrations [163].

STMP crosslinking of PVA was reported by Chaouat *et al.* in 2008 [166]. Transparent and elastic PVA hydrogel films were fabricated under mild fabrication condition at ambient temperature by casting PVA-STMP mixture into petri dishes. The generated PVA-STMP hydrogels showed biocompatibility with vascular cells and resistance to mechanical stress. The films were further sutured or glued to a 2 mm tubular graft and implanted *in vivo* in a rat abdominal aorta model using end-to-end anastomosis for one week. Within the one-week period, the grafts did not exhibit mechanical or thrombotic complications, and 5 out of 6 grafts remained patent, proved the compatibility of the resulted PVA hydrogel with circulatory blood flow. Following up this study, our group developed a dip casting method to prepare small diameter PVA tubular grafts [16]. By dip casting PVA-STMP mixture on cylindrical molds with different sizes, we were able to fabricate PVA tubular grafts with diameter range from 0.9 mm to 6 mm. Additionally, the mechanical properties of the PVA grafts can be adjusted by changing the preparation parameters. We reported that the PVA grafts had a wide range of mechanical properties with compliance ranging from 1 to 6 %/40 mmHg, burst pressure ranging from 200-800 mmHg, and Young's modulus ranging from 200kPa to 2MPa [11, 167]. This flexibility of PVA hydrogels allows us to fabricate PVA small diameter vascular grafts that match the stiffness of native blood vessels.

In addition to tunable mechanical properties, the hemocompatibility of STMP crosslinked PVA hydrogels was also evaluated. *In vitro* hemocompatibility test using platelet rich plasma showed that STMP-PVA induced similarly low platelet adhesion and activation and thrombin generation with ePTFE, which is a classical material for vascular graft [168]. Later, the STMP-PVA grafts were tested in a whole blood *ex vivo* shunt model. The grafts were reported to have platelet adhesion and fibril accumulation lower than ePTFE clinical controls [169]. Recently, the thrombogenicity of PVA crosslinked by STMP, GA and freeze-thawing was compared [170]. GA-crosslinked PVA increased coagulator factor XII (FXII) activation with presence of cofactors prekallikrein and kininogen and

induced significantly higher platelet attachment. Among the three groups, STMP-PVA hydrogels had lowest FXII activation and platelet attachment and aggregation.

Overall, the studies indicated that the STMP crosslinked PVA could be a promising alternative for synthetic small diameter vascular grafts with tunable mechanical properties and satisfactory blood compatibility. Despite the promising *in vitro* and *in vivo* performances of STMP-PVA small diameter vascular grafts, the hydrophilic nature and lack of cell binding site make PVA biologically inert. Modification on PVA is required to improve endothelial cell adhesion on PVA.

2.4.3 Endothelialization of PVA

Vascular endothelium is supported by its ECM, which contains several adhesive proteins, such as collagen, laminin and fibronectin. Endothelial cells adhered to the ECM proteins by forming integrin and focal adhesions. In order to mimic the natural cellular niche, prior studies have modified PVA with extracellular proteins and peptide sequences [169, 171]. Improved endothelialization was observed, however, the modified surfaces also induced significantly higher platelet deposition [171]. We recently conjugated gelatin, a denatured form of collagen, on PVA [172]. Endothelial cells formed focal adhesions on gelatin modified PVA and had significantly better adhesion and monolayer formation. Moreover, the modification did not induce noticeable change on the platelet adhesion and thrombogenicity of PVA [172].

In addition to ECM protein modification, plasma treatment on PVA has also been demonstrated to improve endothelial cell attachment [173, 174]. O_2, N_2 Ar and NH_3 plasma were studied. All types of plasma increased cell attachment on PVA, and N_2 and NH_3 plasma treated PVA hydrogels had lower platelet attachment compared unmodified PVA. However, the functional groups on plasma treated PVA were shown to be stable for 30 days and had a significantly reduction at 77 days [174], indicating that the treatment may not be suitable for long term storage.

Topographies cues have been elucidated to mediate cell behaviors. Our group previously fabricate PVA films and tubular grafts with various of topographical patterns to improve the endothelial cell responses on PVA [16, 174]. *In vitro* studies suggested that the attachment of endothelial cells on PVA was significantly improved by 2 μm gratings and 1.8 μm concave lenses. Additionally, topographically patterned PVA tubular grafts with diameter of 2 mm and length of 1 cm were implanted in rat infrarenal aorta. Only grafts with 2 μm gratings showed endothelial cell attachment in the lumen [16]. However, although the topographical modification on PVA is promising in improving endothelial cell responses,

it is not sufficient to support endothelial monolayer formation. Thus, combination of biochemical modification with topographical cues will be necessary to improve the endothelialization on PVA.

2.5 Fucoidan as a bioactive molecule

Fucoidan is a sulfated polysaccharide mainly isolated from the matrix of brown seaweeds. It is primarily composed of sulfated L-fucose and different proportions of xylose, mannose, galactose, glucose and uronic acid depending on the species of brown seaweeds [175-177]. The structure of fucoidan is heterogeneous. Two main types of fucoidan backbone were identified as mono-(1-3)-α-L-fucopyranose and repeated alternating (1-3)- and (1-4)-α-L-fucopyranose [178], with sulfate groups locating at C-2, C-3 and/or C-4 of fucose ring **(Fig 2-3)**. Fucoidan was first isolated from brown algae in 1913 by Kylin and now fucoidan has been marketed as dietary supplement in food industry.

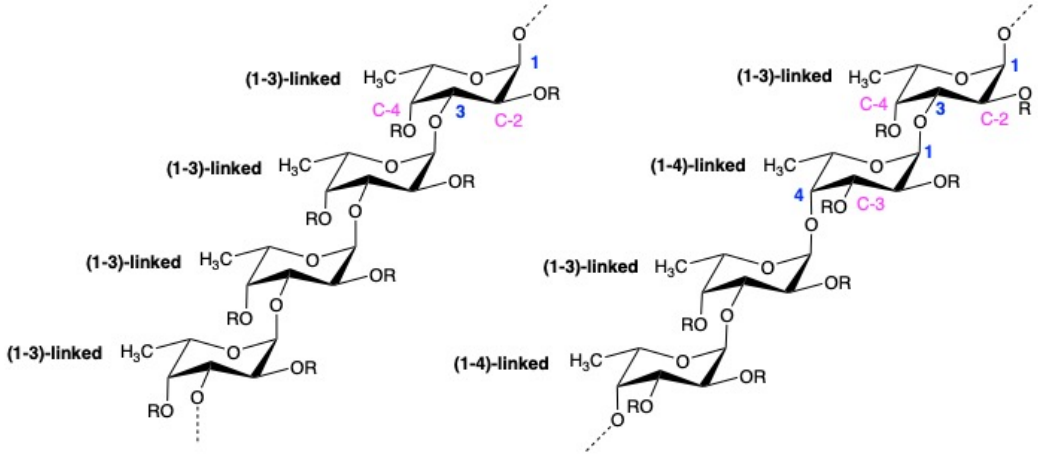


Figure 2-3. Fucoidan structure with mono-(1-3)-α-L-fucopyranose backbone and repeated (1-3)- and (1-4)-α-L-fucopyranose backbone

Since its discovery, fucoidan has attracted steadily increased research interest, attributed to its low toxicity and diverse bioactivities, including anticoagulant, antitumor, anti-inflammatory and antioxidant activities. Increasing numbers of studies have suggested that the bioactivities of fucoidan could contribute to its application in cardiovascular area [12]. Fucoidan has been shown to alleviate atherosclerotic lesions through its anti-inflammatory and anticoagulant effects. Fucoidan reduces leukocyte and platelet adhesion on dysfunctional or damaged endothelium [179] and inhibits thrombin generation [180]. It also inactivates free-radical processes [181], reduces level of cholesterol [182] and inhibits lipid accumulation [183]. The ability of fucoidan to reduce thrombin generation in

microvasculature [184] and to induce angiogenesis through recruitment of endothelial progenitor cells [185] also attenuates myocardial infarction and stimulates revascularization in ischemic regions. In this section, we will review the findings on bioactivities of fucoidan for cardiovascular application from three main aspects: (1) the anticoagulant and antithrombotic activity; (2) the anti-inflammatory activity; and (3) the modulation of vascular cell behaviors.

2.5.1 Anticoagulant and antithrombotic activities

2.5.1.1 Anticoagulant activities

Fucoidan was firstly reported to exhibit anticoagulant activity both *in vitro* and *in vivo* in 1957 by Springer [186]. They found that fucoidan from *Fucus vesiculosus* significantly prolonged prothrombin time (PT) when being injected intravenously to rabbits. Later, similar trend has been observed in other animals [187]. The prolonging of activated partial thromboplastin time (APTT) by fucoidan has been reported by many studies [188-191]. Fucoidans from three sea cucumbers have been shown to prolong APTT is significant but not PT and thrombin time (TT) [192]. Fucoidan from *Hizikia fusiforme* has been reported to prolong APTT distinctly but delay TT slightly [193]. The findings, showing that fucoidan could prolong both APTT and PT, suggest that fucoidan exhibits anticoagulant activity through both intrinsic and extrinsic pathways. The main targets of fucoidan have been identified as factor Xa and thrombin, as shown in **Fig 2-4**.

Factor Xa (FXa) is an activated form of factor X, and it can cleave prothrombin to yield active thrombin. The interaction of fucoidan with FXa is emphasized in the mechanism of the anticoagulant activity of fucoidan. Fucoidan is a potent inhibitor of FXa generation in the intrinsic pathway [194, 195]. Furthermore, fucoidan has been shown to inhibit intrinsic coagulation factor Xase in a concentration-dependent manner [192].

The anticoagulant activity and efficiency of fucoidan is highly dependent on the structure of fucoidan. Among all of the structural features, sulfate content and molecular weight appear to be play the most predominant role. A common consensus is that the anticoagulant effect is positively related to the number of sulfate groups [196], while negatively related to the molecular size [197].

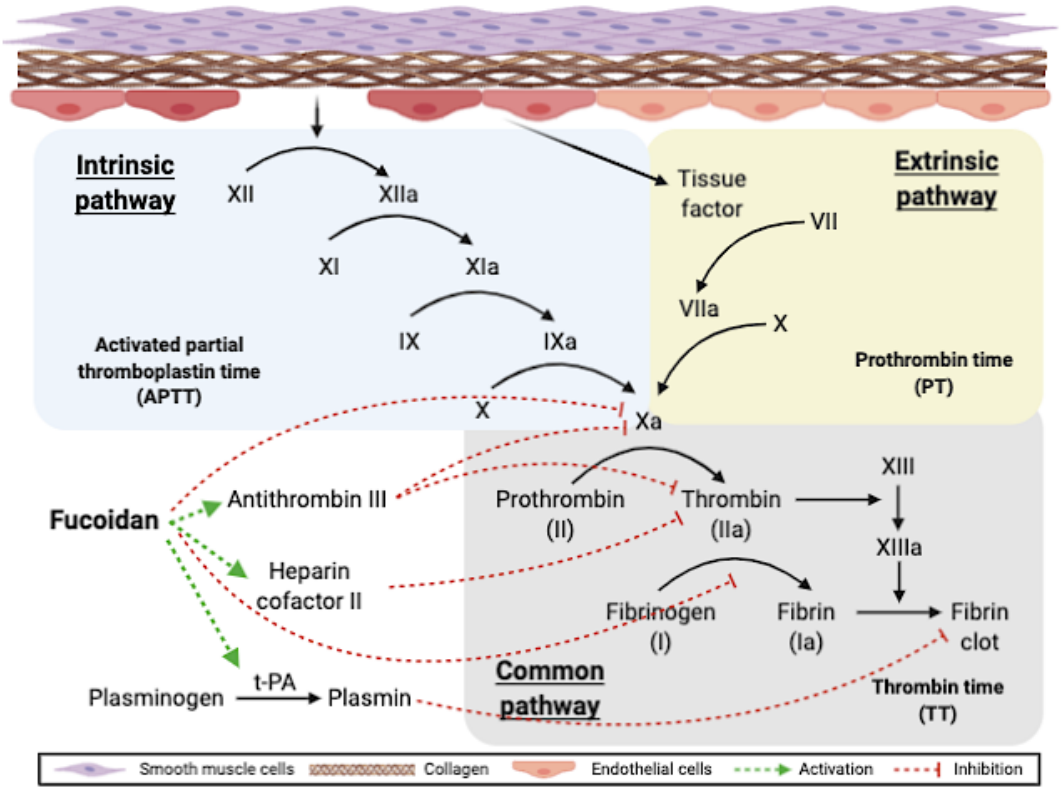


Figure 2-4. Coagulation pathways and the role of fucoidan. Fucoidan exhibits anticoagulant activity by inhibiting FXa formation in the intrinsic pathway [194, 195, 198]. Fucoidan improves the activity of heparin cofactor II and antithrombin III in inactivating thrombin by binding to antithrombin III and heparin cofactor II [199-201]. Fucoidan inhibits fibrinogen-thrombin reaction by binding to the thrombin attacking site in fibrinogen [202, 203]. Fucoidan also promotes fibrinolytic effect by simulating t-PA catalyzed plasminogen activation [204, 205].

2.5.1.2 Thrombin generation

Fucoidan has an inhibitory activity on thrombin generation. Injection of fucoidan inhibits thrombosis by prolonging thrombin clotting time and lag phase of thrombin generation and slowing down the thrombus occlusion caused by endothelial denudation [206]. The thrombin inhibition activity of fucoidan is mainly mediated by heparin cofactor II- and antithrombin III-dependent pathways [201] (**Fig 2-4**). Heparin cofactor II and antithrombin III inactivate thrombin by forming complexes with thrombin, blocking the active site of thrombin. Fucoidan has a high affinity for heparin cofactor II and

is potent in enhancing the rate of heparin cofactor II-thrombin reaction [207]. Fucoidan also bind to antithrombin III, although to a less extent compared to heparin cofactor II [208].

Other mechanisms of the antithrombotic activity of fucoidan have been explored. Fibrin polymerization can be suppressed by fucoidan. Fucoidan binds to fibrinogen, presenting a steric hindrance, thereby inhibiting fibrinogen clotting by thrombin [203]. Plasminogen lyses fibrin once activated and converted to plasmin. Tissue plasminogen activator (t-PA) is the primary activator of plasminogen. Fucoidan was found to be capable of simulating t-PA catalyzed plasminogen activation [209]. A recent study also showed that mixing fucoidan into recombinant t-PA (rt-PA) yielded a greater fibrinolytic effect than rt-PA alone [205]. Richard *et al.* looked into the effect of fucoidan on Protease nexin-I (PN-I), which has a inhibitory effect on thrombin [210]. They observed that fucoidan bound to thrombin, PN-I and PN-I/thrombin complex. The resulting kinetic curve showed that the fucoidan accelerated thrombin inhibition through PN-I.

Among all the studies on antithrombotic activity of fucoidan, little evidence showed that fucoidan has a direct inhibitory effect on thrombin. Ustyuzhanina *et al.* reported that a high concentration of fucoidan and a minimal of 16 saccharide units might be required to achieve a direct inhibition of thrombin [208].

2.5.1.3 Platelets

In addition to the anticoagulant and antithrombotic activities, fucoidan also affects platelet adhesion, aggregation, and activation. Fucoidan has been shown to inhibit thrombin-induced and adenosine diphosphate (ADP)-induced platelet aggregation [177, 211]. Intravenous administration of fucoidan has been shown to cause complete inhibition of platelet aggregation [187] and platelet adhesion to damaged arterial surfaces [179]. Fucoidan has also been shown to inhibit platelet activation by reducing platelet aggregation, decreasing the secretion endothelial microparticles and von Willebrand factor (vWF), and suppressing the intracellular Ca^{2+} influx [212]. However, fucoidan from *Fucus vesiculosus* was also reported to induce irreversible platelet aggregation and cause platelet activation through Src family kinase signaling pathways, which are critical initiators of platelet response to vascular injury [213].

The contradictory results could be explained by the dose and molecular weight differences of the fucoidans used in different studies. The irreversible induction of platelet aggregation by fucoidan from *Fucus vesiculosus* has been shown to only appear at high concentrations (0.5-5 mg/mL). Additionally,

low molecular weight fractions of fucoidan has been shown to induce lower platelet aggregation compared to high molecular weight fucoidans [214]. Other studies have also found that high molecular weight fucoidan caused pro-aggregation response of platelets, while low molecular weight fucoidan inhibited thrombin-induced platelet aggregation [197].

2.5.2 Anti-inflammatory activities

Inflammation has been highlighted and evidenced to play a significant role in the development of cardiovascular pathology, especially atherosclerosis. Fucoidan has been identified as a promising anti-inflammatory agent to treat early-stage atherosclerosis [215]. The anti-inflammatory effect of fucoidan is achieved mainly by inhibiting complement system, binding to selectins and suppressing the activities of several inflammatory enzymes [12].

2.5.2.1 Complement

Fucoidan was first described as a potent inhibitor of complement activation by Blondin *et al.* in 1994 [216, 217]. Later, Zvyagintseva *et al.* showed that fucoidans caused 50% inhibition of alternative complement activation at a concentration from 0.5 to 20 mg/mL, depending on the sources [218]. The inhibition on complement activation by fucoidan is mainly through the classical pathway and to a lesser extent through alternative pathway (**Fig 2-5**). Fucoidan binds to C1q and interferes the association of the C1r2-C1s2 subunit, thus inhibiting the full activation of C1 [219]. Fucoidan also prevents C4 cleavage by forming a complex with C4 [220]. In addition, fucoidan directly inhibits the formation of C3 convertase. By interfering the interaction between C4b and C2, fucoidan inhibits the formation of C4b2a. Also, by decreasing the number of binding sites on factor B for C3b, fucoidan suppressed the generation of C3bBb [216].

The anticomplement activities of fucoidan is structural dependent. High molecular weight has been shown to favor a better anticomplementary activity [221]. The anticomplementary activity of fucoidan has been shown to increase with increasing molecular weight until reaching a plateau [217]. A higher sulfate content in fucoidan has also been shown to benefit the complement inhibition [221].

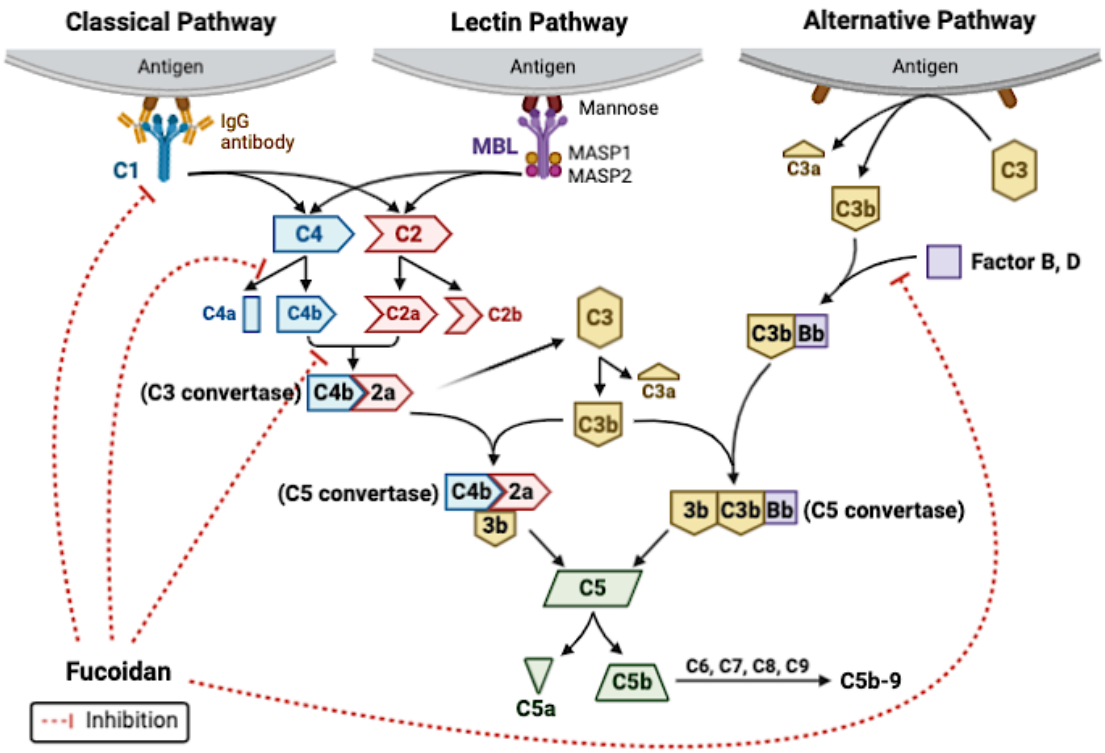


Figure 2-5. Three complement activation pathways and the role of fucoidan in complement activation. Fucoidan inhibits complement activation through the classical pathway by preventing active C1 formation, inhibiting C4 activity by forming a complex with C4, and preventing the binding of C4b and C2a [216, 220]. Fucoidan also inhibits complement activation through the alternative pathway by preventing the binding of factor B to C3b [216].

2.5.2.2 Selectin

Selectins are a group of glycoproteins, playing a vital role in the leukocyte recruitment and accumulation at the sites of inflammation and tissue damage. Fucoidan acts as a ligand to both P- and L-selectin and inhibits their activities. Through binding to the selectins, fucoidan is efficient in inhibiting leukocyte, neutrophil and platelet adhesion to damaged arterial surfaces [179, 184]. In different animal models, pre-treatment of fucoidan has been shown to be efficient in reducing leukocyte rolling and neutrophil migration [222-224]. In addition, fucoidan is able to bind to activated platelets by targeting the P-selectin on the surfaces of activated platelets. Juenet *et al.* reported a nanomolar affinity of fucoidan for the P-selectin expressed by activated platelets in thrombus, which suggests that

fucoidan can be used as carriers for targeting thrombosis [225]. Fucoidan functionalized microcapsules and microparticles can bind to activated platelet aggregates and locate specifically at the abdominal aortic aneurysm thrombotic wall in a rat model [226, 227]. The ability of fucoidan to locate activated platelets in thrombus enables fucoidan to work as a promising molecular imaging agent. Furthermore, fucoidan also shows therapeutic potential in attenuating myocardial infarction by reducing selectin-dependent adhesion of platelets [228].

2.5.2.3 Enzyme activity

Recent studies found out that in addition to the inhibition of complement and selectins, fucoidan also suppresses the activity of several inflammatory enzymes. Dietary intake of low molecular weight fucoidan from *Saccharina japonica* has been shown to markedly downregulate the matrix metalloproteinase (MMP) level, reduce expression of interleukin 1β, TNF-α and monocyte chemotactic protein-1, and limit the growing of abdominal aortic aneurysm (AAA) [229]. MMP-2, also known as type IV collagenase, is responsible for intimal hyperplasia [230, 231]. Fucoidan from *Fucus vesiculosus* specifically inhibits MMP-2 activity and reducs the narrowing of the lumen of the damaged vessels [232]. Administration of fucoidan has also been shown to attenuate MMP activities by suppressing the activation of nuclear factor κB and c-Jun N-terminal kinase (JNK), therefore inhibiting AAA progression [233]

2.5.3 Directing vascular cell behaviors

2.5.3.1 Endothelial cells

Vascular endothelial cells (ECs) serve as a barrier between blood and tissues and participates actively in maintaining homeostasis. Endothelial dysfunction is a major contributor to cardiovascular diseases, such as atherosclerosis, hypertension and diabetes [234]. Endothelial denudation is the primary factor that causes restenosis after surgical interventions to treat cardiovascular diseases [235].

Several studies showed that fucoidan has a protective function for ECs. Chen *et al.* investigated the EC protective activity of fucoidan by measuring the vWF level and the number of endothelial microparticles, which are important indexes of endothelial injury [212]. vWF level was significantly suppressed *in vitro* and *in vivo* in an endothelial injury rat model, and the number of endothelial microparticles stimulated by TNF-α was significantly decreased. Chen *et al.* later studied the relationship between the structural features and EC protective activity of fucoidan from *Saccharina*

japonica [13]. They found that low molecular weight fucoidan were more effective than medium molecular weight fucoidan in protecting ECs. Furthermore, highly sulfated fucoidan appears to be more effective at inducing EC proliferation in the presence of fibroblast growth factors (FGFs). A recent study using dyslipidemia and atherosclerosis mouse models showed that the EC protective activity of fucoidan may be related to its ability to reduce the expression of endothelial dysfunction marker, endothelin-1, and proinflammatory cytokines, TNF-α and IFNγ [236]. Other studies employing fucoidan as functional molecules also suggested that fucoidan could enhance endothelialization on synthetic materials or decellularized scaffold [237, 238].

2.5.3.2 Smooth muscle cells

Vascular smooth muscle cells (SMCs) play significant roles in atherosclerosis, hypertension and intimal hyperplasia formation. Adding fucoidan in cell culture media has been shown to be potent in inhibiting SMC proliferation [239, 240]. McCaffrey *et al.* compared the antiproliferative effect of fucoidan with that of heparin, and fucoidan had significantly more effective inhibition than heparin [14]. This study has also suggested that fucoidan suppresses SMC proliferation through the interaction with transforming growth factor- β1 (TGF-β1). They have also reported that fucoidan can protect TGF-β1 from plasmin degradation and increase the steady state levels of TGF-β1 activity in SMCs in a later study [241]. The inhibition of fucoidan on DNA synthesis, phosphorylation, and nuclear translocation of mitogen-activated protein kinase (MAPK) also contribute to the anti-proliferative effect on SMCs [242, 243]. The antiproliferative effect of fucoidan is affected by the structural features. Sulfation of fucoidan [239] and a minimal of 30 saccharide units [244] have been found to be necessary to exhibit the antiproliferative activity on SMCs.

In addition to inhibiting SMC proliferation, fucoidan suppresses SMC migration. In a recent study in a pulmonary arterial hypertension mouse model, fucoidan (25 mg/kg) inhibited hypoxia and growth factor-stimulated SMC proliferation and migration [245]. Fucoidan alters the synthesis and secretion of fibronectin and thrombospondin substantially [239], which may contribute to the inhibition effect of fucoidan on SMC migration. These inhibitory effects of fucoidan on SMC proliferation and migration have contribute to its mitigating function on the formation of atherosclerotic lesions and suppress intimal hyperplasia formation [246-249].

Overall, all these studies have suggested that fucoidan is a promising biomolecule for cardiovascular application.

2.6 Topographical cues for improved cell responses

Cells are surrounded by a complex microenvironment with geometrically defined structures *in vivo*. The extracellular environment provided three-dimensional (3D) physical cues in micron and sub-micron scale, which plays an essential role in diverse cell processes. To mimic natural extracellular environment, micro- and nano-topographies have been fabricated on substrates and implants to modulate cell processes *in vitro* and regulate cell behaviors *in vivo*.

2.6.1 Topographical cues on hydrogels

Hydrogels are attractive candidates for cellular studies and tissue engineering application. They can be engineered to resemble native extracellular matrix and generate artificial organs. Hydrogels with rigidity that matches body tissues can be developed as platform to study mechanobiology. In order to provide specific cues to modulate cell responses, topographically patterning on hydrogels has been extensively investigated. Surface patterning of a hydrogel can be achieved by various approaches, such as casting, nanoimprinting, electrospinning, multiphoton patterning and 3D printing [250]. The resolution of generated patterns ranging nanoscale to microscale depending on the technique being employed. Different cell behaviors, such as improved cell adhesion, controlled cell migration, increased or decreased cell proliferation and guided stem cell differentiation have been achieved by manipulating the surface topography on the hydrogels.

2.6.1.1 Cell adhesion and morphology

Cell adhesion is essential in cell communication and signalling. However, adhesion of cells on hydrogels that lack of cell binding anchorage or do not support ECM adsorption is challenging. Topographical modification has demonstrated improve cell adhesion on non-adhesive hydrogels.

Poly(2-hydroxyethyl methacrylate) (pHEMA) is a commonly used hydrogel for contact lens. The adhesion and growth of human corneal epithelial cell has demonstrated a significant increase on nano-sized rippled patterned [131] and Lotus leaf topographies [132]. Our previous study on patterned PVA hydrogels showed that ECs had substantially enhanced attachment on 2 μm gratings both *in vitro* and *in vivo* [22, 133]. The promotion effect of topographies on cell adhesion are dependent on topography dimensions. Hepatocytes attachment on heparin hydrogels with gratings of different pitch sizes has been were compared. Gratings with height of 300 nm and pitch of 400 nm supports markedly better attachment than other patterns [134]. Fibroblasts exhibited good adhesion on polyethylene glycol

hydrogels with 3 μm pillars and grooves [135], and grooves with 10 μm in width induced significantly better cell adhesion and spreading [136].

In addition to cell adhesion, substrate topographies can also induce cell morphology change, cell alignment and cytoskeletal re-arrangement. Hydrogels with aligned microfibers and nanofibers are well documented to induce cell alignment along the fibers [251, 252]. Cells are able orient along with fiber axis, form extended protrusions parallel or perpendicular to aligned fibers and form cell-matrix dual alignment. [251]. Similar to aligned fiber, micro- and nano-groove structures on hydrogels are also effective in inducing cell alignment parallel to the grooves. Dimension of grooves was shown to affect cell alignment differently. Robert *et al*. showed that hydrogels with 1.9 μm of grooves by casting method were effective in inducing cell alignment, but cells aligned poorly on grooves with depth less than 1 μm [253]. Adipose-derived stem cells were also shown to exhibit alignment when the topography width is larger than 0.60 μm and height larger than 170 ± 100 nm on elastin-based hydrogel [254]. Cells on micro-well and micropillar structures exhibits distinct morphology compared to on grating structures. Rat bone marrow mesenchymal stem cells have been shown to form a large spherical shape in a pillar substrate but not in a grooved substrate [255]. Preadipocytes on poly(ethylene glycol) (PEG) hydrogel with nano-well structures exhibited spherical but more confined shape compared to unpatterned surfaces [256].

2.6.1.2 Cell migration

Substrate topographies, mainly groove structure or on aligned fibers provides contact guidance, accelerating cell migration. Corneal epithelial cells on microgrooved PEG-based hydrogels have been found to explore larger space and migrate on an average of 100 μm parallel to the ridge and groove topographies. They have also exhibited 50% higher wound healing rate compared to unpatterned surfaces [257]. The efficiency of grooved structure in promoting cell migration has been shown to be affected by groove width and the slope of groove walls. Fibroblasts appears to adhere, align and elongate more on denser patterns on polyurethane-amide (PUA) hydrogels with variable groove width of 1-9 μm [258]. Vicente *et al*. found the orientation of migration tracks with pattern increased with the decreasing of line width [259]. Cells migrate randomly inside wide channels that are larger than cell size, while on narrow channels, cell migrate parallel to the pattern direction. Epithelial cells have shown to increase their motility by 3-fold on the microgrooved PEG hydrogel [260]. By varying the slope of the microgroove walls, the authors found that relatively upright walls may be necessary for increased cell migration [260]. Mechanism underlying this phenomenon has been proposed to be topography-

induced geometry constraint of cell adhesion sites, which results in cell alignment, polarization and directional migration [261].

2.6.1.3 Cell proliferation

Cell proliferation is regulated by the extent and strength of cell adhesion and was reported to be positively correlated with cell flattening [262]. Substrate topographies play a role in cell proliferation through by affecting cell spreading on the substrates. Proliferation of multiple nerve cells has been shown to be promoted by the aligned fibers on silk-graphene hybrid hydrogels [263]. Electronspun fibrin nanofiber hydrogels with hierarchically aligned fibers were designed to promote peripheral nerve regeneration [264]. The nanofibers have shown capability to direct Schwann cells migration and proliferation and accelerating axonal regrowth. On the contrary, grating structures seem to hinder the proliferation of smooth muscle cells. Human aortic smooth muscle cells exhibits significantly lower proliferation on microgrooved tetronic-tyramine hydrogels than on unpatterned hydrogel, regardless of the groove size [265]. Isotropic structures also affect cell proliferation. Human corneal endothelial cells on 1 μm pillar structures have been reported to have higher cell density compared to the unpatterned control [266]. Our previous study on gelatin methacryloyl-based hydrogels showed that human corneal endothelial cells had a higher density on 1 μm pillars [266].

2.6.1.4 Cell differentiation

Stem cells have emerged as important cell source for regenerative medicine due to their differentiation and self-renewal capability. Stem cells have been demonstrated to respond to biophysical and biochemical cues in their natural niche. Stiffness is considered as a key parameter in the microenvironment that directs cell differentiation [267]. The stiffness of hydrogels can be adjusted by changing parameters, such as polymer concentration and crosslinking density, and thus hydrogels have been used as platforms for studying cell differentiation. Hydrogels with topographies have shown potential for culturing stem cells and providing niche for directed stem cell differentiation *in vitro* and *in vivo*.

Microgrooved structures and aligned fibers have been documented to induce neuron differentiation [268, 269]. Neuron differentiation of human embryonic stem cells has been shown to increase as groove pitch decreased, and 2 μm microgrooves can improve neuron growth by 1.7 fold [268]. Hierarchically aligned fibrillar fibrin hydrogel prepared by electrospinning has been shown induce cytoskeletons alignment of human umbilical cord mesenchymal stem cells (hUMSCs), upregulate neural lineage

specific markers and encourage rapid neurite outgrowth [269]. In addition to groove structure and aligned fibers, nanopillars were also found to be promising to enhance neural stem cell differentiation and regulate neurite outgrowths [270]. In addition, micro- and nano-groove structures have been shown to promote osteogenic differentiation [271, 272], myogenesis and myotube alignment [273], and chondrogenic differentiation [274].

2.6.1.5 Mechanism

The mechanisms of regulation behaviors of topographies on cells have been studied. Topography alters protein adsorption on hydrogels. This topography-directed protein adsorption has been reported to contribute to the improved cell adhesion. The presence of serum proteins has been speculated for improved cell adhesion on patterned PEG hydrogels [275]. The presence of serum proteins, especially vitronectin, in culture medium appears to be essential for initial cell attachment and topography is important for establishing durable adhesion and cell spreading. In addition, topography-induced differentiation have also been observed to associate with changes in cell adhesion and morphology, which could be due to geometry-dependent cytoskeletal arrangement [276], changes in actomyosin contractility [277] and focal adhesion signaling [278]. Actin filaments preferentially form and elongate along the directions with least resistance, and consequently leads to aligned cell shape. Similar to cells on other patterned substrates, the role of focal adhesion formation has also been stressed when investigating the mechanism of cell elongation on hydrogels with grating structures. Yip *et al*. reported that fibroblasts formed protrusions in the grating grooves on a polyacrylamide (PAM) hydrogel with 2 μm gratings [279]. Focal adhesions also aligned parallel to the gratings, which also resulted in aligned actin stress fiber formation in the direction parallel to the grating, leading to polarized traction stresses which drive cell elongation. Smooth muscle cells cultured on microgrooved tetronic-tyramine hydrogels have been reported to form localized focal adhesions on the ridges of grooves and less organized focal adhesions in the 2 μm depth of the grooves, which contributes to the alignment of actin networks along the grooves [265]. Similarly, human mesenchymal stem cells also formed long and aligned focal adhesion on 3D printed micro-channeled gelatin hydrogels, while formed small and randomly distributed focal adhesions on unpatterned hydrogels [280]. In addition, the roles of integrins have been emphasized in topography induced cell responses [281, 282]. Micro- and nano-sized topographies have also been elucidated to promote integrin cluster formation between cells and the extracellular matrix [283, 284].

2.6.2 Topographical cues for improved endothelial cell responses

ECs are surrounded by their basement membrane. The vascular basement membrane presents a complex network with pores and fibers that are in submicron and nanoscale [285], providing topographical cue for the activities of ECs in the vascular system. Understanding the effects of these topographies in EC responses and replicating these topographies in synthetic materials can facilitate the development of vascular tissue engineering.

In our previous study, EC responses on 40 different type of topographies were compared [286]. We found that cell density and proliferation were lower on nano- and micro-sized circular topographies, such as pillars, wells, and lenses, compared to grating topographies [286]. Another study comparing the responses of ECs and SMCs on pillar and groove structures also demonstrated that the 1 μm pillars inhibited the growth of ECs and SMCs while the 1 μm grooves promoted EC adhesion and inhibited SMC growth [287]. The possible mechanism has been proposed to be the reduced focal adhesion interaction with circular topographies. Vinculin staining demonstrated that focal adhesions formed by cells on grooved surfaces were elongated and aligned. Only cytosolic vinculin was observed on cells on pillars, which may give rise to disorganized cytoskeleton and decreased cell spreading [287].

ECs are subjected to the shear stress by the blood flow *in vivo* and exhibit elongated morphology and aligned orientation. Aligned fibers and nano- and micro-grooved patterns can induce strong alignment of the ECs. The alignment and elongation of ECs have been reported to be correlated with the re-organization of cytoskeletal components and formation of aligned focal adhesions [288]. Orientation of EC monolayer is beneficial for various endothelial functions. ECs cultured on grooves have been demonstrated to exhibit improved antithrombotic activity with significantly increased production of PGI_2 and t-PA [289]. Moreover, oriented ECs appeared to inhibit the activation of intrinsic coagulation system more effectively compared to ECs on flat surfaces, as indicated by the prolonged TT and APTT. Moreover, alignment of ECs decreases inflammatory signaling of ECS. ECs cultured on aligned nanofibrillar collagen scaffolds have been shown to exhibit 50% less monocyte adhesion compared to those on randomly oriented fibrils [290]. Downregulated expression of VCAM-1 and increased expression of KLF-2 by oriented and elongated ECs have also been observed [291].

ECs respond to topographies differently depending on their origins. A recent study has compared the effects of various topographies on the phenotype and function of venous ECs, arterial EC and stem cell-derived ECs [292]. All ECs displayed similar morphology in response to the substrate topographies. Expression of venous marker, COUP transcription factor 2 (COUP-TFII), in venous ECs was

significantly improved by gratings and micro-pillars, while the expression of arterial marker, NOTCH1, was significantly decreased by gratings. Among all the patterns, 2 μm gratings appears to be the most efficient in depressing the arterial phenotype and augmenting the venous phenotype of venous ECs. Hierarchical micro-gratings with parallel nano-gratings promoted the arterial phenotype and functional maturation of pluripotent stem cell-derived endothelial cells with increased NOTCH1 and Ac-LDL expression. The study indicated that the selection of topographies may need to be customized to a particular cell source.

Endothelial dysfunction can be cause by several diseases, such as diabetes and hypertension. Diseased and healthy ECs have inherently different phenotype, genotype and metabolism [293], and thus may react differently to topographical cues. Our group has previously compared the functional responses of healthy and diabetic human coronary arterial ECs on various isotropic and anisotropic topographies [294]. Concave microlens topography deteriorated the adhesion and angiogenic capability of diabetic endothelial cells, but did not significantly affect the functions of healthy endothelial cells. Grating structure decreased the expression of endothelial nitric oxide synthase (eNOS) and immunogenic genes in healthy ECs, while increased monocyte adhesion and eNOS expression in diabetic cells on grating structures. Additionally, gratings appeared to be more effective in promoting the rate of wound healing of healthy cells compared to diabetic cells.

2.7 Summary

In summary, this chapter introduces the structure of blood vessels and the roles of vascular cells in the pathogenesis of cardiovascular diseases. Currently available commercial vascular grafts and vascular grafts under research and development were reviewed, and the failure mechanism of synthetic small diameter vascular grafts were elaborated. A review on the progresses and strategies to improve the performance small diameter vascular grafts was provided. These highlighted the unmet needs of an off-the-shelf available synthetic vascular graft with improved clinical performance, and the motivation of developing PVA hydrogel vascular graft. Subsequently, the potential of fucoidan as biochemical cues was introduced and their potential in cardiovascular application was presented. Finally, the topographical patterning on hydrogels was reviewed, and the topographical cues for endothelial cell responses were discussed. The literature review presented in this chapter helps to understand the need to develop durable small diameter vascular grafts. The vast research efforts in the field emphasize the importance of surface modification to overcome the shortcomings of current synthetic vascular grafts.

It also reveals the potential and drawbacks of PVA vascular grafts and sheds light on the values of fucoidan and topographical cue for improving the performance of vascular devices.

Based on these findings, this PhD thesis focuses on the effects of fucoidan and topographies on endothelial cell responses and hemocompatibility, and it aims to develop a versatile surface modification method to improve performance of PVA small diameter vascular grafts and to understand the mechanism on how the modifications could lead to the improvement.

Chapter 3

Effect of Fucoidan on Endothelial Cell Adhesion and Hemocompatibility of PVA

Poly(vinyl alcohol) (PVA) hydrogels have tunable mechanical properties and a low thrombogenic surface, which suggests its potential value as a small diameter vascular graft material. However, PVA does not support cell adhesion and thus requires surface modification to encourage endothelialization. This chapter presents a modification of PVA with fucoidan. Fucoidan is a sulfated polysaccharide with anticoagulant and antithrombotic properties, which was shown to potentially increase endothelial cell adhesion and proliferation. By mixing fucoidan with PVA and co-crosslinked by sodium trimetaphosphate (STMP), the modification was achieved without sacrificing mechanical properties. Endothelial cell adhesion and monolayer function were significantly enhanced by the fucoidan modification. *In vitro* and *ex-vivo* studies showed low platelet adhesion and activation and decreased thrombin generation with fucoidan modified PVA. The modification proved to be compatible with gamma sterilization. *In vivo* evaluation of fucoidan modified PVA grafts in rabbits exhibited increased patency rate, endothelialization, and reduced intimal hyperplasia formation.

3.1 Introduction

Vascular diseases remain the leading cause of death globally. Autologous artery or vein grafts are used to bypass or replace occluded blood vessels to restore blood flow, but their availability is limited. Synthetic vascular grafts have been an alternative to autologous grafts for a long time and benefited millions of patients. Commercially available synthetic vascular grafts, such as ePTFE and Dacron®, showed satisfactory long-term performance for larger diameter vessels (>6 mm), but displayed inferior performance in small-diameter applications (<6mm) [58-60]. Yet at small diameter, these synthetic grafts occlude either rapidly subsequent to surgery due to acute thrombosis formation or subsequently due to substantial intimal hyperplasia development in the lumen of vascular grafts and at the anastomoses sites, both of which were speculated to be caused by the lack of functional endothelial coverage [63, 64]. To improve endothelialization, surface modification of synthetic materials is frequently carried out with different strategies. Anticoagulant and antiplatelet coating and conjugations are the most common approaches. Trials using heparin on artificial graft materials have shown suppressed thrombin generation and improved patency rates in animal studies [100, 295, 296]. However, the hemorrhagic effect of heparin raises additional concerns.

Fucoidan has been extensively studied in the past decades for its various biological activities, including anticoagulant, anti-inflammatory, antioxidant, and anticancer properties [297-299]. Despite anticoagulant and antithrombotic activities similar to heparin, fucoidan does not cause hemorrhagic effects [107], making it a promising alternative to heparin. Furthermore, the potentials in promoting endothelial cell growth [300] and suppressing smooth muscle cell proliferation [243] combine to make fucoidan a promising surface modification molecule for synthetic vascular grafts.

Sodium trimetaphosphate (STMP)-crosslinked PVA has tunable mechanical properties that can match native blood vessels [11, 166]. However, the main barrier for developing PVA small diameter vascular grafts is the absence of endothelialization on PVA due to the hydrophilicity and lack of cell binding sites. Our group and other groups have been investigating surface modification strategies to improve the endothelialization of PVA, including plasma treatment [174, 301], surface topographical patterning [16], and peptide and protein coating [168, 169, 171]. However, developing a modification method that both improves endothelialization and maintains a non-thrombogenic surface is still challenging.

In this chapter, we hypothesized that modification of PVA with fucoidan could improve endothelialization without compromising the desirable blood compatibility of PVA. Previous studies using fucoidan to promote endothelialization required the presence of supplementary molecules, such as growth factors and extracellular proteins, or some required multi-layer coating to achieve best performance [237, 302, 303]. Our current study employed fucoidan alone without any supplementary molecules, and the modification was carried out with a mild and simple procedure by mixing fucoidan in aqueous PVA solution followed by STMP crosslinking in ambient conditions. Human vascular endothelial cell adhesion and function on fucoidan modified PVA were studied by characterizing cell density, cell monolayer formation, and cell marker expression. Platelet adhesion, activation, and thrombosis were assessed *in vitro* using rabbit blood and *ex-vivo* in a non-human primate shunt model. Furthermore, we tested the *in vivo* performance of fucoidan modified small diameter PVA grafts in a rabbit carotid artery model. *In situ* endothelialization, patency rate, and restenosis of the grafts were analyzed. Overall, the study highlights the potential of the fucoidan modification to improve endothelialization without compromising the hemocompatibility.

3.2 Materials and methods

3.2.1 Preparation of PVA hydrogels

PVA hydrogels were prepared as previously published [16]. In brief, an aqueous solution of 10% PVA solution was prepared by dissolving PVA powder (average Mw 85,000-124,000, 87%-89% hydrolyzed, Sigma-Aldrich) in deionized (DI) water, followed by autoclaving at 121 °C for 20 min to facilitate dissolving. To crosslink PVA, 15% (w/v) STMP solution was mixed with 10% PVA solution, and 30% (w/v) NaOH was added dropwise to activate the functional groups of PVA and STMP. The obtained solution was either cast on petri dishes to form PVA films or dip-coated on cylinder molds to form tubular grafts. PVA films and tubular grafts were then kept in a cabinet with controlled temperature (20°C) and humidity (60%-70%) until fully crosslinked. Solutions of 10X phosphate buffer solution (PBS), 1X PBS, and DI water were used to rehydrate and de-mold crosslinked PVA hydrogels.

To modify PVA hydrogels, fucoidan (crude, from *Fucus vesiculosus*, Sigma-Aldrich) was mixed with 10% PVA solution (PVA:fucoidan = 30:1 (w/w)) prior to adding STMP and stirred for 24 hours to homogenize. The fucoidan-PVA mixture was then co-crosslinked by STMP as described above (PVA-F).

3.2.2 Sterilization of PVA hydrogels

PVA and PVA-F tubular grafts were sterilized by gamma irradiation before implantation. The gamma sterilization was done at Southern Ontario Centre for Atmospheric Aerosol Research in University of Toronto. The irradiation was carried out with a Co-60 source (G.C. 220) at a dose of 25 kGy.

3.2.3 Scanning electron microscope (SEM) measurement

The PVA and PVA-F samples were dried overnight and mounted on aluminum stubs and imaged by an environmental scanning electron microscope (FEI Quanta FEG 250 ESEM) with energy dispersive X-ray (EDX) microanalysis in high vacuum mode at 20 kV. No coating was applied prior to imaging.

3.2.4 Static water contact angle (WCA) measurement

Water contact angle of PVA and PVA-F films were measure with a JC2000D3 contact angle meter. A 2 µl water drop was deposited onto the hydrated PVA films, and images were captured after the droplet remained stable on the PVA surfaces. The angle value was calculated using ImageJ.

3.2.5 Fucoidan concentration determination

The density of fucoidan on PVA-F films were determined using a metachromatic dye, toluidine blue O (TBO) (Sigma-Aldrich), adopted from a previous published procedure[304]. 1 cm^2 films of PVA and PVA-F were immersed in 500 µl of TBO solution with a concentration of 50 µg/ml and shaken for 1 hr. The absorbance at 631 nm of the supernatant was then measured using Synergy 4 multi-detection microplate reader (BioTek). To quantify the density of fucoidan on PVA-F samples, a calibration curve (as shown in **Fig 3-1**) was generated from free fucoidan solutions with a concentration range from 1.0 µg/ml-1.0 mg/ml. Hexane was added to the free fucoidan solution to remove the fucoidan-toluidine blue complex from the aqueous phase before reading the absorbance. To evaluate stability of the modification, PVA-F samples were stored in PBS at 37 °C for 15 days, 30 days and 60 days, and the density of fucoidan was compared against freshly prepared PVA-F samples.

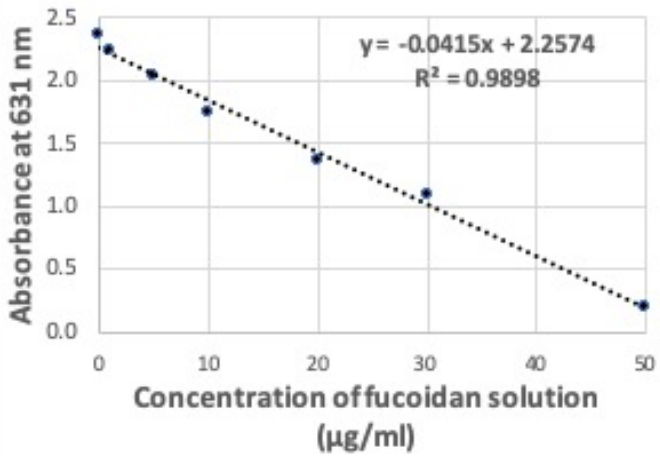


Figure 3-1. Absorbance of Toluidine blue staining at 631 nm with different concentration of free fucoidan solution.

3.2.6 Crosslinking density measurement

Crosslinking density of PVA and PVA-F hydrogels was determined by measuring phosphate concentration with a phosphate assay kit (Abcam). Briefly, around 200 mg of the hydrogel was degraded in 10% nitric acid at 105°C for 1 hour. The solution was diluted with double distilled water. An aliquot of 200 µl sample was then mixed with 30 µl phosphate reagent and incubated for 30 min at room temperature protected from light. The phosphate concentration was measured at 650 nm wavelength using different concentrations of phosphoric acid solutions as standards.

3.2.7 Water content measurement

Hydrated PVA and PVA-F hydrogels were weighed to get initial weight, W_H. The samples were then dehydrated in 60°C oven until reaching stable weight, W_D. The water content was determined by equation: Water content = $(W_H-W_D)/W_H\times100\%$.

3.2.8 Mechanical property test

Compliance test of PVA and PVA-F grafts was carried out by measuring outer diameter change of the grafts at 80 mmHg (D_{80}) and 120 mmHg (D_{120}) internal pressure. Grafts were clamped at one end and the other end was connected to a bag of saline solution through a catheter. The inner pressure of 80 mmHg and 120 mmHg were achieved by changing the height of the saline bag. The diameters of the graft with different inner pressures were measured and the compliance was calculated by Compliance (%/40mmHg) = $(D_{120}-D_{80})/D_{80}\times100\%$. Burst pressure was measured by exposing the grafts to increasing intramural pressure until failure. A segment of the graft was clamped at one end and the other end was linked to a nitrogen gas cylinder through a catheter. A pressure regulator was used to control the pressure supply. Uniaxial tensile tests were measured using a Universal Mechanical Tester (UNMT-2MT, T1377, Center for Tribology, Inc.) at an extension rate of 10 mm/min with a load cell of 10 kg for circumferential test and 100 kg for longitudinal test. The cross-sectional area of the sample was measured by ImageJ.

3.2.9 Endothelial cell adhesion and function assay

Human umbilical vein endothelial cells (HUVECs, passage 3-5, Lonza) were maintained in EGM-2MV medium (Lonza) and seeded on PVA, PVA-F, and glass coverslips with a seeding density of 50,000 cells/cm^2. Cells were cultured for either 2 days until confluent for cell functional marker staining or 24 hours until sub-confluent for extracellular matrix (ECM) protein staining. Cells were fixed with 4% paraformaldehyde (PFA), permeabilized with 0.1% Triton X-100, and blocked with 5% goat serum and 0.3% Triton X-100. Following blocking, the cells were immune-stained with platelet endothelial cell adhesion molecule (PECAM-1, mouse-anti-PECAM-1 at 1:100, monoclonal, Abcam, ab9498), vascular endothelial cadherin (VE-Cad, rabbit anti-VE-Cad at 1:100, polyclonal, Cell Signaling Technology, 2158S), endothelial NOS (eNOS, mouse anti-eNOS at 1:100, monoclonal, Abcam, ab76198), collagen IV antibody (rabbit anti-collagen IV at 1:100, polyclonal, Abcam, ab6586), or laminin antibody (rabbit anti-laminin at 1:100, polyclonal, Alfa Aesar, J65295) with the corresponding AlexaFluor labeled secondary goat antibodies, and counterstained with DAPI to label nuclei. Images

were taken using Zeiss fluorescence microscope (Axio Observer Z1) and analyzed using ImageJ software.

3.2.10 *In vitro* hemocompatibility test

In vitro hemocompatibility was performed on flat samples by incubating samples with rabbit platelet rich plasma (PRP) under orbital shaking condition. Briefly, blood samples were collected from healthy male New Zealand rabbits in polypropylene tubes and primed with 3.8% sodium citrate (1ml per 9 ml blood). Whole blood was centrifuged at 200 g for 10 min to collect PRP. 200 µl of PRP was then incubated on PVA and PVA-F samples for 1 h on an orbital shaker at 200 rpm. Glass coverslips, coated with 500 µl of 0.1 mg/ml bovine collagen type I, were included as positive control, while ePTFE grafts with carbon lining (CARBOFLO®, Bard) were cut open to expose the lumen and used as a negative control. Non-adherent PRP solution was subsequently collected for a real-time thrombin generation assay, while the adhered platelets on PVA samples were washed with ice-cold PBS to remove unattached red blood cells and platelets, and then kept for either SEM or a lactate dehydrogenase (LDH) assay.

Adhered platelets on PVA were fixed with 2.5% glutaraldehyde in PBS for 20 min, and then gradually dehydrated using increasing ethanol concentration. Dehydrated samples were left to dry at room temperature before SEM imaging. To quantify platelets adhered on PVA samples, adherent platelets were lysed with 1% Triton X-100 by incubating at 37°C for 1 hour. The lysate was analyzed with LDH kit (Roche) and the absorbance was measured with a microplate reader at 490 nm.

Realtime thrombin generation assay was done with Technothrombin® Thrombin Generation Assay (TGA) kit (Diapharma) according to the manufacturer's protocol. In brief, after a 1-hour incubation, PRP was collected and diluted with supplied buffer. 40 µl of PRP dilution was added into a 96 well plate, and 50 µl of supplied substrate was added to each sample to initiate the thrombin reaction. The supernatant fluorescence (390 nm/ 460 nm) was measured by the plate reader for 2 hours at 37°C. According to the thrombin generation curve, the starting time of the thrombin generation (Lagtime), maximum thrombin generation rate (Peak), and total amount of generated thrombin (ETP) were analyzed by the manufacturer provided software.

3.2.11 *Ex vivo* shunt assay

Ex-vivo hemocompatibility test was done on tubular samples with whole blood under flow condition in a non-human primate *ex-vivo* shunt model. PVA tubular grafts, 4 mm diameter and 5 cm in length,

were tested in a flowing, whole blood model of thrombosis as described previously [169]. Four juvenile, baboons (Papio Anubis) had a chronic, arteriovenous shunt with radiolabeled platelets and fibrin. The graft was placed between silicone tubing extensions to test over a Brivo NM615 nuclear imaging camera (GE) with 1 hour of blood flow, controlled at 100 mL/min without any antiplatelet therapies. Platelet accumulation was tested dynamically during this time while fibrin accumulation was quantified at the end of the study. Patency in the *ex vivo* shunt model was measured as described previously [305]. In brief, samples were fixed with 3.7% paraformaldehyde, rinsed, and rendered radiopaque. Samples were imaged using X-ray microcomputed tomography (microCT). Data was imported into Amira® and the luminal volume was quantified. This volume was divided by the sample length to give the average luminal area.

These studies were approved by the Oregon National Primate Research Center (ONPRC) Institutional Animal Care and Use Committee. Baboons were cared for at ONPRC according to the ‘‘Guide to the Care and Use of Laboratory Animals’’ prepared by the Committee on Care & Use of Laboratory Animals of the Institute of Laboratory Animal Resources, National Research Council (International Standard Book, Number 0-309-05377-3, 1996).

3.2.12 Implantation of fucoidan modified small diameter vascular grafts

Implantation of the small diameter vascular grafts was done as previously published [306]. Briefly, New Zealand White rabbits (male, weight 3.5-4.0 kg, Charles River laboratories) were anaesthetized by giving 400-800 ml/min oxygen and gas isoflurane (1-3%) through endotracheal intubation. Heparin (200 IU/kg) was given intravenously prior to arterial clamping. Segments (2 cm) of unmodified PVA grafts (n=5) and PVA-F grafts (n=6) with inner diameter of 1.7 mm (parameters are as shown in **Table 3-1**) were anastomosed onto the right carotid artery, with end-to-side anastomosis, using 8-0 Nylon suture (AD Surgical). Aspirin (15 mg/kg) was administered post-surgery until endpoint. ePTFE grafts (2 cm, n=4, Zeus) with 2 mm inner diameter were included as positive controls. Ultrasound doppler imaging and measurements were done using SonixTouch (Analogic Ultrasound, Peabody) and 10.0 MHz probe at midpoints (14 days) and endpoints (28-31 days) to detect blood flow and check graft patency. At endpoint, rabbits were euthanized with sodium pentobarbital (100 mg/kg). The grafts altogether with native arteries and corresponding left carotid arteries were explanted and fixed in 4% PFA for 72 hours. The fixed grafts were serially dehydrated, parafilm embedded, and sectioned in the middle of the grafts and at the proximal and distal anastomoses. H&E, immunohistochemistry and

immunofluorescence staining were carried out to measure luminal patent area, analyze intimal hyperplasia and detect endothelial cells, respectively.

All rabbit studies were approved (#AUPP 16-09) by the Animal Care Committee according to the Canadian Council on Animal Care's Guidelines, the requirements of Province of Ontario's Animals for Research Act, and the University of Waterloo's Guidelines for the Use of Animals in Research and Teaching.

3.2.13 Statistics

For ex vivo shunt study, PVA samples (n=4-8 per group) were tested along with a collagen-coated expanded polytetrafluoroethylene (ePTFE, n=2) positive control and a clinical ePTFE control (W.L. Gore, n=2). Platelet data were analyzed using a multi-way repeated measures linear mixed effects model against PVA type and time. In order to increase model precision a fractional polynomial term (time × ln(time)) and all relevant interactions were added as model fixed effects. Fibrin data were tested for normality using a q-q plot and homogeneity of variance with a Levene's test. After determining that these data failed these ANOVA assumptions, fibrin and platelet data were natural log transformed, with 0.01 added to each value to avoid exclusion of any zero values. Luminal patent area was analyzed with a one-way ANOVA to compare only the three PVA test samples.

Other statistical analysis was performed using GraphPad Prism 7. The values of all data were presented as mean ± Standard Deviation (SD). To determine statistical significance, t-test, one-way ANOVA test with Tukey's *post hoc* test and two-way ANOVA with Sidak's *post hoc* test were used. Statistical significance criterion was set at p value of <0.05.

Table 3-1. Parameters and mechanical properties of implanted ePTFE, PVAg, PVA-Fg grafts and rabbit common carotid arteries (Rb CCA). Human saphenous vein (SV) and internal thoracic artery (ITA) were included as clinical comparisons.

	Outer diameter (mm)	Inner diameter (mm)	Wall thickness (mm)	Compliance (%/40mmHg)	Burst pressure (mmHg)
ePTFE	2.09±0.05	2.07±0.05	0.13±0.04	0.70±0.18	-
PVAg	2.08±0.06	1.70±0.05	0.39±0.05	1.26±0.17	780±71

PVA-Fg	2.10±0.07	1.71±0.08	0.40±0.09	1.59±0.52	906±76
Rb CCA	-	2.00±0.31 [307]	~0.22 [308]	2.57±0.04 [309]	-
Human SV	4.2±0.6 [310]	-	0.45 [310]	8.8±4.2%/100 mmHg [311]	1599±877 [311]
Human ITA	-	2.05-2.19 [312]	0.50-0.51 [313]	11.5±3.9%/100 mmHg [311]	3196±1264[311]

3.3 Results

3.3.1 Characterization of fucoidan modified PVA hydrogels

The fucoidan modification of PVA was achieved by mixing fucoidan into PVA solution and co-crosslinked by STMP, as shown in **Fig 3-2A**. SEM images showed the structures on the surface of PVA and PVA-F hydrogels (**Fig 3-2B**). The unmodified PVA hydrogels had a smooth surface, while PVA-F hydrogels exhibited irregular structures on the surfaces. Surface energy of PVA and PVA-F was determined by measuring static water contact angle. PVA-F surface showed a slightly lower water contact angle possibly due to the hydrophilicity of fucoidan (**Fig 3-2C**). The presence of fucoidan on PVA-F was visually verified from the purple color change of toluidine blue staining, as shown in **Fig 3-2D**. Fucoidan density on PVA-F samples was quantified to be an average of 53.4±2.0 μg/cm^2. PVA-F films were stored in PBS at 37°C for up to 60 days to determine to stability of fucoidan modification. Fucoidan density after incubation for 15 days, 30 days and 60 days was 43.5±15.4 μg/cm^2, 42.2±12.4 μg/cm^2 and 36.8±5.5 μg/cm^2, respectively. No significant differences of fucoidan density were observed over time ($p=0.3025$) (**Fig 3-2E**). EDX was also carried out to analyze the element composition on PVA-F samples. The atomic percentage of sulfur is 0.12±0.03%, confirming the presence of fucoidan (**Fig 3-2F**).

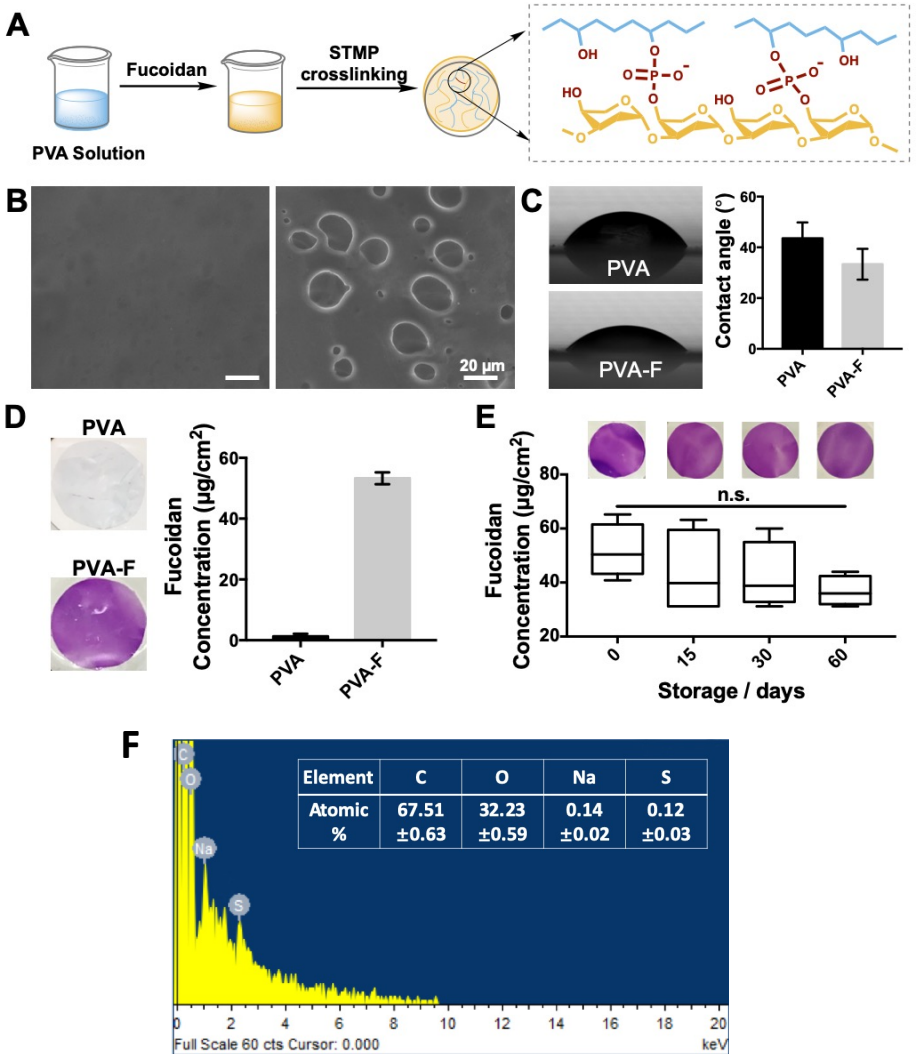


Figure 3-2. (A) Schematic diagram of polyvinyl alcohol-fucoidan (PVA-F) preparation procedure. (B) Scanning electron microscopy (SEM) images showed the structures on PVA (left) and PVA-F (right) surfaces. (C) Static water contact angle of PVA and PVA-F surfaces. (n=6, p=0.0554). (D) Fucoidan density on PVA-F samples was determined by toluidine blue staining. (E) Stability of fucoidan modification was determined by toluidine blue staining at day 0, 15, 30 and 60. n=3, no significant decrease was observed. (F) EDX spectrum of PVA-F samples showed sulfur element, confirming the presence of fucoidan. The table shows the atomic percentage of carbo, oxygen, sodium and sulfur and SD (n=3).

3.3.2 Biomechanical properties of fucoidan modified PVA hydrogels

PVA-F showed significantly higher phosphate content (**Fig 3-3A**), indicating a significantly higher chemical crosslinking density. Water content of PVA-F hydrogels (66.07±1.69%) was not significantly different from unmodified PVA hydrogels (64.27±2.22%) (**Fig 3-3B**).

Mechanical properties of PVA and PVA-F hydrogels were characterized. Compliance was determined *in vitro* by measuring the diameter increase of PVA and PVA-F tubular grafts from 80 mmHg to 120 mmHg internal pressure. PVA and PVA-F grafts had a compliance of 1.63±0.15 (%/40 mmHg) and 1.73±0.10 (%/40 mmHg), respectively (**Fig 3-3C**). With higher crosslinking density, PVA-F hydrogels were significantly stronger with a burst pressure of 831.50±75.43 mmHg, while unmodified PVA hydrogels had a burst pressure of 752.55±56.16 mmHg (**Fig 3-3D**, $p<0.05$, n=3). The tensile Young's modulus of PVA and PVA-F hydrogels were measured in both longitudinal and circumferential directions. Longitudinal Young's modulus for PVA hydrogels was 1.28±0.25 MPa and was increased to 1.57±0.29 MPa for PVA-F hydrogels (**Fig 3-3E**). Similarly, the circumferential Young's modulus was higher for PVA-F hydrogels (1.22±0.09 MPa) compared to PVA hydrogels (1.08±0.03 MPa) (**Fig 3-3F**), and a significant increase was observed ($p<0.05$, n=3).

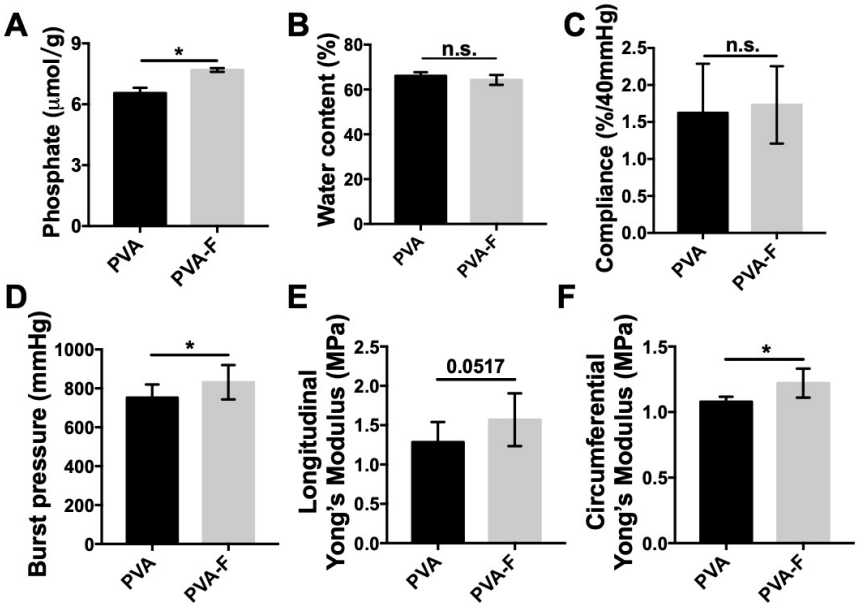


Figure 3-3. Mechanical properties of PVA and PVA-F samples. (A) Crosslinking density of PVA-F samples is significantly higher than PVA samples (n=5). (B) Water content of PVA and PVA-F hydrogels (n=3). (C) Compliance of PVA and PVA-F samples (n=3). (D) Burst pressure of PVA and

PVA-F samples (n=5). (E) Longitudinal tensile Young's modulus of PVA and PVA-F samples (n=3). (F) Circumferential tensile Young's modulus of PVA and PVA-F samples (n=3). * denotes statistical significance using t-test with $p < 0.05$, n=3.

3.3.3 Endothelial cell adhesion on fucoidan modified PVA hydrogels

To evaluate the potential of PVA-F hydrogels for endothelialization, HUVECs adhesion on PVA, PVA-F, and glass coverslips was analyzed. HUVECs exhibited good attachment and spreading and formed confluent monolayers on PVA-F hydrogels and glass coverslips, while only few cells were attached on unmodified PVA hydrogels and failed to form monolayers (**Fig 3-4A and Fig 3-5**). The cell density on PVA-F hydrogels (816 ± 217 cells/mm^2) was significantly higher than that on unmodified PVA (48 ± 16 cells/mm^2, $p<0.0001$), and was comparable to that on glass (965 ± 80 cells/mm^2, $p=0.3076$) (**Fig 3-4B**).

HUVECs on all substrates were immuno-stained with CD31, VE-Cadherin, and eNOS to examine the cell monolayer function. As shown in **Fig 3-4A** and **Fig 3-5**, strong eNOS expression was presented from cells on PVA-F and glass coverslips. The CD31 and VE-Cadherin were expressed strongly at the cell boundaries of the HUVECs on PVA-F and glass coverslips, while only in the cell cytoplasm on unmodified PVA. The quantification of protein expression of HUVECs on PVA-F and glass coverslips was as shown in **Fig 3-4C**, cells on unmodified PVA were not taken into calculation due to low cell numbers. Cells on PVA-F showed similar CD31 and VE-Cadherin expression levels as those on glass, the eNOS expression on PVA-F was significantly higher than on glass ($p<0.05$). Extracellular matrix protein, collagen IV and laminin, produced by HUVECs were also stained and as shown in **Fig 3-4D**. Both collagen IV and laminin were deposited by HUVECs on PVA-F, and the expression levels of both proteins was similar to those on glass coverslips (**Fig 3-4E**).

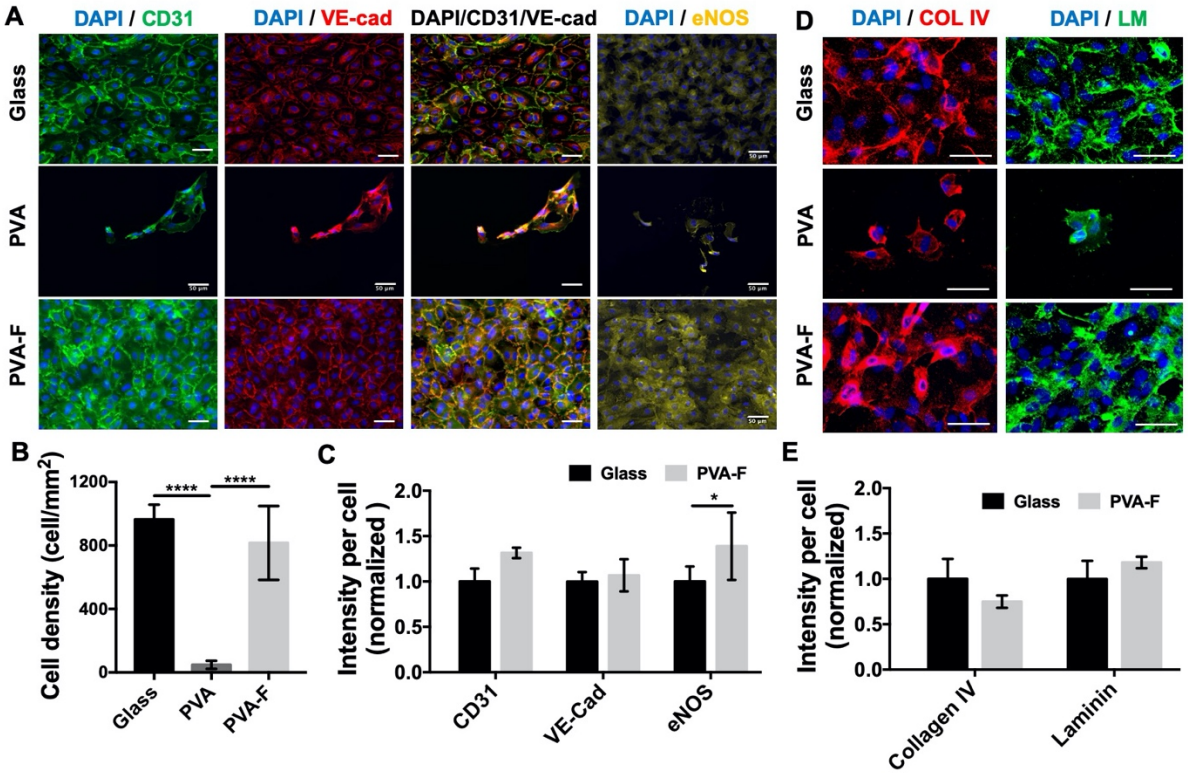


Figure 3-4. Endothelial cell adhesion on PVA and PVA-F samples. (A) Representative fluorescence images of human umbilical vein endothelial cells (HUVECs) on PVA and PVA-F samples after 48 hr culture. Scale bar = 50 µm. (B) Average cell density on PVA and PVA-F samples. **** denotes statistical significance using one-way ANOVA with $p < 0.0001$, n=5. (C) CD31, VE-cadherin and eNOS expression of HUVEC monolayer on PVA-F samples (data normalized to glass). HUVECs on glass cover slip were included in analysis as a positive control. HUVECs on PVA samples were not taken into analysis. * denotes statistical significance using t-test with $p < 0.05$, n=5. (D) Representative fluorescence images of collagen type IV (COL IV) and laminin (LM) deposited by HUVECs on PVA and PVA-F samples after 24 hr culture samples (data normalized to glass). HUVECs on glass cover slip were included in analysis as a positive control. Scale bar = 50 µm. (E) Collagen type IV and laminin expression of HUVECs on PVA-F samples (data normalized to glass). HUVECs on PVA samples were not taken into analysis due to low cell number. No statistical significance was observed, n=3.

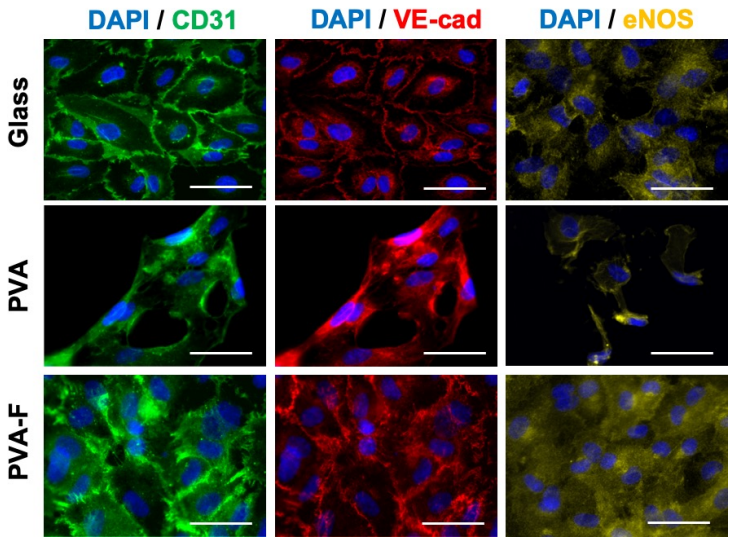


Figure 3-5. Representative images of human umbilical vein endothelial cells (HUVECs) on glass coverslips, PVA and PVA-F samples at a high magnification. (Scale bar =50 μm).

3.3.4 *In vitro* hemocompatibility of fucoidan modified PVA hydrogels

To examine the platelet behaviors on PVA and PVA-F hydrogels, we performed an LDH assay to measure the platelet adhesion and SEM to examine the morphology of attached platelets. The platelets on collagen coated glass were well spread, while the platelets on PVA and ePTFE were rounded (**Fig 3-6A**). More platelets were attached on PVA-F, and the platelets appeared to form more pseudopods compared with those on ePTFE and PVA. The LDH absorbance of collagen coated glass samples was significantly higher than ePTFE, PVA, and PVA-F, but no significant difference was observed among ePTFE, PVA, and PVA-F groups (**Fig 3-6B**). The results indicated that fucoidan modification did not increase platelet adhesion or activation.

Thrombogenicity of the PVA-F hydrogels was examined by a real-time thrombin generation assay. As the kinetic thrombin generation curved shows in **Fig 3-6C**, thrombin was generated at much faster rate and a larger amount on collagen coated glass compared to ePTFE, PVA, and PVA-F. The quantitative parameters, lagtime, peak, and ETP (**Fig 3-6D-F**) confirmed the observation in the kinetic curves. Collagen coated glass had a significantly shorter lagtime, higher peak thrombin generation, and more thrombin generation in total. Also, PVA-F had lower thrombin generation compared to PVA and ePTFE, though no statistical significance was observed.

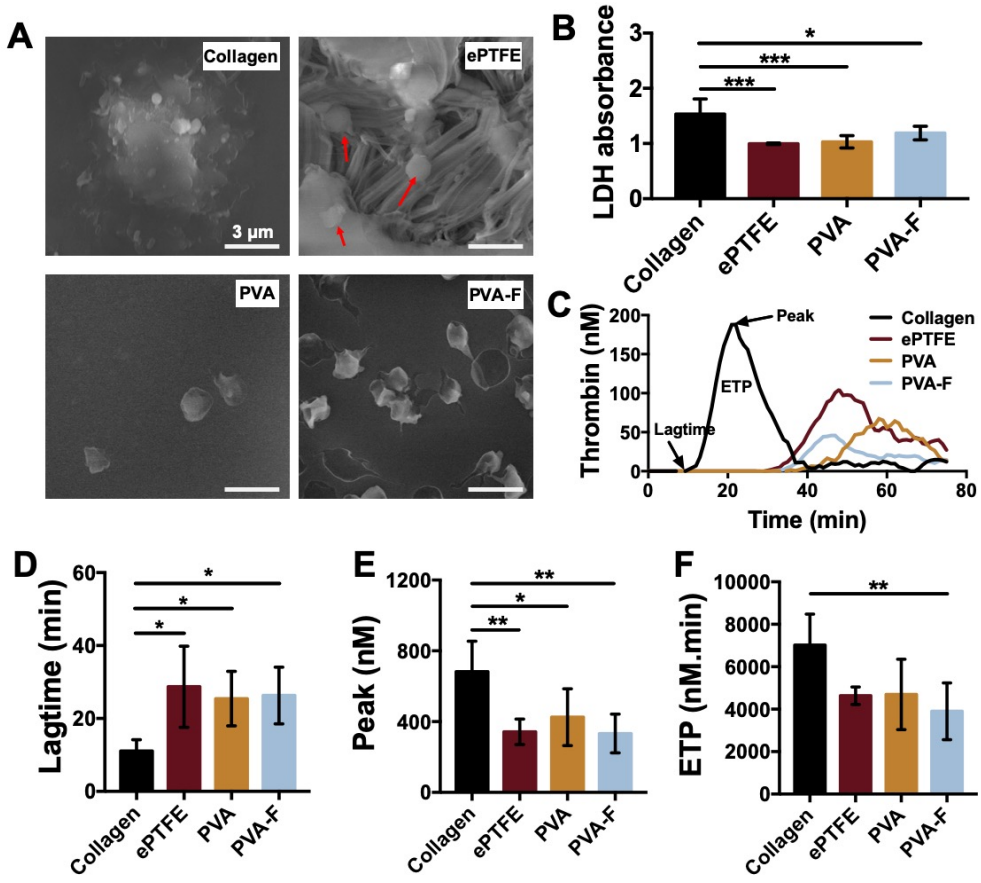


Figure 3-6. *In vitro* hemocompatibility tests of PVA and PVA-F samples. (A) Platelet adhesion and morphology on collagen coated glass cover (positive control), ePTFE (clinical control, platelets are as indicated with arrows), PVA and PVA-F. (B) Quantification of platelet adhesion determined by lactate dehydrogenase (LDH) assay. (C) Real-time thrombin generation assay. Lag-time (D) represents the time taken to start forming thrombin. Peak (E) represents the maximum thrombin generation rate. (F) represents endogenous thrombin potential (ETP). n=5, *, **and *** indicate a significant difference using one-way ANOVA with $p < 0.05$, $p < 0.01$, and $p < 0.001$, respectively.

3.3.5 Gamma sterilization of fucoidan modified PVA hydrogels

Sterilization is required for implantation. To examine if gamma irradiation would affect the fucoidan modified PVA hydrogels, we compared the compliance, water contact angle, cell adhesion, and thrombin generation of fucoidan modified PVA hydrogels before and after gamma irradiation.

Compliance, burst pressure and contact angle of both PVA and PVA-F grafts were not significantly changed after gamma irradiation (**Fig 3-7**).

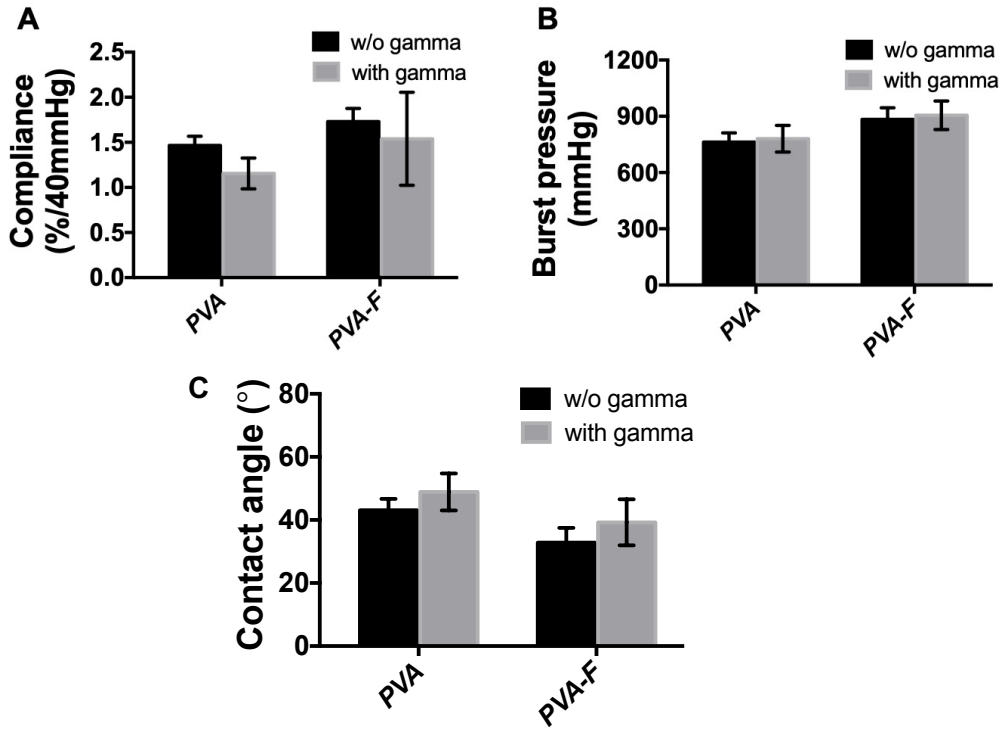


Figure 3-7. Compliance (A), burst pressure (B), and water contact angle (C) of PVA and PVA-F samples with and without gamma sterilization. No significant difference was observed among all groups of samples.

HUVECs attached well on both non-gamma treated (PVA-F) and gamma treated samples (PVA-Fg) (**Fig 3-8**), and the cell density was significantly higher on PVA-Fg samples (**Fig 3-9A**). Moreover, the expression levels of CD31 and eNOS from ECs on PVA-F and PVA-Fg showed no significant difference (**Fig 3-9B** and **C**). The gamma irradiation also did not significantly change the thrombin formation on both unmodified PVA and PVA-F samples (**Fig 3-9D-F**). Overall, the properties of PVA-F hydrogels were not significantly altered by the gamma irradiation.

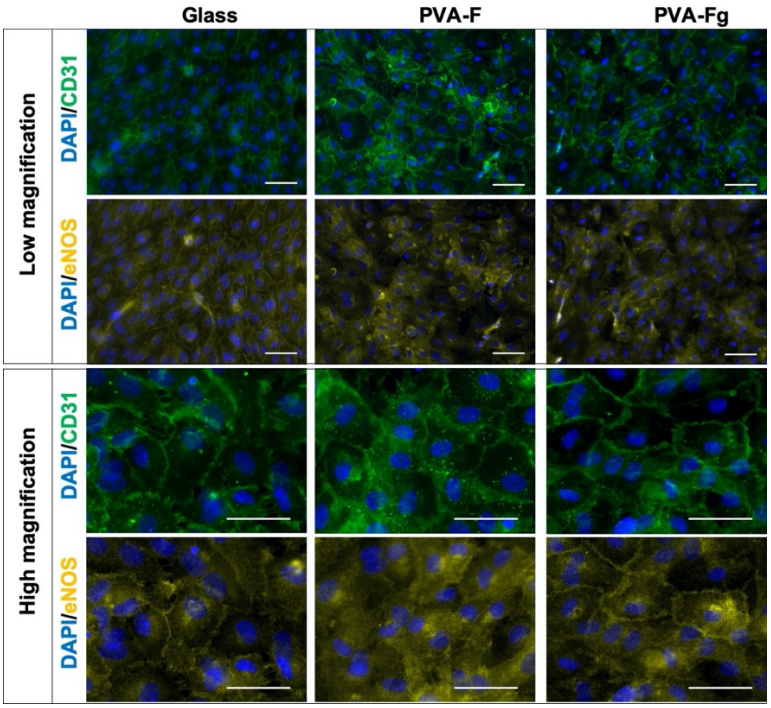


Figure 3-8. Representative images of HUVECs on non-gamma treated PVA-F and gamma sterilized (PVA-Fg) samples. Glass coverslips were included as positive control. (Scale bar =50 µm).

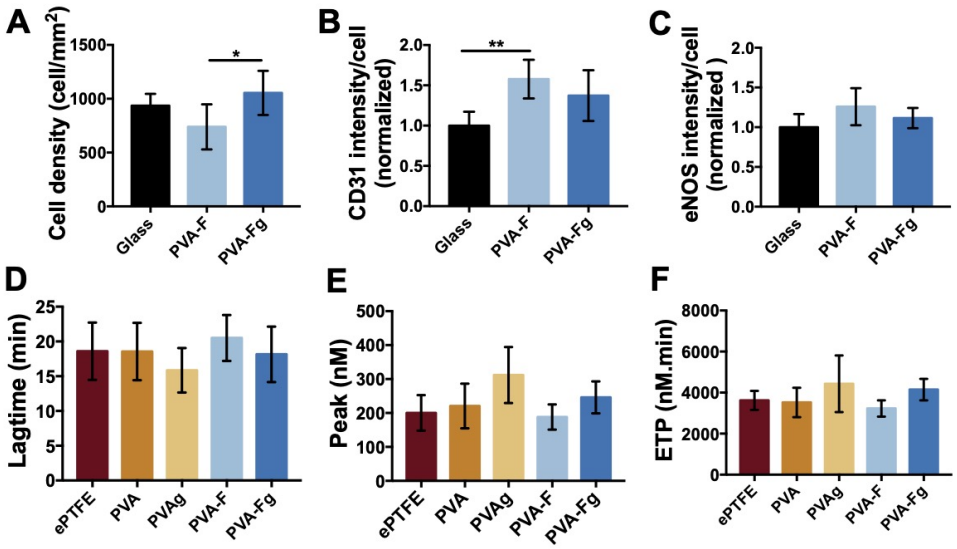


Figure 3-9. Gamma sterilization effect on PVA-F samples. (A) Average cell density on PVA-F samples non-treated (PVA-F) and gamma sterilized (PVA-Fg). CD31 (B) and eNOS (C) expression

of HUVECs on before and after gamma sterilized PVA-F sample (data normalized to glass). n=5, * and ** denotes statistical significance using one-way ANOVA with $p < 0.05$ and $p < 0.01$, respectively. Lagtime (D), Peak (E) and ETP (F) of real-time thrombin generation on non-treated and gamma sterilized samples (n=3).

3.3.6 *Ex-vivo* shunt study of fucoidan-modified PVA grafts

PVA, PVA-F, and PVA-Fg tubular grafts were tested in an *ex-vivo* baboon shunt model, with collagen coated ePTFE grafts and normal ePTFE grafts as controls. The platelets (**Fig 3-10A**) fibrin accumulation (**Fig 3-10B**), and average luminal patent area (**Fig 3-10C**) during the 1-hour testing period did not exhibit any significant differences, though there was a borderline insignificance in platelet accumulation among PVA, PVA-F and PVA-Fg groups (p=0.0523). PVA-F and PVA-Fg grafts had the lowest amount of platelet and fibrin accumulation, although after gamma sterilization, PVA-Fg had slightly increased fibrin accumulation, but still lower than PVA and the ePTFE control groups. PVA-Fg had the highest average luminal area.

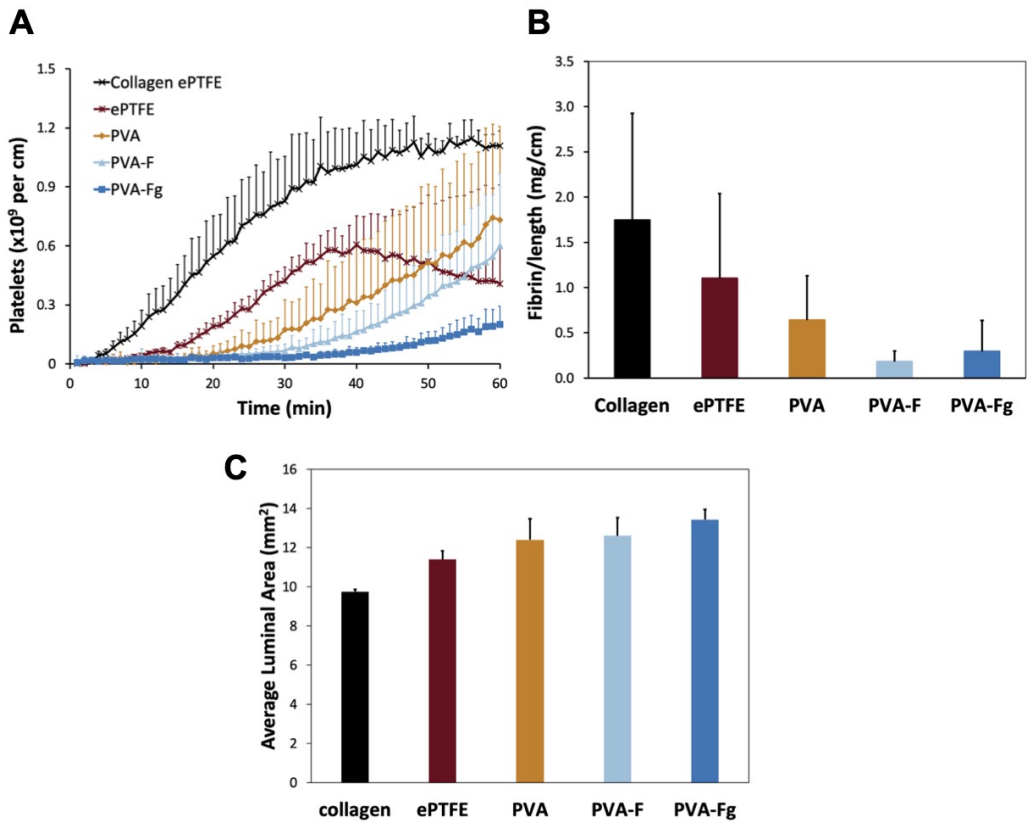


Figure 3-10. *Ex-vivo* shunt study. Platelet accumulation (A), fibrin accumulation (B) and average luminal patent area (C) data are displayed as mean ± SD for all samples. Collagen and ePTFE controls are shown for comparison but were not included in the statistical comparison due to low sample size. No significant differences were observed between the various PVA samples for the platelet (p=0.0523), fibrin (p=0.201 for the 1-way ANOVA), or patent area (p=0.109 for the 1-way ANOVA) data.

3.3.7 *In-vivo* study of fucoidan modified PVA small diameter vascular graft

Sterilized PVAg, PVA-Fg, and ePTFE grafts were implanted in a rabbit right carotid artery model with end-to-side anastomosis, as shown in Fig 3-11. The dimensions of the implanted grafts were shown in **Fig 3-12A**. The PVA and PVA-F grafts were 1.7 mm in diameter and 2 cm in length with curvature of 1.4 cm radius in the middle. The ePTFE grafts were straight with 2.0 mm in diameter and 2 cm in length. Parameters of the implanted grafts with comparisons to native arteries were shown in **Table 3-1**. The grafts were implanted in an end-to-side anastomotic technique, as shown in **Fig 3-12C**. After 1-month implantation, ePTFE (n=4), PVAg (n=5), and PVA-Fg (n=5) grafts had a patency rate of 75%, 40%, and 80%, respectively (**Fig 3-12B**). The ultrasound detection showed that PVA-Fg grafts still maintained strong flow after 1 month while PVAg grafts were either occluded or had minimal flow (**Fig 3-12D**). It was also observed that the blood flow inside ePTFE grafts had big animal variations (**Fig 12E**).

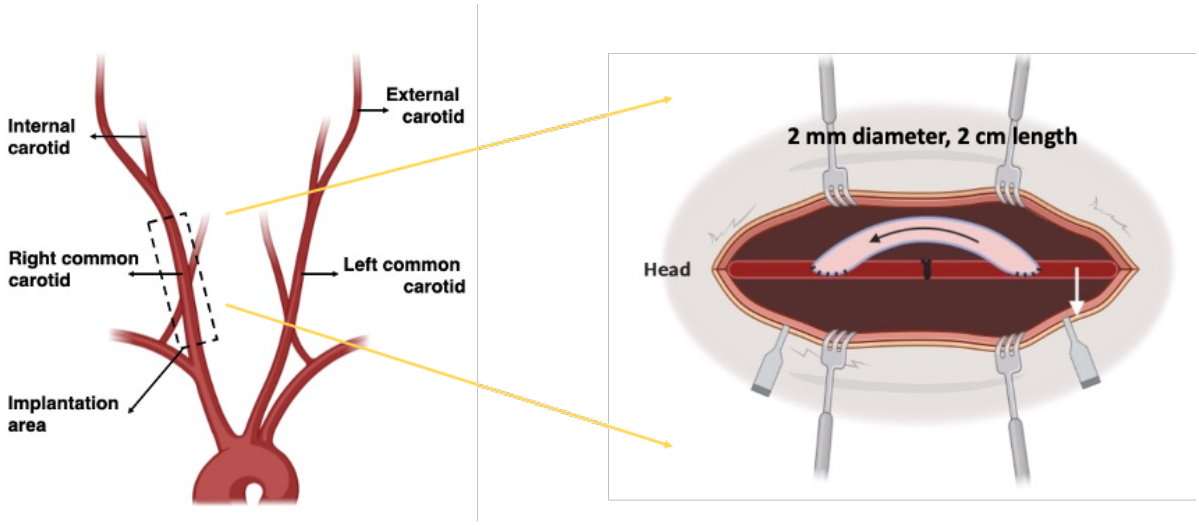


Figure 3-11. Implantation of PVA-based small vascular graft (2 mm in diameter and 2 cm in length) in rabbit right common carotid artery model with end-to-side anastomosis.

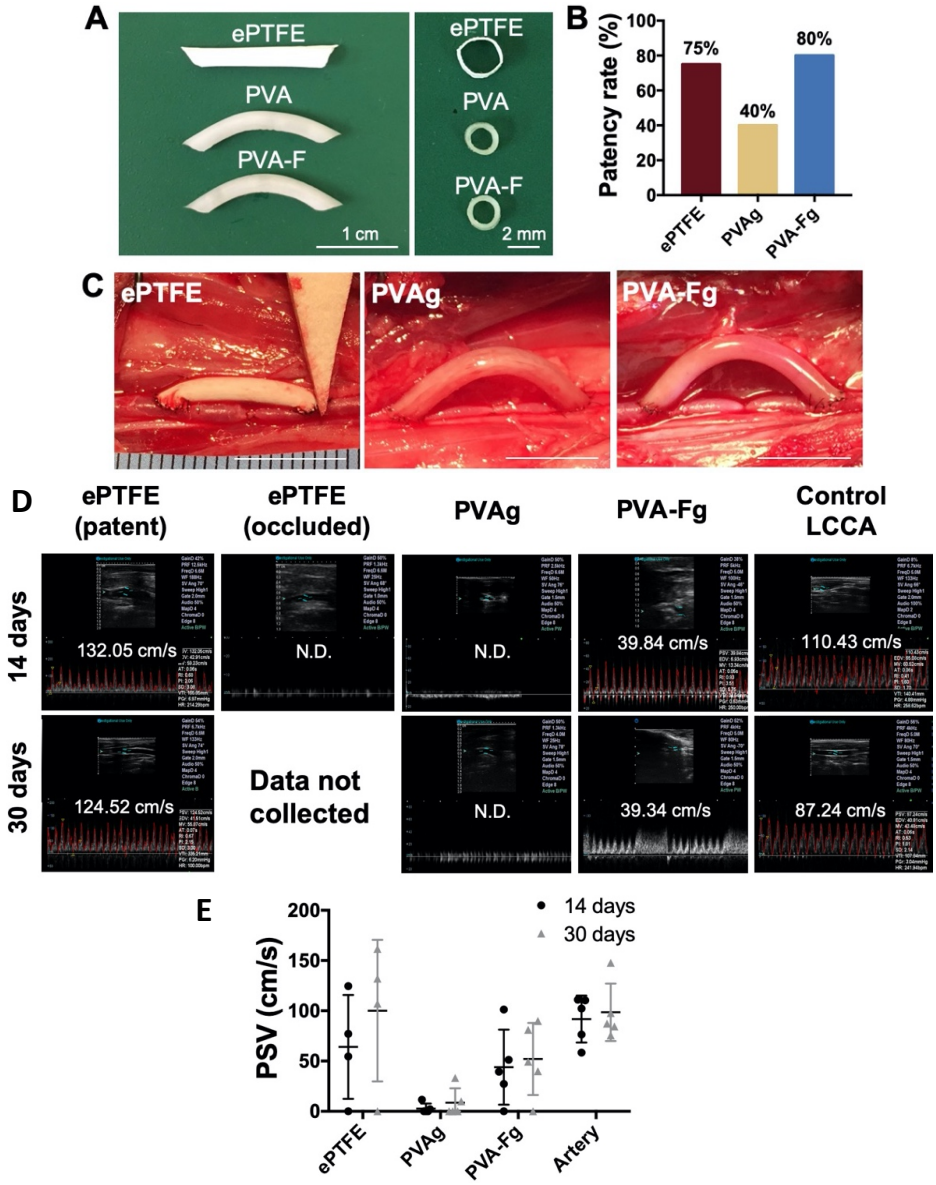


Figure 3-12. Implantation of ePTFE, PVAg, and PVA-Fg grafts. (A) Dimensions of implanted grafts. (B) Patency rate of ePTFE (n=4), PVAg (N=5), and PVA-Fg (n=5). (C) Representative images of ePTFE graft, PVAg graft, and PVA-Fg graft after implantation. Scale bar=1cm. (D) Ultrasound images of PVAg, PVA-Fg and ePTFE grafts and corresponded arteries and peak systolic flow

velocity inside the grafts and arteries after 14 days and 30 days implantation. (N.D. indicates not determined). (E) Peak systolic velocity (PSV) inside the grafts and arteries at day 14 and day 30. Non-detectable PSV was regarded as 0.

After 1 month of implantation, the grafts and contralateral native artery were harvested. The grafts were sectioned at the anastomotic sites (P and D) and the middle (M) as shown in **Fig 3-13A,** for H&E and immunofluorescent staining. As shown in **Fig 3-13B**, the PVA-Fg grafts had a layer of cells on the luminal surfaces, while no cells were presented on plain PVAg surfaces. Immunofluorescent staining showed that the cells on PVA-Fg lumen expressed endothelial cell marker (CD31 and eNOS), indicating endothelial cell coverage on PVA-Fg lumens (**Fig 3-13 C and D)**. Immunofluorescent staining of P,D, and M sections revealed the adhesion of endothelial cells at both anastomosis and in the middle of the graft (**Fig 3-14**). The ePTFE grafts used in this study had a porous structure, the CD31 and eNOS positive staining in ePTFE graft may likely have come from the endothelial cells trapped inside the porous structures.

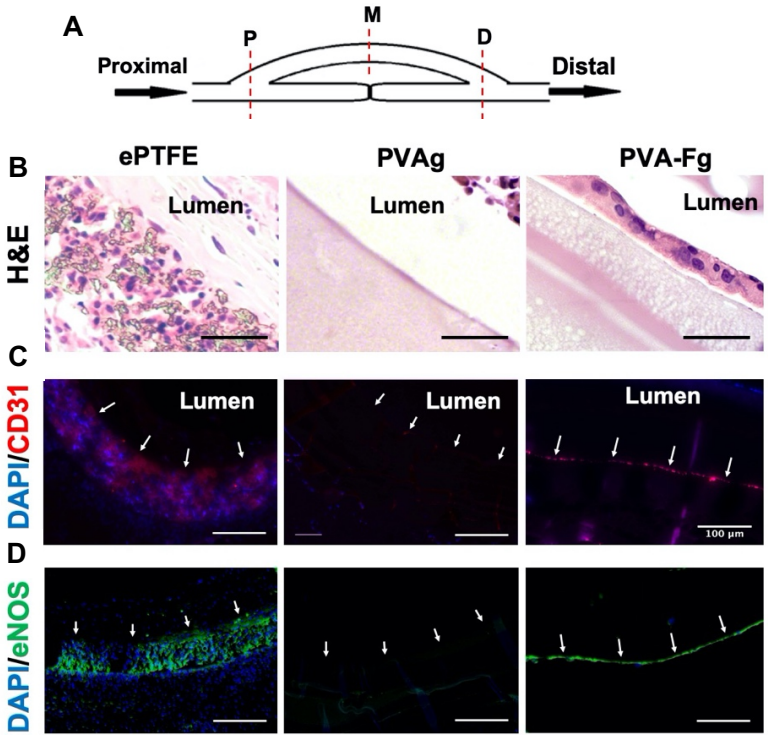


Figure 3-13. *In-vivo* endothelialization of PVA-Fg grafts. (A) Schematic diagram of sectioning positions of the grafts. (B) H&E staining of middle section of explanted vascular grafts. PVA-Fg showed a layer of cells on the luminal surfaces. Scale bar = 50 μm. (C) Immunofluorescence staining

of the middle section of explanted vascular grafts. Arrows indicate luminal surfaces. Scale bar = 100 μm. CD31 positive signals in PVA-Fg samples indicated the presence of endothelial cells. (D) Immunofluorescence staining of the middle section of explanted vascular grafts. Arrows indicate luminal surfaces. Scale bar = 100 μm. The eNOS positive signals indicated that the endothelial cells inside PVA-Fg samples expressed eNOS proteins.

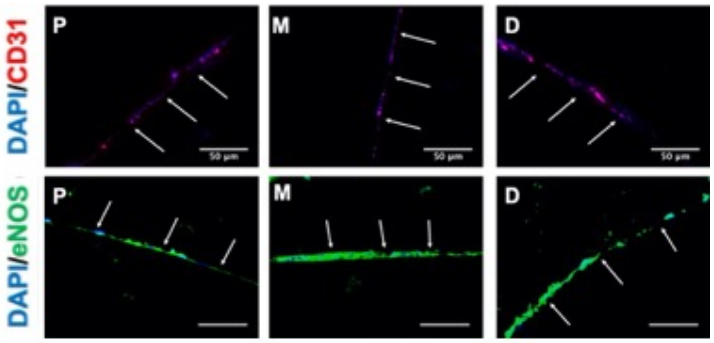


Figure 3-14. CD31 and DAPI staining showed endothelial cells at the proximal anastomoses (P) and distal anastomoses (D) and in the middle of the PVA-Fg graft (M). Arrows indicate luminal side of graft. (C) eNOS and DAPI staining showed the endothelial cells expressed eNOS. Arrows indicate luminal side of graft. Scale bar = 50μm.

The H&E stained cross-sections of the grafts were pictured (**Fig 3-15A**) and the stenosis percentage at the anastomotic junctions was quantified by dividing the area of stenosis to the luminal area of the grafts. PVA-Fg grafts showed a lower percentage of stenosis than PVAg grafts at both proximal and distal anastomotic sites, while the stenosis percentage for ePTFE grafts varied from 10% to 90% (**Fig 3-15B and C**). The intimal hyperplasia inside the lumens of ePTFE, PVA and PVA-F grafts all showed α-SMA positive staining (**Fig 3-15D**), which indicates the presence of smooth muscle cells in the intimal hyperplasia. Ki67 staining showed the presence of proliferating cells presented in the intimal hyperplasia, but the density of proliferating cells was low (**Fig 3-15E**). In general, the PVA-Fg grafts showed a better *in-vivo* performance than plain PVAg grafts and exhibited *in situ* endothelialization.

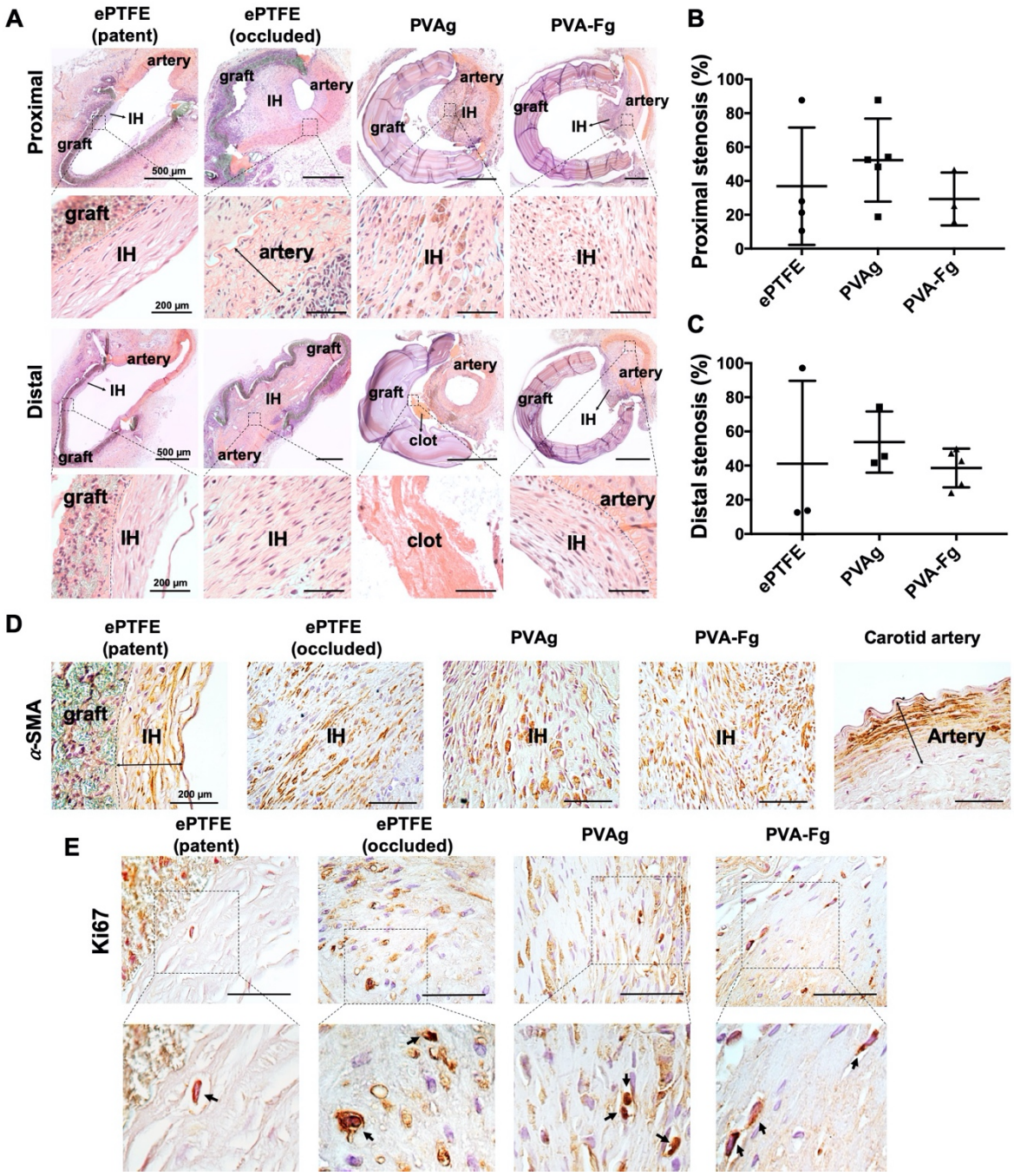


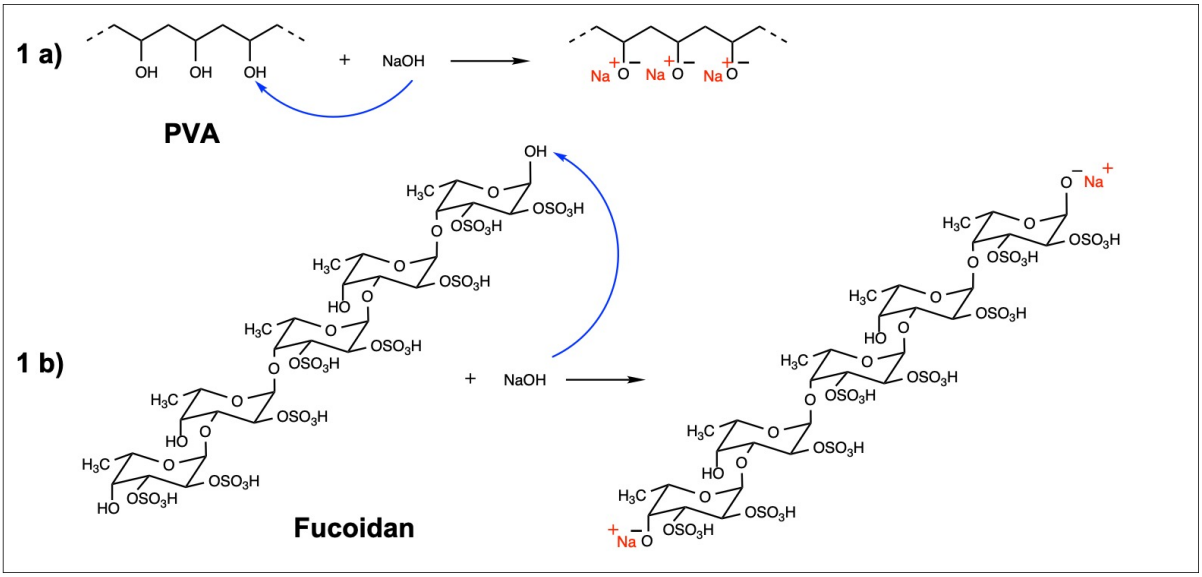
Figure 3-15. Proximal and distal anastomotic stenosis of ePTFE, PVAg, and PVA-Fg grafts. (A) Representative H&E staining images of patent ePTFE, occluded ePTFE, PVAg, and PVA-Fg grafts. IH indicates intimal hyperplasia. (B) Stenosis percentage of ePTFE, PVAg, and PVA-Fg grafts at proximal anastomoses. (C) Stenosis percentage of ePTFE, PVAg, and PVA-Fg grafts at distal anastomoses. (Graft sections with missing pieces were not taken into calculation.) PVA-Fg grafts

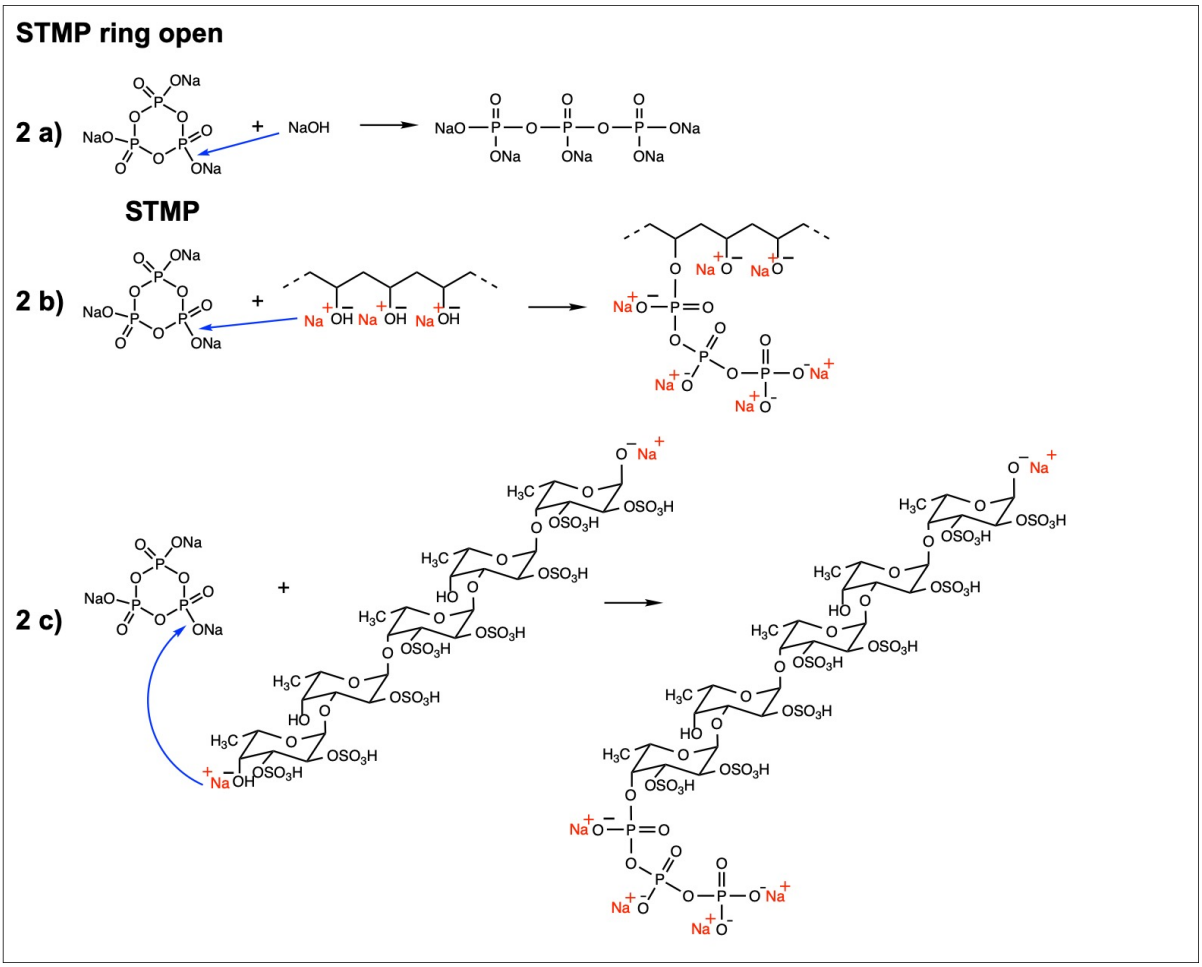
showed lower percentage of stenosis at both proximal and distal anastomosis than unmodified PVAg grafts. (D) α-SMA staining of patent ePTFE, occluded ePTFE, PVAg and PVA-Fg grafts confirmed the presence of smooth muscle cells in the intimal hyperplasia. Scale bar=200 μm. (E) Ki67 staining of patent ePTFE, occluded ePTFE, PVAg and PVA-Fg grafts showed the presence of proliferating cells, but in a low density. Scale bar=50 μm.

3.4 Discussion

Despite decades of development for synthetic vascular grafts, the performance of synthetic vascular grafts with diameters smaller than 6 mm is still disappointing due to the poor patency rate. One of the main reasons for failure is the lack of endothelialization of the synthetic materials, which leads to severe thrombosis formation and intimal hyperplasia formation. Surface modification of synthetic vascular grafts is required to reduce early-stage blood clotting formation and to enhance *in situ* endothelialization for long term patency. Proteins, such as ECM components, and anticoagulants, such as heparin, are frequently used molecules to encourage better vascular graft performance, however, these modifications both cause other complications [314, 315]. Many protein modifications improve the endothelial cell attachment but at the same time promote platelet attachment and activation [316-318], which further increases the chance of thrombus formation and graft occlusion. Coating and immobilizing heparin on synthetic vascular grafts has been shown to reduce platelet adhesion and thrombin generation [100, 105, 319, 320], but with the risk of hemorrhagic effect and heparin-induced thrombocytopenia [321, 322]. To develop a reliable modification, our work studied the ability of a fucoidan modification to promote endothelial cell adhesion and blood compatibility of PVA hydrogels. Fucoidan was chosen due to its ability to de-activate thrombin and inhibit thrombin generation without causing hemorrhagic effect [107, 194, 323]. Other studies also showed that hydrogels functionalized with fucoidan could dictate the release of vascular endothelial growth factors from the hydrogel and promote re-endothelialization [237, 302]. In our study, fucoidan was used to modify STMP-crosslinked PVA hydrogels. The fucoidan modification of PVA was achieved by simply mixing fucoidan with the PVA solution, and then crosslinked by STMP in the presence of NaOH. Due the viscosity of PVA solution and decreased solubility of fucoidan in a basic solution, the dispersion of fucoidan in PVA solution may not be even, and thus the generated PVA-F hydrogels had rougher surfaces compared to plain PVA. In addition, the difference of viscosity and solubility may have caused a change in the evaporation rate of water during PVA-F hydrogel fabrication, which would also lead to a rougher

surface [169]. We found that the surface structures of PVA-F samples were around 10-20 μm. Our previous study compared the cell adhesion on 10 μm pillars and lenses with unpatterned surfaces, and the cell adhesion did not show a significant difference [286]. Also, we found that topographies without other biochemical modifications do not support endothelial cells to form monolayers on PVA [16]. Thus, we speculate that the surface roughness of PVA-F was not a significant contributor to the improved endothelialization. Previous studies have shown that platelets and thrombogenicity can be manipulated by topographies with the same size range as platelets or below, and submicron sized pillars had more exhibit significant effects on platelet response [324]. Additionally, our previous studies using PVA/gelatin also observed uneven surfaces, but no significant difference of platelets adherent was observed [168]. Thus, we speculate that the surface roughness on PVA-MF samples did not significantly affect the thrombogenicity of PVA-MF samples. Modifications of hydrogels by mixing with functional molecules has been extensively studied [168, 171, 315], however, the main problem of physically mixing is the low stability. Slow leaching of the functional molecules from the grafts/scaffolds was shown [325] and will gradually decrease the activity of the biomolecule and change the mechanical properties of the material. To assess the stability of the fucoidan mixing modification presented in this study, we stored the PVA-F hydrogels for up to 2 months and measured the fucoidan density using toluidine blue staining. During the 2-month storage, minimal change of fucoidan concentration was found (**Fig 3-2E**). This is because that fucoidan was not only physically mixed into PVA hydrogels, but also chemically linked to PVA chain by the STMP crosslinking. STMP crosslinking of pullulan has been studied elsewhere, and the reaction mechanism has been proposed [163, 165]. Herein, we propose a similar crosslinking process as shown in **Fig 3-16**, and the phosphate assay proved the presence of phosphate crosslinking bonds in both PVA and PVA-F hydrogels (**Fig 3-3A**).


1 a)
NaOH
PVA
1 b)
NaOH
Fucoidan


STMP ring open
2 a)
NaOH
STMP
2 b)
2 c)

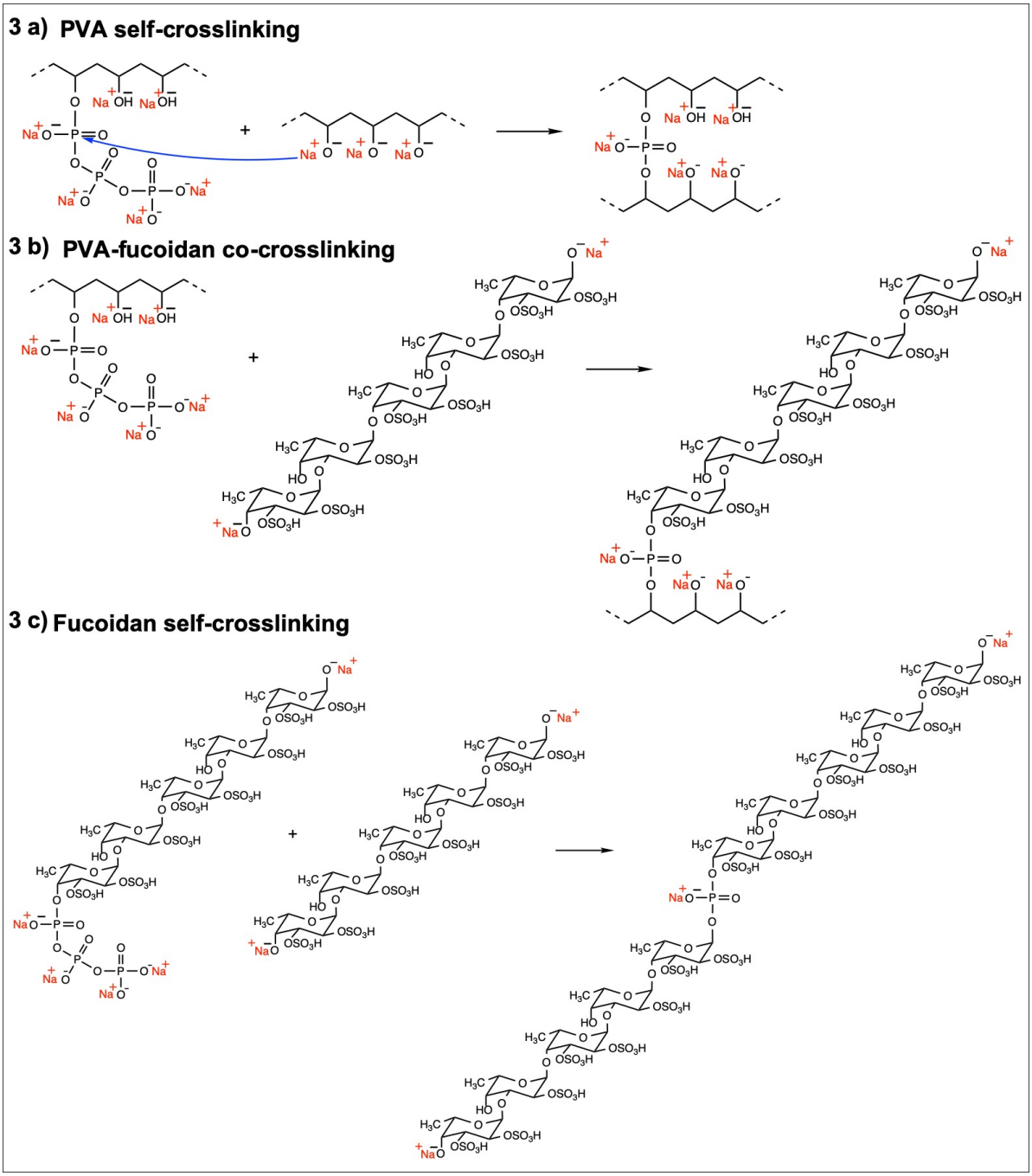


Figure 3-16. Proposed crosslinking process of PVA and PVA-F hydrogels by sodium trimetaphosphate (STMP).

One of the main advantages of the STMP-crosslinked PVA for small diameter vascular grafts is their tunable mechanical properties. According to our previous studies, by adjusting the crosslinking density and fabrication parameters, we were able to fabricate PVA grafts with compliance up to 4.00±3.41%/40mmHg [11, 166], matching that of rabbit carotid artery (3.1%/40mmHg) [326] and human brachial artery (1.3-3.3%/40mmHg) [327]. In this study, we examined the effect of fucoidan modification on the mechanical properties of PVA grafts. Results showed that the PVA-F grafts exhibited a higher chemical crosslinking density compared to plain PVA as measured by phosphate density, further proving that fucoidan is not only physically mixed into PVA, but also chemically crosslinked to PVA through STMP. The higher chemical crosslinking density of PVA-F also yielded stronger grafts with higher burst pressure (**Fig 3-3D**) and Young's modulus (**Fig 3-3E and F**). However, the compliance was not significantly altered by fucoidan modification (**Fig 3-3C**). Our recent study found that the compliance of PVA vascular graft was affected by the overall crosslinking of PVA [167]. During the fabrication procedure, STMP was used to chemically crosslink PVA and the residue OH groups in PVA chains could contribute to physical crosslinking of PVA. In this study, although chemical crosslinking density was increased after fucoidan modification, we did not see a significant difference in water content, which indicates that the overall crosslinking density may not be significantly altered. Additionally, the compliance of PVA vascular grafts fabricated with the lay-by-layer dip casting method could also be affected by the interlayer adhesive shear stress. The increase in interlayer adhesion could increase the burst pressure without sacrificing the compliance. The effect of fucoidan on the interlayer adhesive force will need to be further confirmed.

Unmodified PVA does not support cells adhesion, and our previous studies have tried different modifications, including plasma treatment [174, 301] and incorporation of proteins and peptides to enhance endothelial cell adhesion [168, 169, 171]. Fucoidan was previously found to stimulate endothelial proliferation and potentiated endothelial cell growth and migration with the presence of fibroblast growth factor-1 (FGF-1) [300]. Other studies also suggested that fucoidan binds to integrin $\alpha_M\beta_2$ and promotes the FGF-2-induced overexpression of integrin α_6 in human umbilical endothelial cells, which could further promote neovascularization [185, 328-330]. In this study, after modifying PVA with fucoidan, HUVECs displayed a substantially enhanced adhesion on PVA-F, while without modification, PVA had minimal cell attachment, which was consistent to our previous observations [16, 171]. HUVECs on PVA-F and glass coverslips had similar densities and showed cobblestone morphology. Other than adhesion and spreading, endothelial cells are required to form into a tight-knit and confluent monolayer to maintain its function as a semipermeable barrier. Platelets/endothelial cell

adhesion molecule-1 (PECAM1), also known as CD31, is expressed at endothelial cell-cell junctions, and is shown to be important to restore endothelial integrity [331]. Vascular endothelial cadherin (VE-cadherin) is an important type of adherens junctions, which is critical to control endothelial permeability and maintain cell-cell adhesion [332]. The HUVECs on PVA-F expressed strong CD31 and VE-Cadherin at the cell boundaries, indicating the integrity of endothelial cell monolayer. Endothelial nitric-oxide synthase (eNOS) is expressed in vascular endothelial cells and produces nitric oxide, which is known to regulate the vascular tone as well as smooth muscle cell proliferation [333]. HUVECs on PVA-F expressed eNOS, and the amount of eNOS is higher than HUVECs on glass cover slips. All of these cell marker expression measurements indicated that the HUVECs not only attached to the PVA-F surfaces, but also functioned as mature endothelial monolayers.

Hemocompatibility is an essential property of vascular grafts to prevent acute thrombosis formation after implantation. In our study, both *in vitro* and *ex-vivo* hemocompatibility tests were performed. *In vitro* hemocompatibility test was done with rabbit platelet rich plasma under shaking condition to prevent platelet aggregation and sedimentation. *Ex vivo* shunt study was done in a non-human primate model, which has similar physiology to human, to study the thrombogenicity of the grafts under physiological flow. PVA has low platelets attachment and low thrombin generation [168, 169], and fucoidan-modified PVA showed similar or slightly better hemocompatibility compared to plain PVA. We speculate that the good hemocompatibility was due to the ability of fucoidan to inhibit thrombin generation and platelets aggregation. Fucoidan has antithrombotic activity as tested in different *in vivo* models [107, 333]. It was found that the antithrombotic activity of fucoidan was mediated by heparin cofactor II [323], and fucoidan molecules inhibit thrombin generation by blocking the formation of intrinsic factor Xa [194]. Our real-time thrombin generation test observed slower and less thrombin generation on PVA-F compared to PVA samples (**Fig 3-6C-F**), supporting the antithrombotic activity of fucoidan. The fucoidan we used here is crude *fucus vesiculosus* fucoidan, with a molecular weight range from 20 kDa to 200 kDa and a sulfate content of 32% [334]. In previous studies, *fucus vesiculosus* fucoidan displayed anticoagulant properties, but did not prevent thrombin-induced platelet aggregation [177]. Durig et al. also found *fucus vesiculosus* fucoidan could induce irreversible platelet aggregation [335]. However, in our study, slightly more platelets were attached on PVA-F samples, but no platelet aggregation was observed (**Fig 3-6A**) after 1-hour incubation with rabbit platelet rich plasma. *Ex-vivo* shunt results in a non-human primate model also showed a low number of platelet and fibrin accumulation after 1-hour of whole blood flow with no antiplatelet or anticoagulant therapies (**Fig 3-10**).

Sterilization is required to remove micro-organisms before implantation, and gamma irradiation is one the most commonly used sterilization methods for biomaterial clinical use. Gamma irradiation is known to be able to cause chain scission [336], and studies also found that gamma irradiation could cause branching and crosslinking [337, 338], which combine to raise the concern that mechanical properties of the implants may be altered due to gamma sterilization. Our compliance and burst pressure measurement of PVA and PVA-F grafts before and after gamma sterilization did not show a significant difference (**Fig 3-7**). Previous studies also revealed that gamma irradiation changes the surface and biological properties of biomaterials [339, 340]. Srinivas *et al.*[339] found that gamma treated gels had a decreased surface hydrophilicity with increased dose, and cell adhesion and proliferation were found to be enhanced. A similar trend was observed from our PVA and PVA-F hydrogels. Although contact angle was not significantly increased (**Fig 3-7C**), HUVEC density on gamma treated PVA-F hydrogels was significantly higher than non-gamma treated samples (**Fig 3-9A-C**). Denizli *et al.* showed that gamma irradiation drastically increased the blood protein adsorption on polycarbonate films, which could increase the risk of thrombus formation and platelet accumulation and activation [341]. Our studies also showed that after gamma irradiation, the thrombin generation was slightly increased for both unmodified PVA and PVA-F (**Fig 3-9D-F**). *Ex-vivo* shunt study also exhibited a slightly higher fibrin accumulation on gamma treated PVA-F (PVA-Fg) compared to non-gamma treated PVA-F, however, the difference was not significant, and the accumulation level was still lower than plain PVA (**Fig 3-10**). Overall, the *ex-vivo* shunt results were in line with the *in vitro* hemocompatibility test results that fucoidan modification did not increase platelets activation and thrombin generation, and gamma sterilization did not significantly change the hemocompatibility of PVA-F samples.

After confirming the *in vitro* and *ex vivo* performance of PVA-F, *in vivo* performance of PVA-F grafts was evaluated in a rabbit right carotid artery model with an end-to-side anastomotic technique. Previous studies have shown that when positioned in rabbit carotid artery with an end-to-end anastomosis, ePTFE grafts had a failure rate of 11.2% in the first 2 weeks due to thrombotic occlusion, or lost patency after 16 weeks due to intimal hyperplasia formation [342, 343]. We observed similar results in our ePTFE implantation with end-to-side anastomosis. Occluded ePTFE was occluded by the time of first ultrasound detection at day 14, as shown in **Fig 3-12D**, which was caused by thrombus formation, while patent ePTFE remained good flow until the endpoint. Similarly, most unmodified PVA grafts occluded by day 14, which could also be due to the thrombus formation. Gamma sterilized PVA-F grafts (PVA-Fg) yielded a much higher patency rate (**Fig 3-12B**) and maintained a stronger flow after 1 month compared to PVAg grafts (**Fig 3-12D** and **E**), which could be benefitted from the

endothelial cell attachment (**Fig 3-13**). In addition to endothelial coverage on the surface, low intimal hyperplasia formation is also essential to maintain long term patency. The anastomotic junctions of graft and artery are prone to generate intimal hyperplasia due to the abnormal smooth muscle cell proliferation and migration. In our study, the majority of the cells in the intimal hyperplasia regions of all types of implanted grafts was identified as smooth muscle cells (**Fig 3-15D**), however, the Ki67 staining showed that most of the smooth muscle cells were not in proliferating state (**Fig 3-15E)**. Previous study reported the time course of cell proliferation in the intimal hyperplasia using an angioplasty model [344], and found out that the cellular proliferation in the intimal hyperplasia largely subsided by day 14 after injury, which was in line with our observation that there were low number of proliferating cells in the intimal hyperplasia at one month after implantation. Fucoidan was shown to be a potent inhibitor of smooth muscle cell proliferation through inhibiting mitogen-activated protein kinase pathway in a similar manner as heparin [239, 243]. In our study, PVA-Fg grafts had a lower stenosis percentage at both proximal and distal anastomoses compared to PVAg grafts (**Fig 3-15**), which could be attributed to the inhibition effect of fucoidan on smooth muscle cell proliferation at an early stage after implantation. ePTFE grafts are the gold standards for large diameter vascular grafts, however, ePTFE grafts with small diameters are not suitable due to the frequent intimal hyperplasia formation and blood clotting. The ePTFE grafts with 2 mm diameter were included in this study as clinical controls, and most of the ePTFE grafts showed strong blood flow after 1-month implantation. However, significant intimal hyperplasia was observed on the ePTFE grafts and the patency varied from sample to sample. It is worth mentioning that the ePTFE grafts we used for implantation have thinner wall and porous structure compared to other clinical available ePTFE grafts as shown in **Table 3-1**. Although the performance of PVA-F grafts and ePTFE grafts cannot be compared due to the differences in grafts size and wall thickness, the ePTFE grafts are still valuable clinical controls.

This study has demonstrated that the fucoidan modification was capable to improve endothelialization and hemocompatibility of PVA, and also enhanced the *in vivo* performance of PVA small diameter vascular grafts.

3.5 Conclusions

This chapter presented a fucoidan modification on PVA hydrogels to enhance endothelialization and hemocompatibility. The presence of fucoidan on PVA substantially improves the endothelial cell adhesion and coverage on PVA while maintaining the hemocompatibility of PVA. The *in vivo* test of the fucoidan modified PVA small diameter grafts exhibited promising results with a higher patency

rate and remarkably lower intimal hyperplasia formation. The results suggest the potential of fucoidan as surface modification molecule for small diameter PVA grafts as well as broader application to development of other vascular implants and devices.

Chapter 4

Development and Optimization of Fucoidan Conjugation for Enhanced Endothelial Attachment and Hemocompatibility

Bioconjugation is a useful technique to incorporate bioactive molecules to synthetic and natural materials. The study in this chapter developed a versatile fucoidan conjugation method for vascular graft application. Fucoidan and aminated fucoidan were conjugated to PVA hydrogels through carbonyldiimidazole (CDI) chemistry. The conjugation method was compared with other modification approaches for their effects on surface properties, endothelialization and hemocompatibility. Conjugation with aminated fucoidan on PVA significantly improved endothelial cell adhesion while maintaining low platelet adhesion, activation and thrombin generation. The conjugation method did not affect surface topography or mechanical properties. The amination of fucoidan was achieved using ethylenediamine (EDA), and the bioactivities of aminated fucoidan on endothelial cells and hemocompatibility can be optimized by adjusting EDA ratio. The performance of fucoidan conjugated PVA was also altered by the species of fucoidan source and amination methods of fucoidan. The developed fucoidan conjugation method can also be applied to ePTFE, and significantly improved the endothelial cell adhesion on ePTFE both *in vitro* and *in vivo*.

4.1 Introduction

Fucoidan is a sulfated polysaccharide with versatile bioactivities, such as anticoagulant, anticancer, and anti-inflammatory activities [178]. It has attracted broad research interests in pharmaceutical and biomedical areas. The bioactivities of fucoidan are modulated by various factors, including species of the source that fucoidan is isolated from, molecular weight, and chemical structures [345]. Increasing number of studies have identified the potential of fucoidan in cardiovascular applications. Fucoidan is capable of reducing leukocyte and platelet adhesion on dysfunctional or damaged endothelium [179], inhibiting thrombin generation [180], and inactivating free-radical processes [181]. These functions have been showed to alleviate atherosclerotic lesions. In addition, fucoidan exhibits endothelial protective function by reducing the expression of endothelial dysfunction marker, endothelin-1, and proinflammatory cytokines, TNFα and IFNγ [236]. Employing fucoidan as a surface modification molecule has also demonstrated the ability of fucoidan to improve endothelialization on synthetic and decellularized scaffolds [237, 238, 346]. Surface modification of fucoidan has been mainly achieved by coating. A fucoidan coated metal stent has shown inhibited smooth muscle cell proliferation and

reduced restenosis [347]. In addition, a layer-by-layer coating of fucoidan and laminin has shown reduced platelet adhesion and increased endothelial adhesion [238]. However, researchers found that the fucoidan coating could result in the changes of surface morphology of the material and even distribution of fucoidan molecules [348]. Furthermore, the short stability of the coating may limit the long-term storage and affect the long-term *in vivo* performance.

Surface conjugation of bioactive molecules on a synthetic material is another important surface modification approach in biomedical and tissue engineering applications. Reaction with carbonyldiimidazole (CDI) is a promising strategy for bioconjugation. CDI can activate carboxylic acid groups, hydroxyl groups and amine groups, forming imidazole active intermediates. These intermediates can further conjugate to other nucleophiles [349]. We have previously explored the CDI reaction between polyvinyl alcohol hydrogels (PVA) and amine-containing molecules [172, 350]. The success of the conjugation was evidenced by X-ray photoelectron spectroscopy and Fourier-transform infrared spectroscopy.

Inspired by these findings, in this study, we aim to develop a fucoidan conjugation modification through CDI reaction. We hypothesize that fucoidan can be presented to enhance endothelial cell attachment without affecting the hemocompatibility, surface topography or mechanical properties, and the methods to present fucoidan will significantly affect the surface chemistry and bioactivities for vascular endothelial cells and hemocompatibility. Fucoidan could be conjugated to PVA via its hydroxyl groups. In addition to the conjugation via hydroxyl group, conjugation via aminated group was also investigated. Fucoidan was aminated with ethylenediamine (EDA), and the effect of EDA was examined. Other methods to incorporate fucoidan on PVA, including mixing and coating, were studied and compared. Their effects on the surface property, endothelialization, and hemocompatibility of PVA were compared. Lastly, the conjugation of fucoidan was applied to ePTFE and the function of conjugated fucoidan on endothelialization of ePTFE was evaluated both *in vitro* and *in vivo*.

4.2 Materials and methods

4.2.1 Preparation of PVA hydrogels

Unpatterned PVA hydrogels were prepared as described in Section 3.2.1. Patterned PVA hydrogels were prepared as previously published [16]. Briefly, polydimethylsiloxane (PDMS; Sylgard 184, Dow Corning) with various topographies was used as molds for PVA hydrogels. All PDMS molds were treated with air plasma for 1 min to increase surface energy. To prepare patterned PVA films,

crosslinking PVA solution was casted on plasma treated PDMS molds and centrifuged at 1500 rpm for 1 hour. To prepared PVA tubular grafts, a thin layer of patterned PDMS film was rolled around a cylinder rod prior to plasma treatment. The cylinder rod was then plasma-treated and immersed in crosslinking PVA solution, followed by sonication for 1 hour at 49 kHz. Afterwards, crosslinking PVA solution was dip-coated on the cylinder rod to form tubular grafts. PVA films and tubular grafts were kept in cabinet with controlled temperature and humidity until fully crosslinked. Solutions of 10X phosphate buffer solution (PBS), 1X PBS, and DI water were used to rehydrate and de-mold crosslinked PVA hydrogels.

4.2.2 Amination of fucoidan

Amination of fucoidan using ethylenediamine (EDA, Sigma-Aldrich) was adopted from a previously published method [351]. Briefly, fucoidan (*Fucus vesiculosus*, Marinova) was aminated using ethylenediamine through carbonyldiimidazole (CDI, Sigma-Aldrich) reaction. Fucoidan (100 mg) was dissolved in 5 ml formamide, followed by the addition of 4 mg of CDI. After 1 hour of stirring, different amount of EDA was added into the mixture and reacted under stirring overnight. The solution was then dialyzed in 3500 Da cut-off dialysis tubes against DI water for 5 days at room temperature and freeze dried.

Amine group on fucoidan was determined using fluorescamine adopted from a previous protocol [351]. Briefly, 0.5 mg/ml aminated fucoidan was dissolved in PBS. 1.5 ml of aminated fucoidan solution was mixed with 0.5 ml of 3 mg/ml fluorescamine solution and incubated in darkness for 30 min. The fluorescence was measured at the excitation wavelength of 400 nm and the emission wavelength of 460 nm using a plate reader. Ethylenediamine was used as a standard.

4.2.3 Modification of PVA hydrogels with fucoidan

PVA hydrogels were dried overnight at 60°C to remove moisture. The hydrogels were then activated in 100 mg/ml CDI solution in dimethyl sulfoxide (DMSO) for 1 hour at room temperature with 100 rpm shaking. The CDI-activated PVA hydrogels were then wash 3 times in 1X PBS to remove excess CDI and incubated in 10 mg/ml aminated fucoidan (PVA-CDI-aF) or 10 mg/ml native fucoidan (PVA-CDI-F) solution at 37°C overnight. As a comparison, PVA hydrogels was directly incubated in 10 mg/ml native fucoidan solution at 37°C overnight (PVA-SF). The fucoidan modified PVA hydrogels prepared as described in Section 3.2.1 were also included as a comparison (PVA-MF).

4.2.4 Toluidine blue staining

Toluidine blue staining of fucoidan modified PVA hydrogels was done as described in Section 3.2.5.

4.2.5 X-ray photoelectron spectroscopy (XPS) measurement

X-ray photoelectron spectroscopy (XPS) was used to study the element composition on the surfaces of the samples. XPS survey spectra were measured in a Thermo-VG Scientific ESCALab 250 microprobe equipped with a monochromatic Al Kα source (1486.6 eV) at Waterloo Advanced Technology Laboratory (University of Waterloo, Waterloo, ON). The measurement is carried out under ultra-high vacuum (UHV) conditions with pass energy of 50eV. The incidence angle of X-ray to sample was set at 45°, and the take-off angle was set at 90°. The atom percentage was calculated in CasaXPS software.

4.2.6 Water contact angle measurement

Water contact angle of PVA and fucoidan modified PVA films were measured either with a JC2000D3 contact angle meter or using a captive bubble method with an optical contact angle system (OCA20, Future Digital Scientific Corp). For the measurement with contact angle meter, a 2 μl water drop was deposited onto the hydrated PVA films, and images were captured after the droplet remained stable on the PVA surfaces. The angle value was calculated using ImageJ. For captive bubble method, PVA film samples were immersed in DI water, and an air bubble (4 μl) was injected into water through a syringe. The bubble was allowed to attach to the surface of samples and imaged by a camera. The contact angle was then calculated by a SCA20 software.

4.2.7 Mechanical property test

PVA vascular grafts (2 mm inner diameter) modified with fucoidan by different methods were fabricated for compliance and burst pressure tests, as described in Section 3.2.8.

4.2.8 Sterilization treatment

Sterilization with gamma irradiation was done as described in Section 3.2.2. Sterilization with ethylene oxide (EtO) was done at Oregon National Primate Research Center (ONPRC) with the following procedure: sterilization with ethylene oxide (EtO) gas was performed with the following process parameters: preconditioning phase for 90 minutes at 55°C and minimum relative humidity (RH) of 70% at puncture, EtO exposure phase for 60 minutes with EtO concentration of 759 mg/L at pressure range 400-650 mbar, and aeration phase for 12 hours at 55°C.

4.2.9 Endothelial cell adhesion assays

Human umbilical vein endothelial cells (HUVECs, p 3-5, Lonza) were maintained in EGM-2 medium (Lifeline). HUVECs were seeded on PVA samples at a seeding density of 50,000 cells/cm^2 and cultured overnight to allow adhesion before live/dead staining. Live/dead staining was done according to supplier's protocol (ThermoFisher scientific). Briefly, cells were washed once with 1x Dulbecco's phosphate-buffered saline (DPBS) and incubated with the mixture of calcein AM and ethidium homodimer-1 for 30 min. The cells were then washed once with 1x DPBS before imaging.

Immunofluorescence staining of endothelial cells was done as described in Section 3.2.9. Briefly, HUVECs (p 3-5) or human coronary artery endothelial cells (HCAECs, p 3-5) were seeded on PVA samples at a seeding density of 50,000 cells/cm^2 and cultured for 3 days until confluent. Confluent cells were washed once with 1x DPBS, fixed with 4% paraformaldehyde (PFA), permeabilized with 0.1% Triton X-100, and blocked with 5% goat serum and 0.3% Triton X-100. Following blocking, the cells were stained with vascular endothelial cadherin (VE-cad, 1:100, Cell Signaling Technology) and counterstained with DAPI to label nuclei. Images were taken using Zeiss fluorescence microscope (Axio Observer Z1) and analyzed using ImageJ software.

4.2.10 *In vitro* hemocompatibility test

In vitro hemocompatibility test was done as described in Section 3.2.10

4.2.11 Ex-vivo hemocompatibility test

Ex-vivo hemocompatibility test was done in an ex-vivo shunt model as described in Section 3.2.11.

4.2.12 Fucoidan modification on ePTFE

To activate ePTFE surface for modification, ePTFE films was heated in oven at 120°C for 3 hours, followed by treatment with air plasma for 10 min. The plasma-treated ePTFE was then directly put in 1M NaOH solution and stir for 2 hours at room temperature. The samples were subsequently washed with DI water and dried in oven for 1 hour at 120°C, followed by reaction in CDI solution for 1 hour. The CDI activated ePTFE was washed three times with 1X PBS, and subsequently incubated in aminated fucoidan solution overnight (ePTFE-plas-NaOH-aF). ePTFE samples that were not treated with NaOH after plasma treatment were also included as a comparison (ePTFE-plas-aF).

4.2.13 Implantation of ePTFE vascular graft

Fucoidan-modified ePTFE tubular graft was prepared by suturing the ePTFE films with interrupted stitches along the tube. The graft was EtO sterilized prior to implantation. ePTFE graft (2 mm inner diameter, 5 mm in in length) was implanted in rabbit right common carotid artery with end-to-end anastomosis. The surgery was done as described in Section 3.2.12. Ultrasound doppler imaging and measurements were done using Siemens Acuson X300 ultrasound system with a VF 8-3+ (8-3 MHz) linear transducer and imaging frequency of 10 MHz at midpoints (14 days) and endpoints (28 days) to detect blood flow and check graft patency. The explanted graft was section into 3 segments and immunofluorescently stained against VE-cadherin and CD31.

4.2.14 Statistics

All statistical analysis was performed using GraphPad Prism 8. The values of all data were presented as mean ± Standard Deviation (SD). To determine statistical significance, t-test, one-way ANOVA with Tukey's post hoc test and two-way ANOVA with Sidak's post hoc test were used. Statistical significance criterion was set at p value of <0.05.

4.3 Results

4.3.1 Comparison of fucoidan conjugation with other fucoidan modification methods

4.3.1.1 Preparation of fucoidan modified PVA with conjugation and other methods

As discussed in chapter 3, PVA hydrogels could be modified by mixing fucoidan in PVA solution followed by STMP crosslinking (PVA-MF). However, PVA-MF samples displayed rough surface morphology with irregular micro-sized structures and were not compatible with topographical patterning, as shown in Fig **4-1**. The results demonstrated that PVA-MF is not appropriate to fabricate topographically patterned PVA hydrogels

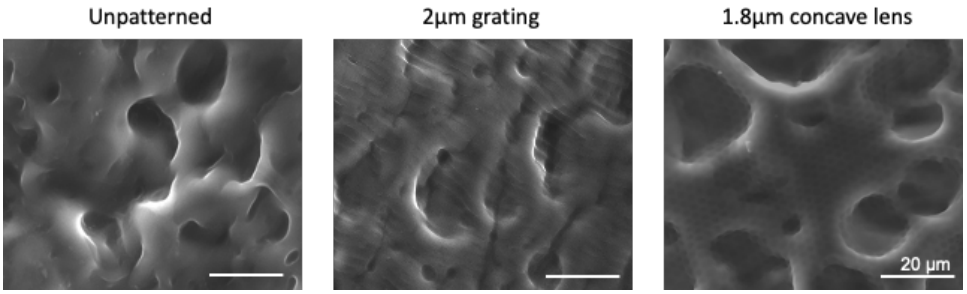


Figure 4-1. SEM images of unpatterned PVA-MF and PVA-MF with 2 μm gratings and 1.8 μ concave lenses.

In order to develop a fucoidan modification method that does not sacrifice surface roughness, other fucoidan modifications of PVA were done by several methods as shown in **Fig 4-2**. PVA-SF was prepared by soaking PVA films in fucoidan solution. To conjugate fucoidan directly to PVA, PVA was first activated with CDI (PVA-CDI), followed by incubation in native fucoidan solution (PVA-CDI-F). To conjugate aminated fucoidan, PVA-CDI was incubated in aminated fucoidan solution (PVA-CDI-aF). In this section, the surface properties and biological activities of PVA-MF, PVA-SF, PVA-CDI-F, and PVA-CDI-aF were compared.

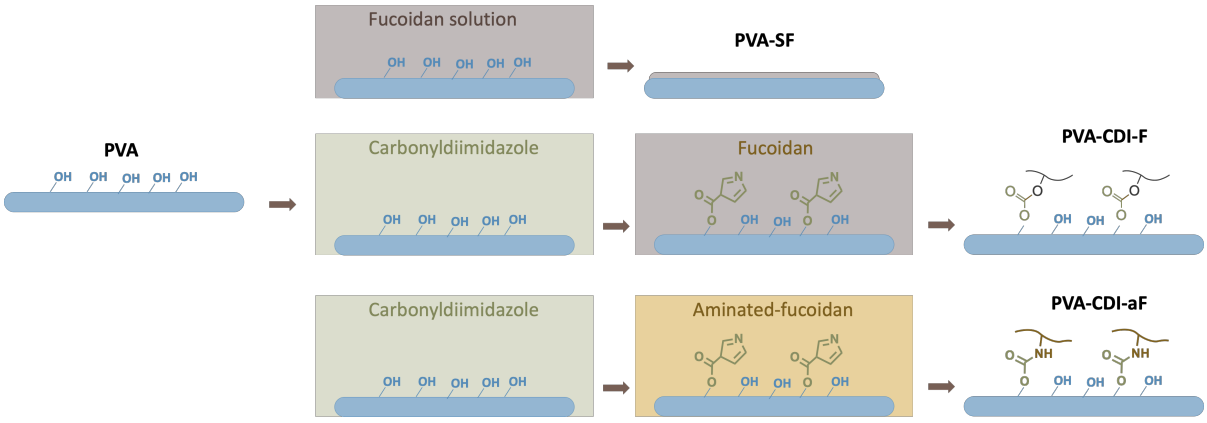


Figure 4-2. Schematic diagram of preparation procedure of PVA-SF, PVA-CDI-F and PVA-CDI-aF.

4.3.1.2 Amination of fucoidan

To facilitate conjugation reaction, fucoidan was aminated by EDA through CDI reaction. To prove the success of fucoidan amination, ^{1}H NMR spectroscopy was done to characterize fucoidan, CDI-activated fucoidan (fucoidan-CDI), and aminated fucoidan (Fucoidan-CDI-EDA) (**Fig 4-3**). The spectrum of fucoidan showed α-anomeric protons (H-1) at 5-5.6 ppm, ring protons (H-2 to H-5) at 3.1-4.8 ppm, O-acetyl groups at 2.1-2.2 ppm, and methyl protons (H-6) at 1-1.4 ppm. The spectrum of fucoidan-CDI showed the characteristic peaks of imidazole at 7.4-8.5 ppm. Methylene protons from EDA was observed at 3.05 ppm and 3.3 ppm in the spectrum of Fucoidan-CDI-EDA. Furthermore, after CDI reaction, the signals from α-anomeric protons at 5-5.6 ppm and ring protons around 4.5-4.8 ppm

decreased, which indicated that the CDI not only reacted with the functional groups at the sugar ring but also caused a ring open reaction.

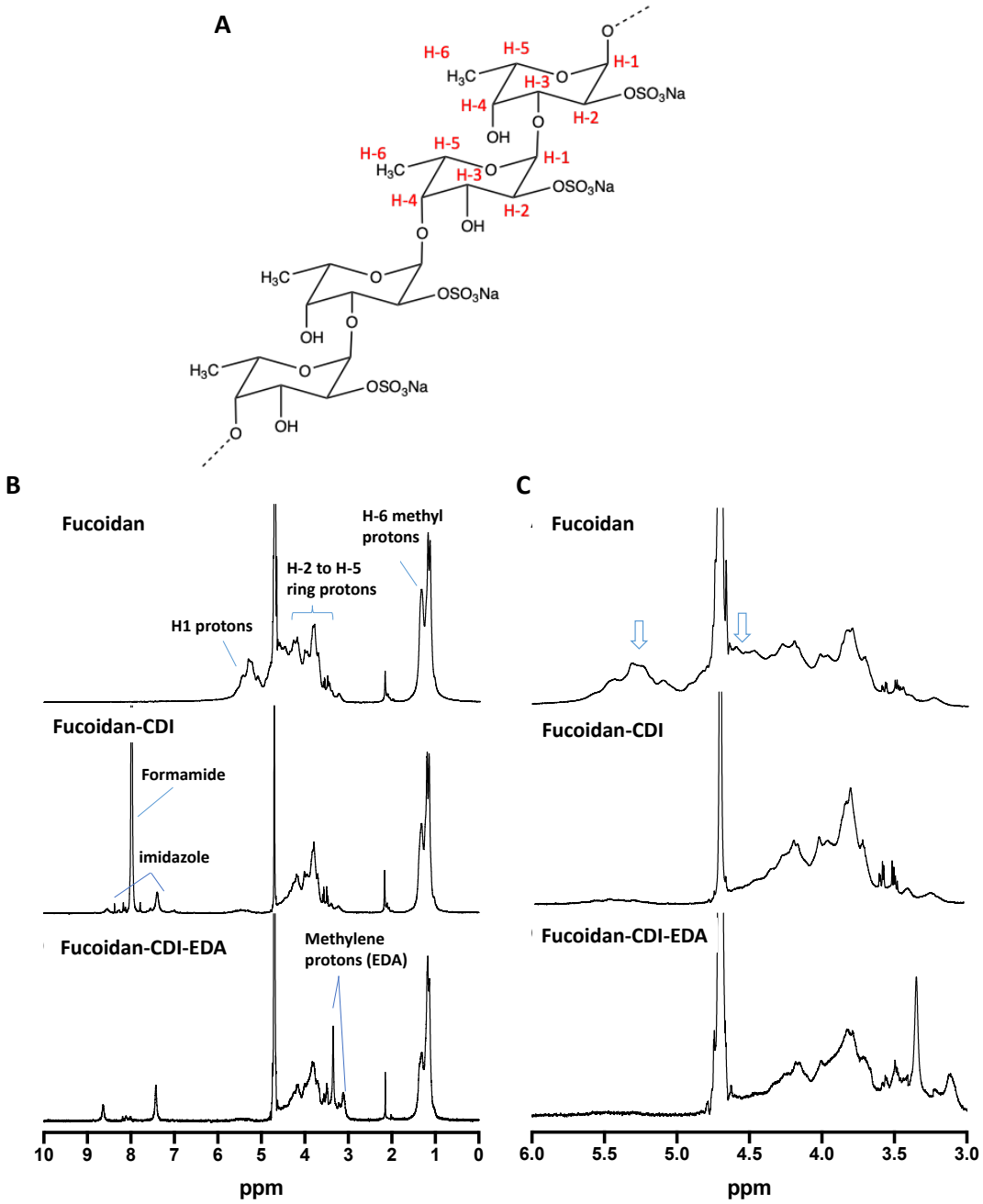
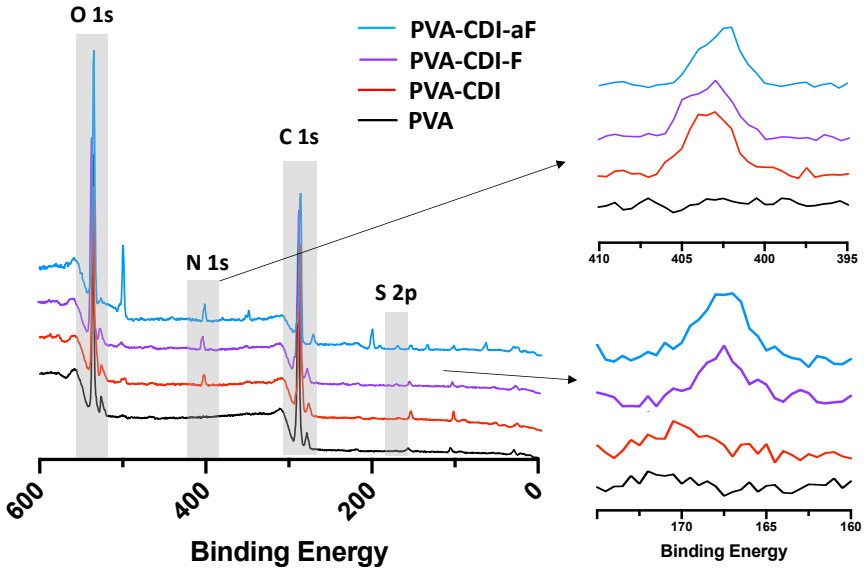


Figure 4-3. Chemical structure of fucoidan (A) and ^{1}H NMR spectra of fucoidan, CDI-activated fucoidan and EDA aminated fucoidan (B and C).

4.3.1.3 XPS characterization of fucoidan and aminated fucoidan conjugated PVA

XPS survey scan was used to confirm the conjugation reaction between fucoidan, aminated fucoidan and PVA. PVA-CDI, PVA-CDI-F, and PVA-CDI-aF samples showed significant N1s peaks, and PVA-CDI-F and PVA-CDI-aF showed S2p peaks (**Fig 4-4**), confirming the presence of fucoidan on conjugated PVA samples. Fucoidan conjugation on PVA also induced changes in surface atom percentage. Comparing to unmodified PVA, O% of PVA-CDI-F and PVA-CDI-aF increased from 25.5% to 32.4% and 31.4%, respectively, while C% decreased from 74.8% to 63.4% and 64.3%, respectively. The difference was not statistically significant. The C% and O% did not show a big difference between PVA-CDI-F and PVA-CDI-aF samples.



Atom %	C	N	O	S
PVA	74.8±1.6	N.D.	25.2±1.6	N.D.
PVA-CDI	71.4±0.69	4.7±0.4	23.9±1.9	N.D.
PVA-CDI-F	63.4±2.2	3.5±0.2	32.4±2.0	0.8±0.1
PVA-CDI-aF	64.3±2.3	3.4±0.3	31.4±1.9	0.9±0.1

Figure 4-4. X-ray photoelectron spectroscopy (XPS) survey scan of PVA, PVA-CDI, PVA-CDI-F, and PVA-CDI-aF. The table shows the atomic %age of carbon, nitrogen and oxygen and sulfur. SD (n = 3). N.D. = not detectable.

4.3.1.4 Surface characterization of fucoidan modified PVA

The surface properties of fucoidan modified PVA hydrogels with different methods were compared. SEM imaging was used to examine the surface morphology (**Fig 4-5**). PVA-MF showed significant increased roughness on the unpatterned samples, while the other groups all had smooth surfaces. 5 μm gratings were fabricated on PVA hydrogels to assess the compatibility of fucoidan modifications with topographical patterning. PVA-MF samples did not show clear patterned structures PVA, while PVA-SF, PVA-CDI-F, and PVA-CDI-aF all had good fidelity of the topography.

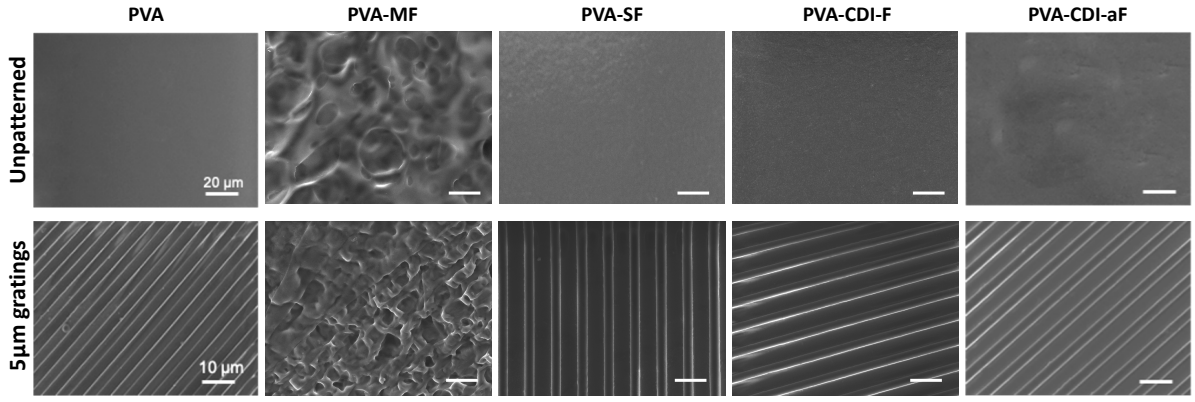


Figure 4-5. SEM images of unpatterned and 5 μm gratings PVA, PVA-MF, PVA-SF, PVA-CDI-F and PVA-CDI-aF.

Surface energy of PVA and fucoidan modified PVA was determined by measuring static water contact angle (**Fig 4-6A**). PVA-SF had an average contact angle value of 48°, significantly higher than PVA modified by the other methods. None of the fucoidan modified PVA had significant difference in contact angle compared to unmodified PVA. Fucoidan concentration was measurement by toluidine blue staining. PVA-MF had significantly higher fucoidan concentration (52.4 μg/cm^2) on the surfaces compared to PVA modified by other methods ($p<0.0005$) (**Fig 4-6B**). Among all the modification methods, PVA-SF had the lowest fucoidan concentration, with an average of 5.2 μg/cm^2. PVA-CDI-F and PVA-CDI-aF did not exhibit significant difference in fucoidan concentration.

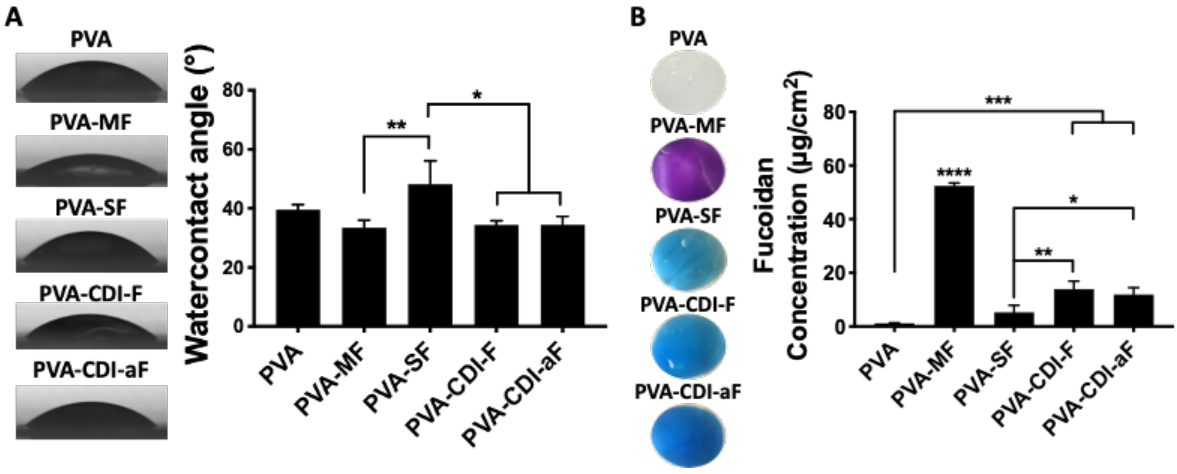


Figure 4-6. Effect of fucoidan modification methods on the surface properties. (A) Water contact angle. N=4, * and ** indicate a significant difference using one-way ANOVA with $p < 0.05$ and $p < 0.01$, respectively. (B) Toluidine blue staining. N=3, * , **, *** and **** indicate a significant difference using one-way ANOVA with $p<0.05$, $p < 0.01$, $p < 0.005$ and $p < 0.0005$, respectively.

4.3.1.5 Mechanical properties

The effects of fucoidan modification methods on the mechanical properties of PVA grafts were tested by measuring compliance and burst pressure of PVA vascular graft with 2 mm inner diameter. As shown in Fig 4-7, no significant difference on compliance and burst pressure was observed among all the tested groups, indicating that the fucoidan modification did not alter the mechanical properties of PVA significantly.

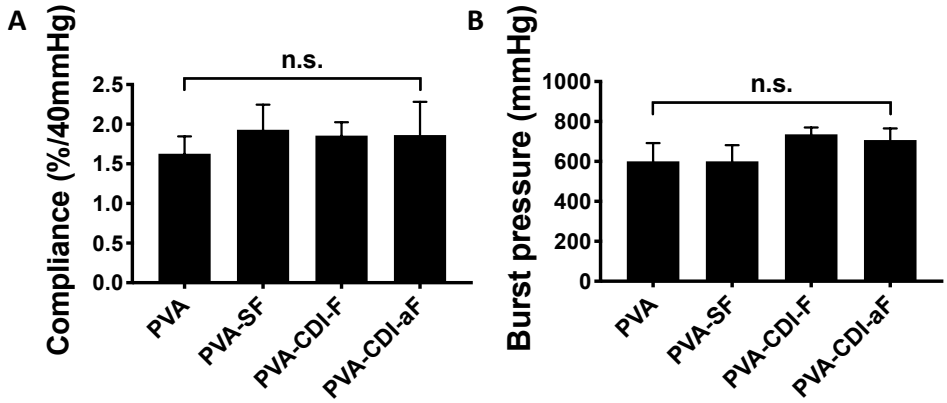


Figure 4-7. Compliance (A) and burst pressure (B) of PVA, PVA-SF, PVA-CDI-F and PVA-CDI-aF grafts. N=3, no significant difference was observed.

4.3.1.6 Endothelial cell adhesion

ECs were seeded on fucoidan-modified PVA to determine the influence of fucoidan modification methods on EC adhesion and function. Live/dead staining of HUVECs showed significantly more live cells on all fucoidan modified PVA samples compared to PVA (**Fig 4-8A**). Cell viability results also demonstrated that the cell viability was significantly improved by fucoidan modification (**Fig 4-8C**). Cell density, spreading and monolayer formation function were evaluated by staining HUVECs with DAPI, CD31 and VE-cadherin. Endothelial monolayers were formed on all fucoidan modified PVA samples as shown in **Fig 4-8B**, with significantly higher cell density compared to unmodified PVA ($p \leq 0.0005$) (**Fig 4-8D**). Expression of cell-cell junction markers, CD31 and VE-cadherin, was compared among all the modified PVA samples. Unmodified PVA was not included in the comparison due to low number of adhered cells. All cells on fucoidan modified PVA expressed strong CD31 and VE-cadherin, and the expression was seen at the cell boundaries (**Fig 4-8B**). The quantification results showed PVA-CDI-F and PVA-CDI-aF had higher CD31 expression than PVA-MF and PVA-SF, as shown in **Fig 4-8E**. The expression of VE-cadherin did not demonstrate a significant difference among all the groups.

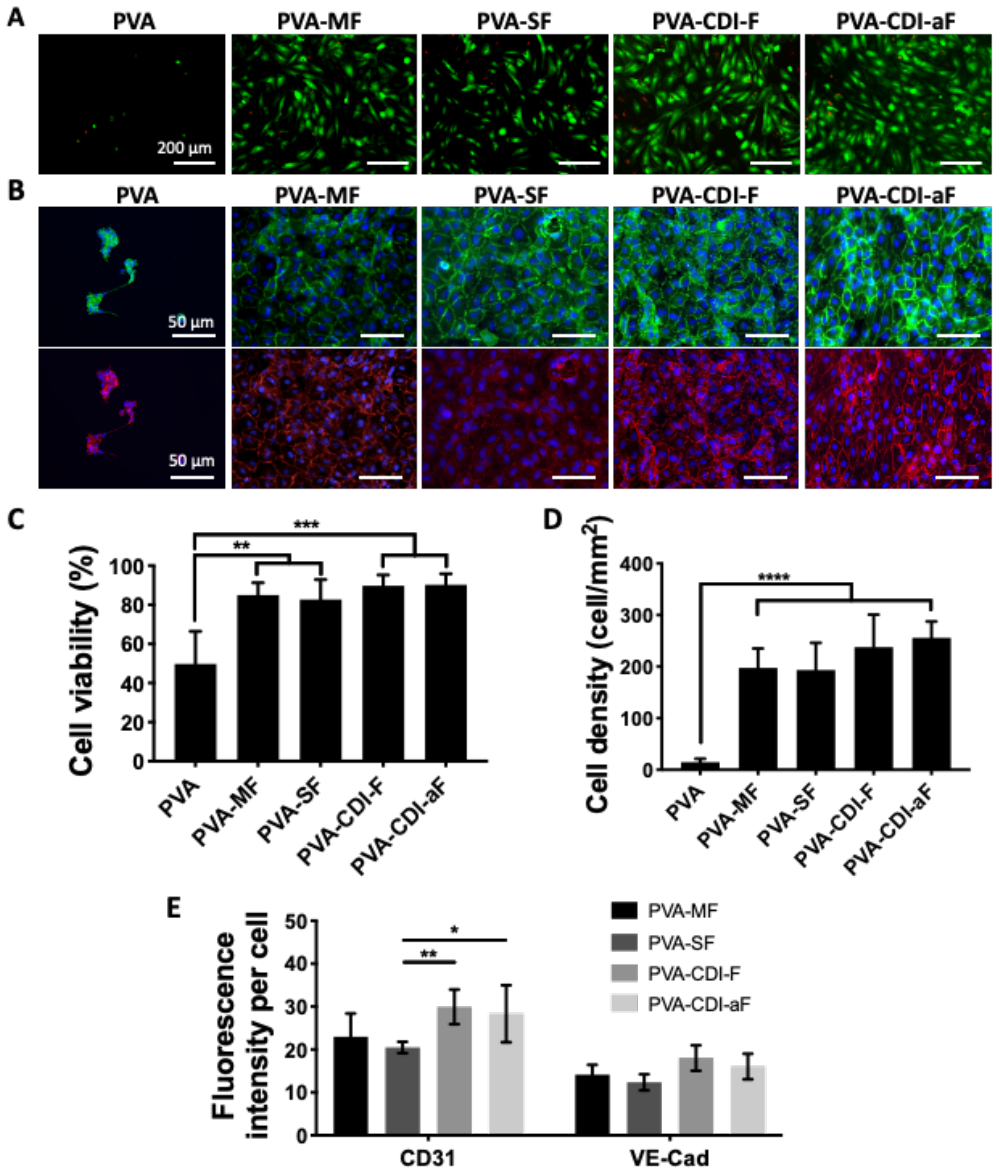


Figure 4-8. Endothelialization on fucoidan modified PVA with different modification methods. (A) Representative live/dead staining of cells on PVA and fucoidan modified PVA samples. Scale bar = 200 µm. (B) Endothelial cell monolayer formation on PVA and fucoidan modified PVA. Representative immunofluorescent images of endothelial cells on PVA and fucoidan modified PVA. Scale bar = 50 µm. Blue denotes nuclei, green denotes VE-cadherin and red denotes CD31. Cell viability (C), cell density (D) and VE-cadherin and CD31 expression (E) of endothelial cells on PVA and fucoidan modified PVA. N=6, *, **, *** and **** indicate a significant difference using one-way ANOVA with $p < 0.05$, $p < 0.01$, $p < 0.005$ and $p < 0.0005$, respectively.

4.3.1.7 Hemocompatibility

To examine the effects of modification methods on the hemocompatibility of PVA-fucoidan hydrogels and tubular grafts, *in vitro* hemocompatibility test with rabbit platelet rich plasma and *ex vivo* hemocompatibility test using a non-human primate shunt model were carried out.

Platelet morphology and adhesion on PVA and fucoidan modified PVA samples were assessed by SEM imaging and LDH assay. SEM images (**Fig 4-9A**) showed that platelet adhesion was significantly higher on collagen coated glass, PVA-SF, and PVA-CDI-F, which was in line with the quantification results from LDH assay (**Fig 4-9B**). Adhered platelets on collagen coated glass were spread and activated, while the platelets on ePTFE, PVA, and fucoidan-modified PVA remained rounded morphology. No significant difference was seen among the ePTFE, PVA, PVA-MF, and PVA-CDI-aF groups. Real-time thrombin generation assay did not exhibit a significant difference in lagtime (**Fig 4-9C**). Peak thrombin generation rate and total thrombin generation was significantly higher on collagen-coated glass, PVA-SF and PVA-CDI-F (**Fig 4-9D and E**). ePTFE, PVA, PVA-MF, and PVA-CDI-aF exhibited comparable thrombogenicity.

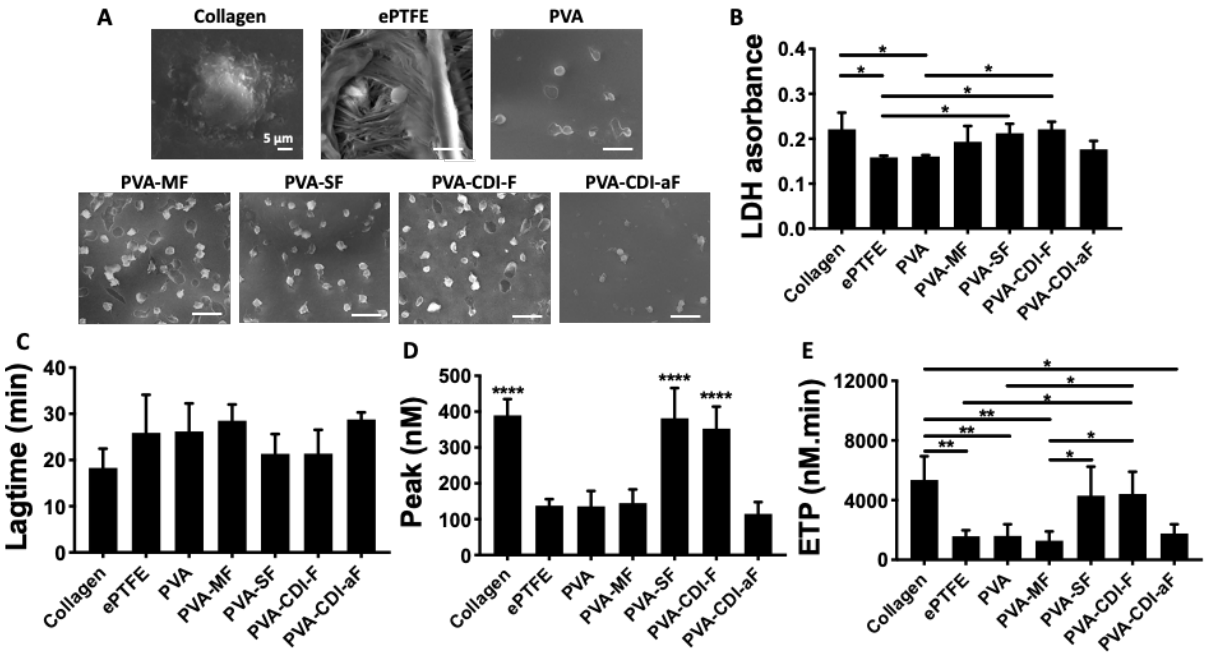


Figure 4-9. *In vitro* hemocompatibility of fucoidan modified PVA. (A) Representative SEM images of platelets on PVA and fucoidan modified PVA. (B) Quantification of platelet adhesion determined by lactate dehydrogenase (LDH) assay. (C) (D) and (E) Realtime thrombin generation. Lag-time (C)

represents the time taken to start forming thrombin. Peak (D) represents the maximum thrombin generation rate. ETP (E) represents endogenous thrombin potential. n=5, *, ** and **** indicate a significant difference using one-way ANOVA with $p < 0.05$, $p < 0.01$ and $p < 0.0005$, respectively.

PVA and fucoidan modified tubular grafts were then exposed to flowing blood for *ex vivo* thrombosis testing. Unmodified PVA samples had low platelet and fibrin accumulation compared to the positive and clinical controls. The PVA-SF and PVA-CDI-F grafts had high platelet adhesion, slimier to a collagen coated ePTFE graft control (**Fig 4-10A and B**). We observed a significant decrease in platelet attachment and fibrin accumulation onto PVA-CDI-aF grafts when compared to PVA-SF and PVA-CDI-F grafts. Additionally, PVA-CDI-aF grafts had significantly higher patent luminal area after 1 hour of blood flow (**Fig 4-10C**), and 3-dimensional and cross-sectional images of the PVA-CDI-aF grafts also exhibited less thrombi (**Fig 4-10D).**

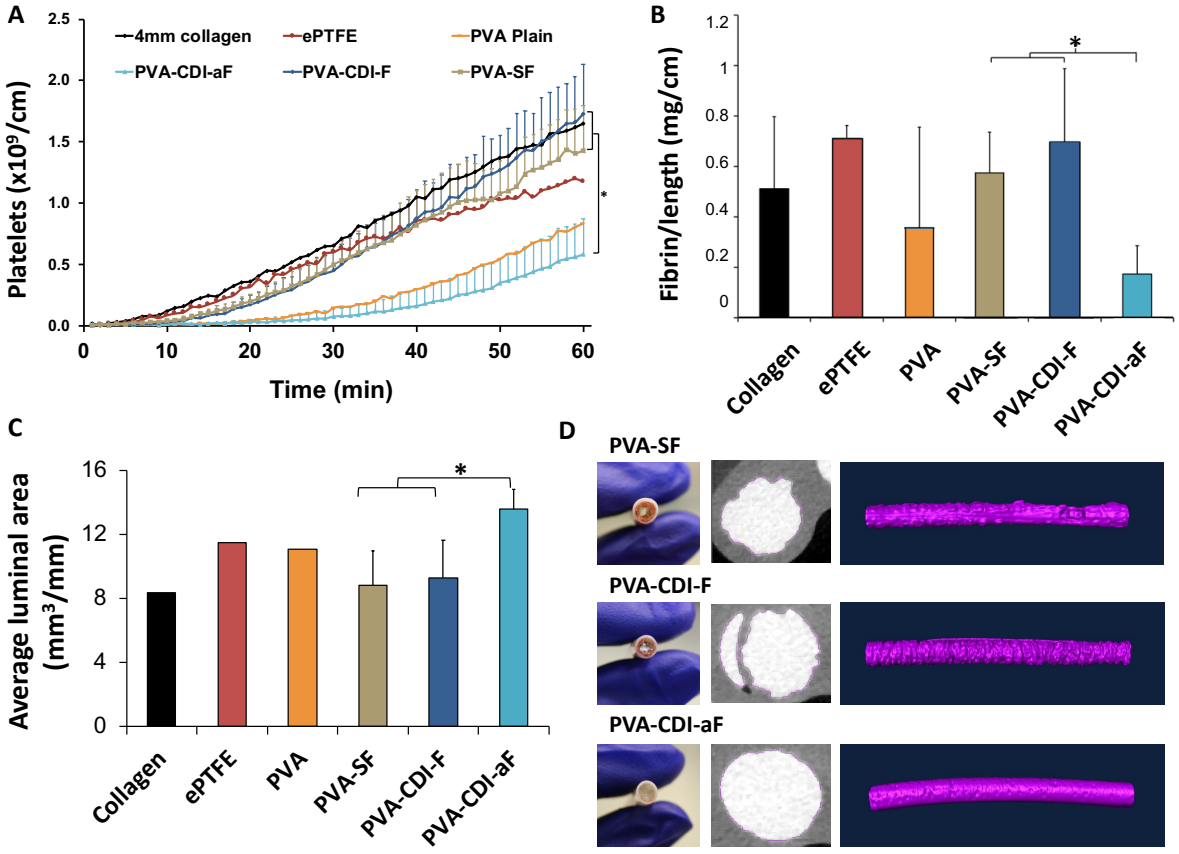


Figure 4-10. *Ex vivo* hemocompatibility of plain PVA and fucoidan modified PVA vascular graft. Platelet accumulation (A), fibrin accumulation (B) and average luminal patent area (C) data are displayed as mean ± SD for all samples. Collagen–coated ePTFE, (n=2), ePTFE (n=2), PVA (n=2) and fucoidan modified PVA (n=6) grafts were tested. Statistical analysis was performed using a one-way ANOVA with Tukey's HSD *post hoc* testing ($p < 0.001$). * indicates statistical significance. (D) Three-dimensional surface volume renderings of microCT cross-sectional ROI selections showing thrombi in the lumen of tested samples.

Overall, the results showed that the modification methods to present fucoidan on PVA could lead to different surface and biological activities on endothelialization and hemocompatibility. Both PVA-CDI-F and PVA-CDI-aF exhibited significant improvement on endothelial cell adhesion without changing the surface chemistry and topography, but PVA-CDI-F induced more severe platelet adhesion and thrombin generation. Thus, PVA-CDI-F was not further pursued. In next two sections, the effects of preparation parameters on the properties of PVA-CDI-aF and the optimization of PVA-CDI-aF were studied.

4.3.2 Characterization of aminated fucoidan-conjugated PVA hydrogel with various preparation methods

4.3.2.1 Comparison with reduction amination method

Reduction of carboxylic acid with borane has been applied to aminate fucoidan by targeting the reducing end. Here, we compared the aminated fucoidans prepared by EDA reaction and borane reduction. Fluorescamine reaction showed that borane-prepared fucoidan had higher number of amine groups in the fucoidan molecules compared to EDA-prepared fucoidan (**Fig 4-11A**). Thrombin generation assay showed that borane-prepared fucoidan induced a significantly higher thrombin generation (**Fig 4-11C and D**). This suggests that aminated fucoidan prepared by EDA may have a better antithrombin activity.

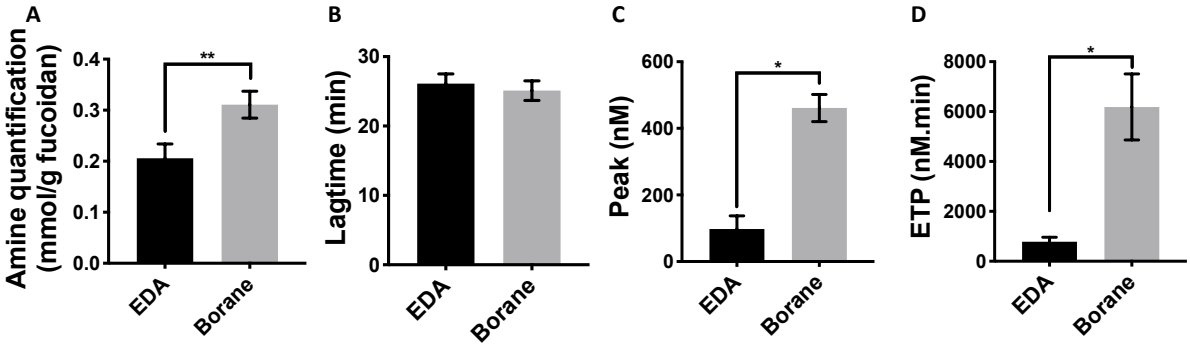


Figure 4-11. Comparison of amination methods. (A) Amine quantification of fucoidan aminated by EDA and borane reduction reaction. N=3, ** indicates a significant difference using unpaired t test with $p < 0.01$. (B)(C)(D) Hemocompatibility of PVA modified by aminated fucoidan using different amination methods. N=2, * indicates a significant difference using unpaired t test with $p < 0.05$.

4.3.2.2 Comparison of sources of fucoidan

Fucus vesiculosus (fv) and *Undaria pinnatifida* (up) seaweeds are two main sources for fucoidan. We aminated fucoidan from both sources and compared their bioactivities. PVA-CDI-aF_{fv} exhibited a significantly better EC adhesion compared to PVA-CDI-aF_{up}. Although PVA-CDI-aF_{up} had a higher cell density compared to unmodified PVA, the cells failed to form monolayers on the PVA-CDI-aF_{up} samples (**Fig 4-12A**). Thrombin generation assay did not exhibit a significance among all the tested groups (**Fig 4-12B**).

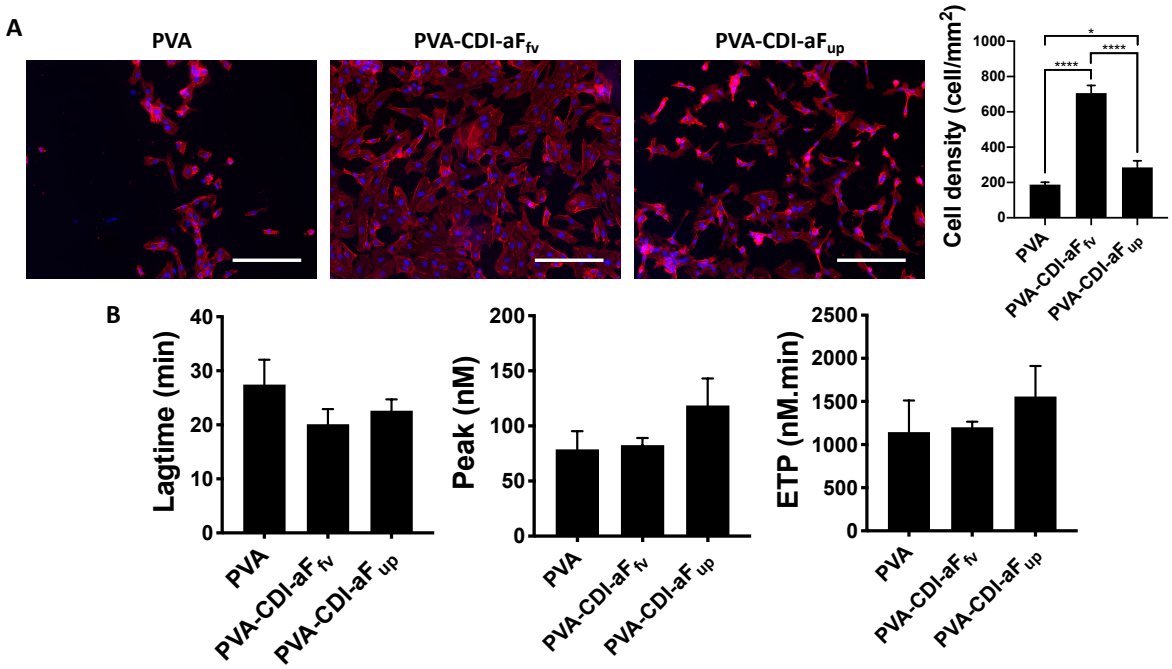


Figure 4-12. Comparison of fucoidan from *Fucus vesiculosus* and *Undaria pinnatifida.* (A) Endothelialization on PVA-CDI-aF$_{fv}$ and PVA-CDI-aF$_{up}$. Scale bar = 200 µm. Blue denotes nuclei, and red denotes F-actin. N=3, *, *** and **** indicate a significant difference using one-way ANOVA with $p < 0.05$, $p < 0.005$ and $p < 0.0005$, respectively. (B) Thrombin generation on PVA-CDI-aF$_{fv}$ and PVA-CDI-aF$_{up}$. N=2, no statistical significance was observed.

4.3.2.3 Effect of sterilization

Gamma irradiation and EtO treatment are two commonly used sterilization approaches for implants. We examined the effect the sterilization on the biological activities of fucoidan conjugated PVA. EC adhesion on PVA-CDI-aF hydrogels were not affected by the sterilization. HUVECs adhered well and formed monolayers on unsterilized, gamma-treated and EtO-treated PVA-CDI-aF samples, and the cell density was significantly higher than unmodified PVA samples ($p<0.0005$) (**Fig 4-13A and B**). Thrombin generation assay showed that gamma irradiation on unmodified PVA has significantly higher peak thrombin generation rate compared to unsterilized PVA and all PVA-CDI-aF samples. EtO treatment on both unmodified PVA and PVA-CDI-aF exhibited a slightly lower thrombin generation, however, the difference was not statistically significant (**Fig 4-13C-E**).

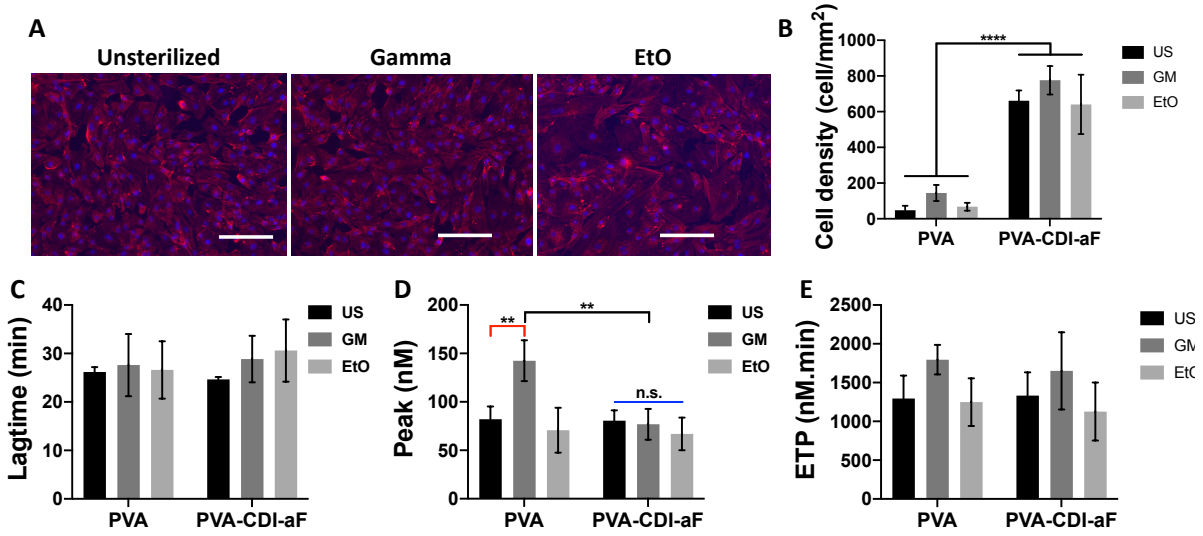


Figure 4-13. Effect of terminal sterilization methods on endothelial cell adhesion and thrombin generation of PVA-CDI-aF. (A) Representative immunofluorescence staining images of HUVECs on PVA-CDI-aF sterilized by different methods. Scale bar = 200 μm. Blue denotes nuclei, and red denotes F-actin. (B) Cell density on PVA and PVA-CDI-aF samples with different sterilization methods. N=3, **** indicate a significant difference using two-way ANOVA with $p < 0.0005$. (C)(D)(E) Thrombin generation on PVA and PVA-CDI-aF samples with different sterilization methods. N=3, ** indicate a significant difference using two-way ANOVA with $p < 0.01$.

4.3.3 Optimization of fucoidan conjugation based on surface and biological characterization

Fucoidan amination was achieved using ethylenediamine (EDA). Adjusting the amount of EDA used in the amination reaction of fucoidan could result in fucoidans with different amine groups and in turn affect the surface properties and biological functions of modified PVA. A series of aminated fucoidans were prepared by adding different amount of EDA (**Fig 4-14A**). Among all the aminated fucoidans, aF25 had the highest amine groups on the fucoidan molecules. Moreover, the effects of the number of amine groups on surface properties of fucoidan conjugated PVA were compared. PVA-CDI-aF10 had a higher water contact angle compared to PVA-CDI-aF2 and PVA-CDI-aF25 (**Fig 4-15A**). The concentration of conjugated fucoidan in PVA was also altered by the number of amine groups, and

PVA-CDI-aF25 had a significantly higher fucoidan concentration compared to PVA-CDI-aF5 (**Fig 4-14B**).

A

Sample ID	Mass fucoidan (mg)	Mass CDI (mg)	EDA (µg)	Molar ratio FC:CDI:EDA
FC	10	0	0	-
aF0	10	0.4	0	-
aF2	10	0.4	12	1:25:2
aF5	10	0.4	30	1:25:5
aF10	10	0.4	60	1:25:10
aF25	10	0.4	150	1:25:25

B

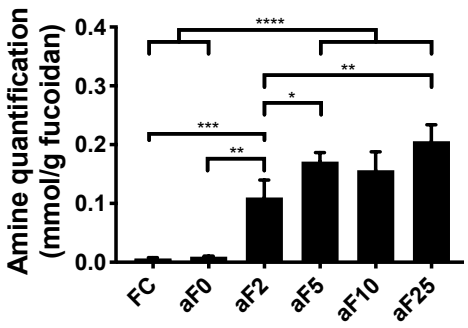


Figure 4-14. Preparation of aminated fucoidan with different EDA ratio. (A) Preparation of aminated fucoidan (aF) using different concentration of ethylenediamine (EDA). (B) Quantification of amine groups on aminated fucoidan. N=3, *, **, *** and **** indicate a significant difference using one-way ANOVA with $p < 0.05$, $p < 0.01$, $p < 0.005$ and $p < 0.0005$, respectively.

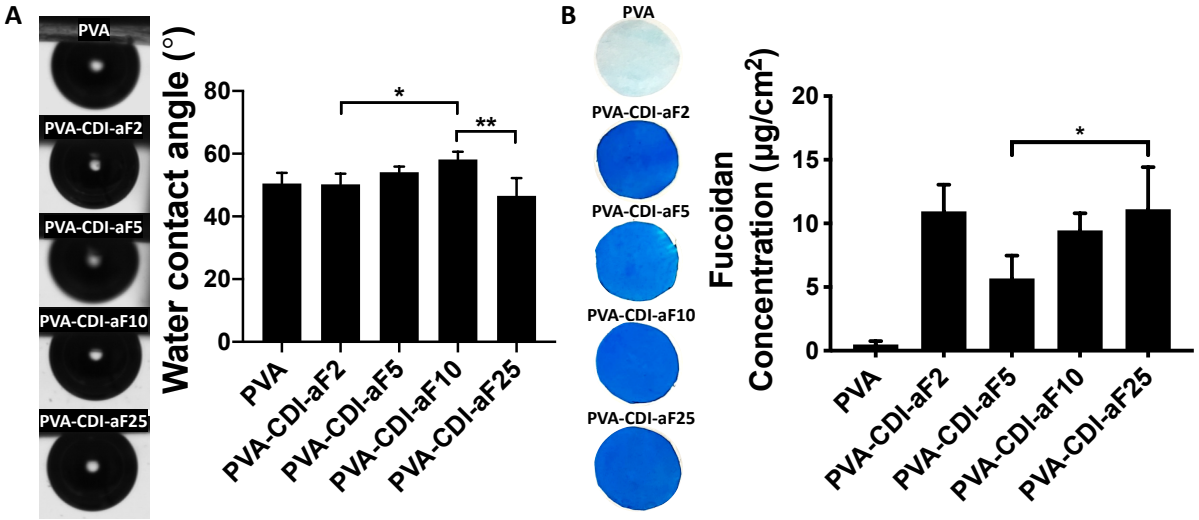


Figure 4-15. Effect of EDA ratio on the surface properties of PVA-CDI-aF samples. (A) Water contact angle of PVA-CDI-aF. N=4, * and ** indicate a significant difference using one-way ANOVA with $p < 0.05$ and $p < 0.01$, respectively. (B) Toluidine blue staining of PVA-CDI-aF. N=3, * indicates a significant difference using one-way ANOVA with $p < 0.05$.

The effect of EDA ratio on the EC responses were determined by live/dead staining of HUVECs and immunofluorescence staining of HCAECs against VE-cadherin. As shown in **Fig 4-16A**, PVA-CDI-aF samples exhibited a better cell adhesion and viability compared to unmodified PVA. More adhered cells were seen on PVA-CDI-aF2 and PVA-CDI-aF25 groups. The cell viability of PVA-CDI-aF2 and PVA-CDI-aF25 was significantly higher than unmodified PVA (**Fig 4-16C**). Furthermore, endothelial monolayer formation was examined. Although a significantly higher cell density was seen on all PVA-CDI-aF samples compared to unmodified PVA (**Fig 4-16D**), only PVA-CDI-aF25 supported a confluent endothelial monolayer formation (**Fig 4-16B**). VE-cadherin expression on PVA-CDI-aF5 and PVA-CDI-aF10 was mainly in the cytoplasm, while cells on PVA-CDI-aF25 expressed strong VE-cadherin at the cell-cell junctions.

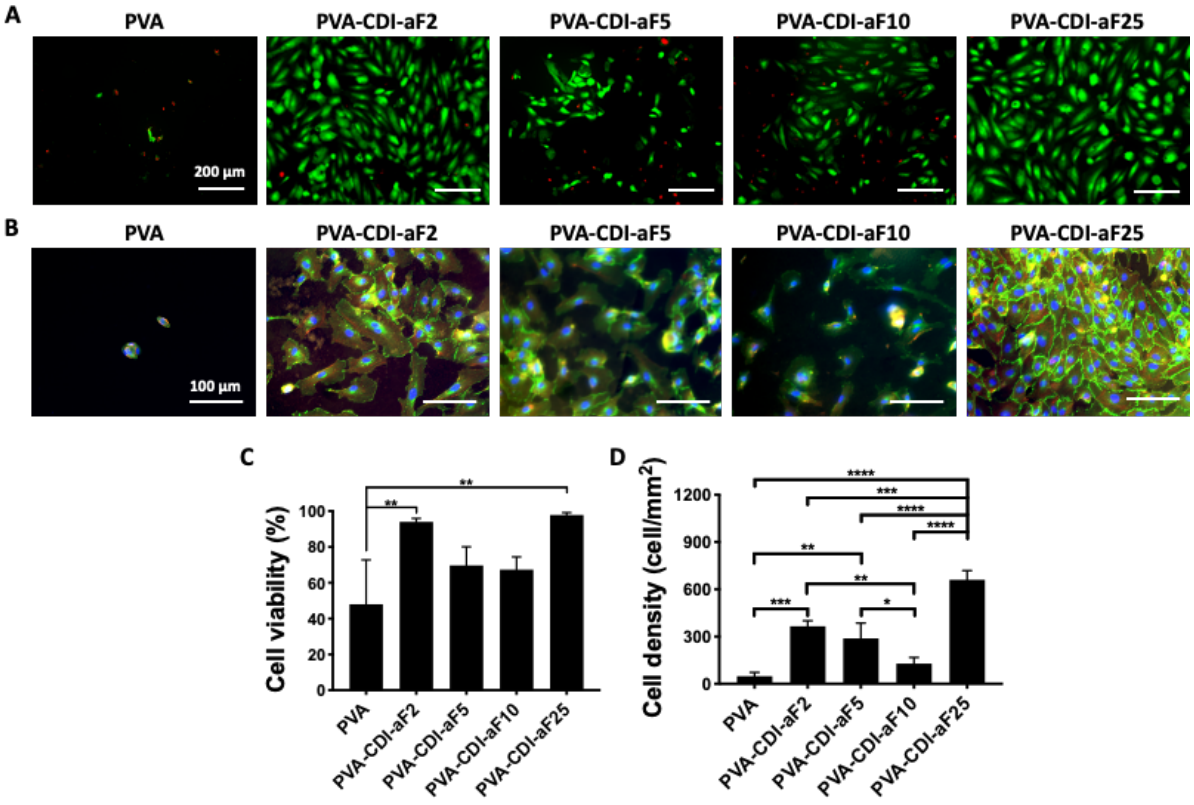


Figure 4-16. Effect of EDA ratio on endothelial cell adhesion on PVA with aminated fucoidan (PVA-CDI-aF)**.** (A) Representative live/dead staining images of HUVECs on PVA-CDI-aF. Scale bar = 200 µm. (B) Representative immunofluorescent images of HCAECs on PVA-CDI-aF. Scale bar = 100 µm. Blue denotes nuclei, green denotes VE-cadherin and red denotes F-actin. Cell viability (C) and density (D) of endothelial cells on PVA with aminated fucoidan. N=3, *, **, *** and **** indicate a

significant difference using one-way ANOVA with $p < 0.05$, $p < 0.01$, $p < 0.005$ and $p < 0.0005$, respectively.

Hemocompatibility tests of PVA and PVA-CDI-aF samples were done with rabbit platelet rich plasma. SEM images showed that the platelets on both PVA and PVA-CDI-aF samples had rounded shape (**Fig 4-17A**). SEM and LDH assay did not demonstrate a significant difference in platelet adhesion among all the groups (**Fig 4-17B**). In the real-time thrombin generation assay, PVA-CDI-aF2 and PVA-CDI-aF5 induced thrombin generation significantly faster than unmodified PVA. PVA-CDI-aF25 had a lagtime longer than PVA-CDI-aF2. Moreover, PVA-CDI-aF10 has significantly higher peak thrombin generation rate and total thrombin generation compared unmodified PVA (**Fig 4-17C-E**).

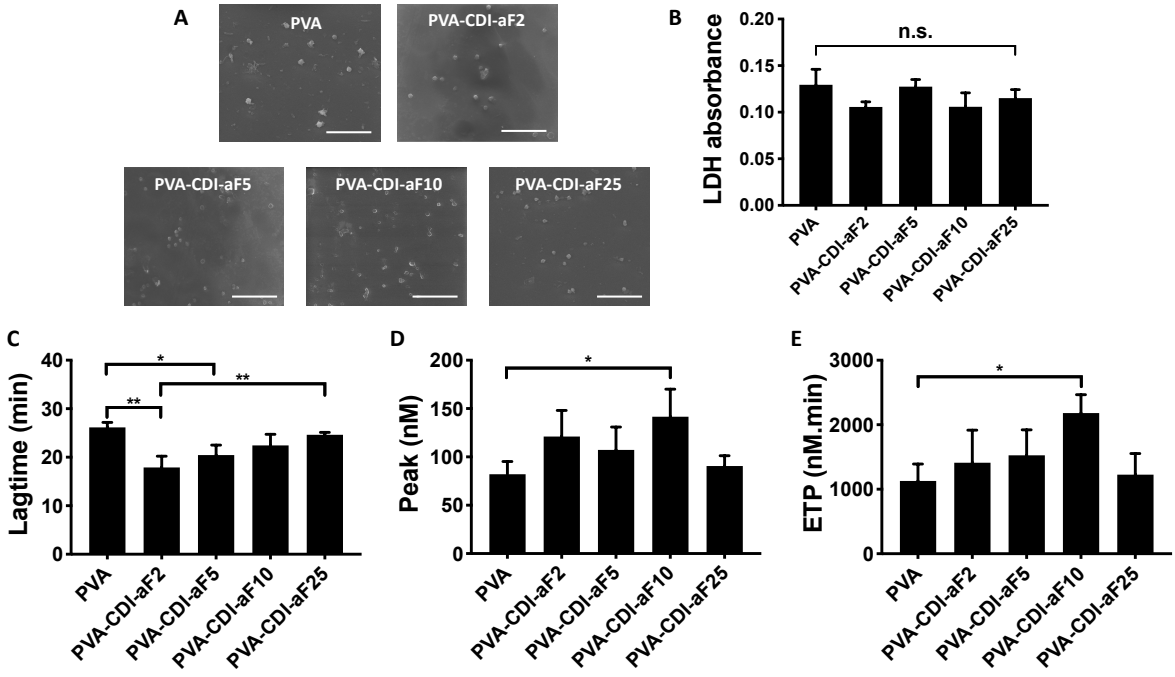


Figure 4-17. Effect of EDA ratio on hemocompatibility of PVA with aminated fucoidan (PVA-CDI-aF). (A) Representative SEM images of platelets on PVA-CDI-aF samples. Scale bar = 10 µm. (B) Quantification of platelet adhesion determined by lactate dehydrogenase (LDH) assay. (C) (D) and (E) Realtime thrombin generation. N=4, * and ** indicate a significant difference using one-way ANOVA with $p < 0.05$ and $p < 0.01$, respectively.

Overall, the results showed that the conjugation of aminated fucoidan has a significant enhance on endothelialization on PVA while maintaining a good hemocompatibility. The EDA ratio used in the preparation of aminated fucoidan play a role in mediating the surface characteristics and the biological functions of PVA-CDI-aF. aF25 appeared to exhibit the most favorable bioactivities, and thus was chosen for the following studies.

4.3.4 Fucoidan conjugation on ePTFE

In order to further explore the potential application of fucoidan conjugation on other synthetic materials, in this section, we investigated the effect of fucoidan conjugation on ePTFE, which is a typical material for synthetic vascular graft. ePTFE is inert and plasma treatment on ePTFE was done to activate the surfaces prior to fucoidan conjugation. Treatment of ePTFE with NaOH was shown to increase the number of OH functional groups on ePTFE [352]. As shown in **Fig 4-18A**, the presence of fucoidan on ePTFE surfaces was confirmed by the color change in the toluidine blue staining. However, without NaOH treatment, ePTFE-plas-aF showed light and uneven staining, indicating that the fucoidan concentration on ePTFE was low and the distribution was not uniform. ePTFE-plas-NaOH-aF samples exhibited a darker color and a more homogeneous fucoidan distribution on the surfaces.

The endothelialization on ePTFE and fucoidan modified ePTFE was evaluated by live/dead staining of HUVECs. The majority of the cells on ePTFE samples were dead. ePTFE-plas-NaOH-aF samples had more adhered cells compared to the other groups (**Fig 4-18B**). Density of live cells on the ePTFE samples was calculated, and ePTFE-plas-NaOH-aF had significantly higher cell density compared to the other groups. The cell density on ePTFE-plas-aF samples also exhibited a statistical significance compared to ePTFE, but was not significantly higher ePTFE-plas samples (**Fig 4-18C**). ePTFE-plas-NaOH-aF samples were selected to proceed hemocompatibility test and *in vivo* study.

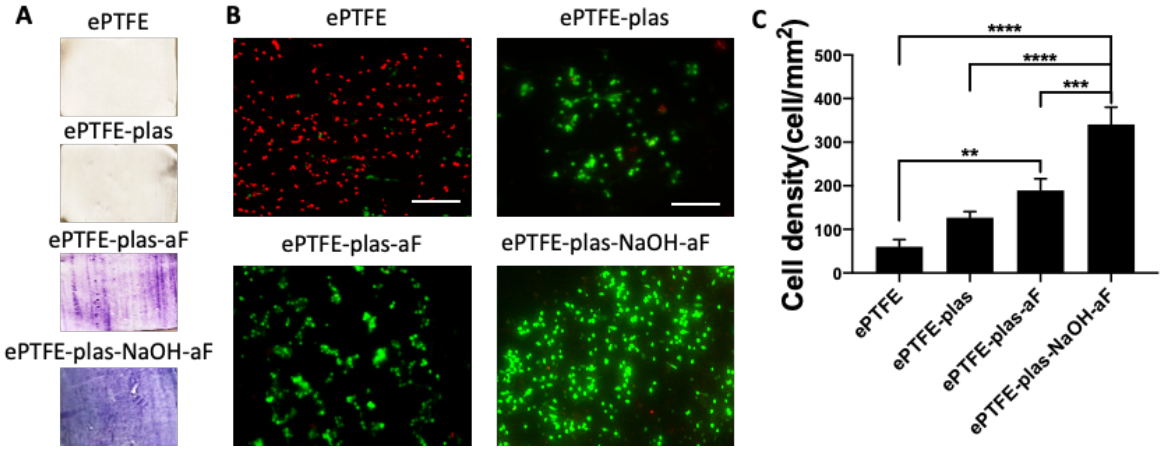


Figure 4-18. Characterization and cell adhesion on fucoidan conjugated ePTFE. (A) Toluidine blue staining of ePTFE and fucoidan modified ePTFE. (B) Representative live/dead staining images of HUVECs on ePTFE and fucoidan modified ePTFE. Scale bar = 200 µm. (C) Cell density of endothelial cells on ePTFE and fucoidan modified ePTFE. N=3, **, *** and **** indicate a significant difference using one-way ANOVA with $p < 0.01$, $p < 0.005$ and $p < 0.0005$, respectively.

Hemocompatibility of fucoidan conjugated ePTFE was evaluated with rabbit platelet rich plasma. SEM images showed that both ePTFE and fucoidan conjugated ePTFE (ePTFE-plas-NaOH-aF) had low platelet adhesion, and the adhered platelets remained in rounded shape. Collagen coated glass had induced more platelet adhesion and severe platelet spreading (**Fig 4-19A**). LDH absorbance further confirmed the results from SEM that the collagen coated glass had significantly more platelet adhesion than ePTFE and ePTFE-plas-NaOH-aF samples (**Fig 4-19B**). Thrombin generation assay showed the ePTFE-plas-NaOH-aF had significantly prolonged lagtime of thrombin generation and significantly lower total thrombin generation compared to collagen-coated glass. The thrombin generation on ePTFE-plas-NaOH-aF was also slightly but not significantly lower than unmodified ePTFE (**Fig 4-19 C-E**).

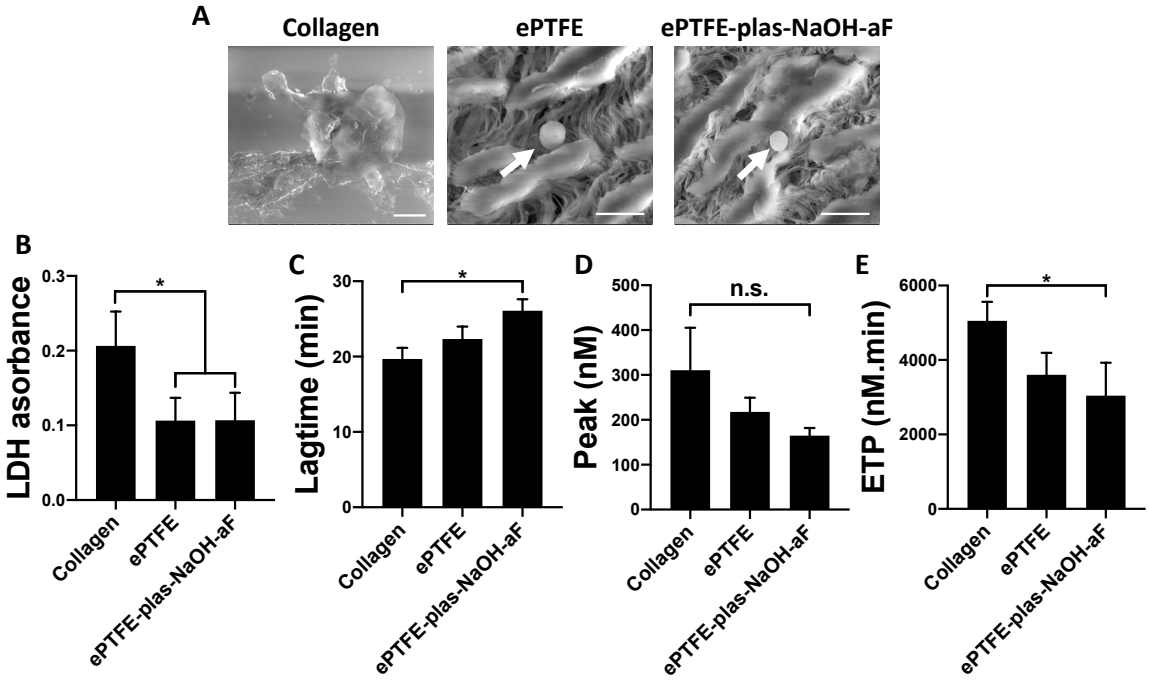


Figure 4-19. *In vitro* hemocompatibility of fucoidan modified ePTFE. (A) Representative SEM images of platelets on collagen coated glass, ePTFE and ePTFE-plas-NaOH-aF. Scale bar = 10 μm. (B) Quantification of platelet adhesion determined by lactate dehydrogenase (LDH) assay. (C) (D) and (E) Realtime thrombin generation. Lag-time (C) represents the time taken to start forming thrombin. Peak (D) represents the maximum thrombin generation rate. ETP (E) represents endogenous thrombin potential. n=3, * indicates a significant difference using one-way ANOVA with $p < 0.05$.

ePTFE graft modified with fucoidan conjugation was implanted in rabbit right common carotid artery. The ultrasound imaging showed that the graft remained patent throughout the 4-week implantation (**Fig 4-20A**). The cross-sections of the graft were stained with H&E staining. Cell attachment was observed at the proximal end of the graft, middle of the graft and the distal end of the graft (**Fig 4-20B**). To further analyze the cell adhesion, the cross-sections of the graft were immunofluorescently stained against VE-cadherin and CD31. Cells exhibited positive staining of VE-cadherin and a weak signal of CD31.

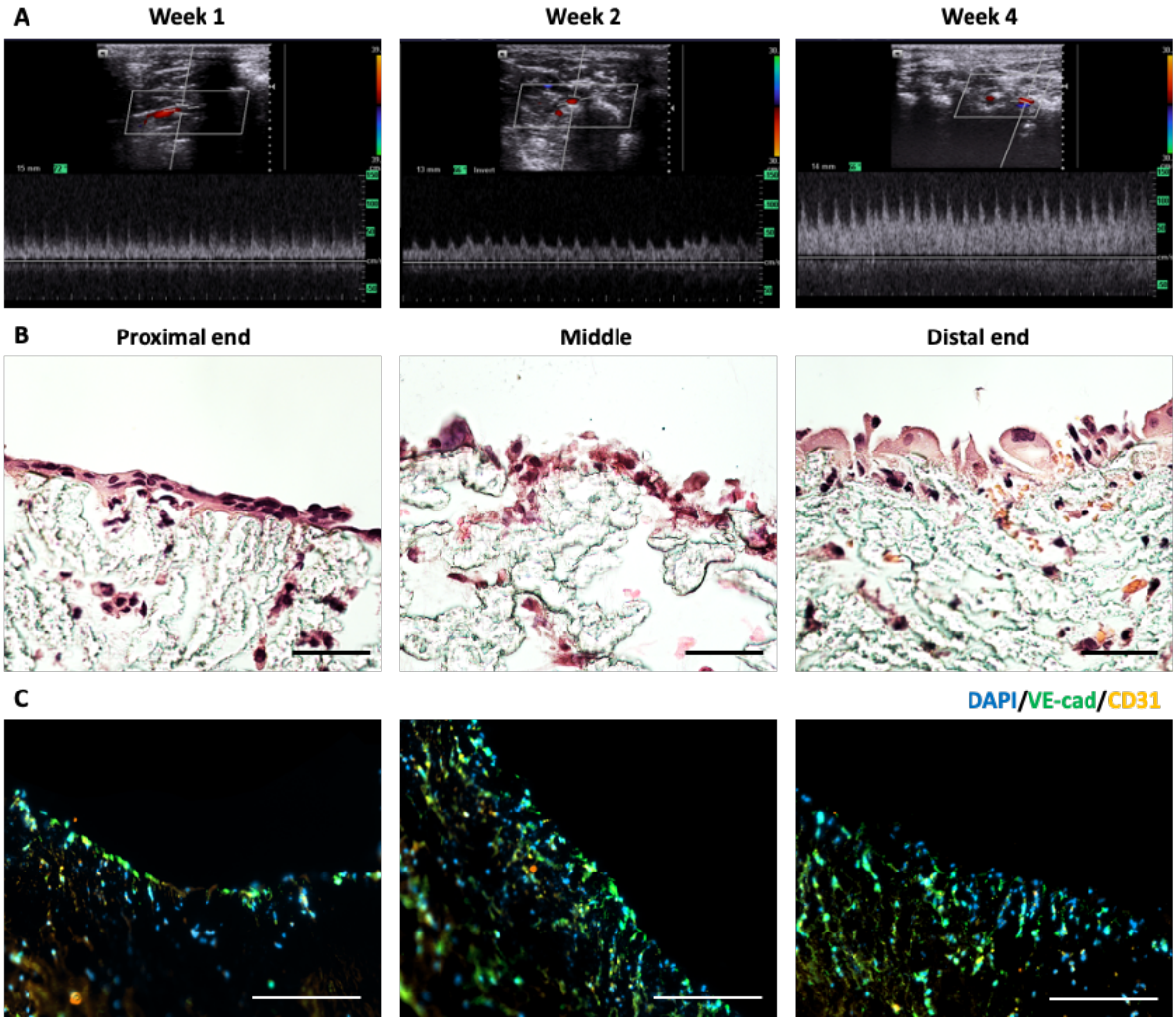


Figure 4-20. *In vivo* study of fucoidan modified ePTFE graft. (A) Blood flow inside the fucoidan modified ePTFE graft at week 1, week 2, and week 4 detected by ultrasound imaging. (B) Cell attachment in the luminal surfaces of fucoidan modified ePTFE grafts. Scale bar = 50 µm. (C) Representative immunofluorescent images of cells in the lumen of fucoidan modified ePTFE graft. Scale bar = 200 µm.

The results in this section indicated that the fucoidan conjugated method developed in this study could also be applied to other synthetic materials to improve the endothelialization.

4.4 Discussion

Fucoidan has attracted broad attention for its diverse bioactivities [353], and various factors, including dose, molecular weight and structural features, affect the biological performance of fucoidan drastically [345]. Most applications of fucoidan have been focusing on coating or mixing. Immobilization of fucoidan on plasma treated polyethylene terephthalate surfaces has exhibited success in promoting thrombin time, however, the surface morphology was significantly altered [348]. In our study, we developed a chemical conjugation method to immobilize fucoidan on synthetic surfaces based on CDI chemistry. The conjugation is applicable to different materials and did not affect the surface morphology.

Both native fucoidan and aminated fucoidan was used for the conjugation. CDI can react with the hydroxyl groups on PVA and form imidazole active intermediates. The CDI-activated PVA can further conjugate native fucoidan through hydroxyl groups or aminated fucoidan via amine groups. To prepare aminated fucoidan, CDI was used to activate fucoidan and EDA provided the amine groups. In the ^{1}H NMR spectra, we observed the characteristic peaks from fucoidan, CDI and ethylenediamine, proving the success of the amination reaction. We also noticed that peaks at 5-5.6 ppm and around 4.5-4.8 ppm decreased after CDI reaction with fucoidan. Many studies on the structure of fucoidan have identified the peaks around 5-5.6 ppm and 1-1.4 ppm as α-anomeric protons and methyl protons, respectively [354, 355]. However, the broadening and overlapping of the peaks from 3.1-4.8 make it difficult to give a complete description of the structural characteristics. Previous studies have used both ^{13}C NMR and ^{1}H NMR, as well as 2-dimensional NMR to identify the corresponding protons [356]. However, the fucoidan used in our study has limited solubility in water and is not soluble in most organic solvent. The ^{13}C NMR of fucoidan did not exhibit clear peaks of fucoidan due to the insufficient concentration of fucoidan.

The effects of fucoidan modification methods on the surface properties and bioactivities of fucoidan modified PVA have been studied. EC adhesion was substantially promoted by all fucoidan modification compared to unmodified PVA, while the hemocompatibility showed drastic differences among different groups, which indicates that in the current experimental setting, cell adhesion may be less sensitive to the modification methods of fucoidan, compared to the coagulation system. The anticoagulant and antithrombotic activities of fucoidan are dependent on multiple factors, such as concentration, molecular weight and sulfate content. Fucoidan with a higher degree of sulfate inhibits coagulation, complement and cytokines more effectively [221]. In addition to anticoagulant activity,

fucoidan also exhibited procoagulant activity depending on the concentration and structure. Typically, procoagulant activity of fucoidan is observed at low concentration, while anticoagulant activity occurs at a high concentration [357]. In our study, PVA-SF had a significant lower fucoidan concentration on the surface compared to PVA-CDI-F and PVA-CDI-aF. This low concentration may have caused the fucoidan on PVA-SF to exhibit procoagulant activity, and thus induced significantly more thrombin generation *in vitro* and higher platelet and fibrin accumulation *ex vivo*. PVA-CDI-F samples had comparable fucoidan concentration with PVA-CDI-aF, however, the PVA-CDI-F had much higher thrombin generation. We speculated that this phenomenon could be attributed by several factors. Firstly, the amine groups on the PVA-CDI-aF samples may contribute to its better hemocompatibility. Addition of aminated groups to fucoidan has been shown to increase its anti-coagulant property. Aminated derivative of fucoidan from *Fucus vesiculosus* was found to be more effective in promoting the stimulation of t-PA-induced plasma clot lysis, and it also exhibited 2.3 times more potent efficiency in accelerating heparin cofactor II-mediated thrombin inhibition than native fucoidan [358]. The beneficial effect of aminated fucoidan on anticoagulant activity was reported to be through the intrinsic pathway, and the change on charge density of fucoidan was suggested to be the potential reason [359]. Secondly, the introduction of EDA on the fucoidan may function as a space molecule and thus enable a more flexible conformation of fucoidan. The flexible conformation has also been shown to benefit the antithrombotic activity of fucoidan [178]. Overall, the conjugation of aminated fucoidan has demonstrated significantly improved endothelialization without affecting hemocompatibility.

We observed that by adjusting the amount of EDA in the amination reaction of fucoidan, the PVA-CDI-aF samples exhibited different surface properties and biological activities. Among all the tested groups, aF25 (EDA:fucoidan=25:1) has the most amine groups on the fucoidan molecules, while aF2 has the least amine groups. However, both PVA-CDI-aF2 and PVA-CDI-aF25 exhibited high concentration of fucoidan on the PVA surfaces as detected by toluidine blue assay. The results suggested that the reduction in amine groups on fucoidan did not necessarily decrease the probability of reaction between CDI-activated PVA and aminated fucoidan. In the hemocompatibility test, PVA-CDI-aF10 exhibited a higher thrombogenicity which could be attributed to its increased water contact angle and lower fucoidan concentration. EC attachment was enhanced by all PVA-CDI-aF samples, although to a lesser extent by PVA-CDI-aF5 and PVA-CDI-aF10, which is likely due to the low surface fucoidan concentration. In the cell monolayer formation study, PVA-CDI-aF25 had significantly better monolayer formation than PVA-CDI-aF2 although they had similar fucoidan concentration on the surfaces. A previous study on EC adhesion on 2-hydroxyethyl methacrylate (HEMA)-based

polyelectrolyte hydrogels showed that increased positive surface charges allowed an enhanced cellular attachment [360]. In our study, aF25 has a higher number of positively charged amine groups, which may be reason of enhanced monolayer formation compared aF2.

Due to the heterogeneous nature of fucoidan, direct amination of fucoidan through hydroxyl groups on the fucose ring is challenging. Aminating fucoidan with diaminopropane at the reducing end by borane reduction has been proven to be successful. We conjugated the aminated fucoidan prepared by both methods on PVA and examined their activity in thrombin generation. Borane reduction prepared aminated fucoidan contained a greater number of amine groups compared to EDA prepared. However, the increased amine groups did not generate a more antithrombotic surface. Severer thrombin generation was observed in borane aminated fucoidan samples compared to EDA aminated fucoidan samples. Similar results were seen in another study that the borane reduction prepared fucoidan exhibited strong interaction with platelets [361].

Fucoidan is mainly isolated from brown seaweeds, and fucoidan isolated from different species of the seaweeds has varied chemical structure and biological activities. Fucoidans from *Fucus vesiculosus* and *Undaria pinnatifida* are two major commercial fucoidan products in the market. Fucoidan from *Fucus vesiculosus* has repeated alternating (1-3)-α-$_{L}$-fucopyranose and (1-4)-α-$_{L}$-fucopyranose [362], while fucoidan from *Undaria pinnatifida* has a mono (1-3)-α-$_{L}$-fucopyranose backbone [363]. This structural difference could contribute to varied bioactivities. In our study, we successfully aminated the fucoidans from both *Uucus vesiculosus* and *Undaria pinnatifida* and the conjugation of these two aminated fucoidans on PVA was achieved. Previous study showed that the anticoagulant activity of fucoidan from *Undaria pinnatifida* was twice that of fucoidans from *Fucus vesiculosus* [364]. However, in our study, the conjugated aminated fucoidans did not exhibit significant differences in thrombogenicity. Moreover, fucoidan from *Undaria pinnatifida* has reported to reduce proliferation and migration of HUVECs, while fucoidan from *Fucus vesiculosus* has been shown to promote EC adhesion and proliferation [237, 346, 365]. This is in line with our observation that EC adhesion on PVA-CDI-aF$_{up}$ was significantly lower than PVA-CDI-aF$_{fv}$.

The potential influence of the surface modification by sterilization could affect the success of translation application of the PVA-CDI-aF. EtO and gamma sterilization are two frequently used terminal sterilization technique. Determination of an appropriate sterilization method is important as the sterilization procedure may change the properties of the material. In our study, we evaluated effects of EtO and gamma sterilization on aminated fucoidan conjugated PVA. The cell adhesion on EtO and

gamma treated PVA-CDI-aF treated samples was comparable. Our previous study has shown an enhanced cell adhesion by gamma irradiation [366]; however, in the study of this chapter, this incremental enhancement was not significant. Platelet adhesion and fibrin accumulation on unmodified PVA has been shown to be elevated by gamma irradiation compared to EtO treatment [366]. Similar trend was observed in our study that the gamma treated PVA had significantly high peak thrombin generation rate. However, this effect was denuded by fucoidan conjugation on PVA. Overall, the terminal sterilization did not alter the bioactivities of the conjugated fucoidan significantly. However, cautions should be paid on the potential increase in thrombogenicity caused by gamma irradiation.

ePTFE is a common clinically used material for synthetic vascular grafts. ePTFE-based vascular graft exhibited high patency rate when replacing large diameter (>6mm) vessels; however, small diameter ePTFE grafts had a low patency rate of 79% at 6 months [61] and 50% at 5 years [62]. Lack of endothelialization has been proposed to be one of the primary causes of occlusion. Many efforts have been spent to improve the endothelialization on by introducing functional molecules to ePTFE. However, ePTFE is inert and thus modifying of ePTFE is challenging due to the lack reactive site. The development of plasma treatment has significantly facilitated the modification of ePTFE [367, 368]. In our study, in order to introduce reactive functional groups for CDI reaction, ePTFE was treated with air plasma. The fucoidan conjugation on plasma treated ePTFE was successfully performed; however, the density of fucoidan was low and the distribution was uneven. Park et al. found that treatment of ePTFE with NaOH could introduce additional hydroxyl (OH) groups on ePTFE [352]. Hence, in our study, we immersed the plasma treated ePTFE in 1M NaOH solution prior to CDI reaction and found that the generated samples showed more evenly distributed fucoidan on the surfaces. This also increased endothelialization on ePTFE. ePTFE itself is known to have low thrombogenicity, the conjugation of fucoidan on the ePTFE surface did not compromise this property. Additionally, our pilot animal study demonstrated the promising efficacy of the fucoidan conjugation in promoting *in vivo* endothelialization on the luminal surface of ePTFE.

4.5 Conclusion

This chapter presents a novel surface conjugation method with animated fucoidan for vascular graft application. This conjugation method exhibited significant improvement on endothelialization of PVA hydrogels without compromising thrombogenicity, surface topography or mechanical properties. The activities of the aminated fucoidan conjugation was affected by the ratio of the amination reagent, species of the fucoidan source and amination methods. In addition, the aminated fucoidan could be

conjugated to ePTFE, and the modified ePTFE demonstrated significantly improved endothelialization both *in vitro* and *in vivo*. Overall, the surface conjugation method with aminated fucoidan developed in this study could be a promising modification approach to improve endothelialization on synthetic materials. More importantly, the results in this study shed light on the importance of selecting proper modification method of fucoidan for desirable bioactivities.

Chapter 5

Combination of Fucoidan and Topographical Modification for Small Diameter Vascular Graft Application

Both biochemical and biophysical cues modulate endothelial cells behaviors. This chapter investigated the synergistic effect of fucoidan conjugation and topographical modification of PVA hydrogels on endothelial cell responses, including cell adhesion, monolayer formation and cell functions. Fucoidan conjugation significantly enhanced the endothelial cell adhesion and promoted cell monolayer formation on PVA. Topographies on fucoidan conjugated PVA mediated cell morphology and monocyte adhesion. Grating structures induced significant cell elongation and alignment. While most topography patterns did not significantly increased monocyte adhesion compared to unpatterned control, the 10 μm gratings and 2 μm pillars triggered more monocyte adhesion on endothelial cell layers. Hemocompatibility of PVA hydrogels was not affected by fucoidan nor topographies. The 2 μm gratings was selected based on cell adhesion, hemocompatibility and monocyte adhesion assay. *In vivo* study showed that fucoidan modified PVA small diameter vascular grafts had stronger blood flow and better endothelialization. The 2 μm gratings on fucoidan modified PVA grafts further improved endothelial coverage along the grafts. Integrin and focal adhesion staining showed that fucoidan improved endothelial cell adhesion by providing binding ligands for integrin β_1, α_2, α_5, α_6, and $\alpha_v\beta_5$. Focal adhesions formed by endothelial cells on fucoidan had similar number and size compared to those on gelatin, but were smaller than those on laminin. Topographies also regulated focal adhesion size, shape and distribution. Preliminary studies showed that 2 μm gratings promoted endothelial cell migration along the grating direction. The enhanced cell adhesion *in vitro* and the enhanced endothelialization *in vivo* could be due to the focal adhesion modulation and cell migration.

5.1 Introduction

Interaction between cells and their extracellular matrix (ECM) plays a fundamental role in regulating cell adhesion, proliferation, differentiation and migration [369]. Like many cell types, endothelial cells (ECs), are surrounded by its own basement membrane, which is mainly composed of contains laminin, collagen type IV, glycosaminoglycans and proteoglycans, such as heparan sulfate proteoglycans [1-3]. The component in the basement membrane provides cell binding anchors and the 3-dimensional arrangement of ECM components provides topographical cues, which combine to modulate the EC behaviors and functions. In addition to the biochemical and biophysical cues provided by the ECM,

vascular ECs are also subjected to fluid shear stress, derived from blood flow. Under physiological shear stress, ECs change phenotype from random orientation to aligned along with flow direction [86, 87]. Oriented and elongated EC morphology have been reported to be beneficial for the anticoagulant and anti-inflammation functions of ECs [370].

To mimic the native ECM environment, many efforts have been spent to incorporate ECM proteins and topographical cues on synthetic materials to stimulate endothelial cell responses. Immobilization of ECM proteins, such as collagen [371], laminin [372] and fibronectin [373], have significantly enhanced the EC adhesion and proliferation on synthetic surfaces. However, the direct contact of ECM proteins on synthetic surface with the blood stream presents a risk of acute thrombosis and platelet activation [119]. Topographical patterning on synthetic substrates have been well established to modulate EC functions. Circular topographies, such as lens and pillars, have been reported to decrease EC proliferation [286], while grooves and aligned fibers have demonstrated promotion on EC proliferation and adhesion [374]. Anisotropic topographies have also been demonstrated to induce EC elongation and alignment. The orientation of EC monolayers on microgrooved and aligned nanofibrillar substrates reduced endothelial adhesiveness for monocytes and platelets and downregulated the expression of intercellular adhesion molecule-1 (ICAM-1) [375]. In our previous study, polyvinyl alcohol (PVA) hydrogels patterned with various dimension of topographies have been prepared to stimulate the interaction between ECs and the PVA hydrogels [16]. Topographies with 2 μm gratings and 1.8 μm concave lens appeared to improved EC adhesion and function compared to unpatterned surfaces. However, the topographical cue alone failed to support EC monolayer formation on PVA, and the incorporation of biochemical modification is necessary to further improve EC adhesion and functions.

In this chapter, we hypothesize that the combination of fucoidan and topographical modification will promote endothelial cell adhesion on PVA hydrogel and enhance the luminal endothelization of PVA small diameter vascular grafts. Micro-sized isotropic and anisotropic topographical patterns were fabricated on PVA hydrogels. Fucoidan conjugation was done on both unpatterned and patterned PVA hydrogels. Platelet adhesion, activation, and thrombosis on fucoidan and topography modified PVA were assessed *in vitro* using rabbit platelet rich plasma. The effects of fucoidan conjugation and topographies on the adhesion, monolayer formation, and function of human umbilical vein endothelial cells (HUVECs) were studied. *In vivo* performance of fucoidan and topography modified PVA grafts were evaluated in a rabbit carotid artery model. *In vivo* endothelialization, blood flow inside the grafts,

and the restenosis were analyzed. Furthermore, the mechanism of improved endothelialization by fucoidan and topography was investigated by studying the integrin expression and focal adhesion formation.

5.2 Materials and methods

5.2.1 Fabrication of patterned PVA hydrogels

Fabrication of PVA hydrogels and patterned PVA hydrogels was done as described in Section 4.2.1.

5.2.2 Fucoidan conjugation on unpatterned and patterned PVA hydrogels

Fucoidan conjugation on PVA hydrogels was done as described in Section 4.2.3

5.2.3 Scanning electron microscope (SEM) measurement

SEM imaging of unpatterned and patterned PVA hydrogels was done as described in Section 3.2.3.

5.2.4 Water contact angle measurement

Water contact angle measurement of PVA hydrogels was done as described in Section 4.2.6.

5.2.5 Sterilization of PVA vascular grafts

PVA vascular grafts were sterilized with EtO treatment prior to implantation, as described in Section 4.2.7.

5.2.6 Endothelial cell adhesion and function assays

Human umbilical vein endothelial cells (HUVECs, p 3-5, Lonza) were maintained in EGM-2 medium (Lifeline). HUVECs were seeded on PVA samples at a seeding density of 50,000 cells/cm^2 and cultured for 3 days until confluent. Cells was washed once with 1x Dulbecco's phosphate-buffered saline (DPBS), fixed with 4% paraformaldehyde (PFA), permeabilized with 0.1% Triton X-100, and blocked with 5% goat serum and 0.3% Triton X-100. Following blocking, the cells were stained with vascular endothelial cadherin (VE-cad, 1:100, Cell Signaling Technology) and counterstained with DAPI to label nuclei. Images were taken using Zeiss fluorescence microscope (Axio Observer Z1) and analyzed using ImageJ software.

5.2.7 Monocyte adhesion assay

HUVECs (P3-P5) were seeded on unpatterned and patterned PVA films at 50,000 cells/cm^2 for 3 days until confluent. The endothelial cell layers were activated by incubation with 2.5 ng/mL Tumor necrosis factor-α (TNF-α, Sigma-Aldrich) in culture media for 5 hours. Human monocytes (U937, p13-14) were labeled with calcein-AM (Fisher scientific) and seeded on activated endothelial cells at 150,000 cells/cm^2. Samples were incubated for 45 min on a shaker, followed by staining against DAPI and platelet endothelial cell adhesion molecule (CD31). Images were taken using Zeiss fluorescence microscope (Axio Observer Z1) and analyzed using ImageJ software.

5.2.8 Gelatin and laminin conjugation on PVA

To compare fucoidan with extracellular matrix, conjugation of gelatin and laminin on PVA was carried out. Briefly, PVA films were dried in oven at 60°C to remove moisture. The hydrogels were then activated in CDI reaction in DMSO for 1 hour at room temperature with 100 rpm shaking. The CDI-activated PVA hydrogels were then wash 3 times in 1X phosphate buffered saline (PBS) to remove excess CDI. To prepare gelatin conjugated PVA, the CDI-activated PVA was incubated in gelatin solution overnight at 37°C. To prepare laminin conjugated PVA, CDI-activated PVA was incubated in poly(L-lysine) overnight at 4°C, followed by incubation in laminin solution for 1 hour at 37°C.

5.2.9 Focal adhesion and integrin staining

Human umbilical vein endothelial cells (HUVECs) (P3-P5) were seeded on plain PVA, unpatterned and patterned fucoidan modified PVA films at 8000 cells/cm^2 overnight. The endothelial cells were then washed once with 1x DPBS, followed by fixation with 4% PFA, permeabilization with 0.1% Triton X-100, and blocking with 5% goat serum and 0.3% Triton X-100. The cells were then immunofluorescently-stained with vinculin (mouse-anti-vinculin at 1:100, Abcam) or integrin β1 (mouse-anti-integrin β1 at 1: 50, DSHB), integrin α2 (mouse-anti-integrin α2 at 1: 60, DSHB), integrin α5 (mouse-anti-integrin α5 at 1: 50, DSHB), integrin α6 (mouse-anti-integrin α6 at 1: 50 , DSHB) and integrin αvβ5 (mouse-anti-integrin αvβ5 at 1: 20, DSHB) with the corresponding AlexaFluor 488 labeled secondary goat antibodies, and counter-stained with DAPI to label nuclei. Images were taken using Zeiss 700 confocal microscope and analyzed using ImageJ software. To analyze the focal adhesions, images were enhanced using CLAHE algorithm in MATLAB, as previous described [376], followed by analyzing using ImageJ to determine the size and density of focal adhesions.

5.2.10 Wound healing assay

Cell migration study was performed with a wound healing assay. Briefly, HUVECs (P4-5) were seeded on unpatterned and 2 μm grating patterned fucoidan modified PVA films. Cells were cultured for 3 days to allow cell monolayer formation. Wound was created by making a scratch on the cell monolayer with a triangular PDMS strip. On the 2 μm grating pattern, the wound was created in perpendicular to the grating axis, to allow cell migration direction to mimic trans-anastomotic migration in vascular graft. The created wound was around 600-700 μm in width. After the scratch was made, detached cells were removed with DPBS washing prior to imaging. The migration of the cells was tracked by taking images of the wounds using a Zeiss fluorescence microscope (Axio Observer Z1) equipped with a motorized stage at pre-determined time points (0h, 6h, 12h, 24h, 36h, 48h, 60h and 72h). The area of the wound at different time points was measured with ImageJ. Percentage of wound closure was calculated by dividing the wound area at different time points to the wound area at 0h.

5.2.11 *In vitro* hemocompatibility test

In vitro hemocompatibility assay was performed as described in Section 3.2.10.

5.2.12 Implantation of PVA small diameter vascular graft

Implantation of PVA small diameter vascular grafts was done as described in Section 3.2.12. Ultrasound doppler imaging and measurements were done using Siemens Acuson X300 ultrasound system with a VF 8-3+ (8-3 MHz) linear transducer and imaging frequency of 10 MHz at midpoints (14 days) and endpoints (28 days) to detect blood flow and check graft patency. The standard practice to investigate stenosis and intimal hyperplasia requires pre-mortal pressurized perfusion. However, due to animal ethical protocol limitation, pre-mortal perfusion could not be performed. Heparin was administrated before euthanization and PFA was injected and pressurized as soon as the vascular graft was isolated. The explanted grafts were paraffin-embedded and sectioned. H&E staining, immunofluorescence staining, and Masson's trichrome staining were on the cross-sectional tissue slides. Stenosis percentage was calculated by dividing the area of stenosis to the luminal area of the grafts from H&E staining images using ImageJ. Collagen and smooth muscle fiber percentage was determined by Masson's trichrome staining. The RGB images from the Masson's trichrome staining were split into monochromatic images using color deconvolution plugin in ImageJ. The blue and red channels were used for calculating percentage of collagen and smooth muscle fibers, respectively. The

percentage was calculated by dividing the area of collagen or smooth muscle fibers to the area of the intimal hyperplasia.

5.2.13 Statistics

All statistical analysis was performed using GraphPad Prism 8. The values of all data were presented as mean ± Standard Deviation (SD). To determine statistical significance, t-test, one-way ANOVA with Tukey's post hoc test and two-way ANOVA with Sidak's post hoc test were used. Statistical significance criterion was set at p value of <0.05.

5.3 Results

5.3.1 Surface characterization of unpatterned and patterned PVA-CDI-aF

PVA hydrogels with topographical patterns of 2 μm gratings (2μG), 5 μm gratings (5μG), 10 μm gratings (10μG), 2 μm pillars (2μP), 1.8 μm concave lenses (CCV) and 1.8 μm convex lenses (CVX) were fabricated successfully and modified with aminated fucoidan conjugation (PVA-CDI-aF). As shown in **Fig 5-1A**, fucoidan conjugation did not mask the topographical patterns on PVA. The PVA-CDI-aF hydrogel samples retained good shape fidelity for all topographies. Water contact angle analysis showed 2 μm gratings exhibited a lower contact angle compared to the circular patterns (**Fig 5-1B**). No significant difference was observed between unpatterned PVA-CDI-aF samples and patterned PVA-CDI-aF samples. Moreover, none of the modified PVA samples exhibit significant difference in water contact angle compared to plain PVA (unmodified and unpatterned), and all samples were still hydrophilic with water contact angle values ranging from 40° to 60°.

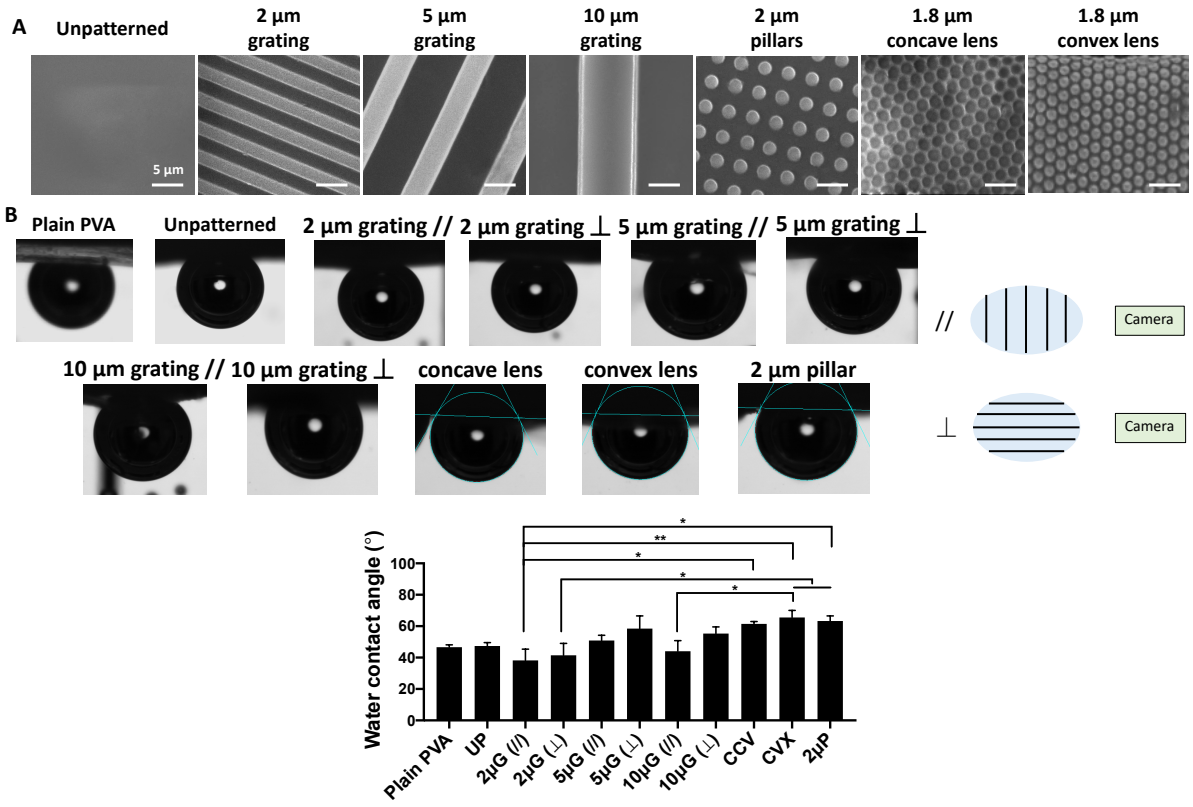


Figure 5-1. Surface characterization of unpatterned and patterned PVA-CDI-aF. (A) SEM images of unpatterned and patterned PVA-CDI-aF. (B) Water contact angel of plain PVA (unmodified and unpatterned), unpatterned and patterned PVA-CDI-aF. n=3, * and ** indicate a significant difference using one-way ANOVA with $p < 0.05$ and $p < 0.01$, respectively.

5.3.2 *In vitro* hemocompatibility of unpatterned and patterned PVA-CDI-aF

In vitro hemocompatibility test was done with rabbit platelet rich plasma. To examine the effect of fucoidan conjugation and topographical patterning on platelet behaviors, we performed SEM imaging to examine the platelet morphology and an LDH assay to quantify the platelet adhesion. The SEM images showed that collagen coated glass samples had more adhered platelets compared to PVA-based samples, and the platelets were spread on the surfaces. All plain PVA and modified PVA samples had low platelet attachment, and the adhered platelets were rounded and exhibited similar morphology (**Fig 5-2A**). The LDH absorbance did not show any statistically significant difference in the number of adhered platelets among the plain PVA and modified PVA groups, although grating samples had a

slightly lower platelet attachment (**Fig 5-2B**). Collagen coated glass had significantly higher platelet adhesion than PVA-based samples. Thrombogenicity was tested in a real-time thrombin generation assay. Three parameters, lagtime, peak thrombin generation rate (peak), and total thrombin generation (ETP) were selected to represent the thrombogenicity. No significance was observed in lagtime, but collagen coated glass had significantly higher peak thrombin generation rate and total thrombin generation. The plain PVA and modified PVA groups did not exhibit significance in thrombin generation assay (**Fig 5-2C-E**). The quantification results showed that the thrombogenicity of PVA was not significantly altered by the fucoidan conjugation nor the topographical patterning.

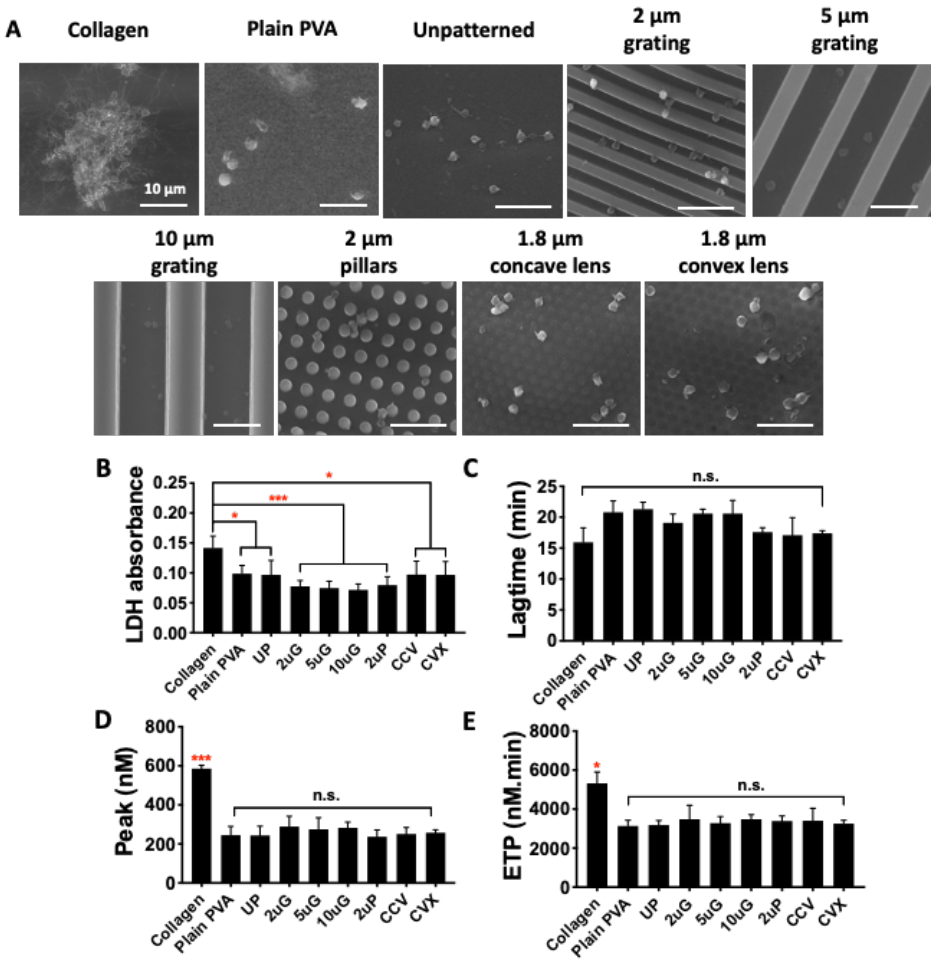


Figure 5-2. *In vitro* hemocompatibility of unpatterned and patterned PVA-CDI-aF. (A) Representative SEM images of platelets on unpatterned and patterned PVA-CDI-aF. (B) Quantification of platelet adhesion determined by lactate dehydrogenase (LDH) assay. (C-E) Realtime thrombin generation. Lag-time (C) represents the time taken to start forming thrombin. Peak

(D) represents the maximum thrombin generation rate. ETP (F) represents endogenous thrombin potential. N=4, * and *** indicate a significant difference using one-way ANOVA with $p < 0.05$ and $p < 0.005$, respectively, n.s. indicates no significance was seen between plain PVA and PVA-CDI-aF samples.

5.3.3 Endothelial cell adhesion and function

Adhesion of HUVECs was investigated on plain PVA, unpatterned PVA-CDI-aF, and patterned PVA-CDI-aF. As shown in **Fig 5-3A**. Only a few numbers of cells were attached on plain PVA samples. The HUVECs on PVA had rounded cell morphology and they were unable to form confluent monolayer within the culture period. Cells on all PVA-CDI-aF samples exhibited good attachment and formed confluent monolayers. The cell density on all PVA-CDI-aF samples was significantly higher than plain PVA (**Fig 5-3B**). Cell spreading on plain PVA and modified PVA was compared. Cells on PVA-CDI-aF samples exhibited a significantly larger cell area compared to those on plain PVA (**Fig 5-3C**). The fluorescence staining of HUVECs showed that VE-cadherin were strongly expressed at the cell boundaries by the cells on PVA-CDI-aF samples, while VE-cadherin expression of cells on plain PVA was observed only in the cell cytoplasm (**Fig 5-3A**).

The comparison of the cell adhesion on unpatterned PVA-CDI-aF and patterned PVA-CDI-aF showed that the topographies on PVA-CDI-aF did not exhibit significant alteration on the cell density and average cell area (**Fig 3-B,C,D**). However, HUVECs on different topographies formed distinguishable morphology. Cells on grating structures had a significant decrease in cell circularity compared to ECs on circular patterns and unpatterned samples. Grating patterns induced noticeable cell elongation and alignment along the grating axis. Moreover, the decrease in cell circularity increases with the grating size (**Fig 3-E**).

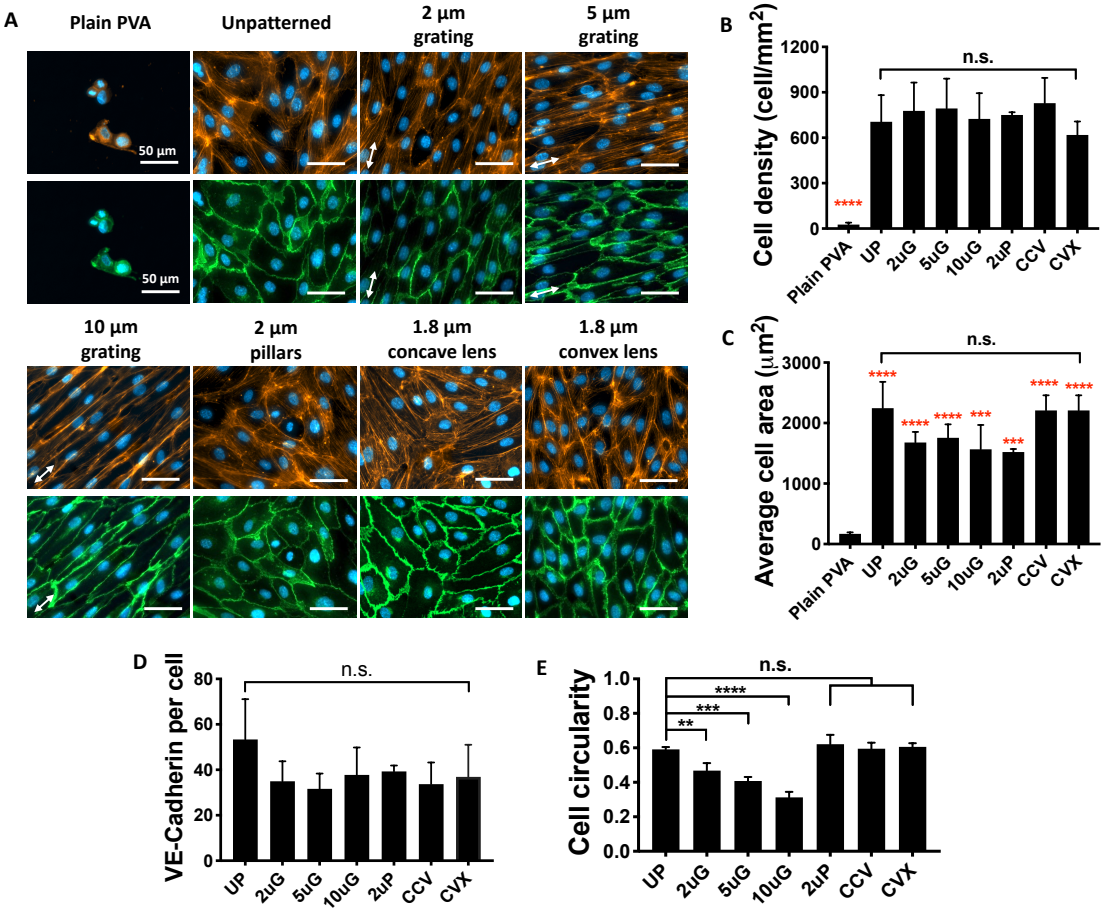


Figure 5-3. Endothelialization on unpatterned and patterned PVA-CDI-aF. (A) Representative immunofluorescent images of endothelial cells plain PVA, unpatterned, and patterned PVA-CDI-aF. Scale bar = 50 µm. Blue denotes nuclei, green denotes VE-cadherin and orange denotes F-actin. Cell density (B), average cell area (C), VE-cadherin expression (D) and cell circularity (E) of endothelial cells on unpatterned and patterned PVA-CDI-aF. N=6, **, *** and **** indicate a significant difference using one-way ANOVA with $p < 0.01$, $p < 0.005$, and $p < 0.0005$, respectively.

Monocyte adhesion on endothelial monolayers was examined to evaluate the effect of topographies on PVA-CDI-aF samples on the interaction of endothelial monolayer with the immune cells. Plain PVA was not included in the study due to the lack of endothelial monolayer formation. Monocyte adhesion density on most of the topographies was not significantly different from the unpatterned (UP) control. However, 10 µm gratings (10µG) and 2 µm pillars (2µP) induced a significantly higher monocyte

adhesion on endothelial monolayers, compared to unpatterned PVA-CDI-aF and 2 μm gratings. No significant difference was observed in the CD31 expression.

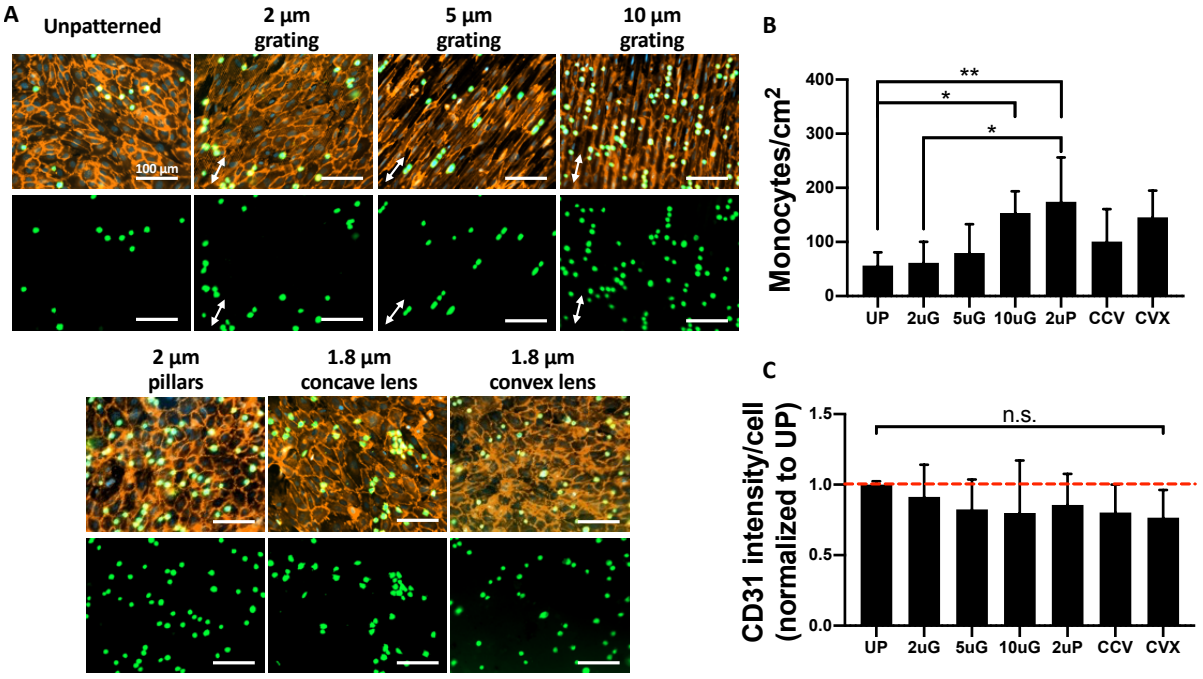


Figure 5-4. Monocyte adhesion on endothelial cells on unpatterned and patterned PVA-CDI-aF. (A) Representative immunofluorescent images of monocytes and endothelial cells on unpatterned and patterned PVA-CDI-aF. Scale bar = 100 μm. Blue denotes nuclei, green denotes monocytes and orange denotes CD31. (B) Monocyte density on unpatterned and patterned PVA-CDI-aF. N=6, * and ** indicate a significant difference using one-way ANOVA with $p < 0.05$ and $p < 0.01$, respectively. (C) CD31 expression of endothelial cells on unpatterned and patterned PVA-CDI-aF. N=6, no statistical significance was observed.

5.3.4 *In vivo* performance of PVA small diameter vascular graft with fucoidan and topography modification

To evaluate the effect of topography and fucoidan conjugation modifications on the *in vivo* endothelialization and patency of PVA grafts, 2 mm in diameter and 2 cm in length PVA small diameter grafts were fabricated and implanted in rabbit right common carotid arteries, as shown in **Fig 3-**11. Three groups of grafts, plain PVA (n=4), unpatterned PVA-CDI-aF (n=4), and PVA-CDI-aF (n=5) with

2 μm gratings luminal pattern were implanted and tested. After 4 weeks of implantation, plain PVA, unpatterned PVA-CDI-aF, and PVA-CDI-aF grafts had patency rate of 75%, 75%, and 80%, respectively. To detect the blood flow changes inside the grafts, ultrasound imaging was done at pre-determined time points 0, 1, 2 and 4 weeks. As shown in **Fig 5-5A**, the blood flow inside the unpatterned PVA-CDI-aF grafts and PVA-CDI-aF grafts with 2 μm gratings was stronger than plain PVA grafts at both 2-week and 4-week time points. The blood flow velocity at midpoint (2 weeks) and endpoint (4 weeks) was shown in **Fig 5-5B and C**. The average flow velocity inside UP PVA-CDI-aF grafts and 2μG PVA-CDI-aF grafts was higher that of plain PVA grafts at both midpoint and endpoint, although the difference was not statistically significant.

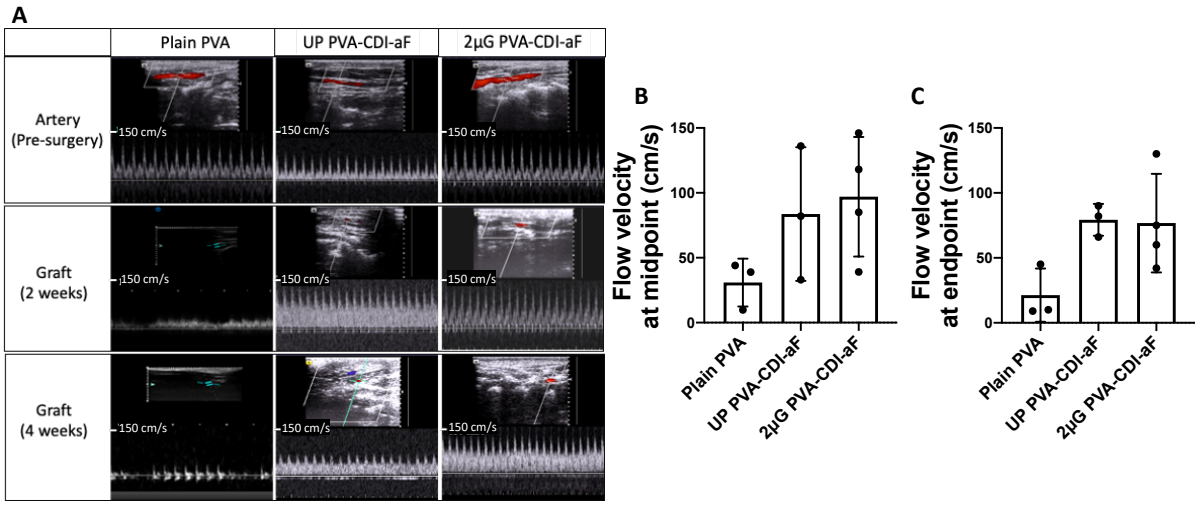


Figure 5-5. Ultrasound imaging of blood flow inside unmodified and modified PVA grafts. (A) Representative ultrasound images of blood flow inside the grafts before surgery, 2 weeks after surgery and 4 weeks after surgery. Flow velocity inside the grafts at midpoint (2 weeks) (B) and at endpoint (after 4-week). UP indicates unpatterned grafts, and 2μG indicates grafts with 2 μm gratings. No statistical significance was observed.

After 4 weeks of implantation, the grafts were harvested and sectioned to examine the endothelial cell attachment inside the luminal surfaces of the grafts. The graft was cut into three segments: close to proximal end, in the mid-point of the graft (B) and close to distal end, as shown in **Fig 5-6B**. Immunofluorescence staining of the cross-sections of the grafts revealed the presence of cells on the luminal surfaces of both UP PVA-CDI-aF and 2μG PVA-CDI-aF grafts. The CD31 and VE-cadherin positive staining of the cells indicated that the cells were endothelial cells. No cell was observed on

plain PVA surfaces. Furthermore, to quantify the endothelialization, the graft that had higher than 50% endothelial coverage on the luminal surface was defined as an endothelialized graft at each of the defined position. As shown in **Fig 5-6C**, none of the plain PVA grafts were endothelialized. 75% of UP PVA-CDI-aF grafts and 80% of 2μG PVA-CDI-aF grafts were endothelialized in the proximal section; 25% of UP PVA-CDI-aF grafts and 60% of 2μG PVA-CDI-aF grafts were endothelialized in the mid-point of the grafts; while 25% of UP PVA-CDI-aF grafts and 40% of 2μG PVA-CDI-aF grafts were endothelialized in the distal section. The endothelial coverage on the luminal surfaces of patent grafts were calculated. Both UP PVA-CDI-aF grafts and 2μG PVA-CDI-aF grafts had significantly higher endothelial coverage compared to plain PVA in the proximal section and distal section. 2μG PVA-CDI-aF grafts also had significantly higher endothelial coverage than plain PVA in the mid-point of the grafts. No significant differences were observed in the percentage of endothelial coverage between UP PVA-CDI-aF grafts and 2μG PVA-CDI-aF grafts (**Fig 5-6D**).

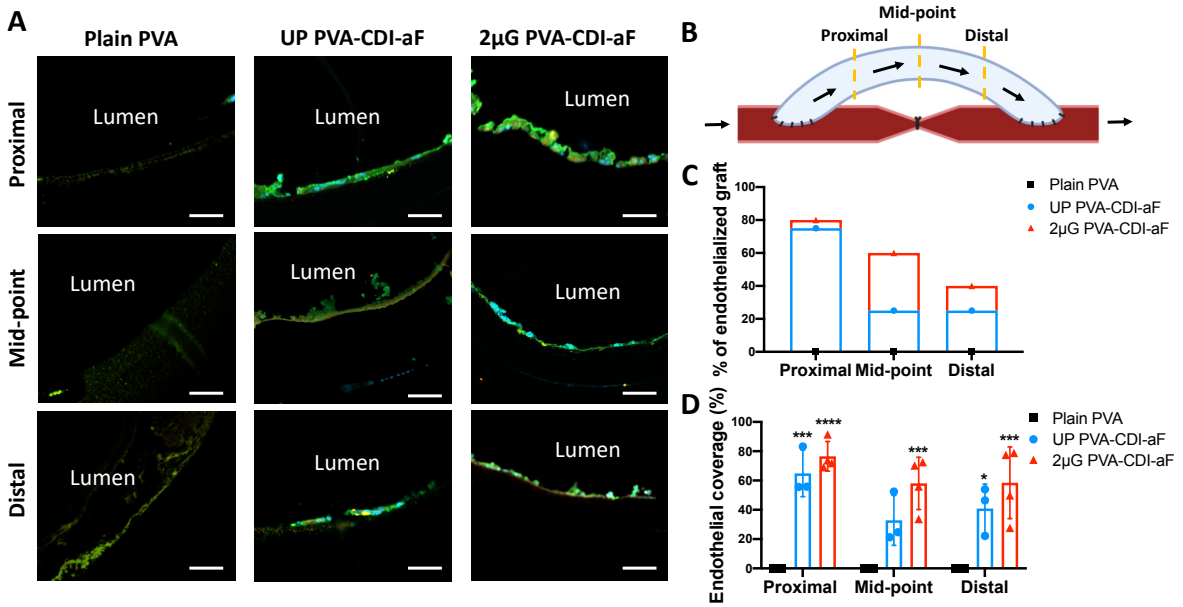


Figure 5-6. *In vivo* endothelialization of PVA small diameter grafts after 4 weeks of implantation. (A) Representative immunofluorescent images of endothelial cells in the lumen of PVA grafts. Scale = 100 μm. Blue denotes nuclei, green denotes VE-cadherin, and orange denotes CD31. (B) Schematic diagram of the sample location. (C) Percentage of grafts that have higher than 50% endothelial cell coverage at each position. (D) Endothelial coverage percentage of patent grafts. N=3 for plain PVA and UP PVA-CDI-aF, n=4 for 2μG PVA-CDI-aF. *, *** and **** indicate a significant difference using two-way ANOVA with $p < 0.05$, $p < 0.005$, and $p < 0.0005$, respectively.

Stenosis of the vascular grafts was estimated by doing H&E staining at the anastomotic junctions of the grafts and arteries. In the plain PVA grafts, a significant amount of blood clot was observed at both proximal and distal anastomoses, while minimal clot was seen in PVA-CDI-aF grafts. The intimal hyperplasia (IH) was presented in anastomotic junctions, and the majority of the IH was located on the floor of the native arteries (**Fig 5-7A**). The stenosis percentage at the anastomotic junctions was quantified by dividing the area of stenosis to the luminal area of the grafts. No statistical significance was observed among the samples, although 2μG PVA-CDI-aF grafts had a slightly lower restenosis percentage at the proximal anastomoses (**Fig 5-7B**).

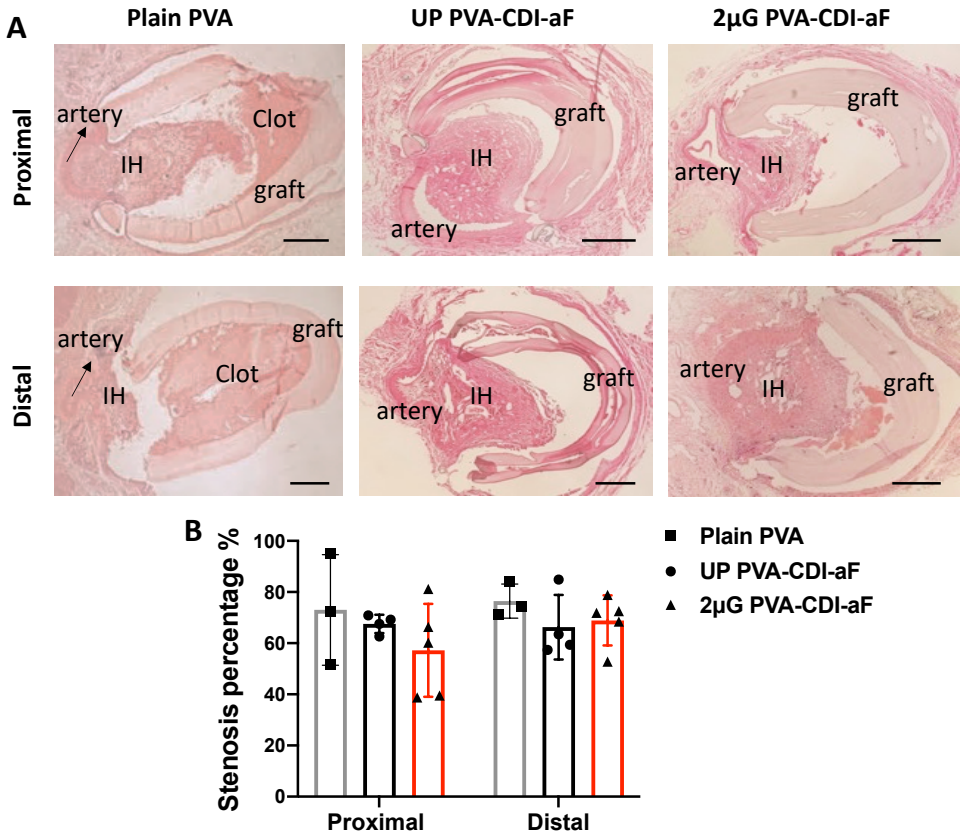


Figure 5-7. Stenosis at the anastomoses of the explanted grafts. (A) Representative hematoxylin and eosin (H&E) images of proximal and distal anastomoses and stenosis percentage. Scale = 500 μm. (B) Stenosis percentage at proximal and distal anastomoses. N=4 for plain PVA and UP PVA-CDI-aF, n=5 for 2μG PVA-CDI-aF, no significance was observed.

To identify the composition of the IH in proximal and distal anastomoses of grafts, the cross-sections around the anastomotic junctions were stained with Masson's trichrome staining. The Masson's trichrome staining showed profuse collagen as well as smooth muscle cells in the IH of all types of grafts (**Fig 5-8A**). The different color channels were split into monochromatic images to analyze the percentage of the total area of individual components. The percentage of collagen and smooth muscle cells were comparable, but a large animal-to-animal variation was observed, especially at the distal anastomosis. No significant difference was seen among the three types of grafts.

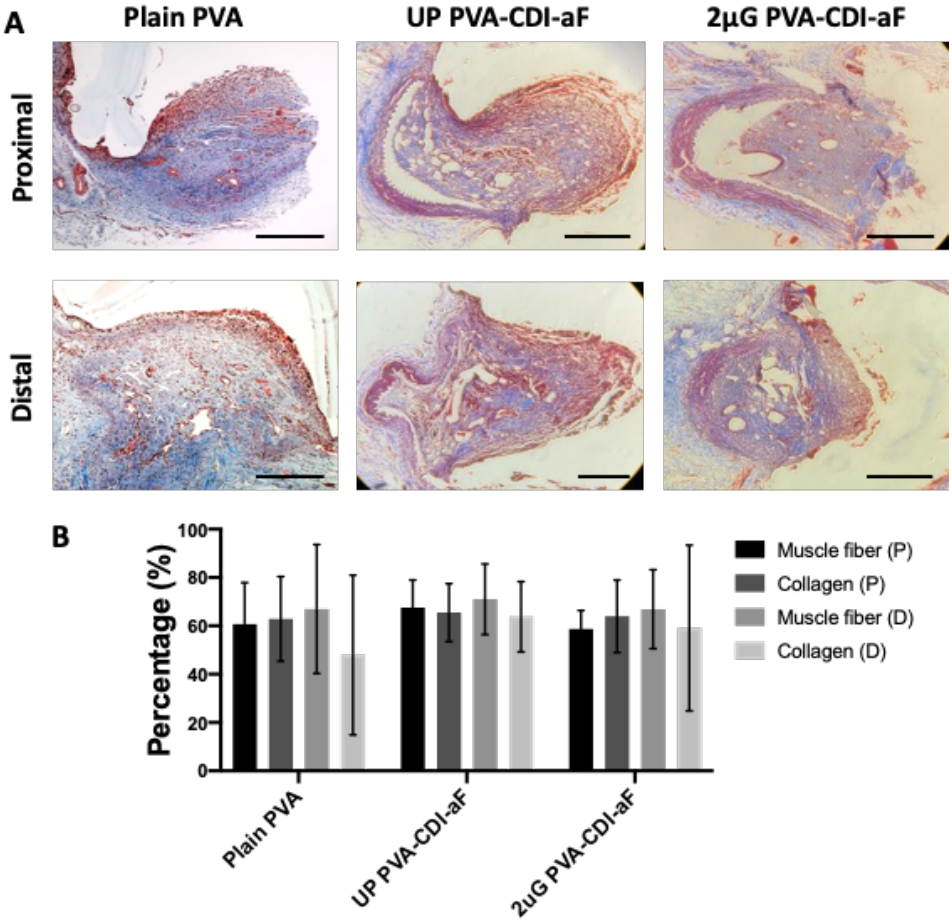


Figure 5-8. Composition of intimal hyperplasia (IH) in proximal and distal anastomoses of grafts. (A) Representative Masson's trichrome staining images of the stenosis in proximal and distal anastomoses of plain PVA, unpatterned PVA-CDI-aF and PVA-CDI-aF grafts with 2 μm gratings. Scale = 500 μm. Blue denotes collagen and red denotes muscle fibers. (B) Percentage of the area collagen and muscle fiber to the area of total IH in the stenosis. P and D indicated the percentage at

the proximal and distal anastomosis, respectively. N=4 for plain PVA and UP PVA-CDI-aF, n=5 for 2μG PVA-CDI-aF. No significance was observed.

5.3.5 Endothelialization was improved through integrin and focal adhesion formation

The *in vitro* and *in vivo* studies demonstrated that the fucoidan conjugation improves the endothelialization on PVA hydrogels, and the topographies could further affect the endothelial cell responses. To explore the potential mechanism, we investigated the integrin expression and the formation of focal adhesions in the HUVECs on fucoidan. Immunofluorescence staining of HUVECs on PVA-CDI-aF samples showed that cells showed spread morphology and exhibited positive staining of integrin subunits β_1, α_2, α_5, α_6, and integrin $\alpha_v\beta_5$, but did not show positive signals for $\alpha_M\beta_2$ (**Fig 5-9**). The integrin subunits α_2, α_5, and α_6 can pair with integrin subunit β_1, forming $\alpha_2\beta_1$, $\alpha_5\beta_1$, and $\alpha_6\beta_1$ dimers that bind to the ligands within ECM proteins. As listed in **Table 5-1**, laminin provides ligands for integrins $\alpha_2\beta_1$, $\alpha_6\beta_1$, and $\alpha_v\beta_5$, and gelatin provides ligand for integrin $\alpha_5\beta_1$.

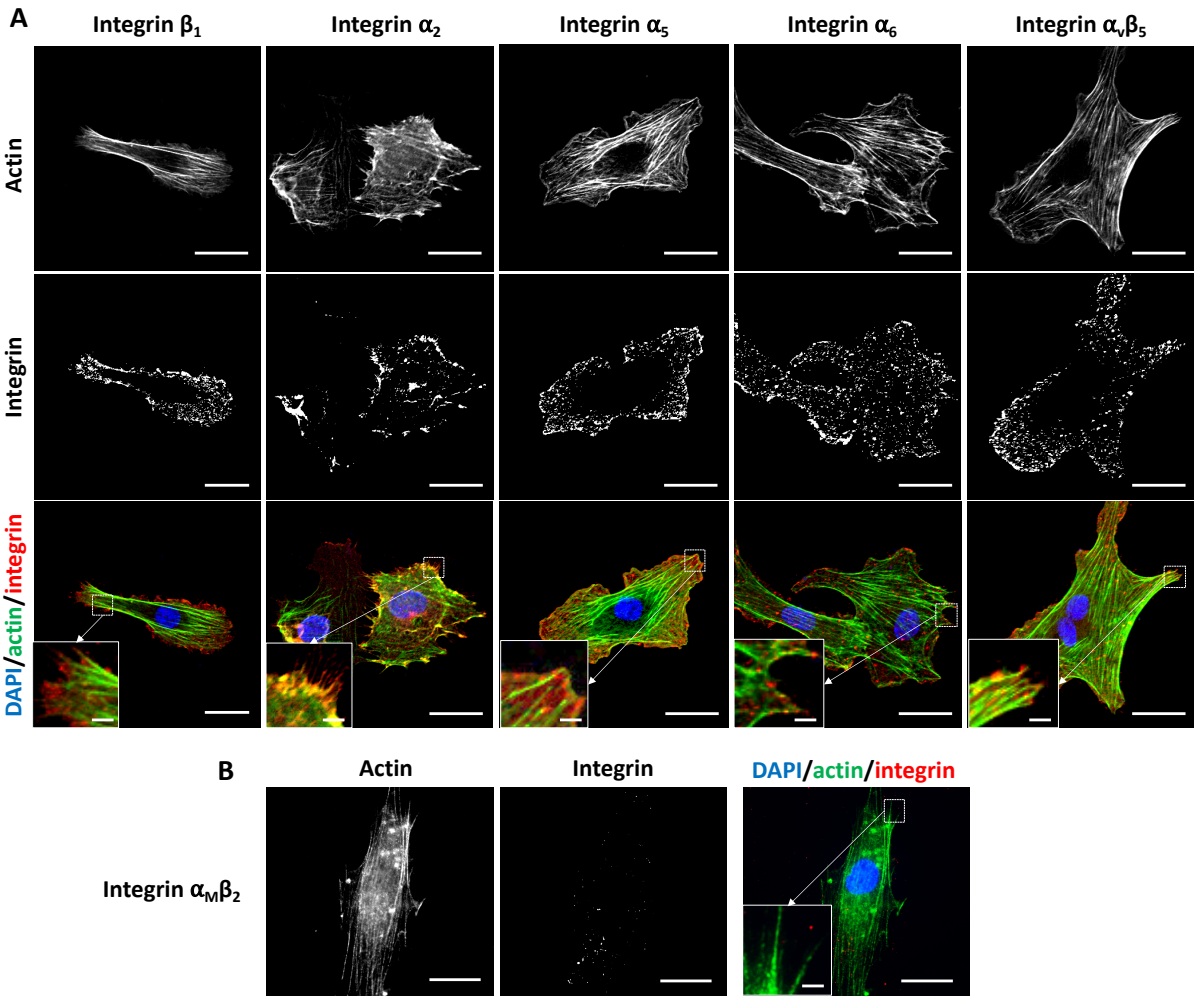


Figure 5-9. Integrin formation by HUVECs on fucoidan. (A) Representative images of integrin subunits β_1, α_2, α_5, α_6, and integrin $\alpha_v\beta_5$ formed by endothelial cells on PVA-CDI-aF. Scale bar = 30 μm. Inset shows magnified view (scale bar = 5 μm). (B) Staining of integrin $\alpha_M\beta_2$ did not show positive signals. Scale bar = 30 μm.

Table 5-1. Integrins form by ECs on extracellular matrix proteins.

Integrins	ligands	Refs
$\alpha_2\beta_1$	Collagen IV, laminin	[377, 378]
$\alpha_5\beta_1$	Gelatin, fibronectin	[379]
$\alpha_6\beta_1$	Laminin	[380]

$\alpha_v\beta_5$	Vitronectin, laminin	[381]

To compare the fucoidan with ECM proteins, gelatin (GEL) and laminin (LMN) were conjugated on PVA through CDI reaction. Focal adhesion (FA) formed by HUVECs on PVA-CDI-aF, PVA-CDI-LMN and PVA-CDI-GEL were compared by staining against vinculin. As shown in **Fig 5-10A**, cells on plain PVA were less spread compared to those on modified PVA, and only a few numbers of mature FAs were seen on plain PVA samples. The quantification analysis confirmed that HUVECs on PVA formed significantly less FAs compared to on PVA-CDI-aF, PVA-CDI-LMN and PVA-CDI-GEL. Similarly, the total area of FAs on PVA was also significantly lower than on the modified PVA samples. In addition, the average size of FAs on plain PVA was significantly smaller than those on PVA-CDI-LMN. Fucoidan and gelatin exhibited similar effects on FA formation. The FA number, average FA size, and total area of FAs did not exhibit significantly difference between PVA-CDI-aF and PVA-CDI-GEL samples. Laminin demonstrated a stronger interaction with ECs compared to fucoidan by forming larger size of FAs.

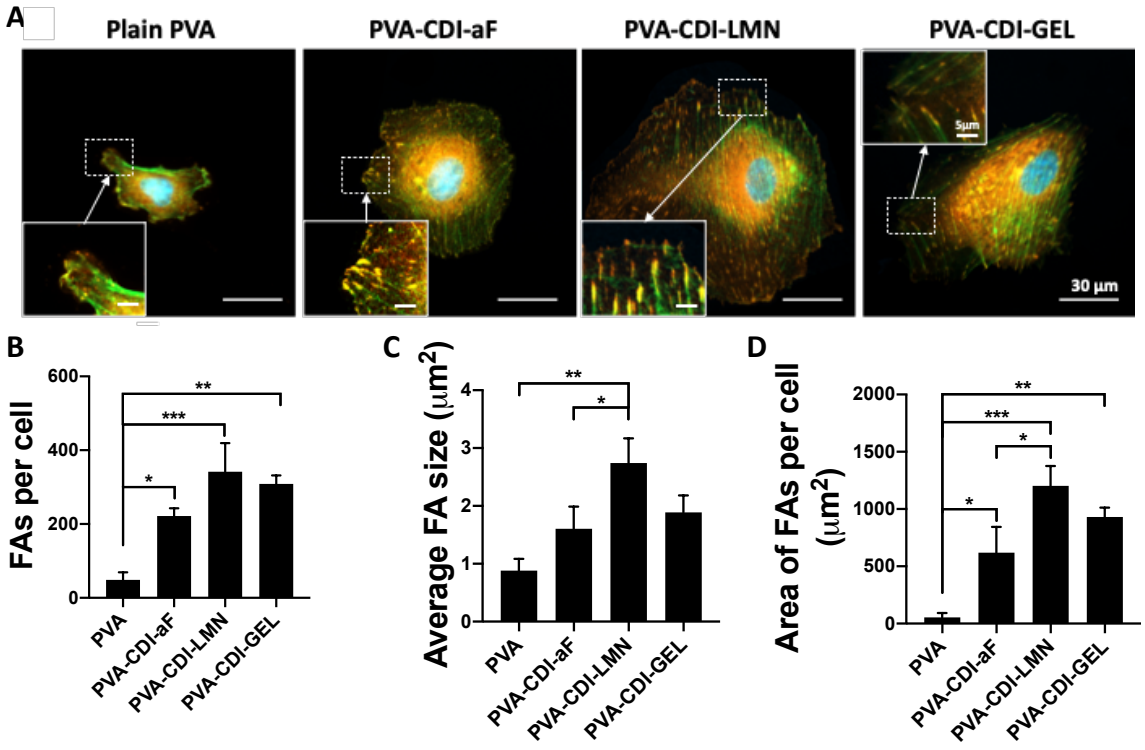


Figure 5-10. Comparison of focal adhesion formation by HUVECs on fucoidan, laminin and gelatin. (A) Representative images of focal adhesions formed by endothelial cells on unmodified PVA, fucoidan conjugated PVA (PVA-CDI-aF), laminin-conjugated PVA (PVA-CDI-LMN) and gelatin conjugated PVA (PVA-CDI-GEL). Blue denotes nuclei, green denotes F-actin and orange denotes vinculin. Scale bar = 30 μm. Inset shows magnified view (scale bar = 5 μm). Number of focal adhesions per cell (B), average focal adhesion size (C) and total area of focal adhesions per cell (D) on unpatterned and patterned PVA-CDI-aF. N=6, *, ** and *** indicate a significant difference using one-way ANOVA with $p < 0.05$, $p < 0.01$ and $p < 0.005$, respectively.

We further assessed the effects of topographical patterns on the FA formation by HUVECs on PVA-CDI-aF samples. Cells showed a spread morphology and formed FA formation on both unpatterned and patterned PVA-CDI-aF samples (**Fig 5-11A**). A difference in the FA shape and distribution among different topographies was observed. On unpatterned and grating surfaces, FAs exhibited elongated shape, and the FAs on the grating structures appeared to align along the grating axis. FAs were observed around the edges of 10 μm gratings. While on the circular topographies, FAs were rounded and FAs on the 2 μm pillars were mainly on the top surfaces of the pillars. Quantification results showed that the number of formed FAs were significantly lower on the 5 μm gratings and 10 μm gratings compared to unpatterned samples, while convex lenses had significantly more FAs compared to gratings. The size of FA was slightly increased on grating structures although the difference was not statistically significant. The overall area of FAs on convex lenses was the highest among all the topographies.

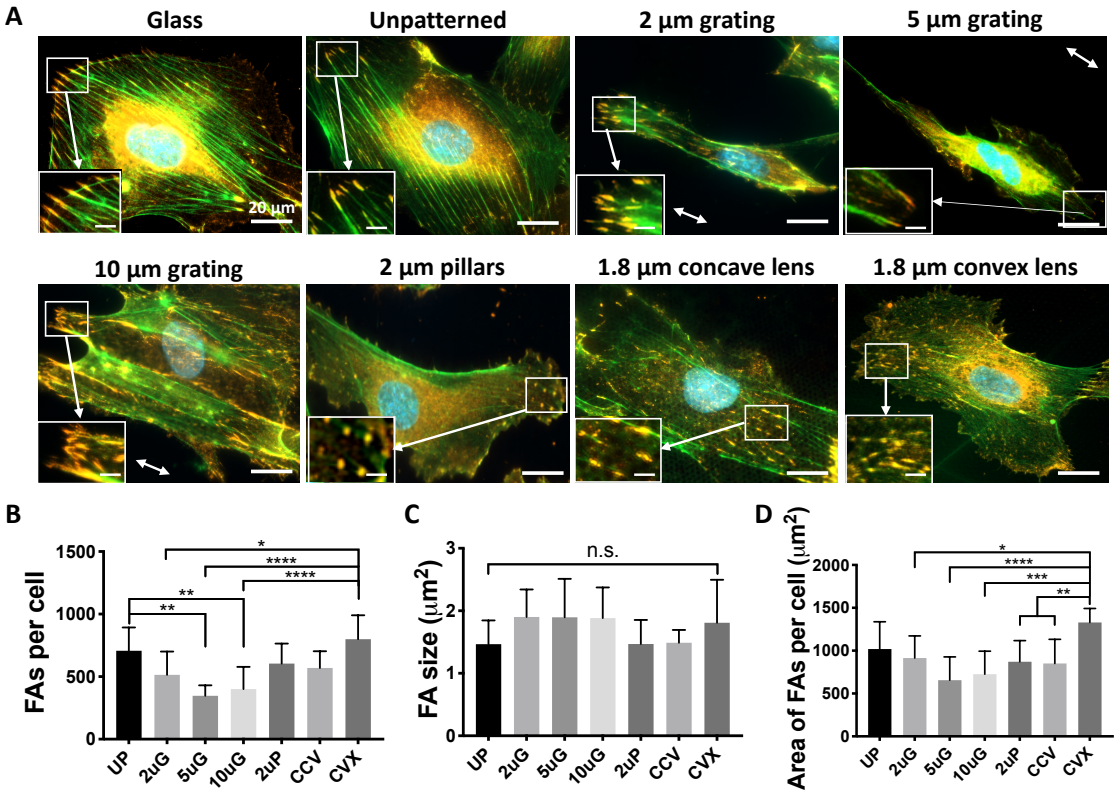


Figure 5-11. Focal adhesion formation by HUVECs on unpatterned and patterned PVA-CDI-aF. (A) Representative immunofluorescence images of focal adhesion formed by HUVECs on unpatterned and patterned PVA-CDI-aF. Scale bar = 20 µm. Blue denotes nuclei, green denotes F-actin and orange denotes vinculin. Inset shows magnified view (scale bar = 5 µm). Number of focal adhesions per cell (B), average focal adhesion size (C) and total area of focal adhesions per cell (D) on unpatterned and patterned PVA-CDI-aF. N=6, *, **, *** and **** indicate a significant difference using one-way ANOVA with $p < 0.05$, $p < 0.01$, $p < 0.005$ and $p < 0.0005$, respectively.

Gratings patterns have been demonstrated to provide contact guidance and enhance cell migration, which could contribute to the better *in vivo* endothelialization [382]. To assess if the combination of fucoidan and 2 µm gratings would also enhance cell migration, an endothelial cell migration study was done on unpatterned and patterned PVA-CDI-aF samples with 2 µm gratings using a wound healing assay. Scratches on 2 µm gratings samples were made perpendicular to the grating axis. As shown in **Fig 12A**, HUVECs on PVA-CDI-aF with 2 µm gratings covered more scratched area at 24h and 48h compared those on unpatterned PVA-CDI-aF, and the wound on 2 µm gratings was fully closed before

72h. The quantification results of wound area showed that the HUVECs on 2 μm gratings had higher percentage of closure at different time points than those on unpatterned PVA-CDI-aF (**Fig 13B**). The results indicate that the cells on 2 μm gratings migrated faster along the grating axis to cover the wounds.

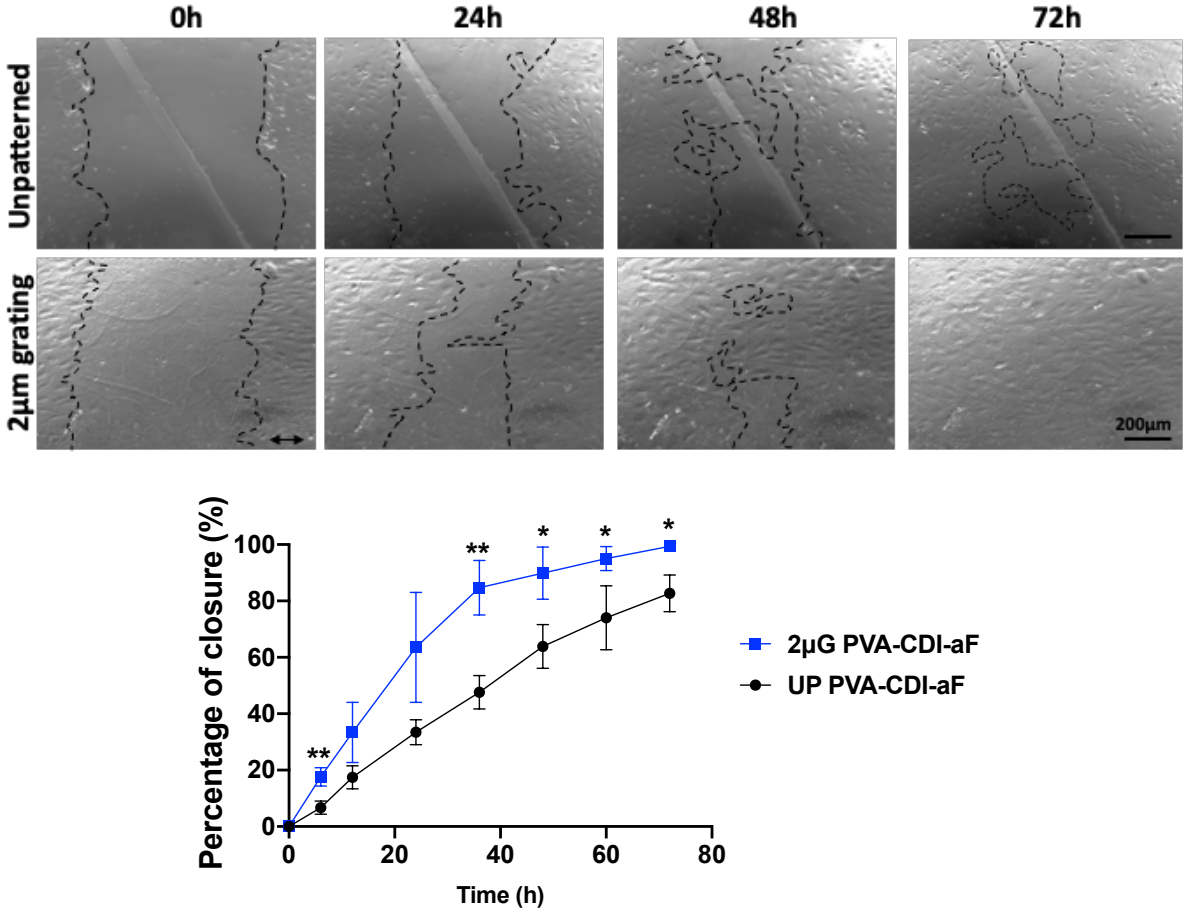


Figure 5-12. Endothelial cell migration with a wound healing assay. Representative images of HUVECs on unpatterned PVA-CDI-aF and PVA-CDI-aF with 2 μm gratings at 0h, 24h, 48h, and 72h after the scratches were made. Scale bar = 200 μm. Arrow indicates the direction of the 2 μm gratings. N=4, * and ** indicate a significant difference using one-way ANOVA with $p < 0.05$ and $p < 0.01$, respectively.

5.4 Discussion

In natural extracellular micro-environment, ECs are subjected to biochemical and biophysical cues provided by the EC basement membrane. Mimicking the natural niche on synthetic substrates by introducing biochemical and topographical modifications on synthetic materials has been a widely explored strategy to mediate EC behaviors and functions. In a previous study from our group, topographical patterning on PVA was successfully achieved by casting PVA solution on patterned PDMS molds [16]. The topographical patterns on PVA hydrogels were found to improve the interactions between the ECs and the substrates, however, without additional surface modification, ECs were not able to form monolayers on patterned PVA. Approaches using plasma treatment demonstrated a significantly improved EC adhesion on patterned PVA, however the plasma treatment is subjected to low stability and the risk of increased platelet adhesion [174]. With the development of the aminated fucoidan conjugation method as described in Chapter 4, we successfully fabricated fucoidan conjugated PVA samples with topographies of various dimensions, including different sizes of grating, pillars and lenses. The SEM images confirmed that the topographies on PVA retained their shape and size fidelity after the conjugation of aminated fucoidan, indicating that the fucoidan conjugation method is compatible with topographical patterning on PVA surface. Topographies have been known to alter the surface energy of a material [383, 384]. In our test, the water contact angle was altered by the topographical patterns; however, this alteration did not significantly change the hydrophilicity compared to unmodified plain PVA.

The effects of substrate topography on endothelial cell responses have received broad research interests, several studies have also reported that the topography could affect platelet adhesion, spreading and activation [385]. The size, aspect ratio and interspacing of the substrate topographies have all been shown to play a role in platelet adhesion [324]. However, in our study, the substrate topographies on PVA did not induce noticeable changes in platelet adhesion nor thrombin generation. We speculated that this phenomenon is attributed to both the resistance of PVA to protein adsorption and the antithrombotic activity of fucoidan. Platelet adhesion and activation on synthetic surfaces are known to be triggered by the deposition of plasma proteins on the material surfaces. PVA is known to resist non-specific protein adsorption [386], which could contribute to the low number of platelet adhesion on PVA samples. Additionally, platelet adhesion on synthetic materials is mediated by surface properties of the materials, such as surface energy and surface charge [387]. In our study, the topographies on

fucoidan conjugated PVA samples did not cause a drastic change in surface energy, which could also explain the results in platelet adhesion.

As previously described, unmodified plain PVA does not support endothelialization. The fucoidan conjugation has significantly enhanced the HUVEC attachment and the HUVEC monolayer formation, regardless of the type of topographies. Despite the similar cell density, cell area, and VE-cadherin expression, the HUVEC morphology on patterned PVA-CDI-aF samples varied vastly. HUVECs on unpatterned and circular patterns had high circularity and exhibited cobblestone morphology, which resembles the morphology of ECs under static condition. While on gratings structures, HUVECs were elongated and aligned, similar to the physiological morphology of EC under blood flow. The elongated and aligned morphology of ECs has been shown to be beneficial for the antithrombotic and anti-inflammatory functions of ECs [291]. The interaction between ECs and the immune system is a vital function of the endothelium *in vivo*. Monocyte adhesion on endothelium and consequent intravasation leads to chronic inflammation and the development and progression of atherosclerosis [388]. Topographical cues have been reported to affect the inflammatory phenotype of endothelial cells and expression of inflammatory cytokines [389]. Our previous studies and a study from another group have suggested that the increased monocyte adhesion is closely related to increased intercellular adhesion molecule-1(ICAM-1) expression [286, 390]. In our monocyte adhesion assay, significantly higher monocyte adhesion was found on 2 μm pillars and 10 μm gratings, which have been reported to induce a greater expression of phospho-AKT and ICAM-1 by the ECs [390]. Additionally, comparing different sizes of gratings, 10 μm appeared to induce a greater expression of inflammatory cytokines interleukin 1 beta (IL-1β) and TNF-α of endothelial cells, which could also explain the increased monocyte adhesion on 10 μm gratings [391]. CD31 is an important regulator of trans-endothelial migration [392]. It also maintains the endothelial cell junctional integrity. In our study, CD31 expression was observed at the cell boundaries on all samples. The topographies did not exhibit a noticeable alteration on the expression level of CD31. This is similar to the observations in the previous studies form our group [286, 294] on PDMS, which may indicate that the CD31 expression is less sensitive to topographies compared to ICAM-1. Overall, based on the *in vitro* EC adhesion and function assessment, we found that the 2 μm gratings induced a more favorable EC morphology but did not induce severe monocyte adhesion, and thus 2 μm gratings were chosen to proceed the *in vivo* study.

The implantation of plain PVA and fucoidan-modified PVA small diameter vascular grafts was done in a rabbit right common carotid artery model. Staining of the cross-sections of the grafts demonstrated

the efficacy of fucoidan conjugation on improving EC adhesion *in vivo*. Plain PVA grafts did not have EC attachment on the luminal surfaces. Significant amount of blood clot formed at the anastomosis and inside the graft due to the lack of endothelial lining, which also leads to a significant reduction in blood flow inside the PVA grafts after 14 days. Trans-anastomotic ingrowth has been proposed as an important mechanism of endothelialization in acellular grafts [393]. The trans-anastomotic ingrowth relies on the migration of host ECs from the anastomosis to the middle of the graft. Migration of ECs *in vivo* could be modulated by shear flow [394]. In a wound healing model, under the fluid shear stress, cells at the upstream side were more elongated and orientated compared to the cells at the downstream. The fluid shear stress also induced more protrusion formation by the cells at the upstream. Therefore, cells at the upstream were shown to have faster migration under fluid shear stress compared to cells at the downstream [395]. This explains our observations that a high proportion of grafts were endothelialized at the proximal side compared to the distal side.

Fucoidan has been reported to interact with several integrins. Fucoidan interact with integrin subunit α_5 and cause re-organization of integrin α_5 on cancer cells [396]. The interaction of fucoidan with β_1 was shown to be important for fucoidan-induced cancer cell apoptosis [397]. Fucoidan was shown to provided binding site for $\alpha_M\beta_2$ in bone marrow myeloid cells [398]. In the presence of FGF-2, fucoidan has been shown to enhance α_6 and β_1 expression of HUVECs [399]. Also, fucoidan alone increased α_6 integrin subunit expression on of endothelial progenitor cells [400]. In our study, HUVECs on fucoidan expressed integrin subunits β_1, α_2, α_5, α_6, and $\alpha_v\beta_5$, but did not express $\alpha_M\beta_2$. These expressed integrins were either reported to have interactions with fucoidan previously or serves as important anchor for EC adhesion. To compare fucoidan with other ECM proteins, we selected laminin, which provides ligands for $\alpha_2\beta_1$, $\alpha_6\beta_1$, and $\alpha_v\beta_5$, and gelatin, which provides ligand for integrin $\alpha_5\beta_1$. Laminin and gelatin were selected also because laminin and collagen are the main ECM components in the vasculature. While we have previously demonstrated the conjugation of gelatin to PVA via CDI-conjugation, direct conjugation of large laminin and collagen negatively impacted bioactivates, including compromised cell adhesion (data not shown). Therefore, gelatin was used as a comparison. The focal adhesion staining showed that fucoidan functioned to provide cell binding anchors to facilitate cell adhesion, similar to ECM protein gelatin and laminin. HUVECs on laminin had larger size of focal adhesion compared to HUVECs on fucoidan. However, laminin modification presents a risk of increased platelet adhesion and activation [401]. As laminin also has other limitations such as short half-life, the bioactivities are sensitive to protein conformation, we postulate that the surface modification with

sulfated polysaccharide fucoidan could be more advantageous for the application in enhancing off-the-shelf vascular grafts.

Our *in vivo* studies have demonstrated that PVA-CDI-aF grafts with 2 μm gratings had higher endothelial coverage at the middle and the distal segments of the grafts compared with unpatterned PVA-CDI-aF grafts. We believe that this is attributed to the increased cell migration on grating structures. In our cell migration study, we observed that endothelial cells on 2 μm gratings had a significantly faster wound closure rate compared to those on unpatterned samples, indicating that cells could migrate faster along the grating axis to cover the wound. Similarly, in a previous study, endothelial cells on grating structures have a faster migration velocity and a longer accumulated migration distance compared to those on unpatterned surface [294]. The phenomenon can be correlated with topography mediated mechano-sensing. The grating-induced physical confinement could drive orientation of FAs and cause cytoskeletal re-arrangement of cells. In our study, we observed that FAs formed HUVECs on grating structures are less but have elongated shape and exhibited alignment along the gratings. This is in line with the findings from our previous study that FAs on gratings were more elongated and exhibited significantly higher aspect ratio on gratings [292]. This alignment of FAs has also been found to contribute to anisotropic traction force parallel to the grating direction [279], which could further mediates the actin stress fiber formation and contact guidance directed cell migration [382].

The IH formation could be driven by multiple factors, such as surgical trauma, lack of endothelialization, and mechanical properties mismatch. Many studies have correlated the anastomotic IH with mechanical injury and fluid dynamics, especially in end-to-side anastomosis model [10, 402]. The geometric discontinuity across the anastomoses between grafts and native blood vessels causes a blood flow disturbance or flow separation around the anastomoses, which causes endothelial injury followed by SMC and myofibroblasts proliferation [83, 84]. In our study, stenosis was observed in the anastomoses of all types of grafts. Intimal hyperplasia (IH) was formed on all grafts but mainly at the floor of the native arteries, while no significant IH was seen on the luminal surfaces of the grafts. We compared the composition of the IH, both collagen and smooth muscle cells were shown to be abundant in the intimal hyperplasia. Additionally, the composition was not significantly different among different groups of samples or between proximal and distal anastomosis. Based on the results, we speculate that the fucoidan conjugation and topography may not play a significant role in the development of IH in

the current experimental settings; the mechanical properties, surgical injury and fluid dynamics may have been the main contributors.

5.5 Conclusion

In summary, this study has focused on the effect of fucoidan conjugation and topographical modification on EC responses. The fucoidan conjugation had significantly improved the endothelialization on PVA hydrogels. Topographies on fucoidan conjugated PVA hydrogels induced different EC morphology and functions. Among all the patterns, 2 μm gratings induced EC alignment and elongation without causing severe monocyte adhesion. *In vivo* studies showed that fucoidan conjugation significantly improved endothelialization and the 2 μm grating luminal pattern further enhanced the endothelial cell coverage along the luminal surfaces of the grafts. Additionally, the mechanism study showed that fucoidan increased EC adhesion by providing receptors for cell adhesion via integrins β_1, α_2, α_5, α_6, and $\alpha_v\beta_5$ and promoting the focal adhesion formation by ECs. The 2 μm gratings further improve the endothelialization by promoting cell migration along grating axis. The results of this study suggested that the combination of fucoidan conjugation and topographical patterning is a promising modification strategy to improve endothelialization on synthetic materials and could be further applied to other blood-contacting devices.

Chapter 6
Conclusions and Recommendations

6.1 Conclusions

The performance of currently available synthetic small diameter vascular grafts has been disappointing due to fast occlusion. Development of other synthetic materials and a versatile surface modification has attracted broad research interests in the cardiovascular research field. Sodium trimetaphosphate-crosslinked PVA has shown its potential to serve as a material for vascular graft application due to its tunable mechanical properties. However, the surface of PVA needs to be modified to allow endothelialization *in vitro* and *in vivo*. This thesis project was set out to develop strategies to improve the surface endothelialization and hemocompatibility of PVA, and to understand the potential mechanism for the improvement. The overall results have demonstrated the hypothesis that fucoidan and topographical modification could improve endothelialization on PVA. Important findings and the research achievements are listed as below.

In chapter 3, fucoidan molecule was incorporated into PVA hydrogels by mixing fucoidan with the PVA during crosslinking. The presence of fucoidan on PVA improved the endothelial cell adhesion on PVA. Cells were able to adhere, spread and form monolayers on modified PVA hydrogels. The *in vitro* and *ex vivo* hemocompatibility tests showed that fucoidan did not increase platelet adhesion, activation and thrombin generation. *In vivo* studies with fucoidan modified PVA small diameter vascular grafts showed that the fucoidan modification could improve the graft patency and support i*n vivo* endothelialization. Overall, the work in this chapter demonstrated that fucoidan is promising molecules to improve endothelial cell adhesion without compromising the hemocompatibility.

In chapter 4, a novel fucoidan conjugation method was developed to improve endothelial cell adhesion on PVA. The modification method is based on carbonyldiimidazole (CDI) chemistry, and both native fucoidan and aminated fucoidan were successfully conjugated to PVA. The fucoidan conjugation was compared with other fucoidan modification approaches. Among all the modification methods, conjugation of aminated fucoidan on PVA appeared to be the most promising with substantially increased endothelial adhesion and the lowest thrombogenicity. This conjugation also exhibited good compatibility with surface topographical patterning and did not alter mechanical properties. The work also demonstrated that various factors, including the ratio of the amination reagent, species of the fucoidan source and amination methods, could affect the activities of aminated fucoidan. Additionally,

conjugated fucoidan not only improved endothelial cell adhesion on PVA but also showed improvement on endothelial cell adhesion and endothelialization of ePTFE both *in vitro* and *in vivo*, respectively. Overall, this work emphasized the importance of choosing proper immobilization methods of fucoidan, and the conjugation method developed in this can be used as a versatile modification method to improve the endothelialization and hemocompatibility of synthetic polymer surface.

In chapter 5, fucoidan conjugation was combined with topographical patterning on PVA to study their synergetic effects on endothelial cell responses, hemocompatibility and graft patency. The fucoidan conjugation improved the endothelial cell adhesion and monolayer formation significantly regardless of the type of patterns that the cells were cultured on. Topographies on the fucoidan-modified PVA affected the endothelial cell morphology and how the endothelial monolayer interact with monocyte. These effects of the surface modifications on endothelial cells was found to be correlated to the integrin binding and focal adhesion formation. Fucoidan on the surface to provided receptors for integrins β_1, α_2, α_5, α_6, and $\alpha_v\beta_5$ that modulate endothelial cell adhesion to extracellular matrix *in vivo*. Meanwhile, topography modulated cell adhesion, cell morphology and guided migration by regulating the focal adhesion formation in the endothelial cells. *In vivo* studies showed that conjugated-fucoidan contributed to patency with a stronger blood flow in PVA small diameter vascular graft. In addition, the combined modification with topography and fucoidan showed better endothelialization on the lumen along the PVA small diameter vascular graft. The findings could benefit the further development of PVA as vascular graft and present as a promising modification strategy for blood contacting surfaces and other vascular devices.

6.2 Recommendations

Based on the results obtained from this thesis, the following recommendations are proposed for future work.

6.2.1 Effect of modification on smooth muscle cells and inflammatory responses

The research presented in this thesis focused on the responses and function of endothelial cells. Smooth muscle cells and inflammatory responses also play a significant role in both the atherosclerosis progression, thrombus formation and intimal hyperplasia formation.

Fucoidan is known to have an antiproliferative effect on smooth muscle cells, and topographies have been reported to alter the smooth muscle cell phenotype and regulate smooth muscle cell proliferation. A systematic study on the responses of smooth muscle cells to fucoidan modification and topographical

cues is recommended. Screening of topographies can be done based on the smooth muscle cell phenotype switch, proliferation and migration rate.

In chapter 5, we examined the effect of topographies on monocyte adhesion to endothelial cell monolayers and found that 10 μm gratings and 2 μm pillars induce more severe monocyte adhesion. A more comprehensive examination is recommended to understand the interactions between topography and fucoidan and immune system. Inflammatory cell adhesion on the material surfaces, expression of pro-inflammatory molecules by endothelial cells, and complement activation can be used as important parameters to determine the effect of modification on inflammatory responses.

6.2.2 The role of mechanical properties

The research presented in this thesis evidenced that fucoidan could improve the *in vivo* endothelialization on PVA. The 2 μm gratings could further promote the endothelial coverage along the graft by inducing a more aligned cell morphology and guided cell migration. This improvement in endothelialization reduced the blood clot formation in the grafts and thus maintaining a stronger blood flow. Mismatch in mechanical properties, especially compliance mismatch, between the artery and graft has been established to be a critical contributor to anastomotic intimal hyperplasia. The mechanical property of PVA prepared by STMP could be manipulated by changing the preparation parameters. In this thesis, the compliance of the implanted PVA grafts is 1.5-1.8 %/40mmHg, which is higher that of ePTFE grafts (0.7 %/40mmHg), but still lower the rabbit carotid arteries (2.57 %/40mmHg). Future studies to optimize the mechanical properties of PVA to match the native artery will be necessary. Understanding the synergetic effects of both surface modification and mechanical properties on the intimal hyperplasia formation and graft patency rate will be of great research interest in this area. Additionally, the complexity of flow pattern in the end-to-side anastomosis model could add up to the complications and contribute to intimal hyperplasia formation. In the future, in addition to mechanical properties, the subsequent hemodynamic, resulted from the compliance mismatch and the end-to-side anastomosis should also be investigated.

6.2.3 Purification of fucoidan

Fucoidan production is relying on the extraction from the seaweeds. Fucoidan product is known to have some contaminants such as alginate, proteins and ashes. Fucoidan used in this study is a crude product with high molecular weight. The large molecular weight increases the difficulty to reveal the chemical structure of modified fucoidan, and the presence of impurities presents a risk of inconsistent

experimental results. This was one of the key challenges and limitations to reveal the chemical structure of the conjugation of native and aminated fucoidan in this study. For future studies, fucoidan with a higher purity or fractioned fucoidan with more defined molecular weight and structural features are recommended. This will also allow the study to get a more comprehensive understanding of the structure-bioactivities relationship of fucoidan.

List of Copyright Permissions

SPRINGER NATURE LICENSE
TERMS AND CONDITIONS

Aug 09, 2021

This Agreement between University of Waterloo -- Yuan Yao ("You") and Springer Nature ("Springer Nature") consists of your license details and the terms and conditions provided by Springer Nature and Copyright Clearance Center.

License Number	5124980695757
License date	Aug 09, 2021
Licensed Content Publisher	Springer Nature
Licensed Content Publication	Nature Reviews Nephrology
Licensed Content Title	The immunology of atherosclerosis
Licensed Content Author	Anton Gisterå et al
Licensed Content Date	Apr 10, 2017
Type of Use	Thesis/Dissertation
Requestor type	academic/university or research institute
Format	electronic

Portion	figures/tables/illustrations
Number of figures/tables/illustrations	1
High-res required	no
Will you be translating?	no
Circulation/distribution	200 - 499
Author of this Springer Nature content	no
Title	Modification of poly(vinyl alcohol) hydrogels for small diameter vascular graft application
Institution name	University of Waterloo
Expected presentation date	Aug 2021
Portions	Figure 1
Requestor Location	University of Waterloo 200 University Ave W Waterloo, ON N2L 3G1 Canada Attn: University of Waterloo
Total	0.00 CAD

Terms and Conditions

Springer Nature Customer Service Centre GmbH
Terms and Conditions

This agreement sets out the terms and conditions of the licence (the **Licence**) between you and **Springer Nature Customer Service Centre GmbH** (the **Licensor**). By clicking 'accept' and completing the transaction for the material (**Licensed Material**), you also confirm your acceptance of these terms and conditions.

1. Grant of License

1. 1. The Licensor grants you a personal, non-exclusive, non-transferable, world-wide licence to reproduce the Licensed Material for the purpose specified in your order only. Licences are granted for the specific use requested in the order and for no other use, subject to the conditions below.

1. 2. The Licensor warrants that it has, to the best of its knowledge, the rights to license reuse of the Licensed Material. However, you should ensure that the material you are requesting is original to the Licensor and does not carry the copyright of another entity (as credited in the published version).

1. 3. If the credit line on any part of the material you have requested indicates that it was reprinted or adapted with permission from another source, then you should also seek permission from that source to reuse the material.

2. Scope of Licence

2. 1. You may only use the Licensed Content in the manner and to the extent permitted by these Ts&Cs and any applicable laws.

2. 2. A separate licence may be required for any additional use of the Licensed Material, e.g. where a licence has been purchased for print only use, separate permission must be obtained for electronic re-use. Similarly, a licence is only valid in the language selected and does not apply for editions in other languages unless additional translation rights have been granted separately in the licence. Any content owned by third parties are expressly excluded from the licence.

2. 3. Similarly, rights for additional components such as custom editions and derivatives require additional permission and may be subject to an additional fee. Please apply to Journalpermissions@springernature.com/bookpermissions@springernature.com for these rights.

2. 4. Where permission has been granted **free of charge** for material in print, permission may also be granted for any electronic version of that work, provided that the material is incidental to your work as a whole and that the electronic version is essentially equivalent to, or substitutes for, the print version.

2. 5. An alternative scope of licence may apply to signatories of the STM Permissions Guidelines, as amended from time to time.

3. Duration of Licence

3. 1. A licence for is valid from the date of purchase ('Licence Date') at the end of the relevant period in the below table:

Scope of Licence	Duration of Licence
Post on a website	12 months
Presentations	12 months
Books and journals	Lifetime of the edition in the language purchased

4. Acknowledgement

4. 1. The Licensor's permission must be acknowledged next to the Licenced Material in print. In electronic form, this acknowledgement must be visible at the same time as the figures/tables/illustrations or abstract, and must be hyperlinked to the journal/book's homepage. Our required acknowledgement format is in the Appendix below.

5. Restrictions on use

5. 1. Use of the Licensed Material may be permitted for incidental promotional use and minor editing privileges e.g. minor adaptations of single figures, changes of format, colour and/or style where the adaptation is credited as set out in Appendix 1 below. Any other changes including but not limited to, cropping, adapting, omitting material that affect the meaning, intention or moral rights of the author are strictly prohibited.

5. 2. You must not use any Licensed Material as part of any design or trademark.

5. 3. Licensed Material may be used in Open Access Publications (OAP) before publication by Springer Nature, but any Licensed Material must be removed from OAP sites prior to final publication.

6. Ownership of Rights

6. 1. Licensed Material remains the property of either Licensor or the relevant third party and any rights not explicitly granted herein are expressly reserved.

7. Warranty

IN NO EVENT SHALL LICENSOR BE LIABLE TO YOU OR ANY OTHER PARTY OR ANY OTHER PERSON OR FOR ANY SPECIAL, CONSEQUENTIAL, INCIDENTAL OR INDIRECT DAMAGES, HOWEVER CAUSED, ARISING OUT OF OR IN CONNECTION WITH THE DOWNLOADING, VIEWING OR USE OF THE MATERIALS REGARDLESS OF THE FORM OF ACTION, WHETHER FOR BREACH OF CONTRACT, BREACH OF WARRANTY, TORT, NEGLIGENCE, INFRINGEMENT OR OTHERWISE (INCLUDING, WITHOUT LIMITATION, DAMAGES BASED ON LOSS OF PROFITS, DATA, FILES, USE, BUSINESS OPPORTUNITY OR CLAIMS OF THIRD PARTIES), AND
WHETHER OR NOT THE PARTY HAS BEEN ADVISED OF THE POSSIBILITY OF SUCH DAMAGES. THIS LIMITATION SHALL APPLY NOTWITHSTANDING ANY FAILURE OF ESSENTIAL PURPOSE OF ANY LIMITED REMEDY PROVIDED HEREIN.

8. Limitations

8. 1. ***BOOKS ONLY:*** Where **'reuse in a dissertation/thesis'** has been selected the following terms apply: Print rights of the final author's accepted manuscript (for clarity, NOT the published version) for up to 100 copies, electronic rights for use only on a personal website or institutional repository as defined by the Sherpa guideline (www.sherpa.ac.uk/romeo/).

8. 2. For content reuse requests that qualify for permission under the STM Permissions Guidelines, which may be updated from time to time, the STM Permissions Guidelines supersede the terms and conditions contained in this licence.

9. Termination and Cancellation

9. 1. Licences will expire after the period shown in Clause 3 (above).

9. 2. Licensee reserves the right to terminate the Licence in the event that payment is not received in full or if there has been a breach of this agreement by you.

Appendix 1 — Acknowledgements:

For Journal Content:
Reprinted by permission from [**the Licensor**]: [**Journal Publisher** (e.g. Nature/Springer/Palgrave)] [**JOURNAL NAME**] [**REFERENCE CITATION**

(Article name, Author(s) Name), [**COPYRIGHT**] (year of publication)

For **Advance Online Publication papers:**
Reprinted by permission from [**the Licensor**]: [**Journal Publisher** (e.g. Nature/Springer/Palgrave)] [**JOURNAL NAME**] [**REFERENCE CITATION** (Article name, Author(s) Name), [**COPYRIGHT**] (year of publication), advance online publication, day month year (doi: 10.1038/sj.[JOURNAL ACRONYM].)

For Adaptations/Translations:
Adapted/Translated by permission from [**the Licensor**]: [**Journal Publisher** (e.g. Nature/Springer/Palgrave)] [**JOURNAL NAME**] [**REFERENCE CITATION** (Article name, Author(s) Name), [**COPYRIGHT**] (year of publication)

Note: For any republication from the British Journal of Cancer, the following credit line style applies:

Reprinted/adapted/translated by permission from [**the Licensor**]: on behalf of Cancer Research UK: : [**Journal Publisher** (e.g. Nature/Springer/Palgrave)] [**JOURNAL NAME**] [**REFERENCE CITATION** (Article name, Author(s) Name), [**COPYRIGHT]** (year of publication)

For **Advance Online Publication** papers:
Reprinted by permission from The [**the Licensor**]: on behalf of Cancer Research UK: [**Journal Publisher** (e.g. Nature/Springer/Palgrave)] [**JOURNAL NAME**] [**REFERENCE CITATION** (Article name, Author(s) Name), [**COPYRIGHT**] (year of publication), advance online publication, day month year (doi: 10.1038/sj.[JOURNAL ACRONYM])

For Book content:
Reprinted/adapted by permission from [**the Licensor**]: [**Book Publisher** (e.g. Palgrave Macmillan, Springer etc) [**Book Title**] by [**Book author**(s)] [**COPYRIGHT**] (year of publication)

Other Conditions:

Version 1.3

Questions? customercare@copyright.com or +1-855-239-3415 (toll free in the US) or +1-978-646-2777.

Bibliography

[1] E.J. Benjamin, P. Muntner, A. Alonso, M.S. Bittencourt, C.W. Callaway, A.P. Carson, A.M. Chamberlain, A.R. Chang, S. Cheng, S.R. Das, F.N. Delling, L. Djousse, M.S.V. Elkind, J.F. Ferguson, M. Fornage, L.C. Jordan, S.S. Khan, B.M. Kissela, K.L. Knutson, T.W. Kwan, D.T. Lackland, T.T. Lewis, J.H. Lichtman, C.T. Longenecker, M.S. Loop, P.L. Lutsey, S.S. Martin, K. Matsushita, A.E. Moran, M.E. Mussolino, M. O'Flaherty, A. Pandey, A.M. Perak, W.D. Rosamond, G.A. Roth, U.K.A. Sampson, G.M. Satou, E.B. Schroeder, S.H. Shah, N.L. Spartano, A. Stokes, D.L. Tirschwell, C.W. Tsao, M.P. Turakhia, L.B. VanWagner, J.T. Wilkins, S.S. Wong, S.S. Virani, n. null, Heart Disease and Stroke Statistics—2019 Update: A Report From the American Heart Association, Circulation 139(10) (2019) e56-e528.
[2] H.H.G. Song, R.T. Rumma, C.K. Ozaki, E.R. Edelman, C.S. Chen, Vascular Tissue Engineering: Progress, Challenges, and Clinical Promise, Cell Stem Cell 22(3) (2018) 340-354.
[3] S. Pashneh-Tala, S. MacNeil, F. Claeyssens, The Tissue-Engineered Vascular Graft—Past, Present, and Future, Tissue Engineering Part B: Reviews 22(1) (2015) 68-100.
[4] Y. Merhi, M. King, R. Guidoin, Acute thrombogenicity of intact and injured natural blood conduits versus synthetic conduits: Neutrophil, platelet, and fibrin(ogen) adsorption under various shear-rate conditions, Journal of Biomedical Materials Research 34(4) (1997) 477-485.
[5] S. Sarkar, K.M. Sales, G. Hamilton, A.M. Seifalian, Addressing thrombogenicity in vascular graft construction, Journal of Biomedical Materials Research Part B: Applied Biomaterials 82B(1) (2007) 100-108.
[6] Y. Heo, Y.M. Shin, Y.B. Lee, Y.M. Lim, H. Shin, Effect of immobilized collagen type IV on biological properties of endothelial cells for the enhanced endothelialization of synthetic vascular graft materials, Colloids and Surfaces B: Biointerfaces 134 (2015) 196-203.
[7] W. Zheng, Z. Wang, L. Song, Q. Zhao, J. Zhang, D. Li, S. Wang, J. Han, X.-L. Zheng, Z. Yang, D. Kong, Endothelialization and patency of RGD-functionalized vascular grafts in a rabbit carotid artery model, Biomaterials 33(10) (2012) 2880-2891.
[8] Y.M. Shin, Y.B. Lee, S.J. Kim, J.K. Kang, J.-C. Park, W. Jang, H. Shin, Mussel-Inspired Immobilization of Vascular Endothelial Growth Factor (VEGF) for Enhanced Endothelialization of Vascular Grafts, Biomacromolecules 13(7) (2012) 2020-2028.
[9] H.J. Salacinski, S. Goldner, A. Giudiceandrea, G. Hamilton, A.M. Seifalian, A. Edwards, R.J. Carson, The Mechanical Behavior of Vascular Grafts: A Review, Journal of Biomaterials Applications 15(3) (2001) 241-278.
[10] Y. Jeong, Y. Yao, E.K.F. Yim, Current understanding of intimal hyperplasia and effect of compliance in synthetic small diameter vascular grafts, Biomaterials Science 8(16) (2020) 4383-4395.
[11] M.F. Cutiongco, M. Kukumberg, J.L. Peneyra, M.S. Yeo, J.Y. Yao, A.J. Rufaihah, C. Le Visage, J.P. Ho, E.K. Yim, Submillimeter Diameter Poly(Vinyl Alcohol) Vascular Graft Patency in Rabbit Model, Front Bioeng Biotechnol 4 (2016) 44.
[12] T. Zaporozhets, N. Besednova, Prospects for the therapeutic application of sulfated polysaccharides of brown algae in diseases of the cardiovascular system: review, Pharmaceutical Biology 54(12) (2016) 3126-3135.
[13] A. Chen, Y. Lan, J. Liu, F. Zhang, L. Zhang, B. Li, X. Zhao, The structure property and endothelial protective activity of fucoidan from Laminaria japonica, International Journal of Biological Macromolecules 105 (2017) 1421-1429.
[14] T.A. McCaffrey, D.J. Falcone, W. Borth, C.F. Brayton, B.B. Weksler, Fucoidan is a non-anticoagulant inhibitor of intimal hyperplasia, Biochemical and Biophysical Research Communications 184(2) (1992) 773-781.

[15] B.D. James, J.B. Allen, Vascular Endothelial Cell Behavior in Complex Mechanical Microenvironments, ACS Biomaterials Science & Engineering 4(11) (2018) 3818-3842.
[16] M.F. Cutiongco, S.H. Goh, R. Aid-Launais, C. Le Visage, H.Y. Low, E.K. Yim, Planar and tubular patterning of micro and nano-topographies on poly(vinyl alcohol) hydrogel for improved endothelial cell responses, Biomaterials 84 (2016) 184-95.
[17] S.J. Liliensiek, J.A. Wood, J. Yong, R. Auerbach, P.F. Nealey, C.J. Murphy, Modulation of human vascular endothelial cell behaviors by nanotopographic cues, Biomaterials 31(20) (2010) 5418-5426.
[18] M. Tennant, J.K. McGeachie, Blood vessel structure and function: a brief update on recent advances, Australian and New Zealand Journal of Surgery 60(10) (1990) 747-753.
[19] D.H. Rohrbach, R. Timpl, Preface, in: D.H. Rohrbach, R. Timpl (Eds.), Molecular and Cellular Aspects of Basement Membrane, Academic Press1993, pp. xvii-xix.
[20] E. Iivanainen, V.-M. Kähäri, J. Heino, K. Elenius, Endothelial cell–Matrix interactions, Microscopy Research and Technique 60(1) (2003) 13-22.
[21] R. Mazurek, J.M. Dave, R.R. Chandran, A. Misra, A.Q. Sheikh, D.M. Greif, Vascular Cells in Blood Vessel Wall Development and Disease, Adv Pharmacol 78 (2017) 323-350.
[22] M.W. Radomski, R.M.J. Palmer, S. Moncada, The anti-aggregating properties of vascular endothelium: interactions between prostacyclin and nitric oxide, British Journal of Pharmacology 92(3) (1987) 639-646.
[23] K. Shimada, M. Kobayashi, S. Kimura, M. Nishinaga, K. Takeuchi, T. Ozawa, Anticoagulant Heparin-like Glycosaminoglycans on Endothelial Cell Surface : 54th Annual Scientific Session of the Japanese Circulation Society, Japanese Circulation Journal 55(10) (1991) 1016-1021.
[24] C. Michiels, Endothelial cell functions, Journal of Cellular Physiology 196(3) (2003) 430-443.
[25] J.S. Pober, W.C. Sessa, Evolving functions of endothelial cells in inflammation, Nature Reviews Immunology 7(10) (2007) 803-815.
[26] J.J. Castellot, Jr., M.L. Addonizio, R. Rosenberg, M.J. Karnovsky, Cultured endothelial cells produce a heparinlike inhibitor of smooth muscle cell growth, J Cell Biol 90(2) (1981) 372-9.
[27] A. Sandoo, J.J.C.S.V. van Zanten, G.S. Metsios, D. Carroll, G.D. Kitas, The endothelium and its role in regulating vascular tone, Open Cardiovasc Med J 4 (2010) 302-312.
[28] J.-B. Michel, Phylogenic Determinants of Cardiovascular Frailty, Focus on Hemodynamics and Arterial Smooth Muscle Cells, Physiological Reviews 100(4) (2020) 1779-1837.
[29] G. Li, S.-J. Chen, S. Oparil, Y.-F. Chen, A. Thompson John, Direct In Vivo Evidence Demonstrating Neointimal Migration of Adventitial Fibroblasts After Balloon Injury of Rat Carotid Arteries, Circulation 101(12) (2000) 1362-1365.
[30] A. Scott Neal, D. Cipolla Gustavo, E. Ross Cheryl, B. Dunn, H. Martin Francis, L. Simonet, N. Wilcox Josiah, Identification of a Potential Role for the Adventitia in Vascular Lesion Formation After Balloon Overstretch Injury of Porcine Coronary Arteries, Circulation 93(12) (1996) 2178-2187.
[31] Y. Shi, E. O'Brien James, A. Fard, D. Mannion John, D. Wang, A. Zalewski, Adventitial Myofibroblasts Contribute to Neointimal Formation in Injured Porcine Coronary Arteries, Circulation 94(7) (1996) 1655-1664.
[32] R.C.M. Siow, C.M. Mallawaarachchi, P.L. Weissberg, Migration of adventitial myofibroblasts following vascular balloon injury: insights from in vivo gene transfer to rat carotid arteries, Cardiovascular Research 59(1) (2003) 212-221.
[33] M.W. Majesky, X.R. Dong, V. Hoglund, G. Daum, W.M. Mahoney, Jr., The adventitia: a progenitor cell niche for the vessel wall, Cells Tissues Organs 195(1-2) (2012) 73-81.
[34] Y. Hu, Q. Xu, Adventitial Biology, Arteriosclerosis, Thrombosis, and Vascular Biology 31(7) (2011) 1523-1529.
[35] A. Gisterå, G.K. Hansson, The immunology of atherosclerosis, Nature Reviews Nephrology 13(6) (2017) 368-380.

[36] S. Sitia, L. Tomasoni, F. Atzeni, G. Ambrosio, C. Cordiano, A. Catapano, S. Tramontana, F. Perticone, P. Naccarato, P. Camici, E. Picano, L. Cortigiani, M. Bevilacqua, L. Milazzo, D. Cusi, C. Barlassina, P. Sarzi-Puttini, M. Turiel, From endothelial dysfunction to atherosclerosis, Autoimmunity Reviews 9(12) (2010) 830-834.
[37] T.L. Cornwell, E. Arnold, N.J. Boerth, T.M. Lincoln, Inhibition of smooth muscle cell growth by nitric oxide and activation of cAMP-dependent protein kinase by cGMP, American Journal of Physiology-Cell Physiology 267(5) (1994) C1405-C1413.
[38] R. Sarkar, D. Gordon, J.C. Stanley, R.C. Webb, Cell cycle effects of nitric oxide on vascular smooth muscle cells, American Journal of Physiology-Heart and Circulatory Physiology 272(4) (1997) H1810-H1818.
[39] M.W. Radomski, R.M. Palmer, S. Moncada, An L-arginine/nitric oxide pathway present in human platelets regulates aggregation, Proceedings of the National Academy of Sciences 87(13) (1990) 5193.
[40] M.W. Radomski, R.M.J. Palmer, S. Moncada, The role of nitric oxide and cGMP in platelet adhesion to vascular endothelium, Biochemical and Biophysical Research Communications 148(3) (1987) 1482-1489.
[41] C. Zhang, The role of inflammatory cytokines in endothelial dysfunction, Basic research in cardiology 103 (2008) 398-406.
[42] A. Milutinović, D. Šuput, R. Zorc-Pleskovič, Pathogenesis of atherosclerosis in the tunica intima, media, and adventitia of coronary arteries: An updated review, Bosn J Basic Med Sci 20(1) (2020) 21-30.
[43] A.C. Doran, N. Meller, C.A. McNamara, Role of Smooth Muscle Cells in the Initiation and Early Progression of Atherosclerosis, Arteriosclerosis, Thrombosis, and Vascular Biology 28(5) (2008) 812-819.
[44] Y. Ishikawa, M. Kimura-Matsumoto, M. Murakami, K. Yamamoto, Y. Akasaka, M. Uzuki, Y. Yuri, N. Inomata, T. Yokoo, T. Ishii, Distribution of smooth muscle cells and macrophages expressing scavenger receptor BI/II in atherosclerosis, Journal of atherosclerosis and thrombosis 16 6 (2009) 829-39.
[45] M. Braun, P. Pietsch, K. Schrör, G. Baumann, S.B. Felix, Cellular adhesion molecules on vascular smooth muscle cells, Cardiovascular Research 41(2) (1999) 395-401.
[46] F. Xu, J. Ji, L. Li, R. Chen, W. Hu, Activation of adventitial fibroblasts contributes to the early development of atherosclerosis: A novel hypothesis that complements the “Response-to-Injury Hypothesis” and the “Inflammation Hypothesis”, Medical Hypotheses 69(4) (2007) 908-912.
[47] F. Xu, J. Ji, L. Li, R. Chen, W.-c. Hu, Adventitial fibroblasts are activated in the early stages of atherosclerosis in the apolipoprotein E knockout mouse, Biochemical and Biophysical Research Communications 352(3) (2007) 681-688.
[48] E. Torsney, Y. Hu, Q. Xu, Adventitial Progenitor Cells Contribute to Arteriosclerosis, Trends in Cardiovascular Medicine 15(2) (2005) 64-68.
[49] A.J. Jolly, S. Lu, K.A. Strand, A.M. Dubner, M.F. Mutryn, R.A. Nemenoff, M.W. Majesky, K.S. Moulton, M.C.M. Weiser-Evans, Heterogeneous subpopulations of adventitial progenitor cells regulate vascular homeostasis and pathological vascular remodeling, Cardiovascular Research (2021).
[50] R.N. Mitchell, P. Libby, Vascular Remodeling in Transplant Vasculopathy, Circulation Research 100(7) (2007) 967-978.
[51] H.a.S. Foundation, Coronary artery disease, 2018. http://www.heartandstroke.ca/heart/conditions/coronary-artery-disease.
[52] S. Goldman, K. Zadina, T. Moritz, T. Ovitt, G. Sethi, G. Copeland Jack, L. Thottapurathu, B. Krasnicka, N. Ellis, J. Anderson Robert, W. Henderson, n. null, Long-term patency of saphenous vein and left internal mammary artery grafts after coronary artery bypass surgery, Journal of the American College of Cardiology 44(11) (2004) 2149-2156.

[53] J.F. Sabik, B.W. Lytle, E.H. Blackstone, P.L. Houghtaling, D.M. Cosgrove, Comparison of Saphenous Vein and Internal Thoracic Artery Graft Patency by Coronary System, The Annals of Thoracic Surgery 79(2) (2005) 544-551.
[54] R.E. Harskamp, R.D. Lopes, C.E. Baisden, R.J. de Winter, J.H. Alexander, Saphenous Vein Graft Failure After Coronary Artery Bypass Surgery: Pathophysiology, Management, and Future Directions, Annals of Surgery 257(5) (2013) 824-833.
[55] Y. Ben-Gal, D.P. Taggart, M.R. Williams, E. Orion, G. Uretzky, R. Shofti, S. Banai, L. Yosef, G. Bolotin, Expandable external support device to improve Saphenous Vein Graft Patency after CABG, Journal of Cardiothoracic Surgery 8(1) (2013) 122.
[56] A.H. Blakemore, A.B. Voorhees, The Use of Tubes Constructed from Vinyon "N" Cloth in Bridging Arterial Defects—Experimental and Clinical, Annals of Surgery 140(3) (1954) 324-333.
[57] S. Ravi, Z. Qu, E.L. Chaikof, Polymeric Materials for Tissue Engineering of Arterial Substitutes, Vascular 17(Supplement 1) (2009) S45-S54.
[58] G.W. Bos, A.A. Poot, T. Beugeling, W.G. van Aken, J. Feijen, Small-Diameter Vascular Graft Prostheses: Current Status, Archives of Physiology and Biochemistry 106(2) (1998) 100-115.
[59] J.J. Bergan, F.J. Veith, V.M. Bernhard, J.S.T. Yao, W.R. Flinn, S.K. Gupta, L.A. Scher, R.H. Samson, J.B. Towne, Randomization of autogenous vein and polytetrafluoroethylene grafts in femoral-distal reconstruction, Surgery 92(6) (1982) 921-930.
[60] W.C. Pevec, R.C. Darling, G.I. L'Italien, W.M. Abbott, Femoropopliteal reconstruction with knitted, nonvelour Dacron versus expanded polytetrafluoroethylene, Journal of Vascular Surgery 16(1) (1992) 60-65.
[61] S. Roll, J. Müller-Nordhorn, T. Keil, H. Scholz, D. Eidt, W. Greiner, S.N. Willich, Dacron vs. PTFE as bypass materials in peripheral vascular surgery--systematic review and meta-analysis, BMC surgery 8 (2008) 22-22.
[62] W.C. Johnson, K.K. Lee, Comparative evaluation of externally supported Dacron and polytetrafluoroethylene prosthetic bypasses for femorofemoral and axillofemoral arterial reconstructions, Journal of Vascular Surgery 30(6) (1999) 1077-1083.
[63] P. Zilla, D. Bezuidenhout, P. Human, Prosthetic vascular grafts: Wrong models, wrong questions and no healing, Biomaterials 28(34) (2007) 5009-5027.
[64] M.A. Hiob, S. She, L.D. Muiznieks, A.S. Weiss, Biomaterials and Modifications in the Development of Small-Diameter Vascular Grafts, ACS Biomaterials Science & Engineering 3(5) (2016) 712-723.
[65] B.H. Walpoth, G.L. Bowlin, The daunting quest for a small diameter vascular graft, Expert Review of Medical Devices 2(6) (2005) 647-651.
[66] S.L. Mitchell, L.E. Niklason, Requirements for growing tissue-engineered vascular grafts, Cardiovascular Pathology 12(2) (2003) 59-64.
[67] R.D. Rudic, E.G. Shesely, N. Maeda, O. Smithies, S.S. Segal, W.C. Sessa, Direct evidence for the importance of endothelium-derived nitric oxide in vascular remodeling, The Journal of Clinical Investigation 101(4) (1998) 731-736.
[68] L.J. Ignarro, G.M. Buga, L.H. Wei, P.M. Bauer, G. Wu, P. del Soldato, Role of the arginine-nitric oxide pathway in the regulation of vascular smooth muscle cell proliferation, Proceedings of the National Academy of Sciences 98(7) (2001) 4202.
[69] M.W. Radomski, R.M.J. Palmer, S. Moncada, ENDOGENOUS NITRIC OXIDE INHIBITS HUMAN PLATELET ADHESION TO VASCULAR ENDOTHELIUM, The Lancet 330(8567) (1987) 1057-1058.
[70] K. Maiellaro, W.R. Taylor, The role of the adventitia in vascular inflammation, Cardiovascular Research 75(4) (2007) 640-648.

[71] S.G.E. Barker, L.C. Tilling, G.C. Miller, J.E. Beesley, G. Fleetwood, G.T. Stavri, P.A. Baskerville, J.F. Martin, The adventitia and atherogenesis: removal initiates intimal proliferation in the rabbit which regresses on generation of a 'neoadventitia', Atherosclerosis 105(2) (1994) 131-144.
[72] X. Xu, H. Lu, H. Lin, M. Ni, H. Sun, C. Li, H. Jiang, F. Li, Y. Zhao, M. Zhang, Y. Zhang, Lymphangiogenesis promotes inflammation and neointimal hyperplasia after adventitia removal in the rat carotid artery, International Journal of Cardiology 134(3) (2009) 426-427.
[73] S.G.E. Barker, J.E. Beesley, P.A. Baskerville, J.F. Martin, The influence of the adventitia on the presence of smooth muscle cells and macrophages in the arterial intima, European Journal of Vascular and Endovascular Surgery 9(2) (1995) 222-227.
[74] R. Kornowski, M.K. Hong, F.O. Tio, O. Bramwell, H. Wu, M.B. Leon, In-Stent Restenosis: Contributions of Inflammatory Responses and Arterial Injury to Neointimal Hyperplasia, Journal of the American College of Cardiology 31(1) (1998) 224.
[75] P. Roy-Chaudhury, B.S. Kelly, M.A. Miller, A. Reaves, J. Armstrong, N. Nanayakkara, S.C. Heffelfinger, Venous neointimal hyperplasia in polytetrafluoroethylene dialysis grafts, Kidney International 59(6) (2001) 2325-2334.
[76] J.R. Hoch, V.K. Stark, N. van Rooijen, J.L. Kim, M.P. Nutt, T.F. Warner, Macrophage depletion alters vein graft intimal hyperplasia, Surgery 126(2) (1999) 428-437.
[77] R. Ross, Atherosclerosis — An Inflammatory Disease, New England Journal of Medicine 340(2) (1999) 115-126.
[78] A.C. Newby, A.B. Zaltsman, Molecular mechanisms in intimal hyperplasia, The Journal of Pathology 190(3) (2000) 300-309.
[79] S. Goetze, X.-P. Xi, Y. Kawano, H. Kawano, E. Fleck, A. Hsueh Willa, E. Law Ronald, TNF-α–Induced Migration of Vascular Smooth Muscle Cells Is MAPK Dependent, Hypertension 33(1) (1999) 183-189.
[80] C. Kanthou, O. Benzakour, G. Patel, J. Deadman, V.V. Kakkar, F. Lupu, Thrombin Receptor Activating Peptide (TRAP) Stimulates Mitogenesis, c-fos and PDGF-A Gene Expression in Human Vascular Smooth Muscle Cells, Thromb Haemost 74(05) (1995) 1340-1347.
[81] T. Nakajima, I. Kitajima, H. Shin, I. Takasaki, K. Shigeta, K. Abeyama, Y. Yamashita, T. Tokioka, Y. Soejima, I. Maruyama, Involvement of NF-κB Activation in Thrombin-Induced Human Vascular Smooth Muscle Cell Proliferation, Biochemical and Biophysical Research Communications 204(2) (1994) 950-955.
[82] C.A. McNamara, I.J. Sarembock, L.W. Gimple, J.W. Fenton, 2nd, S.R. Coughlin, G.K. Owens, Thrombin stimulates proliferation of cultured rat aortic smooth muscle cells by a proteolytically activated receptor, The Journal of Clinical Investigation 91(1) (1993) 94-98.
[83] V.S. Sottiurai, S. Lim Sue, E.L. Feinberg, II, W.L. Bringaze, A.T. Tran, R.C. Batson, Distal anastomotic intimal hyperplasia: Biogenesis and etiology, European Journal of Vascular Surgery 2(4) (1988) 245-256.
[84] V.S. Sottiurai, J.S.T. Yao, R.C. Batson, S.L. Sue, R. Jones, Y.A. Nakamura, Distal Anastomotic Intimal Hyperplasia: Histopathologic Character and Biogenesis, Annals of Vascular Surgery 3(1) (1989) 26-33.
[85] A.J. Reininger, U. Heinzmann, C.B. Reininger, P. Friedrich, L.J. Wurzinger, Flow mediated fibrin thrombus formation in an endothelium-lined model of arterial branching, Thrombosis Research 74(6) (1994) 629-641.
[86] B.J. Ballermann, A. Dardik, E. Eng, A. Liu, Shear stress and the endothelium, Kidney International 54 (1998) S100-S108.
[87] A.M. Malek, S.L. Alper, S. Izumo, Hemodynamic Shear Stress and Its Role in Atherosclerosis, JAMA 282(21) (1999) 2035-2042.

[88] S. Nadaud, M. Philippe, J.-F. Arnal, J.-B. Michel, F. Soubrier, Sustained Increase in Aortic Endothelial Nitric Oxide Synthase Expression In Vivo in a Model of Chronic High Blood Flow, Circulation Research 79(4) (1996) 857-863.
[89] M. Ojha, Wall shear stress temporal gradient and anastomotic intimal hyperplasia, Circulation Research 74(6) (1994) 1227-1231.
[90] A.V. Sterpetti, A. Cucina, L.S. D'Angelo, B. Cardillo, A. Cavallaro, Shear stress modulates the proliferation rate, protein synthesis, and mitogenic activity of arterial smooth muscle cells, Surgery 113(6) (1993) 691-699.
[91] M. Haga, A. Yamashita, J. Paszkowiak, B.E. Sumpio, A. Dardik, Oscillatory shear stress increases smooth muscle cell proliferation and akt phosphorylation, Journal of Vascular Surgery 37(6) (2003) 1277-1284.
[92] M. Southgate Kay, D. Mehta, B. Izzat Mohammed, C. Newby Andrew, D. Angelini Gianni, Increased Secretion of Basement Membrane–Degrading Metalloproteinases in Pig Saphenous Vein Into Carotid Artery Interposition Grafts, Arteriosclerosis, Thrombosis, and Vascular Biology 19(7) (1999) 1640-1649.
[93] M. Mayr, Y. Hu, P. Hainaut, Q. Xu, Mechanical stress-induced DNA damage and rac-p38MAPK signal pathways mediate p53-dependent apoptosis in vascular smooth muscle cells, The FASEB Journal 16(11) (2002) 1423-1425.
[94] J.H. Haga, Y.-S.J. Li, S. Chien, Molecular basis of the effects of mechanical stretch on vascular smooth muscle cells, Journal of Biomechanics 40(5) (2007) 947-960.
[95] E. Wilson, F. Vives, T. Collins, E. Ives Harlan, Strain-Responsive Regions in the Platelet-Derived Growth Factor-A Gene Promoter, Hypertension 31(1) (1998) 170-175.
[96] S. Aslani, M. Kabiri, S. HosseinZadeh, H. Hanaee-Ahvaz, E.S. Taherzadeh, M. Soleimani, The applications of heparin in vascular tissue engineering, Microvascular Research 131 (2020) 104027.
[97] K. Daenens, S. Schepers, I. Fourneau, S. Houthoofd, A. Nevelsteen, Heparin-bonded ePTFE grafts compared with vein grafts in femoropopliteal and femorocrural bypasses: 1- and 2-year results, Journal of Vascular Surgery 49(5) (2009) 1210-1216.
[98] J.M.M. Heyligers, H.J.M. Verhagen, J.I. Rotmans, C. Weeterings, P.G. de Groot, F.L. Moll, T. Lisman, Heparin immobilization reduces thrombogenicity of small-caliber expanded polytetrafluoroethylene grafts, Journal of Vascular Surgery 43(3) (2006) 587-591.
[99] P.H. Lin, C. Chen, R.L. Bush, Q. Yao, A.B. Lumsden, S.R. Hanson, Small-caliber heparin-coated ePTFE grafts reduce platelet deposition and neointimal hyperplasia in a baboon model, Journal of Vascular Surgery 39(6) (2004) 1322-1328.
[100] R.A. Hoshi, R. Van Lith, M.C. Jen, J.B. Allen, K.A. Lapidos, G. Ameer, The blood and vascular cell compatibility of heparin-modified ePTFE vascular grafts, Biomaterials 34(1) (2013) 30-41.
[101] P.C. Caracciolo, P. Diaz-Rodriguez, I. Ardao, D. Moreira, F. Montini-Ballarin, G.A. Abraham, A. Concheiro, C. Alvarez-Lorenzo, Evaluation of human umbilical vein endothelial cells growth onto heparin-modified electrospun vascular grafts, International Journal of Biological Macromolecules 179 (2021) 567-575.
[102] Z. Xu, Z. Feng, L. Guo, L. Ye, Z. Tong, X. Geng, C. Wang, X. Jin, X. Hui, Y. Gu, Biocompatibility evaluation of heparin-conjugated poly(ε-caprolactone) scaffolds in a rat subcutaneous implantation model, Journal of Materials Science: Materials in Medicine 31(8) (2020) 76.
[103] J. Gao, Y. Wang, S. Chen, D. Tang, L. Jiang, D. Kong, S. Wang, Electrospun poly-ε-caprolactone scaffold modified with catalytic nitric oxide generation and heparin for small-diameter vascular graft, RSC Advances 7(30) (2017) 18775-18784.
[104] M. Zhou, Z. Liu, Z. Wei, C. Liu, T. Qiao, F. Ran, Y. Bai, X. Jiang, Y. Ding, Development and Validation of Small-diameter Vascular Tissue From a Decellularized Scaffold Coated With Heparin and Vascular Endothelial Growth Factor, Artificial Organs 33(3) (2009) 230-239.

[105] Y. Yao, J. Wang, Y. Cui, R. Xu, Z. Wang, J. Zhang, K. Wang, Y. Li, Q. Zhao, D. Kong, Effect of sustained heparin release from PCL/chitosan hybrid small-diameter vascular grafts on anti-thrombogenic property and endothelialization, Acta Biomaterialia 10(6) (2014) 2739-2749.
[106] F. Zia, K.M. Zia, M. Zuber, S. Tabasum, S. Rehman, Heparin based polyurethanes: A state-of-the-art review, International Journal of Biological Macromolecules 84 (2016) 101-111.
[107] S.-K. Min, O.-C. Kwon, S. Lee, K.-H. Park, J.-K. Kim, An Antithrombotic Fucoidan, Unlike Heparin, Does Not Prolong Bleeding Time in a Murine Arterial Thrombosis Model: A Comparative Study of Undaria pinnatifida sporophylls and Fucus vesiculosus, Phytotherapy Research 26(5) (2012) 752-757.
[108] S. Asadpour, H. Yeganeh, J. Ai, H. Ghanbari, A novel polyurethane modified with biomacromolecules for small-diameter vascular graft applications, Journal of Materials Science 53(14) (2018) 9913-9927.
[109] F. Zhang, T. Bambharoliya, Y. Xie, L. Liu, H. Celik, L. Wang, O. Akkus, M.W. King, A hybrid vascular graft harnessing the superior mechanical properties of synthetic fibers and the biological performance of collagen filaments, Materials Science and Engineering: C 118 (2021) 111418.
[110] S.K. Williams, L.B. Kleinert, V. Patula-Steinbrenner, Accelerated neovascularization and endothelialization of vascular grafts promoted by covalently bound laminin type 1, Journal of Biomedical Materials Research Part A 99A(1) (2011) 67-73.
[111] J.S. Budd, K.E. Allen, P.R.F. Bell, R.F.L. James, The effect of varying fibronectin concentration on the attachment of endothelial cells to polytetrafluoroethylene vascular grafts, Journal of Vascular Surgery 12(2) (1990) 126-130.
[112] G. De Visscher, L. Mesure, B. Meuris, A. Ivanova, W. Flameng, Improved endothelialization and reduced thrombosis by coating a synthetic vascular graft with fibronectin and stem cell homing factor SDF-1α, Acta Biomaterialia 8(3) (2012) 1330-1338.
[113] S.L. Bellis, Advantages of RGD peptides for directing cell association with biomaterials, Biomaterials 32(18) (2011) 4205-4210.
[114] L.V. Antonova, A.M. Seifalian, A.G. Kutikhin, V.V. Sevostyanova, E.O. Krivkina, A.V. Mironov, A.Y. Burago, E.A. Velikanova, V.G. Matveeva, T.V. Glushkova, E.A. Sergeeva, G.Y. Vasyukov, Y.A. Kudryavtseva, O.L. Barbarash, L.S. Barbarash, Bioabsorbable Bypass Grafts Biofunctionalised with RGD Have Enhanced Biophysical Properties and Endothelialisation Tested In vivo, Frontiers in Pharmacology 7(136) (2016).
[115] J.M. Bastijanic, R.E. Marchant, F. Kligman, M.T. Allemang, R.O. Lakin, D. Kendrick, V.S. Kashyap, K. Kottke-Marchant, In vivo evaluation of biomimetic fluorosurfactant polymer-coated expanded polytetrafluoroethylene vascular grafts in a porcine carotid artery bypass model, Journal of Vascular Surgery 63(6) (2016) 1620-1630.e4.
[116] D. Yao, Z. Qian, J. Zhou, G. Peng, G. Zhou, H. Liu, Y. Fan, Facile incorporation of REDV into porous silk fibroin scaffolds for enhancing vascularization of thick tissues, Materials Science and Engineering: C 93 (2018) 96-105.
[117] H.-W. Jun, J.L. West, Modification of polyurethaneurea with PEG and YIGSR peptide to enhance endothelialization without platelet adhesion, Journal of Biomedical Materials Research Part B: Applied Biomaterials 72B(1) (2005) 131-139.
[118] G. Peng, D. Yao, Y. Niu, H. Liu, Y. Fan, Surface Modification of Multiple Bioactive Peptides to Improve Endothelialization of Vascular Grafts, Macromolecular Bioscience 19(5) (2019) 1800368.
[119] P. Konrad, P. Dougan, D. Bergqvist, Acute thrombogenicity of collagen coating of dacron grafts: An experimental study in sheep, European Journal of Vascular Surgery 6(1) (1992) 67-72.
[120] L.V. Antonova, A.M. Seifalian, A.G. Kutikhin, V.V. Sevostyanova, V.G. Matveeva, E.A. Velikanova, A.V. Mironov, A.R. Shabaev, T.V. Glushkova, E.A. Senokosova, G.Y. Vasyukov, E.O. Krivkina, A.Y. Burago, Y.A. Kudryavtseva, O.L. Barbarash, L.S. Barbarash, Conjugation with RGD

Peptides and Incorporation of Vascular Endothelial Growth Factor Are Equally Efficient for Biofunctionalization of Tissue-Engineered Vascular Grafts, International Journal of Molecular Sciences 17(11) (2016).
[121] K. Wang, Q. Zhang, L. Zhao, Y. Pan, T. Wang, D. Zhi, S. Ma, P. Zhang, T. Zhao, S. Zhang, W. Li, M. Zhu, Y. Zhu, J. Zhang, M. Qiao, D. Kong, Functional Modification of Electrospun Poly(ε-caprolactone) Vascular Grafts with the Fusion Protein VEGF–HGFI Enhanced Vascular Regeneration, ACS Applied Materials & Interfaces 9(13) (2017) 11415-11427.
[122] V.V. Sevostyanova, V.G. Matveeva, L.V. Antonova, E.A. Velikanova, A.R. Shabaev, E.A. Senokosova, E.O. Krivkina, G.Y. Vasyukov, T.V. Glushkova, Y.A. Kudryavtseva, O.L. Barbarash, L.S. Barbarash, Constructing a blood vessel on the porous scaffold modified with vascular endothelial growth factor and basic fibroblast growth factor, AIP Conference Proceedings 1783(1) (2016) 020204.
[123] L. Antonova, A. Kutikhin, V. Sevostianova, E. Velikanova, V. Matveeva, T. Glushkova, A. Mironov, E. Krivkina, A. Shabaev, E. Senokosova, L. Barbarash, bFGF and SDF-1α Improve In Vivo Performance of VEGF-Incorporating Small-Diameter Vascular Grafts, Pharmaceuticals 14(4) (2021).
[124] L. West-Livingston, Y.M. Ju, H. Lee, R.L. Geary, A. Atala, S.J. Lee, Antibody-Conjugated Electrospun Vascular Scaffolds to Enhance In Situ Endothelialization, ACS Applied Bio Materials 3(7) (2020) 4486-4494.
[125] Q. Lin, X. Ding, F. Qiu, X. Song, G. Fu, J. Ji, In situ endothelialization of intravascular stents coated with an anti-CD34 antibody functionalized heparin–collagen multilayer, Biomaterials 31(14) (2010) 4017-4025.
[126] G. Camci-Unal, J.W. Nichol, H. Bae, H. Tekin, J. Bischoff, A. Khademhosseini, Hydrogel surfaces to promote attachment and spreading of endothelial progenitor cells, Journal of Tissue Engineering and Regenerative Medicine 7(5) (2013) 337-347.
[127] J.I. Rotmans, J.M.M. Heyligers, H.J.M. Verhagen, E. Velema, M.M. Nagtegaal, D.P.V. de Kleijn, F.G. de Groot, E.S.G. Stroes, G. Pasterkamp, In Vivo Cell Seeding With Anti-CD34 Antibodies Successfully Accelerates Endothelialization but Stimulates Intimal Hyperplasia in Porcine Arteriovenous Expanded Polytetrafluoroethylene Grafts, Circulation 112(1) (2005) 12-18.
[128] W. Mrówczyński, A. Rungatscher, F. Buchegger, J.-C. Tille, S. Namy, O. Ratib, M. Kutryk, B.H. Walpoth, Biological effects of anti-CD34-coated ePTFE vascular grafts. Early in vivo experimental results, Kardiochir Torakochirurgia Pol 11(2) (2014) 182-190.
[129] S. Lu, P. Zhang, X. Sun, F. Gong, S. Yang, L. Shen, Z. Huang, C. Wang, Synthetic ePTFE Grafts Coated with an Anti-CD133 Antibody-Functionalized Heparin/Collagen Multilayer with Rapid in vivo Endothelialization Properties, ACS Applied Materials & Interfaces 5(15) (2013) 7360-7369.
[130] B. Marelli, A. Alessandrino, S. Farè, G. Freddi, D. Mantovani, M.C. Tanzi, Compliant electrospun silk fibroin tubes for small vessel bypass grafting, Acta Biomaterialia 6(10) (2010) 4019-4026.
[131] S. Enomoto, M. Sumi, K. Kajimoto, Y. Nakazawa, R. Takahashi, C. Takabayashi, T. Asakura, M. Sata, Long-term patency of small-diameter vascular graft made from fibroin, a silk-based biodegradable material, Journal of Vascular Surgery 51(1) (2010) 155-164.
[132] K. Tanaka, D. Fukuda, Y. Higashikuni, Y. Hirata, I. Komuro, T. Saotome, Y. Yamashita, T. Asakura, M. Sata, Biodegradable Extremely-Small-Diameter Vascular Graft Made of Silk Fibroin can be Implanted in Mice, Journal of Atherosclerosis and Thrombosis advpub (2020).
[133] X. Gong, H. Liu, X. Ding, M. Liu, X. Li, L. Zheng, X. Jia, G. Zhou, Y. Zou, J. Li, X. Huang, Y. Fan, Physiological pulsatile flow culture conditions to generate functional endothelium on a sulfated silk fibroin nanofibrous scaffold, Biomaterials 35(17) (2014) 4782-4791.
[134] D. Wang, H. Liu, Y. Fan, Silk fibroin for vascular regeneration, Microscopy Research and Technique 80(3) (2017) 280-290.

[135] S.G. Wise, M.J. Byrom, A. Waterhouse, P.G. Bannon, M.K.C. Ng, A.S. Weiss, A multilayered synthetic human elastin/polycaprolactone hybrid vascular graft with tailored mechanical properties, Acta Biomaterialia 7(1) (2011) 295-303.
[136] F.O. Obiweluozor, G.A. Emechebe, D.-W. Kim, H.-J. Cho, C.H. Park, C.S. Kim, I.S. Jeong, Considerations in the Development of Small-Diameter Vascular Graft as an Alternative for Bypass and Reconstructive Surgeries: A Review, Cardiovascular Engineering and Technology 11(5) (2020) 495-521.
[137] Z. Mosala Nezhad, A. Poncelet, L. de Kerchove, P. Gianello, C. Fervaille, G. El Khoury, Small intestinal submucosa extracellular matrix (CorMatrix®) in cardiovascular surgery: a systematic review, Interactive CardioVascular and Thoracic Surgery 22(6) (2016) 839-850.
[138] B. Han, F. Xue, C. Fan, X. Mo, Surface heparinization and blood compatibility modification of small intestinal submucosa (SIS) for small-caliber vascular regeneration, Bio-Medical Materials and Engineering 28 (2017) 213-222.
[139] M.T. Koobatian, S. Row, R.J. Smith Jr, C. Koenigsknecht, S.T. Andreadis, D.D. Swartz, Successful endothelialization and remodeling of a cell-free small-diameter arterial graft in a large animal model, Biomaterials 76 (2016) 344-358.
[140] N. L'Heureux, S. Pâquet, R. Labbé, L. Germain, F.A. Auger, A completely biological tissue-engineered human blood vessel, The FASEB Journal 12(1) (1998) 47-56.
[141] T.N. McAllister, M. Maruszewski, S.A. Garrido, W. Wystrychowski, N. Dusserre, A. Marini, K. Zagalski, A. Fiorillo, H. Avila, X. Manglano, J. Antonelli, A. Kocher, M. Zembala, L. Cierpka, L.M. de la Fuente, N. L'Heureux, Effectiveness of haemodialysis access with an autologous tissue-engineered vascular graft: a multicentre cohort study, The Lancet 373(9673) (2009) 1440-1446.
[142] R. Wenger, M.-N. Giraud, 3D Printing Applied to Tissue Engineered Vascular Grafts, Applied Sciences 8(12) (2018).
[143] Y. Mori, H. Tokura, M. Yoshikawa, Properties of hydrogels synthesized by freezing and thawing aqueous polyvinyl alcohol solutions and their applications, Journal of Materials Science 32(2) (1997) 491-496.
[144] B. Singh, L. Pal, Sterculia crosslinked PVA and PVA-poly(AAm) hydrogel wound dressings for slow drug delivery: Mechanical, mucoadhesive, biocompatible and permeability properties, Journal of the Mechanical Behavior of Biomedical Materials 9 (2012) 9-21.
[145] G. Fundueanu, M. Constantin, P. Ascenzi, Poly(vinyl alcohol) microspheres with pH- and thermosensitive properties as temperature-controlled drug delivery, Acta Biomaterialia 6(10) (2010) 3899-3907.
[146] A. Kumar, S.S. Han, PVA-based hydrogels for tissue engineering: A review, International Journal of Polymeric Materials and Polymeric Biomaterials 66(4) (2017) 159-182.
[147] E.A. Kamoun, E.-R.S. Kenawy, X. Chen, A review on polymeric hydrogel membranes for wound dressing applications: PVA-based hydrogel dressings, Journal of Advanced Research 8(3) (2017) 217-233.
[148] J.L. Holloway, A.M. Lowman, G.R. Palmese, The role of crystallization and phase separation in the formation of physically cross-linked PVA hydrogels, Soft Matter 9(3) (2013) 826-833.
[149] S. Gupta, S. Goswami, A. Sinha, A combined effect of freeze--thaw cycles and polymer concentration on the structure and mechanical properties of transparent PVA gels, Biomedical Materials 7(1) (2012) 015006.
[150] N.A. Peppas, Turbidimetric studies of aqueous poly (vinyl alcohol) solutions, Die Makromolekulare Chemie: Macromolecular Chemistry and Physics 176(11) (1975) 3433-3440.
[151] S. Jiang, S. Liu, W. Feng, PVA hydrogel properties for biomedical application, Journal of the Mechanical Behavior of Biomedical Materials 4(7) (2011) 1228-1233.
[152] E. Otsuka, A. Suzuki, A simple method to obtain a swollen PVA gel crosslinked by hydrogen bonds, Journal of applied polymer science 114(1) (2009) 10-16.

[153] H.S. Mansur, C.M. Sadahira, A.N. Souza, A.A.P. Mansur, FTIR spectroscopy characterization of poly (vinyl alcohol) hydrogel with different hydrolysis degree and chemically crosslinked with glutaraldehyde, Materials Science and Engineering: C 28(4) (2008) 539-548.
[154] J. Gough, C. Scotchford, S. Downes, Cytotoxicity of glutaraldehyde crosslinked collagen/poly(vinyl alcohol) films is by the mechanism of apoptosis, Journal of biomedical materials research 61 1 (2002) 121-30.
[155] W. Chen, Y. Hou, Z. Tu, L. Gao, R. Haag, pH-degradable PVA-based nanogels via photo-crosslinking of thermo-preinduced nanoaggregates for controlled drug delivery, Journal of Controlled Release 259 (2017) 160-167.
[156] J.-O. Jeong, J.-S. Park, Y.-A. Kim, S.-J. Yang, S.-I. Jeong, J.-Y. Lee, Y.-M. Lim, Gamma Ray-Induced Polymerization and Cross-Linking for Optimization of PPy/PVP Hydrogel as Biomaterial, Polymers 12(1) (2020).
[157] K.M. El Salmawi, Gamma Radiation-Induced Crosslinked PVA/Chitosan Blends for Wound Dressing, Journal of Macromolecular Science, Part A 44(5) (2007) 541-545.
[158] B.-z. Li, L.-j. Wang, D. Li, Y.L. Chiu, Z.-j. Zhang, J. Shi, X.D. Chen, Z.-h. Mao, Physical properties and loading capacity of starch-based microparticles crosslinked with trisodium trimetaphosphate, Journal of Food Engineering 92(3) (2009) 255-260.
[159] F. Gao, D. Li, C.-h. Bi, Z.-h. Mao, B. Adhikari, Preparation and characterization of starch crosslinked with sodium trimetaphosphate and hydrolyzed by enzymes, Carbohydrate Polymers 103 (2014) 310-318.
[160] V. Dulong, S. Lack, D. Le Cerf, L. Picton, J.P. Vannier, G. Muller, Hyaluronan-based hydrogels particles prepared by crosslinking with trisodium trimetaphosphate. Synthesis and characterization, Carbohydrate Polymers 57(1) (2004) 1-6.
[161] A. Bejenariu, M. Popa, V. Dulong, L. Picton, D. Le Cerf, Trisodium trimetaphosphate crosslinked xanthan networks: synthesis, swelling, loading and releasing behaviour, Polymer Bulletin 62(4) (2009) 525-538.
[162] S. Lack, V. Dulong, D. Le Cerf, L. Picton, J.F. Argillier, G. Muller, Hydrogels Based on Pullulan Crosslinked with sodium trimetaphosphate (STMP): Rheological study, Polymer Bulletin 52(6) (2004) 429-436.
[163] V. Dulong, R. Forbice, E. Condamine, D. Le Cerf, L. Picton, Pullulan–STMP hydrogels: a way to correlate crosslinking mechanism, structure and physicochemical properties, Polymer Bulletin 67(3) (2011) 455-466.
[164] Y. Sang, O. Prakash, P.A. Seib, Characterization of phosphorylated cross-linked resistant starch by 31P nuclear magnetic resonance (31P NMR) spectroscopy, Carbohydrate Polymers 67(2) (2007) 201-212.
[165] S. Lack, V. Dulong, L. Picton, D.L. Cerf, E. Condamine, High-resolution nuclear magnetic resonance spectroscopy studies of polysaccharides crosslinked by sodium trimetaphosphate: a proposal for the reaction mechanism, Carbohydrate Research 342(7) (2007) 943-953.
[166] M. Chaouat, C. Le Visage, W.E. Baille, B. Escoubet, F. Chaubet, M.A. Mateescu, D. Letourneur, A Novel Cross-linked Poly(vinyl alcohol) (PVA) for Vascular Grafts, Advanced Functional Materials 18(19) (2008) 2855-2861.
[167] Y. Jeong, Y. Yao, T.H. Mekonnen, E.K.F. Yim, Changing Compliance of Poly(Vinyl Alcohol) Tubular Scaffold for Vascular Graft Applications Through Modifying Interlayer Adhesion and Crosslinking Density, Frontiers in Materials 7(456) (2021).
[168] J.M. Ino, E. Sju, V. Ollivier, E.K. Yim, D. Letourneur, C. Le Visage, Evaluation of hemocompatibility and endothelialization of hybrid poly(vinyl alcohol) (PVA)/gelatin polymer films, J Biomed Mater Res B Appl Biomater 101(8) (2013) 1549-59.
[169] M.F. Cutiongco, D.E. Anderson, M.T. Hinds, E.K. Yim, In vitro and ex vivo hemocompatibility of off-the-shelf modified poly(vinyl alcohol) vascular grafts, Acta Biomater 25 (2015) 97-108.

[170] N.M. Bates, C. Puy, P.L. Jurney, O.J.T. McCarty, M.T. Hinds, Evaluation of the Effect of Crosslinking Method of Poly(Vinyl Alcohol) Hydrogels on Thrombogenicity, Cardiovascular Engineering and Technology 11(4) (2020) 448-455.
[171] D.E.J. Anderson, K.P. Truong, M.W. Hagen, E.K.F. Yim, M.T. Hinds, Biomimetic modification of poly(vinyl alcohol): Encouraging endothelialization and preventing thrombosis with antiplatelet monotherapy, Acta Biomaterialia 86 (2019) 291-299.
[172] M. Rizwan, Y. Yao, M.B. Gorbet, J.W. Tse, D.E.J. Anderson, M.T. Hinds, E.K.F. Yim, One-Pot Covalent Grafting of Gelatin on Poly(Vinyl Alcohol) Hydrogel to Enhance Endothelialization and Hemocompatibility for Synthetic Vascular Graft Applications, ACS Applied Bio Materials 3(1) (2020) 693-703.
[173] P.L. Jurney, D.E.J. Anderson, G. Pohan, E.K.F. Yim, M.T. Hinds, Reactive Ion Plasma Modification of Poly(Vinyl-Alcohol) Increases Primary Endothelial Cell Affinity and Reduces Thrombogenicity, Macromolecular Bioscience 18(11) (2018) 1800132.
[174] G. Pohan, P. Chevallier, D.E.J. Anderson, J.W. Tse, Y. Yao, M.W. Hagen, D. Mantovani, M.T. Hinds, E.K.F. Yim, Luminal Plasma Treatment for Small Diameter Polyvinyl Alcohol Tubular Scaffolds, Frontiers in Bioengineering and Biotechnology 7(117) (2019).
[175] N.A. Ushakova, G.E. Morozevich, N.E. Ustyuzhanina, M.I. Bilan, A.I. Usov, N.E. Nifantiev, M.E. Preobrazhenskaya, Anticoagulant activity of fucoidans from brown algae, Biochemistry (Moscow) Supplement Series B: Biomedical Chemistry 3(1) (2009) 77-83.
[176] W. Jin, Q. Zhang, J. Wang, W. Zhang, A comparative study of the anticoagulant activities of eleven fucoidans, Carbohydrate Polymers 91(1) (2013) 1-6.
[177] A. Cumashi, N.A. Ushakova, M.E. Preobrazhenskaya, A. D'Incecco, A. Piccoli, L. Totani, N. Tinari, G.E. Morozevich, A.E. Berman, M.I. Bilan, A.I. Usov, N.E. Ustyuzhanina, A.A. Grachev, C.J. Sanderson, M. Kelly, G.A. Rabinovich, S. Iacobelli, N.E. Nifantiev, I. and on behalf of the Consorzio Interuniversitario Nazionale per la Bio-Oncologia, A comparative study of the anti-inflammatory, anticoagulant, antiangiogenic, and antiadhesive activities of nine different fucoidans from brown seaweeds, Glycobiology 17(5) (2007) 541-552.
[178] Li, F. Lu, X. Wei, R. Zhao, Fucoidan: structure and bioactivity, Molecules 13(8) (2008) 1671-1695.
[179] P. Chauvet, J.-G. Bienvenu, J.-F. Théorêt, J.-G. Latour, Y. Merhi, Inhibition of platelet-neutrophil interactions by fucoidan reduces adhesion and vasoconstriction after acute arterial injury by angioplasty in pigs, Journal of Cardiovascular Pharmacology 34(4) (1999) 597-603.
[180] Mourão, Perspective on the use of sulfated polysaccharides from marine organisms as a source of new antithrombotic drugs, Marine Drugs 13(5) (2015) 2770-2784.
[181] A. Tariq, M. Athar, J. Ara, V. Sultana, S. Ehteshamul-Haque, M. Ahmad, Biochemical evaluation of antioxidant activity and polysaccharides fractions in seaweeds, Global Journal of Environmental Science and Management 1(1) (2015) 47-62.
[182] H.D. Cuong, T.T.T. Thuy, T.T. Huong, B.M. Ly, T.T.T. Van, Structure and hypolipidaemic activity of fucoidan extracted from brown seaweed Sargassum henslowianum, Natural Product Research 29(5) (2015) 411-415.
[183] T. Yokota, M. Nagashima, M. Ghazizadeh, O. Kawanami, Increased effect of fucoidan on lipoprotein lipase secretion in adipocytes, Life Sciences 84(15) (2009) 523-529.
[184] Thorlacius, Vollmar, Seyfert, Vestweber, Menger, The polysaccharide fucoidan inhibits microvascular thrombus formation independently from P- and l-selectin function in vivo, European Journal of Clinical Investigation 30(9) (2000) 804-810.
[185] F. Zemani, D. Benisvy, I. Galy-Fauroux, A. Lokajczyk, S. Colliec-Jouault, G. Uzan, A.M. Fischer, C. Boisson-Vidal, Low-molecular-weight fucoidan enhances the proangiogenic phenotype of endothelial progenitor cells, Biochemical Pharmacology 70(8) (2005) 1167-1175.

[186] G.F. Springer, H.A. Wurzel, G.M. McNeal, N.J. Ansell, M.F. Doughty, Isolation of anticoagulant fractions from crude fucoidin, Proceedings of the Society for Experimental Biology and Medicine 94(2) (1957) 404-409.
[187] I.P.J. Alwayn, J.Z. Appel Iii, C. Goepfert, L. Buhler, D.K.C. Cooper, S.C. Robson, Inhibition of platelet aggregation in baboons: therapeutic implications for xenotransplantation, Xenotransplantation 7(4) (2000) 247-257.
[188] F. Haroun-Bouhedja, M. Ellouali, C. Sinquin, C. Boisson-Vidal, Relationship between sulfate groups and biological activities of fucans, Thrombosis Research 100(5) (2000) 453-459.
[189] T.A. Kuznetsova, N.N. Besednova, A.N. Mamaev, A.P. Momot, N.M. Shevchenko, T.N. Zvyagintseva, Anticoagulant activity of fucoidan from brown algae Fucus evanescens of the Okhotsk Sea, Bulletin of Experimental Biology and Medicine 136(5) (2003) 471-473.
[190] Kim, Y.-K. Koo, M.-K. Jung, H.R. Moon, S.M. Kim, A. Synytsya, H.S. Yun-Choi, Y.S. Kim, J.K. Park, Y.I. Park, Anticoagulating activities of low-molecular weight fuco-oligosaccharides prepared by enzymatic digestion of fucoidan from the sporophyll of Korean Undaria pinnatifida, Archives of Pharmacal Research 33(1) (2010) 125-131.
[191] W.A.J.P. Wijesinghe, Y. Athukorala, Y.J. Jeon, Effect of anticoagulative sulfated polysaccharide purified from enzyme-assistant extract of a brown seaweed Ecklonia cava on Wistar rats, Carbohydrate Polymers 86(2) (2011) 917-921.
[192] F. Shang, R. Mou, Z. Zhang, N. Gao, L. Lin, Z. Li, M. Wu, J. Zhao, Structural analysis and anticoagulant activities of three highly regular fucan sulfates as novel intrinsic factor Xase inhibitors, Carbohydrate Polymers 195 (2018) 257-266.
[193] Li, R.X. Zhao, X.J. Wei, Anticoagulant activity of fucoidan from Hizikia fusiforme, Agro Food Industry Hi-Tech 19(1) (2008) 22-24.
[194] T. Nishino, A. Fukuda, T. Nagumo, M. Fujihara, E. Kaji, Inhibition of the generation of thrombin and factor Xa by a fucoidan from the brown seaweed Ecklonia kurome, Thrombosis Research 96(1) (1999) 37-49.
[195] E.S. Lapikova, N.N. Drozd, A.S. Tolstenkov, V.A. Makarov, T.N. Zvyagintseva, N.M. Shevchenko, I.U. Bakunina, N.N. Besednova, T.A. Kuznetsova, Inhibition of thrombin and factor Xa by Fucus evanescens fucoidan and its modified analogs, Bulletin of Experimental Biology and Medicine 146(3) (2008) 328-333.
[196] K. Park, E. Cho, M.-J. In, D.C. Kim, H.J. Chae, Physicochemical properties and bioactivity of brown seaweed fucoidan prepared by ultra high pressure-assisted enzyme treatment, Korean Journal of Chemical Engineering 29(2) (2012) 221-227.
[197] Zhao, S. Dong, J. Wang, F. Li, A. Chen, B. Li, A comparative study of antithrombotic and antiplatelet activities of different fucoidans from Laminaria japonica, Thrombosis Research 129(6) (2012) 771-778.
[198] N.N. Drozd, A.S. Tolstenkov, V.A. Makarov, T.A. Kuznetsova, N.N. Besednova, N.M. Shevchenko, T.N. Zvyagintseva, Pharmacodynamic parameters of anticoagulants based on sulfated polysaccharides from marine algae, Bulletin of Experimental Biology and Medicine 142(5) (2006) 591-593.
[199] S. Colliec, A.M. Fischer, J. Tapon-Bretaudiere, C. Boisson, P. Durand, J. Jozefonvicz, Anticoagulant properties of a fucoidan fraction, Thrombosis Research 64(2) (1991) 143-154.
[200] R. Minix, V.M. Doctor, Interaction of fucoidan with proteases and inhibitors of coagulation and fibrinolysis, Thrombosis Research 87(5) (1997) 419-429.
[201] M.B. Mansour, R. Balti, L. Yacoubi, V. Ollivier, F. Chaubet, R.M. Maaroufi, Primary structure and anticoagulant activity of fucoidan from the sea cucumber Holothuria polii, International Journal of Biological Macromolecules 121 (2019) 1145-1153.

[202] T. Nishino, Y. Aizu, T. Nagumo, Antithrombin activity of a fucan sulfate from the brown seaweed Ecklonia kurome, Thrombosis Research 62(6) (1991) 765-773.
[203] T. Nishino, H. Ura, T. Nagumo, The relationship Between the sulfate content and the antithrombin activity of an α(1→2)-fucoidan purified from a commercial fucoidan fraction, Botanica Marina 38(1-6) (1995) 187-194.
[204] S. Soeda, S. Sakaguchi, H. Shimeno, A. Nagamatsu, Fibrinolytic and anticoagulant activities of highly sulfated fucoidan, Biochemical Pharmacology 43(8) (1992) 1853-1858.
[205] R. Ghebouli, S. Loyau, M. Maire, P. Saboural, J.P. Collet, M. Jandrot-Perrus, D. Letourneur, F. Chaubet, J.B. Michel, Amino-fucoidan as a vector for rtPA-induced fibrinolysis in experimental thrombotic events, Thrombosis and Haemostasis 118(1) (2018) 42-53.
[206] S. Mauray, E. De Raucourt, F. Chaubet, O. MaÏGa-Revel, C. Sternberg, A.M. Fischer, Comparative anticoagulant activity and influence on thrombin generation of dextran derivatives and of a fucoidan fraction, Journal of Biomaterials Science, Polymer Edition 9(4) (1998) 373-387.
[207] F.C. Church, J.B. Meade, R.E. Treanor, H.C. Whinna, Antithrombin activity of fucoidan. The interaction of fucoidan with heparin cofactor II, antithrombin III, and thrombin, Journal of Biological Chemistry 264(6) (1989) 3618-3623.
[208] Ustyuzhanina, N.A. Ushakova, K.A. Zyuzina, M.I. Bilan, A.L. Elizarova, O.V. Somonova, A.V. Madzhuga, V.B. Krylov, M.E. Preobrazhenskaya, A.I. Usov, M.V. Kiselevskiy, N.E. Nifantiev, Influence of fucoidans on hemostatic system, Marine Drugs 11(7) (2013) 2444-2458.
[209] S. Soeda, Y. Ohmagari, H. Shimeno, A. Nagamatsu, Preparation of oversulfated fucoidan fragments and evaluation of their antithrombotic activities, Thrombosis Research 72(3) (1993) 247-256.
[210] B. Richard, M.C. Bouton, S. Loyau, D. Lavigne, D. Letourneur, M. Jandrot-Perrus, V. Arocas, Modulation of protease nexin-I activity by polysaccharides, Thrombosis and Haemostasis 95(2) (2006) 229-235.
[211] E.S. Jeong, Y.H. Yoon, J.K. Kim, Contrasting correlation in the inhibition response of ADP-induced platelet aggregation and the anti-coagulant activities of algal fucoidans derived from Eisenia bicyclis and Undaria pinnatifida sporophylls (Mekabu), Fisheries and Aquatic Sciences 12(3) (2009) 194-202.
[212] A. Chen, F. Zhang, J. Shi, X. Zhao, M. Yan, Mechanism study of endothelial protection and inhibits platelet activation of low molecular weight fucoidan from Laminaria japonica, Journal of Ocean University of China 15(5) (2016) 918-922.
[213] Y.A. Senis, A. Mazharian, J. Mori, Src family kinases: at the forefront of platelet activation, Blood 124(13) (2014) 2013-2024.
[214] T. Carvalho G. de Azevedo, M.E.B. Bezerra, M.d.G.d.L. Santos, L.A. Souza, C.T. Marques, N.M.B. Benevides, E.L. Leite, Heparinoids algal and their anticoagulant, hemorrhagic activities and platelet aggregation, Biomedicine & Pharmacotherapy 63(7) (2009) 477-483.
[215] N.P. Patil, V. Le, A.D. Sligar, L. Mei, D. Chavarria, E.Y. Yang, A.B. Baker, Algal polysaccharides as therapeutic agents for atherosclerosis, Frontiers in Cardiovascular Medicine 5(153) (2018).
[216] C. Blondin, E. Fischer, C. Boisson-Vidal, M.D. Kazatchkine, J. Jozefonvicz, Inhibition of complement activation by natural sulfated polysaccharides (fucans) from brown seaweed, Molecular Immunology 31(4) (1994) 247-253.
[217] C. Blondin, F. Chaubet, A. Nardella, C. Sinquin, J. Jozefonvicz, Relationships between chemical characteristics and anticomplementary activity of fucans, Biomaterials 17(6) (1996) 597-603.
[218] T.N. Zvyagintseva, N.M. Shevchenko, I.V. Nazarova, A.S. Scobun, P.A. Luk'yanov, L.A. Elyakova, Inhibition of complement activation by water-soluble polysaccharides of some far-eastern brown seaweeds, Comparative Biochemistry and Physiology - C Pharmacology Toxicology and Endocrinology 126(3) (2000) 209-215.

[219] B. Tissot, F. Gonnet, A. Iborra, C. Berthou, N. Thielens, G.J. Arlaud, R. Daniel, Mass spectrometry analysis of the oligomeric C1q protein reveals the B chain as the target of trypsin cleavage and interaction with fucoidan, Biochemistry 44(7) (2005) 2602-2609.
[220] B. Tissot, B. Montdargent, L. Chevolot, A. Varenne, S. Descroix, P. Gareil, R. Daniel, Interaction of fucoidan with the proteins of the complement classical pathway, Biochimica et Biophysica Acta (BBA) - Proteins and Proteomics 1651(1) (2003) 5-16.
[221] G. Kopplin, A.M. Rokstad, H. Mélida, V. Bulone, G. Skjåk-Bræk, F.L. Aachmann, Structural characterization of fucoidan from Laminaria hyperborea: assessment of coagulation and inflammatory properties and their structure-function relationship, ACS Applied Bio Materials 1(6) (2018) 1880-1892.
[222] M.E. Preobrazhenskaya, A.E. Berman, V.I. Mikhailov, N.A. Ushakova, A.V. Mazurov, A.V. Semenov, A.I. Usov, N.E. Nifant'ev, N.V. Bovin, Fucoidan inhibits leukocyte recruitment in a model peritoneal inflammation in rat and blocks interaction of P-selectin with its carbohydrate ligand, Biochemistry and Molecular Biology International 43(2) (1997) 443-451.
[223] J.P. Gaboury, P. Kubes, Reductions in physiologic shear rates lead to CD11/CD18-dependent, selectin-independent leukocyte rolling in vivo, Blood 83(2) (1994) 345-350.
[224] M. Omata, N. Matsui, N. Inomata, T. Ohno, Protective effects of polysaccharide fucoidin on myocardial ischemia- reperfusion injury in rats, Journal of Cardiovascular Pharmacology 30(6) (1997) 717-724.
[225] M. Juenet, R. Aid-Launais, B. Li, A. Berger, J. Aerts, V. Ollivier, A. Nicoletti, D. Letourneur, C. Chauvierre, Thrombolytic therapy based on fucoidan-functionalized polymer nanoparticles targeting P-selectin, Biomaterials 156 (2018) 204-216.
[226] Li, M. Juenet, R. Aid-Launais, M. Maire, V. Ollivier, D. Letourneur, C. Chauvierre, Development of polymer microcapsules functionalized with fucoidan to target P-selectin overexpressed in cardiovascular diseases, Advanced Healthcare Materials 6(4) (2017) 1601200.
[227] Bonnard, G. Yang, A. Petiet, V. Ollivier, O. Haddad, D. Arnaud, L. Louedec, L. Bachelet-Violette, S.M. Derkaoui, D. Letourneur, C. Chauvierre, C. Le Visage, Abdominal aortic aneurysms targeted by functionalized polysaccharide microparticles: a new tool for SPECT imaging, Theranostics 4(6) (2014) 592-603.
[228] K. Tanaka, M. Ito, M. Kodama, M. Tomita, S. Kimura, M. Hoyano, W. Mitsuma, S. Hirono, H. Hanawa, Y. Aizawa, Sulfated polysaccharide fucoidan ameliorates experimental autoimmune myocarditis in rats, Journal of Cardiovascular Pharmacology and Therapeutics 16(1) (2010) 79-86.
[229] M. Zhou, Y. Ding, L. Cai, Y. Wang, C. Lin, Z. Shi, Low molecular weight fucoidan attenuates experimental abdominal aortic aneurysm through interfering the leukocyte-endothelial cells interaction, Molecular Medicine Reports 17(5) (2018) 7089-7096.
[230] J.I. Rotmans, E. Velema, H.J.M. Verhagen, J.D. Blankensteijn, D.P.V. de Kleijn, E.S.G. Stroes, G. Pasterkamp, Matrix metalloproteinase inhibition reduces intimal hyperplasia in a porcine arteriovenous-graft model, Journal of Vascular Surgery 39(2) (2004) 432-439.
[231] K. Kishi, M. Muramatsu, D. Jin, K. Furubayashi, S. Takai, H. Tamai, M. Miyazaki, The effects of Chymase on matrix metalloproteinase-2 activation in neointimal hyperplasia after balloon injury in dogs, Hypertension Research 30(1) (2007) 77-83.
[232] T. Fujimura, K. Tsukahara, S. Moriwaki, T. Kitahara, T. Sano, Y. Takema, Treatment of human skin with an extract of Fucus vesiculosus changes its thickness and mechanical properties, J Cosmet Sci 53(1) (2002) 1-9.
[233] S.H. Tsai, J.C. Wang, W.I. Liao, Y.J. Hsu, C.Y. Lin, M.T. Liao, P.H. Huang, S.J. Lin, Fucoidan attenuates angiotensin II-induced abdominal aortic aneurysms through the inhibition of c-Jun N-terminal kinase and nuclear factor κB activation, Journal of Vascular Surgery 68(6) (2018) 72S-81S.e1.

[234] H. Haybar, S. Shahrabi, H. Rezaeeyan, R. Shirzad, N. Saki, Endothelial cells: from dysfunction mechanism to pharmacological effect in cardiovascular disease, Cardiovascular Toxicology 19(1) (2019) 13-22.
[235] E.D. Verrier, E.M. Boyle, Endothelial cell injury in cardiovascular surgery, The Annals of Thoracic Surgery 62(3) (1996) 915-922.
[236] T.A. Kuznetsova, L.A. Ivanushko, E.V. Persiyanova, S.P. Ermakova, N.N. Besednova, Markers of systemic inflammation in experimental dyslipidemia induced by P-407: Modulation with fucoidan from brown alga Fucus evanescens, Bulletin of Experimental Biology and Medicine 166(6) (2019) 766-769.
[237] N. Marinval, M. Morenc, M.N. Labour, A. Samotus, A. Mzyk, V. Ollivier, M. Maire, K. Jesse, K. Bassand, A. Niemiec-Cyganek, O. Haddad, M.P. Jacob, F. Chaubet, N. Charnaux, P. Wilczek, H. Hlawaty, Fucoidan/VEGF-based surface modification of decellularized pulmonary heart valve improves the antithrombotic and re-endothelialization potential of bioprostheses, Biomaterials 172 (2018) 14-29.
[238] Wang, C. Ye, H. Su, J. Wang, Y. Wang, H. Wang, A. Zhao, N. Huang, Layer-by-layer self-assembled laminin/fucoidan films: Towards better hemocompatibility and endothelialization, RSC Advances 6(61) (2016) 56048-56055.
[239] P. Vischer, E. Buddecke, Different action of heparin and fucoidan on arterial smooth muscle cell proliferation and thrombospondin and fibronectin metabolism, European Journal of Cell Biology 56(2) (1991) 407-414.
[240] D. Logeart, D. Letourneur, J. Jozefonvicz, P. Kern, Collagen synthesis by vascular smooth muscle cells in the presence of antiproliferative polysaccharides, Journal of Biomedical Materials Research 30(4) (1996) 501-508.
[241] T.A. McCaffrey, D.J. Falcone, D. Vicente, B. Du, S. Consigli, W. Borth, Protection of transforming growth factor β activity by heparin and fucoidan, Journal of Cellular Physiology 159(1) (1994) 51-59.
[242] M.K. Patel, B. Mulloy, K.L. Gallagher, L. O'Brien, A.D. Hughes, The antimitogenic action of the sulphated polysaccharide fucoidan differs from heparin in human vascular smooth muscle cells, Thrombosis and Haemostasis 87(1) (2002) 149-154.
[243] P. Religa, M. Kazi, J. Thyberg, Z. Gaciong, J. Swedenborg, U. Hedin, Fucoidan inhibits smooth muscle cell proliferation and reduces mitogen-activated protein kinase activity, European Journal of Vascular and Endovascular Surgery 20(5) (2000) 419-426.
[244] D. Logeart, S. Prigent-Richard, C. Boisson-Vidal, F. Chaubet, P. Durand, J. Jozefonvicz, D. Letourneur, Fucans, sulfated polysaccharides extracted from brown seaweeds, inhibit vascular smooth muscle cell proliferation. II. Degradation and molecular weight effect, European journal of cell biology 74(4) (1997) 385-390.
[245] T. Novoyatleva, B. Kojonazarov, A. Owczarek, S. Veeroju, N. Rai, I. Henneke, M. Böhm, F. Grimminger, H.A. Ghofrani, W. Seeger, N. Weissmann, R.T. Schermuly, Evidence for the fucoidan/p-selectin axis as a therapeutic target in hypoxia-induced pulmonary hypertension, American Journal of Respiratory and Critical Care Medicine 199(11) (2019) 1407-1420.
[246] J.-F. Deux, A. Meddahi-Pellé, F. Bree, I. Bataille, J.-B. Michel, D. Letourneur, Comparative studies on the mechanisms of action of four polysaccharides on arterial restenosis, Journal of Biomaterials Science, Polymer Edition 20(5-6) (2009) 689-702.
[247] Xu, W. Zhu, T. Wang, L. Jin, T. Liu, X. Li, Z. Guan, Z. Jiang, X. Meng, J. Wang, Y. Guo, Low molecule weight fucoidan mitigates atherosclerosis in ApoE (-/-) mouse model through activating multiple signal pathway, Carbohydrate Polymers 206 (2019) 110-120.
[248] N. Roux, E. Brakenhielm, C. Freguin-Bouillant, F. Lallemand, J.P. Henry, O. Boyer, C. Thuillez, D. Plissonnier, Progenitor cell mobilizing treatments prevent experimental transplant arteriosclerosis, Journal of Surgical Research 176(2) (2012) 657-665.

[249] Kim, I.-H. Bae, K.S. Lim, J.-K. Park, D.S. Park, S.-Y. Lee, E.-J. Jang, M.S. Ji, D.S. Sim, Y.J. Hong, Y. Ahn, J.C. Park, J.G. Cho, J.C. Kang, I.-S. Kim, M.H. Jeong, A method for coating fucoidan onto bare metal stent and in vivo evaluation, Progress in Organic Coatings 78 (2015) 348-356.
[250] B.G. Munoz-Robles, I. Kopyeva, C.A. DeForest, Surface Patterning of Hydrogel Biomaterials to Probe and Direct Cell–Matrix Interactions, Advanced Materials Interfaces 7(21) (2020) 2001198.
[251] C.D. Paul, A. Hruska, J.R. Staunton, H.A. Burr, K.M. Daly, J. Kim, N. Jiang, K. Tanner, Probing cellular response to topography in three dimensions, Biomaterials 197 (2019) 101-118.
[252] Y. Yang, J. Sun, X. Liu, Z. Guo, Y. He, D. Wei, M. Zhong, L. Guo, H. Fan, X. Zhang, Wet-spinning fabrication of shear-patterned alginate hydrogel microfibers and the guidance of cell alignment, Regenerative Biomaterials 4(5) (2017) 299-307.
[253] R.B. Vernon, M.D. Gooden, S.L. Lara, T.N. Wight, Microgrooved fibrillar collagen membranes as scaffolds for cell support and alignment, Biomaterials 26(16) (2005) 3131-3140.
[254] A. Paul, M. Stührenberg, S. Chen, D. Rhee, W.K. Lee, T.W. Odom, S.C. Heilshorn, A. Enejder, Micro- and nano-patterned elastin-like polypeptide hydrogels for stem cell culture, Soft Matter 13(34) (2017) 5665-5675.
[255] Z. Li, Y. Gong, S. Sun, Y. Du, D. Lü, X. Liu, M. Long, Differential regulation of stiffness, topography, and dimension of substrates in rat mesenchymal stem cells, Biomaterials 34(31) (2013) 7616-7625.
[256] D.Y. Fozdar, X. Wu, C.W. Patrick, S. Chen, Micro-well texture printed into PEG hydrogels using the FILM nanomanufacturing process affects the behavior of preadipocytes, Biomedical Microdevices 10(6) (2008) 839-849.
[257] B. Yanez-Soto, S.J. Liliensiek, J.Z. Gasiorowski, C.J. Murphy, P.F. Nealey, The influence of substrate topography on the migration of corneal epithelial wound borders, Biomaterials 34(37) (2013) 9244-9251.
[258] D.-H. Kim, K. Han, K. Gupta, K.W. Kwon, K.-Y. Suh, A. Levchenko, Mechanosensitivity of fibroblast cell shape and movement to anisotropic substratum topography gradients, Biomaterials 30(29) (2009) 5433-5444.
[259] G. de Vicente, M.C. Lensen, Topographically and elastically micropatterned PEG-based hydrogels to control cell adhesion and migration, European Polymer Journal 78 (2016) 290-301.
[260] K. Kushiro, T. Sakai, M. Takai, Slope-Dependent Cell Motility Enhancements at the Walls of PEG-Hydrogel Microgroove Structures, Langmuir 31(37) (2015) 10215-10222.
[261] R.J. Petrie, A.D. Doyle, K.M. Yamada, Random versus directionally persistent cell migration, Nature Reviews Molecular Cell Biology 10(8) (2009) 538-549.
[262] L. Bacakova, E. Filova, M. Parizek, T. Ruml, V. Svorcik, Modulation of cell adhesion, proliferation and differentiation on materials designed for body implants, Biotechnology Advances 29(6) (2011) 739-767.
[263] L. Wang, D. Song, X. Zhang, Z. Ding, X. Kong, Q. Lu, D.L. Kaplan, Silk–Graphene Hybrid Hydrogels with Multiple Cues to Induce Nerve Cell Behavior, ACS Biomaterials Science & Engineering 5(2) (2019) 613-622.
[264] J. Du, J. Liu, S. Yao, H. Mao, J. Peng, X. Sun, Z. Cao, Y. Yang, B. Xiao, Y. Wang, P. Tang, X. Wang, Prompt peripheral nerve regeneration induced by a hierarchically aligned fibrin nanofiber hydrogel, Acta Biomaterialia 55 (2017) 296-309.
[265] I. Jun, S.J. Kim, E. Choi, K.M. Park, T. Rhim, J. Park, K.D. Park, H. Shin, Preparation of biomimetic hydrogels with controlled cell adhesive properties and topographical features for the study of muscle cell adhesion and proliferation, Macromolecular bioscience 12(11) (2012) 1502-1513.
[266] M. Rizwan, G.S.L. Peh, H.-P. Ang, N.C. Lwin, K. Adnan, J.S. Mehta, W.S. Tan, E.K.F. Yim, Sequentially-crosslinked bioactive hydrogels as nano-patterned substrates with customizable stiffness and degradation for corneal tissue engineering applications, Biomaterials 120 (2017) 139-154.

[267] M. d'Angelo, E. Benedetti, M.G. Tupone, M. Catanesi, V. Castelli, A. Antonosante, A. Cimini, The Role of Stiffness in Cell Reprogramming: A Potential Role for Biomaterials in Inducing Tissue Regeneration, Cells 8(9) (2019).
[268] D. Lu, C.-S. Chen, C.-S. Lai, S. Soni, T. Lam, C. Le, E.Y.T. Chen, T. Nguyen, W.-C. Chin, Microgrooved Surface Modulates Neuron Differentiation in Human Embryonic Stem Cells, in: K. Turksen (Ed.), Human Embryonic Stem Cell Protocols, Springer New York, New York, NY, 2016, pp. 281-287.
[269] S. Yao, X. Liu, S. Yu, X. Wang, S. Zhang, Q. Wu, X. Sun, H. Mao, Co-effects of matrix low elasticity and aligned topography on stem cell neurogenic differentiation and rapid neurite outgrowth, Nanoscale 8(19) (2016) 10252-10265.
[270] J.M. Lee, W.S. Kang, K.G. Lee, H.-Y. Cho, B. Conley, C.D. Ahrberg, J.H. Lim, S.J. Mo, S.G. Mun, E.-J. Kim, J.-W. Choi, K.-B. Lee, S.J. Lee, B.G. Chung, Combinatorial biophysical cue sensor array for controlling neural stem cell fate, Biosensors and Bioelectronics 156 (2020) 112125.
[271] B. Duan, C. Xu, S. Das, J.M. Chen, J.T. Butcher, Spatial Regulation of Valve Interstitial Cell Phenotypes within Three-Dimensional Micropatterned Hydrogels, ACS Biomaterials Science & Engineering 5(3) (2019) 1416-1425.
[272] Z. Ding, G. Lu, W. Cheng, G. Xu, B. Zuo, Q. Lu, D.L. Kaplan, Tough Anisotropic Silk Nanofiber Hydrogels with Osteoinductive Capacity, ACS Biomaterials Science & Engineering 6(4) (2020) 2357-2367.
[273] J. Park, J.H. Choi, S. Kim, I. Jang, S. Jeong, J.Y. Lee, Micropatterned conductive hydrogels as multifunctional muscle-mimicking biomaterials: Graphene-incorporated hydrogels directly patterned with femtosecond laser ablation, Acta Biomaterialia 97 (2019) 141-153.
[274] C.L. Nemeth, K. Janebodin, A.E. Yuan, J.E. Dennis, M. Reyes, D.-H. Kim, Enhanced chondrogenic differentiation of dental pulp stem cells using nanopatterned PEG-GelMA-HA hydrogels, Tissue Engineering Part A 20(21-22) (2014) 2817-2829.
[275] V.A. Schulte, M. Diez, M. Möller, M.C. Lensen, Topography-Induced Cell Adhesion to Acr-sP(EO-stat-PO) Hydrogels: The Role of Protein Adsorption, Macromolecular Bioscience 11(10) (2011) 1378-1386.
[276] V.A. Schulte, M. Díez, M. Möller, M.C. Lensen, Surface Topography Induces Fibroblast Adhesion on Intrinsically Nonadhesive Poly(ethylene glycol) Substrates, Biomacromolecules 10(10) (2009) 2795-2801.
[277] S. Ankam, C.K. Lim, E.K.F. Yim, Actomyosin contractility plays a role in MAP2 expression during nanotopography-directed neuronal differentiation of human embryonic stem cells, Biomaterials 47 (2015) 20-28.
[278] B.K.K. Teo, S.T. Wong, C.K. Lim, T.Y.S. Kung, C.H. Yap, Y. Ramagopal, L.H. Romer, E.K.F. Yim, Nanotopography Modulates Mechanotransduction of Stem Cells and Induces Differentiation through Focal Adhesion Kinase, ACS Nano 7(6) (2013) 4785-4798.
[279] A.K. Yip, A.T. Nguyen, M. Rizwan, S.T. Wong, K.-H. Chiam, E.K.F. Yim, Anisotropic traction stresses and focal adhesion polarization mediates topography-induced cell elongation, Biomaterials 181 (2018) 103-112.
[280] A. Tijore, S.A. Irvine, U. Sarig, P. Mhaisalkar, V. Baisane, S. Venkatraman, Contact guidance for cardiac tissue engineering using 3D bioprinted gelatin patterned hydrogel, Biofabrication 10(2) (2018) 025003.
[281] M.J. Dalby, N. Gadegaard, R.O. Oreffo, Harnessing nanotopography and integrin–matrix interactions to influence stem cell fate, Nature materials 13(6) (2014) 558-569.
[282] H. Zheng, Y. Tian, Q. Gao, Y. Yu, X. Xia, Z. Feng, F. Dong, X. Wu, L. Sui, Hierarchical micro-nano topography promotes cell adhesion and osteogenic differentiation via integrin α2-PI3K-AKT signaling axis, Frontiers in Bioengineering and Biotechnology 8 (2020) 463.

[283] A. Sales, K. Ende, J. Diemer, A.R. Kyvik, J. Veciana, I. Ratera, R. Kemkemer, J.P. Spatz, J. Guasch, Cell type-dependent integrin distribution in adhesion and migration responses on protein-coated microgrooved substrates, ACS Omega 4(1) (2019) 1791-1800.
[284] J.Y. Lim, A.D. Dreiss, Z. Zhou, J.C. Hansen, C.A. Siedlecki, R.W. Hengstebeck, J. Cheng, N. Winograd, H.J. Donahue, The regulation of integrin-mediated osteoblast focal adhesion and focal adhesion kinase expression by nanoscale topography, Biomaterials 28(10) (2007) 1787-1797.
[285] S.J. Liliensiek, P. Nealey, C.J. Murphy, Characterization of endothelial basement membrane nanotopography in rhesus macaque as a guide for vessel tissue engineering, Tissue Eng Part A 15(9) (2009) 2643-2651.
[286] M. Kukumberg, Y. Yao, S.H. Goh, D.J.H. Neo, J.Y. Yao, E.K.F. Yim, Evaluation of the Topographical Influence on the Cellular Behavior of Human Umbilical Vein Endothelial Cells, Advanced Biosystems 2(6) (2018) 1700217.
[287] Y. Ding, Z. Yang, C.W.C. Bi, M. Yang, S.L. Xu, X. Lu, N. Huang, P. Huang, Y. Leng, Directing Vascular Cell Selectivity and Hemocompatibility on Patterned Platforms Featuring Variable Topographic Geometry and Size, ACS Applied Materials & Interfaces 6(15) (2014) 12062-12070.
[288] P. Uttayarat, G.K. Toworfe, F. Dietrich, P.I. Lelkes, R.J. Composto, Topographic guidance of endothelial cells on silicone surfaces with micro- to nanogrooves: Orientation of actin filaments and focal adhesions, Journal of Biomedical Materials Research Part A 75A(3) (2005) 668-680.
[289] J.-y. Chen, M. Hu, H. Zhang, B.-c. Li, H. Chang, K.-f. Ren, Y.-b. Wang, J. Ji, Improved Antithrombotic Function of Oriented Endothelial Cell Monolayer on Microgrooves, ACS Biomaterials Science & Engineering 4(6) (2018) 1976-1985.
[290] N.F. Huang, J. Okogbaa, J.C. Lee, A. Jha, T.S. Zaitseva, M.V. Paukshto, J.S. Sun, N. Punjya, G.G. Fuller, J.P. Cooke, The modulation of endothelial cell morphology, function, and survival using anisotropic nanofibrillar collagen scaffolds, Biomaterials 34(16) (2013) 4038-4047.
[291] K.B. Vartanian, M.A. Berny, O.J.T. McCarty, S.R. Hanson, M.T. Hinds, Cytoskeletal structure regulates endothelial cell immunogenicity independent of fluid shear stress, American Journal of Physiology-Cell Physiology 298(2) (2009) C333-C341.
[292] S. Arora, S. Lin, C. Cheung, E.K.F. Yim, Y.-C. Toh, Topography elicits distinct phenotypes and functions in human primary and stem cell derived endothelial cells, Biomaterials 234 (2020) 119747.
[293] G. Eelen, P. de Zeeuw, M. Simons, P. Carmeliet, Endothelial Cell Metabolism in Normal and Diseased Vasculature, Circulation Research 116(7) (2015) 1231-1244.
[294] M.F.A. Cutiongco, B.M.X. Chua, D.J.H. Neo, M. Rizwan, E.K.F. Yim, Functional differences between healthy and diabetic endothelial cells on topographical cues, Biomaterials 153 (2018) 70-84.
[295] X. Qiu, B.L.-P. Lee, X. Ning, N. Murthy, N. Dong, S. Li, End-point immobilization of heparin on plasma-treated surface of electrospun polycarbonate-urethane vascular graft, Acta Biomaterialia 51 (2017) 138-147.
[296] S. Dimitrievska, C. Cai, A. Weyers, J.L. Balestrini, T. Lin, S. Sundaram, G. Hatachi, D.A. Spiegel, T.R. Kyriakides, J. Miao, G. Li, L.E. Niklason, R.J. Linhardt, Click-coated, heparinized, decellularized vascular grafts, Acta Biomaterialia 13 (2015) 177-187.
[297] B. Li, F. Lu, X. Wei, R. Zhao, Fucoidan: Structure and Bioactivity, Molecules 13(8) (2008).
[298] M.T. Ale, J.D. Mikkelsen, A.S. Meyer, Important Determinants for Fucoidan Bioactivity: A Critical Review of Structure-Function Relations and Extraction Methods for Fucose-Containing Sulfated Polysaccharides from Brown Seaweeds, Marine Drugs 9(10) (2011).
[299] I.P.S. Fernando, D. Kim, J.-W. Nah, Y.-J. Jeon, Advances in functionalizing fucoidans and alginates (bio)polymers by structural modifications: A review, Chemical Engineering Journal 355 (2019) 33-48.

[300] J.-L. Giraux, S. Matou, A. Bros, J. Tapon-Bretaudière, D. Letourneur, A.-M. Fischer, Modulation of human endothelial cell proliferation and migration by fucoidan and heparin, European Journal of Cell Biology 77(4) (1998) 352-359.
[301] J.M. Ino, P. Chevallier, D. Letourneur, D. Mantovani, C. Le Visage, Plasma functionalization of poly(vinyl alcohol) hydrogel for cell adhesion enhancement, Biomatter 3(4) (2013) e25414.
[302] A. Purnama, R. Aid-Launais, O. Haddad, M. Maire, D. Mantovani, D. Letourneur, H. Hlawaty, C. Le Visage, Fucoidan in a 3D scaffold interacts with vascular endothelial growth factor and promotes neovascularization in mice, Drug Delivery and Translational Research 5(2) (2015) 187-197.
[303] Y. Wang, C.R. Ye, H. Su, J. Wang, Y.A. Wang, H.H. Wang, A.S. Zhao, N. Huang, Layer-by-layer self-assembled laminin/fucoidan films: towards better hemocompatibility and endothelialization, Rsc Adv 6(61) (2016) 56048-56055.
[304] P.K. Smith, A.K. Mallia, G.T. Hermanson, Colorimetric method for the assay of heparin content in immobilized heparin preparations, Analytical Biochemistry 109(2) (1980) 466-473.
[305] A. Gupta, C.M. Johnston, M.T. Hinds, D.E. Anderson, Quantifying physical thrombus characteristics on cardiovascular biomaterials using microCT, Methods and Protocols (Unpublished results).
[306] D.E.J. Anderson, G. Pohan, J. Raman, F. Konecny, E.K.F. Yim, M.T. Hinds, Improving Surgical Methods for Studying Vascular Grafts in Animal Models, Tissue Engineering Part C: Methods 24(8) (2018) 457-464.
[307] J.S. Lee, M.G. Hamilton, J.M. Zabramski, Variations in the anatomy of the rabbit cervical carotid artery, Stroke 25(2) (1994) 501-503.
[308] T. Matsumoto, E. Okumura, Y. Miura, M. Sato, Mechanical and dimensional adaptation of rabbit carotid artery culturedin vitro, Medical & Biological Engineering & Computing 37(2) (1999) 252-256.
[309] G. Pohan, Endothelialisation of Polyvinyl Alcohol Small Diameter Vascular Graft, UWSpace, 2018.
[310] P. Human, T. Franz, J. Scherman, L. Moodley, P. Zilla, Dimensional analysis of human saphenous vein grafts: Implications for external mesh support, The Journal of Thoracic and Cardiovascular Surgery 137(5) (2009) 1101-1108.
[311] G. Konig, T.N. McAllister, N. Dusserre, S.A. Garrido, C. Iyican, A. Marini, A. Fiorillo, H. Avila, W. Wystrychowski, K. Zagalski, M. Maruszewski, A.L. Jones, L. Cierpka, L.M. de la Fuente, N. L'Heureux, Mechanical properties of completely autologous human tissue engineered blood vessels compared to human saphenous vein and mammary artery, Biomaterials 30(8) (2009) 1542-1550.
[312] N. Ohtani, K. Kiyokawa, H. Asada, T. Kawakami, M. Haga, N. Akasaka, Evaluation of an internal thoracic artery as a coronary artery bypass graft by intercostal duplex scanning ultrasonography, The Japanese Journal of Thoracic and Cardiovascular Surgery 49(6) (2001) 343.
[313] R. Marx, T.W. Jax, G. Plehn, C.M. Schannwell, M. Horlitz, R.M. Klein, H. Lapp, H. Gülker, Morphological differences of the internal thoracic artery in patients with and without coronary artery disease – evaluation by duplex-scanning, European Journal of Cardio-Thoracic Surgery 20(4) (2001) 755-759.
[314] A. de Mel, G. Jell, M.M. Stevens, A.M. Seifalian, Biofunctionalization of Biomaterials for Accelerated in Situ Endothelialization: A Review, Biomacromolecules 9(11) (2008) 2969-2979.
[315] X. Ren, Y. Feng, J. Guo, H. Wang, Q. Li, J. Yang, X. Hao, J. Lv, N. Ma, W. Li, Surface modification and endothelialization of biomaterials as potential scaffolds for vascular tissue engineering applications, Chemical Society Reviews 44(15) (2015) 5680-5742.
[316] C. Tang, F. Kligman, C.C. Larsen, K. Kottke-Marchant, R.E. Marchant, Platelet and endothelial adhesion on fluorosurfactant polymers designed for vascular graft modification, Journal of Biomedical Materials Research Part A 88A(2) (2009) 348-358.

[317] U. Hersel, C. Dahmen, H. Kessler, RGD modified polymers: biomaterials for stimulated cell adhesion and beyond, Biomaterials 24(24) (2003) 4385-4415.
[318] S.-h. Hsu, S.-h. Sun, D.C. Chen, Improved Retention of Endothelial Cells Seeded on Polyurethane Small-diameter Vascular Grafts Modified by a Recombinant RGD-containing Protein, Artificial Organs 27(12) (2003) 1068-1078.
[319] P.C. Begovac, R.C. Thomson, J.L. Fisher, A. Hughson, A. Gällhagen, Improvements in GORE-TEX® vascular graft performance by Carmeda® bioactive surface heparin immobilization, European Journal of Vascular and Endovascular Surgery 25(5) (2003) 432-437.
[320] M. Bosiers, K. Deloose, J. Verbist, H. Schroë, G. Lauwers, W. Lansink, P. Peeters, Heparin-bonded expanded polytetrafluoroethylene vascular graft for femoropopliteal and femorocrural bypass grafting: 1-year results, Journal of Vascular Surgery 43(2) (2006) 313-318.
[321] M.R.H.M. van Sambeek, C.M. Segeren, L.C. van Dijk, J.A. van Essen, D.W.J. Dippel, H. van Urk, Endovascular Repair of an Extracranial Internal Carotid Artery Aneurysm Complicated by Heparin-Induced Thrombocytopenia and Thrombosis, Journal of Endovascular Therapy 7(5) (2000) 353-358.
[322] S. Thakur, J.P. Pigott, A.J. Comerota, Heparin-induced thrombocytopenia after implantation of a heparin-bonded polytetrafluoroethylene lower extremity bypass graft: A case report and plan for management, Journal of Vascular Surgery 49(4) (2009) 1037-1040.
[323] F.C. Church, J.B. Meade, R.E. Treanor, H.C. Whinna, Antithrombin Activity of Fucoidan - the Interaction of Fucoidan with Heparin Cofactor-Ii, Antithrombin-Iii, and Thrombin, J Biol Chem 264(6) (1989) 3618-3623.
[324] L.B. Koh, I. Rodriguez, S.S. Venkatraman, The effect of topography of polymer surfaces on platelet adhesion, Biomaterials 31(7) (2010) 1533-1545.
[325] M. Atlan, T. Simon-Yarza, J.M. Ino, V. Hunsinger, L. Corte, P. Ou, R. Aid-Launais, M. Chaouat, D. Letourneur, Design, characterization and in vivo performance of synthetic 2 mm-diameter vessel grafts made of PVA-gelatin blends, Sci. Rep. 8 (2018).
[326] T. Matsumoto, E. Okumura, T. Shirono, E. Sho, H. Masuda, M. Sato, Flow-Induced Changes in Dimensions and Mechanical Properties of Rabbit Common Carotid Arteries, JSME International Journal Series C Mechanical Systems, Machine Elements and Manufacturing 48(4) (2005) 477-483.
[327] D.A. Salzer, P.J. Medeiros, R. Craen, J.K. Shoemaker, Neurogenic-nitric oxide interactions affecting brachial artery mechanics in humans: roles of vessel distensibility vs. diameter, American Journal of Physiology-Regulatory, Integrative and Comparative Physiology 295(4) (2008) R1181-R1187.
[328] D. Chabut, A.-M. Fischer, S. Colliec-Jouault, I. Laurendeau, S. Matou, B. Le Bonniec, D. Helley, Low Molecular Weight Fucoidan and Heparin Enhance the Basic Fibroblast Growth Factor-Induced Tube Formation of Endothelial Cells through Heparan Sulfate-Dependent α6 Overexpression, Molecular Pharmacology 64(3) (2003) 696.
[329] S. Matou, D. Helley, D. Chabut, A. Bros, A.-M. Fischer, Effect of fucoidan on fibroblast growth factor-2-induced angiogenesis in vitro, Thrombosis Research 106(4) (2002) 213-221.
[330] G. Sarlon, F. Zemani, L. David, J.P. Duong Van Huyen, B. Dizier, F. Grelac, S. Colliec-Jouault, I. Galy-Fauroux, P. Bruneval, A.M. Fischer, J. Emmerich, C. Boisson-Vidal, Therapeutic effect of fucoidan-stimulated endothelial colony-forming cells in peripheral ischemia, Journal of Thrombosis and Haemostasis 10(1) (2012) 38-48.
[331] P. Lertkiatmongkol, D. Liao, H. Mei, Y. Hu, P.J. Newman, Endothelial functions of platelet/endothelial cell adhesion molecule-1 (CD31), Curr Opin Hematol 23(3) (2016) 253-259.
[332] D. Vestweber, VE-Cadherin, Arteriosclerosis, Thrombosis, and Vascular Biology 28(2) (2008) 223-232.
[333] K.-W. Kwak, K.-S. Cho, O.-J. Hahn, K.-H. Lee, B.-Y. Lee, J.-J. Ko, K.-H. Chung, Biological effects of fucoidan isolated from Fucus vesiculosus on thrombosis and vascular cells, Korean J Hematol 45(1) (2010) 51-57.

[334] J.H. Fitton, D.N. Stringer, S.S. Karpiniec, Therapies from Fucoidan: An Update, Mar Drugs 13(9) (2015) 5920-5946.
[335] J. Dürig, T. Bruhn, K.-H. Zurborn, K. Gutensohn, H.D. Bruhn, L. Béress, Anticoagulant fucoidan fractions from Fucus vesiculosus induce platelet activation in vitro, Thrombosis Research 85(6) (1997) 479-491.
[336] A.C. Ouano, D.E. Johnson, B. Dawson, L.A. Pederson, Chain scission efficiency of some polymers in γ-radiation, Journal of Polymer Science: Polymer Chemistry Edition 14(3) (1976) 701-711.
[337] H. Otaguro, L.F.C.P. de Lima, D.F. Parra, A.B. Lugão, M.A. Chinelatto, S.V. Canevarolo, High-energy radiation forming chain scission and branching in polypropylene, Radiation Physics and Chemistry 79(3) (2010) 318-324.
[338] Á. Sáfrány, B. Beiler, K. László, F. Svec, Control of pore formation in macroporous polymers synthesized by single-step γ-radiation-initiated polymerization and cross-linking, Polymer 46(9) (2005) 2862-2871.
[339] A. Srinivas, A. Ramamurthi, Effects of Gamma-Irradiation on Physical and Biologic Properties of Crosslinked Hyaluronan Tissue Engineering Scaffolds, Tissue Engineering 13(3) (2007) 447-459.
[340] A.M. Matuska, P.S. McFetridge, The effect of terminal sterilization on structural and biophysical properties of a decellularized collagen-based scaffold; implications for stem cell adhesion, Journal of Biomedical Materials Research Part B: Applied Biomaterials 103(2) (2015) 397-406.
[341] F.K. Denizli, O. Güven, Competitive adsorption of blood proteins on gamma-irradiated-polycarbonate films, Journal of Biomaterials Science, Polymer Edition 13(2) (2002) 127-139.
[342] W.S. Cassel, R.A. Mason, R. Campbell, G.B. Newton, J.C.K. Hui, F. Giron, An Animal Model for Small-Diameter Arterial Grafts, Journal of Investigative Surgery 2(2) (1989) 181-186.
[343] M.J. Byrom, P.G. Bannon, G.H. White, M.K.C. Ng, Animal models for the assessment of novel vascular conduits, Journal of Vascular Surgery 52(1) (2010) 176-195.
[344] L. Geary Randolph, J.K. Williams, D. Golden, G. Brown Deanna, E. Benjamin Marshall, R. Adams Michael, Time Course of Cellular Proliferation, Intimal Hyperplasia, and Remodeling Following Angioplasty in Monkeys With Established Atherosclerosis, Arteriosclerosis, Thrombosis, and Vascular Biology 16(1) (1996) 34-43.
[345] Wang, M. Xing, Q. Cao, A. Ji, H. Liang, S. Song, Biological activities of fucoidan and the factors mediating its therapeutic effects: A review of recent studies, Marine Drugs 17(3) (2019) 183.
[346] Y. Yao, A.M. Zaw, D.E.J. Anderson, M.T. Hinds, E.K.F. Yim, Fucoidan functionalization on poly(vinyl alcohol) hydrogels for improved endothelialization and hemocompatibility, Biomaterials 249 (2020) 120011.
[347] J. Kim, I.-H. Bae, K. Lim, J. Park, D. Park, S.-Y. Lee, E.-J. Jang, M. Ji, D. Sim, Y. Hong, Y. Ahn, J. Park, J. Cho, J. Kang, I.-S. Kim, M. Jeong, A method for coating fucoidan onto bare metal stent and in vivo evaluation, Progress in Organic Coatings 78 (2015) 348-356.
[348] K. Ozaltin, M. Lehocky, P. Humpolicek, J. Pelkova, A. Di Martino, I. Karakurt, P. Saha, Anticoagulant Polyethylene Terephthalate Surface by Plasma-Mediated Fucoidan Immobilization, Polymers 11(5) (2019).
[349] J.M. Goddard, D. Erickson, Bioconjugation techniques for microfluidic biosensors, Anal Bioanal Chem 394(2) (2009) 469-479.
[350] N.M. Bates, H.E. Heidenreich, M.E. Fallon, Y. Yao, E.K.F. Yim, M.T. Hinds, D.E.J. Anderson, Bioconjugation of a Collagen-Mimicking Peptide Onto Poly(vinyl alcohol) Encourages Endothelialization While Minimizing Thrombosis, Frontiers in Bioengineering and Biotechnology 8(1467) (2020).
[351] A.N. Lukyanov, R.M. Sawant, W.C. Hartner, V.P. Torchilin, PEGylated dextran as long-circulating pharmaceutical carrier, Journal of Biomaterials Science, Polymer Edition 15(5) (2004) 621-630.

[352] H. Park, S. Lee, S.H. Jeong, U.H. Jung, K. Park, M.G. Lee, S. Kim, J. Lee, Enhanced Moisture-Reactive Hydrophilic-PTFE-Based Flexible Humidity Sensor for Real-Time Monitoring, Sensors (Basel) 18(3) (2018) 921.
[353] A. Klettner, Fucoidan as a potential therapeutic for major blinding diseases-A hypothesis, Marine Drugs 14(2) (2016).
[354] M. Alwarsamy, R. Gooneratne, R. Ravichandran, Effect of fucoidan from Turbinaria conoides on human lung adenocarcinoma epithelial (A549) cells, Carbohydrate Polymers 152 (2016).
[355] I.P.S. Fernando, K.K.A. Sanjeewa, K.W. Samarakoon, W.W. Lee, H.-S. Kim, N. Kang, P. Ranasinghe, H.-S. Lee, Y.-J. Jeon, A fucoidan fraction purified from Chnoospora minima; a potential inhibitor of LPS-induced inflammatory responses, International Journal of Biological Macromolecules 104 (2017) 1185-1193.
[356] M.-J. ClÈment, B. Tissot, L. Chevolot, E. Adjadj, Y. Du, P. Curmi, R. Daniel, NMR characterization and molecular modeling of fucoidan showing the importance of oligosaccharide branching in its anticomplementary activity, Glycobiology 20 7 (2010) 883-94.
[357] M. Dockal, S. Till, S. Knappe, H.J. Ehrlich, F. Scheiflinger, Anticoagulant activity and mechanism of non-anticoagulant sulfated polysaccharides, Blood 118(21) (2011) 1208-1208.
[358] S. Soeda, Y. Ohmagari, H. Shimeno, A. Nagamatsu, Preparation of aminated fucoidan and its evaluation as an antithrombotic and antilipemic agent, Biological & Pharmaceutical Bulletin 17(6) (1994) 784-788.
[359] Wang, Q. Zhang, Z. Zhang, Y. Hou, H. Zhang, In-vitro anticoagulant activity of fucoidan derivatives from brown seaweed Laminaria japonica, Chinese Journal of Oceanology and Limnology 29(3) (2011) 679-685.
[360] S. Kim, A.E. English, K.D. Kihm, Surface elasticity and charge concentration-dependent endothelial cell attachment to copolymer polyelectrolyte hydrogel, Acta Biomaterialia 5(1) (2009) 144-151.
[361] L. Bachelet-Violette, A.K.A. Silva, M. Maire, A. Michel, O. Brinza, P. Ou, V. Ollivier, A. Nicoletti, C. Wilhelm, D. Letourneur, C. Ménager, F. Chaubet, Strong and specific interaction of ultra small superparamagnetic iron oxide nanoparticles and human activated platelets mediated by fucoidan coating, RSC Advances 4(10) (2014) 4864-4871.
[362] C. Oliveira, N.M. Neves, R.L. Reis, A. Martins, T.H. Silva, A review on fucoidan antitumor strategies: From a biological active agent to a structural component of fucoidan-based systems, Carbohydrate Polymers 239 (2020).
[363] H. Cao, M. Mikkelsen, M. Lezyk, L. Bui, V. Tran, A. Silchenko, M. Kusaykin, T. Pham, B. Truong, J. Holck, A. Meyer, Novel Enzyme Actions for Sulphated Galactofucan Depolymerisation and a New Engineering Strategy for Molecular Stabilisation of Fucoidan Degrading Enzymes, Marine Drugs 16 (2018) 422.
[364] Zhang, S. Till, S. Knappe, C. Quinn, J. Catarello, G.J. Ray, F. Scheiflinger, C.M. Szabo, M. Dockal, Screening of complex fucoidans from four brown algae species as procoagulant agents, Carbohydrate Polymers 115 (2015) 677-685.
[365] C. Ye, Y. Wang, H. Su, P. Yang, N. Huang, M. F. Maitz, A. Zhao, Construction of a fucoidan/laminin functional multilayer to direction vascular cell fate and promotion hemocompatibility, Materials Science and Engineering: C 64 (2016) 236-242.
[366] G. Pohan, S. Mattiassi, Y. Yao, A.M. Zaw, D.E.J. Anderson, M.F.A. Cutiongco, M.T. Hinds, E.K.F. Yim, Effect of ethylene oxide sterilization on polyvinyl alcohol hydrogel compared to gamma radiation, Tissue Engineering Part A (2020).
[367] D. Mantovani, M. Castonguay, J.F. Pageau, M. Fiset, G. Laroche, Ammonia RF-Plasma Treatment of Tubular ePTFE Vascular Prostheses, Plasmas and Polymers 4(2) (1999) 207-228.

[368] H.-H. Chien, K.-J. Ma, C.-H. Kuo, S.-W. Huang, Effects of plasma power and reaction gases on the surface properties of ePTFE materials during a plasma modification process, Surface and Coatings Technology 228 (2013) S477-S481.
[369] A. Sainio, H. Järveläinen, Extracellular matrix-cell interactions: Focus on therapeutic applications, Cellular Signalling 66 (2020) 109487.
[370] F. Lupu, G. Kinasewitz, K. Dormer, The role of endothelial shear stress on haemodynamics, inflammation, coagulation and glycocalyx during sepsis, Journal of Cellular and Molecular Medicine 24(21) (2020) 12258-12271.
[371] T.J. Herbst, J.B. McCarthy, E.C. Tsilibary, L.T. Furcht, Differential effects of laminin, intact type IV collagen, and specific domains of type IV collagen on endothelial cell adhesion and migration, Journal of Cell Biology 106(4) (1988) 1365-1373.
[372] K.R. Kidd, D.D. Ponte, A.L. Stone, J.B. Hoying, R.B. Nagle, S.K. Williams, Stimulated Endothelial Cell Adhesion and Angiogenesis with Laminin-5 Modification of Expanded Polytetrafluoroethylene, Tissue Engineering 11(9-10) (2005) 1379-1391.
[373] T. Pompe, F. Kobe, K. Salchert, B. Jørgensen, J. Oswald, C. Werner, Fibronectin anchorage to polymer substrates controls the initial phase of endothelial cell adhesion, Journal of Biomedical Materials Research Part A 67A(2) (2003) 647-657.
[374] B. Dreier, J.Z. Gasiorowski, J.T. Morgan, P.F. Nealey, P. Russell, C.J. Murphy, Early responses of vascular endothelial cells to topographic cues, Am J Physiol Cell Physiol 305(3) (2013) C290-C298.
[375] N.F. Huang, E.S. Lai, A.J.S. Ribeiro, S. Pan, B.L. Pruitt, G.G. Fuller, J.P. Cooke, Spatial patterning of endothelium modulates cell morphology, adhesiveness and transcriptional signature, Biomaterials 34(12) (2013) 2928-2937.
[376] R. Muhammad, S.H. Lim, S.H. Goh, J.B.K. Law, M.S.M. Saifullah, G.W. Ho, E.K.F. Yim, Sub-100 nm patterning of TiO2 film for the regulation of endothelial and smooth muscle cell functions, Biomaterials Science 2(12) (2014) 1740-1749.
[377] P.A. Underwood, F.A. Bennett, A. Kirkpatrick, P.A. Bean, B.A. Moss, Evidence for the location of a binding sequence for the α2β1 integrin of endothelial cells, in the β1 subunit of laminin, Biochemical Journal 309(3) (1995) 765-771.
[378] P. Vandenberg, A. Kern, A. Ries, L. Luckenbill-Edds, K. Mann, K. Kühn, Characterization of a type IV collagen major cell binding site with affinity to the alpha 1 beta 1 and the alpha 2 beta 1 integrins, Journal of Cell Biology 113(6) (1991) 1475-1483.
[379] A. Post, E. Wang, E. Cosgriff-Hernandez, A Review of Integrin-Mediated Endothelial Cell Phenotype in the Design of Cardiovascular Devices, Annals of Biomedical Engineering 47(2) (2019) 366-380.
[380] R.H. Kramer, Y.F. Cheng, R. Clyman, Human microvascular endothelial cells use beta 1 and beta 3 integrin receptor complexes to attach to laminin, Journal of Cell Biology 111(3) (1990) 1233-1243.
[381] F.F. Isik, N.S. Gibran, Y.-C. Jang, L. Sandell, S.M. Schwartz, Vitronectin decreases microvascular endothelial cell apoptosis, Journal of Cellular Physiology 175(2) (1998) 149-155.
[382] A. Ray, O. Lee, Z. Win, R.M. Edwards, P.W. Alford, D.-H. Kim, P.P. Provenzano, Anisotropic forces from spatially constrained focal adhesions mediate contact guidance directed cell migration, Nature Communications 8(1) (2017) 14923.
[383] P.M. Hansson, A. Swerin, J. Schoelkopf, P.A. Gane, E. Thormann, Influence of surface topography on the interactions between nanostructured hydrophobic surfaces, Langmuir 28(21) (2012) 8026-8034.
[384] C. Piao, J.E. Winandy, T.F. Shupe, From hydrophilicity to hydrophobicity: A critical review: Part I. Wettability and surface behavior, Wood and Fiber Science 42(4) (2010) 490-510.
[385] R. Sandmann, S.S.G. Henriques, F. Rehfeldt, S. Köster, Micro-topography influences blood platelet spreading, Soft Matter 10(14) (2014) 2365-2371.

[386] D.A. Barrett, M. Hartshome, M.A. Hussain, P. Shaw, M. Davies, Resistance to Nonspecific Protein Adsorption by Poly(vinyl alcohol) Thin Films Adsorbed to a Poly(styrene) Support Matrix Studied Using Surface Plasmon Resonance, Analytical chemistry 73 (2001) 5232-9.
[387] S.N. Rodrigues, I.C. Gonçalves, M.C.L. Martins, M.A. Barbosa, B.D. Ratner, Fibrinogen adsorption, platelet adhesion and activation on mixed hydroxyl-/methyl-terminated self-assembled monolayers, Biomaterials 27(31) (2006) 5357-5367.
[388] J. Mestas, K. Ley, Monocyte-endothelial cell interactions in the development of atherosclerosis, Trends in cardiovascular medicine 18(6) (2008) 228-232.
[389] H. Jeon, J.H. Tsui, S.I. Jang, J.H. Lee, S. Park, K. Mun, Y.C. Boo, D.-H. Kim, Combined Effects of Substrate Topography and Stiffness on Endothelial Cytokine and Chemokine Secretion, ACS Applied Materials & Interfaces 7(8) (2015) 4525-4532.
[390] Y. Liu, W. Deng, L. Yang, X. Fu, Z. Wang, P. van Rijn, Q. Zhou, T. Yu, Biointerface topography mediates the interplay between endothelial cells and monocytes, RSC Advances 10(23) (2020) 13848-13854.
[391] J. Liang, S. Gu, X. Mao, Y. Tan, H. Wang, S. Li, Y. Zhou, Endothelial Cell Morphology Regulates Inflammatory Cells Through MicroRNA Transferred by Extracellular Vesicles, Frontiers in Bioengineering and Biotechnology 8(369) (2020).
[392] F. Liao, H.K. Huynh, A. Eiroa, T. Greene, E. Polizzi, W.A. Muller, Migration of monocytes across endothelium and passage through extracellular matrix involve separate molecular domains of PECAM-1, J Exp Med 182(5) (1995) 1337-1343.
[393] P.F. Sánchez, E.M. Brey, J.C. Briceño, Endothelialization mechanisms in vascular grafts, Journal of Tissue Engineering and Regenerative Medicine 12(11) (2018) 2164-2178.
[394] S. Li, N.F. Huang, S. Hsu, Mechanotransduction in endothelial cell migration, Journal of Cellular Biochemistry 96(6) (2005) 1110-1126.
[395] P.-P. Hsu, S. Li, Y.-S. Li, S. Usami, A. Ratcliffe, X. Wang, S. Chien, Effects of Flow Patterns on Endothelial Cell Migration into a Zone of Mechanical Denudation, Biochemical and Biophysical Research Communications 285(3) (2001) 751-759.
[396] J.M. Liu, J. Bignon, F. Haroun-Bouhedja, P. Bittoun, J. Vassy, S. Fermandjian, J. Wdzieczak-Bakala, C. Boisson-Vidal, Inhibitory Effect of Fucoidan on the Adhesion of Adenocarcinoma Cells to Fibronectin, Anticancer Research 25(3B) (2005) 2129.
[397] Y. Yamasaki, M. Yamasaki, H. Tachibana, K. Yamada, Important Role of β1-Integrin in Fucoidan-Induced Apoptosis via Caspase-8 Activation, Bioscience, Biotechnology, and Biochemistry 76(6) (2012) 1163-1168.
[398] A.s. Hidalgo, A.J. Peired, L.A. Weiss, Y. Katayama, P.S. Frenette, The integrin αMβ2 anchors hematopoietic progenitors in the bone marrow during enforced mobilization, Blood 104(4) (2004) 993-1001.
[399] S. Matou-Nasri, D. Helley, D. Chabut, A. Bros, A.-M. Fischer, Effect of fucoidan on fibroblast growth factor-2-induced angiogenesis in vitro, Thrombosis research 106 (2002) 213-21.
[400] F. Zemani, D. Benisvy, I. Galy-Fauroux, A. Lokajczyk, S. Colliec-Jouault, G. Uzan, A. Fischer, C. Boisson-vidal, Low-molecular-weight fucoidan enhances the proangiogenic phenotype of endothelial progenitor cells, Biochemical pharmacology 70 (2005) 1167-75.
[401] O. Inoue, K. Suzuki-Inoue, O.J.T. McCarty, M. Moroi, Z.M. Ruggeri, T.J. Kunicki, Y. Ozaki, S.P. Watson, Laminin stimulates spreading of platelets through integrin alpha6beta1-dependent activation of GPVI, Blood 107(4) (2006) 1405-1412.
[402] H.S. Bassiouny, S. White, S. Glagov, E. Choi, D.P. Giddens, C.K. Zarins, Anastomotic intimal hyperplasia: Mechanical injury or flow induced, Journal of Vascular Surgery 15(4) (1992) 708-717.